

Dissertation
submitted to the
Combined Faculties of the Natural Sciences and for
Mathematics
of the Ruperto-Carola University of Heidelberg, Germany
for the degree of
Doctor of Natural Sciences

Put forward by
MSc. Patrick Blaser
Born in Heidelberg
Oral examination: 28.06.2017

The application of radiogenic neodymium isotopes
as a palaeo water mass tracer in the subpolar
North Atlantic

Referees: Prof. Dr. Norbert Frank

Prof. Dr. Werner Aeschbach

The application of radiogenic neodymium isotopes as a palaeo water mass tracer in the subpolar North Atlantic

The formation of North Atlantic Deep Water (NADW) is a complex and important mechanism coupling the large oceanic reservoir of heat and carbon to the highly climate relevant atmospheric reservoir. In order to study the role of deep water formation during the last deglaciation, proxies archived in marine sediments are required. One proxy for the identification of local deep waters and their mixing is the isotope composition of seawater-derived Nd (Nd IC). An accurate interpretation of this proxy, however, requires good knowledge of the Nd ICs of water mass end members. In this thesis the distribution, reactivity, and mobility of Nd in deep sea sediments was assessed in detail. This investigation evidences a general immobility of Nd in sediments and results in a refinement of existing methods for the extraction of an authigenic Nd IC from bulk sediments of varying compositions. The subsequent reconstruction of deep water Nd ICs across the subpolar North Atlantic allows for the investigation of changes in the formation of NADW and the Nd IC it carries. The results show the first direct evidence that a prominent transient Nd IC change of deep NADW during the Holocene originated in its source waters, probably in the Nordic Seas.

Die Verwendung von radiogenen Neodymisotopen als Paläo-Wassermassentracer im subpolaren Nordatlantik

Die Bildung von Nordatlantischem Tiefenwasser (NADW) ist ein komplexer und entscheidender Mechanismus der das große ozeanische Kohlenstoff- und Wärmereservoir an das äußerst klimarelevante atmosphärische Reservoir koppelt. Um die Rolle der Tiefenwasserbildung während der letzten Deglaziation zu untersuchen bedarf es Proxies die in marinen Sedimenten archiviert sind. Ein solcher Proxy für die Identifikation von lokalen Tiefenwassern und deren Mischung ist die isotopische Zusammensetzung von Nd aus Meerwasser (Nd IC). Für die genaue Interpretation ist allerdings eine gute Kenntnis der Nd IC der Quellwasser-massen Voraussetzung. In dieser Arbeit wird zunächst die Verteilung, Reaktionsfreudigkeit und Mobilität von Nd in Tiefseesedimenten im Detail untersucht. Diese Analyse bestätigt eine allgemeine Immobilität von Nd im Sediment und resultiert in einer Überarbeitung existierender Methoden für die Extraktion von authigenem Nd aus Gesamtsedimenten unterschiedlicher Zusammensetzung. Die anschließende Rekonstruktion von Tiefenwasser Nd IC an verschiedenen Stellen des subpolaren Nordatlantik erlaubt die Untersuchung von Veränderungen in der Bildung von NADW und seiner Isotopensignatur. Die Ergebnisse liefern den ersten direkten Beweis, dass eine markante vorübergehende Veränderung der Nd IC im tiefen NADW während des Holozäns ihren Ursprung in seinen Quellwasser-massen hat, vermutlich jenen aus der Grönlandsee.

Contents

	Page
1 Introduction	10
2 Basics	12
2.1 Oceans and climate	12
2.1.1 Ocean circulation during the last glacial-interglacial cycle . . .	13
2.1.2 Proxies for past ocean circulation	15
2.2 Nd in the environment	17
2.3 Nd isotopes as a water mass tracer	18
2.4 Nd in deep sea sediments	20
2.4.1 Archives of seawater-derived Nd	20
2.4.2 Nd bearing components in common deep sea sediments	22
2.5 The role of the subpolar North Atlantic	24
2.5.1 Hydrography of the subpolar North Atlantic	24
2.5.2 Sedimentology of the subpolar North Atlantic	28
3 Methods	30
3.1 Sample treatment	30
3.1.1 Bulk sediment leaches	30
3.1.2 Total digestions	32
3.1.3 Foraminifera analyses	32
3.2 Mass spectrometric measurements	32
3.2.1 Element abundance measurements	33
3.2.2 Nd isotope measurements	38
4 The extraction of authigenic Nd from marine sediments	40
4.1 Methods	40
4.2 Results	44
4.3 Discussion	51
4.3.1 Carbonate dissolution	51
4.3.2 Hydrogenetic Fe-Mn oxyhydroxides	52
4.3.3 Quantification of Nd contributions from different sediment fractions	53
4.3.4 The influence of non-biogenic carbonates	57
4.3.5 Elemental ratios as proxies for non-hydrogenetic contamination	57
4.3.6 Implications for an improved acid-reductive leaching method .	58
4.4 Summary	60

5	Reactivity and mobility of Nd in Northeast Atlantic sediments	61
5.1	Introduction	61
5.2	Methods	62
5.2.1	Sites and sediment samples	62
5.2.2	Sediment handling and measurements	64
5.3	Results	65
5.3.1	Sediment stratigraphy	65
5.3.2	Radiogenic Nd isotopes	66
5.3.3	Leachate composition	68
5.4	Discussion	72
5.4.1	No evidence for vertical diffusion of REEs in the sediment	72
5.4.2	Interaction between detrital and authigenic phases	73
5.4.3	Characteristics in the record from Site IODP U1308	77
5.4.4	Impact of detrital sediments on local bottom water Nd IC	78
5.4.5	Northeast Atlantic deep water Nd ICs during the LGM	84
5.5	Summary	84
6	Nd isotopes in the subpolar North Atlantic during the deglaciation	86
6.1	Introduction	86
6.2	The hydrography of the subpolar North Atlantic since last glacial	87
6.3	Study sites	88
6.4	Results and Discussion	92
6.4.1	Integrity of leached Nd ICs as past bottom water signatures	94
6.4.2	Changes in past deep water provenance	99
6.5	Synthesis and summary	109
7	Conclusion and Outlook	111
8	Publications of the author	116
9	Bibliography	117
A	Supplementary Material	139
A.1	Site locations	139
A.2	Hydrographic sections and water mass Nd characteristics	140
A.3	Supplement to chapter 5	144
A.4	Supplement to chapter 6	147
A.5	Quantification of the authigenic fraction via sediment leaches	151
A.6	Additional figures	154
B	Lists	158
B.1	List of Figures	158
B.2	List of Tables	160
B.3	List of abbreviations	161

*How inappropriate to call this planet Earth, when
clearly it is Ocean.*

- Arthur C. Clarke

1 Introduction

The global ocean is the largest highly dynamical actor in the climate system. Covering 71 % of Earth's surface and exhibiting very low albedo, it receives most of the sun's radiation energy and stores or redistributes it. The same surface also couples the large ocean carbon reservoir to the small but highly dynamic and climatically relevant carbon reservoir of the atmosphere. While astronomical parameters have clearly controlled the general climate states during the Pleistocene's 40 to 100 thousand years long glacial-interglacial cycles (e.g. Paillard [1998]), rapid climate transitions during glacials and at glacial terminations evidence a strong modulation by the ocean-atmosphere system. These episodes of rapid global climate change seem to have been connected to reorganisations in the ocean's deep overturning circulation, stratification, and carbon export into the depth (Adkins [2013]). For example, during the last glacial the interface between North Atlantic Deep Water (NADW) and the underlying southern sourced Antarctic Bottom Water (AABW) was shallower and more stable than today. It is hypothesised that the termination of this strong stratification at the end of the glacial led to the release of CO₂ to the atmosphere, thereby accelerating global warming (Skinner et al. [2010]). One fundamental goal of climate science is to improve our understanding of the coupling between climatic and oceanic changes during such rapid transitions. The formation of NADW in the subpolar North Atlantic and its southward export is coupled to a strong northward flux of warm surface waters from the low latitudes. The associated heat flux is a crucial mechanism for inter hemispheric heat exchange, leading to a latitudinal moderation of global temperatures, as evidenced by the moderate climate in northern Europe. For these reasons, the reconstruction of past NADW formation and advection has drawn increased attention of scientists in the last decades. However, since density driving properties of ocean water masses like temperature or salinity are not preserved, palaeoceanographers need to rely on archived indirect proxies of these or other water mass specific properties.

One rather novel proxy is the radiogenic neodymium isotope composition (Nd IC) of seawater, archived in deep sea sediments. While the Nd IC is not related to the water's temperature or salinity, it exhibits a quasi-conservative behaviour in the major deep ocean basins (Piepgras et al. [1979]; Tachikawa et al. [2017]). It can therefore be used to trace the water mass provenance and mixing in the past. The Nd IC is furthermore not influenced by biological cycling or gas exchange, making it a promising addition to traditional biogeochemical proxies. However, for an accurate and possibly quantitative analysis of past seawater Nd ICs, a detailed knowledge of the Nd ICs of water mass mixing end members is a necessary condition. Today, the Nd isotopic signature of NADW is mostly assumed to not have varied significantly.

While there is evidence for such constancy during the Last Glacial Maximum (LGM) and on long time scales (van de Flierdt et al. [2006]; Foster et al. [2007]), several studies from the deep Northwest Atlantic have reconstructed Nd ICs that cannot be explained with a constant northern end member (Roberts et al. [2010]; Wilson et al. [2014]; Böhm et al. [2015]; Howe et al. [2016c]). Retracing the mechanism of formation of NADW and its Nd IC, however, is complicated by the fact that it involves deep convection in two different regions and at least four distinct water masses in the subpolar North Atlantic. Furthermore, the marginal continents deliver Nd of extremely different isotopic compositions by continental weathering; a process which itself can be assumed to be acutely climate sensitive. And finally, the intense interaction of highly dynamic deep currents leads to exchange processes of Nd from seawater and sediments, thereby violating the conservative behaviour of the Nd IC (Lacan and Jeandel [2004a,b, 2005b]). It is thus an important step in the further development of the Nd isotope proxy to investigate its behaviour in the region of NADW formation, the subpolar North Atlantic, during periods of climatic changes.

The last transition from glacial climate into the warm Holocene is, apart from its significance for climate studies, extraordinarily well suited as a testing ground for the investigation of proxy systematics. It is certainly the best studied past time range and comprises the enormous glacial-interglacial reorganisation, as well as several centennial range climate events which have been doubtlessly linked to changes in Atlantic circulation (e.g. Stouffer et al. [2006]). Therefore it is the target of this thesis to investigate the deep water Nd IC across the subpolar North Atlantic reconstructed from sediment core profiles spanning the last glacial, the glacial transition, and the Holocene. However, at the start of this thesis there was no method available that was suited to extract archived seawater-derived Nd from a large variety of deep sea sediments, notably with carbonate contents ranging from 50 to 0% and volcanic material as well as detrital carbonate presenting serious sources of labile contaminant Nd. Furthermore, it was not known whether the largely variable pelagic input of different detrital material during volcanic eruptions or episodes of increased iceberg rafting from the continental margins led to significant imprints in seawater or authigenic Nd ICs. Hence, based on existing bulk sediment leaching methods (Gutjahr et al. [2007]), a revised leaching scheme was developed and extensively tested in order to understand the distribution and reactivity of sedimentary Nd isotopes (chapter 4). The reactivity of massive fluxes of detrital material and the mobility of Nd in sedimentary pore waters was then investigated with a set of sediment cores from the deep Northeast Atlantic (chapter 5). And finally, down core profiles of bottom water Nd ICs were analysed from four sites across the subpolar North Atlantic spanning the abovementioned age range (chapter 6). These records show clear evidence for changes in end member Nd ICs occurring during the LGM and mid Holocene. The latter could help to explain the cause for concomitant Nd IC changes beyond modern water mass end members observed in the deep Northwest Atlantic (Roberts et al. [2010]; Howe et al. [2016c]).

2 Basics

In order to lay the theoretical foundations for this thesis, the basics of ocean circulation and its interaction with the global climate system, climatic changes from the last glacial into today's warm period, and our possibilities of reconstructing such changes are briefly explained in this chapter. Focus will be set on the use and application of authigenic (seawater-derived) Nd isotopes and on peculiarities of the subpolar North Atlantic at the end of this chapter.

2.1 Oceans and climate

The oceans represent the largest dynamical reservoir of heat and greenhouse gases like carbon dioxide in the climate system. Covering about 71 % of Earth's surface, they receive most of the incoming radiation energy and can effectively exchange gases with the atmosphere. In the deep ocean, however, matter like carbon can be withheld from the Earth's surface and either be deposited on the sea floor or rapidly brought back to the atmosphere once large scale circulation allows it. The oceans are in a constant motion, circulating warm and salty surface water from low to high latitudes, where it releases energy, becomes more dense than underlying water, and eventually sinks into the deep. The movement at the ocean's surface is mainly driven by wind stress. Thus, the combination of wind, evaporation, and cooling leads to the steady supply of dense water to the high latitudes and the production of deep water (Fig. 2.1). In contrast, so called upwelling of deep water occurs mainly in the low latitude Pacific and Indian oceans, where deep water slowly rises towards the surface and the overturning loop is completed. This process of thermohaline circulation is an important mechanism by which heat is redistributed from low to high latitudes, especially in the northern hemisphere today (e.g. Broecker [1991]).

The meridional circulation is thus an important mediator of global climate. The location of deep water formation zones is relatively well constrained today. In the South, dense AABW is formed in the Weddell and Ross Seas. The only deep water formation sites of the northern hemisphere today are located in the Labrador and Greenland Seas in the northern North Atlantic Ocean (see Fig. 2.1). The resulting water masses are important end members for the subsequent formation of NADW in the subpolar North Atlantic. Its southward advection leads to a strong Atlantic Meridional Overturning Circulation (AMOC, see Fig. 2.2a). The southward water volume flux of NADW is estimated at some 18 Sv (Talley et al. [2003], 1 Sv = $10^6 \text{ m}^3/\text{s}$). The strong overturning is evidenced in the results of average deep water residence time calculations. For the Atlantic Ocean, the mean residence time of deep water is around 180 years, whereas in the larger and less well ventilated

Pacific it is rather around 1000 years (Broecker and Peng [1982]). This deep convection of recently ventilated water and its subsequent advection is also an important supplier of oxygen into the deep ocean (c.f. Fig. A.17 in the appendix). Numerous studies indicate that the production of NADW and thus the AMOC were significantly weakened during glacial times. A detailed quantitative transient description of the AMOC's behaviour through the last glacial/interglacial cycles would significantly improve our understanding of the global climate system and our capability of forecasting future climate change.

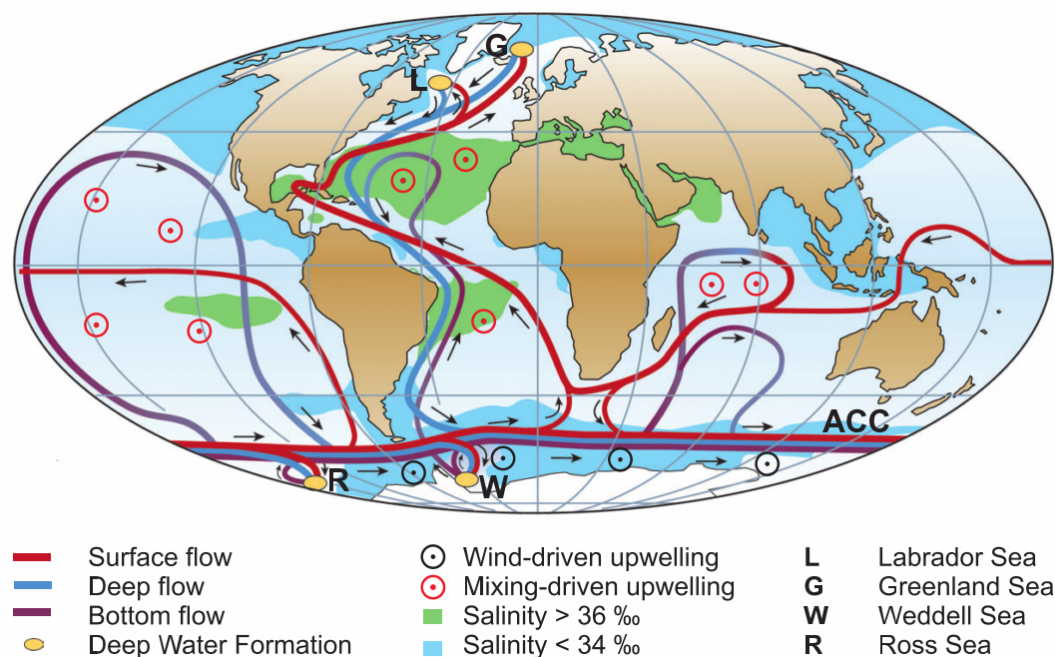
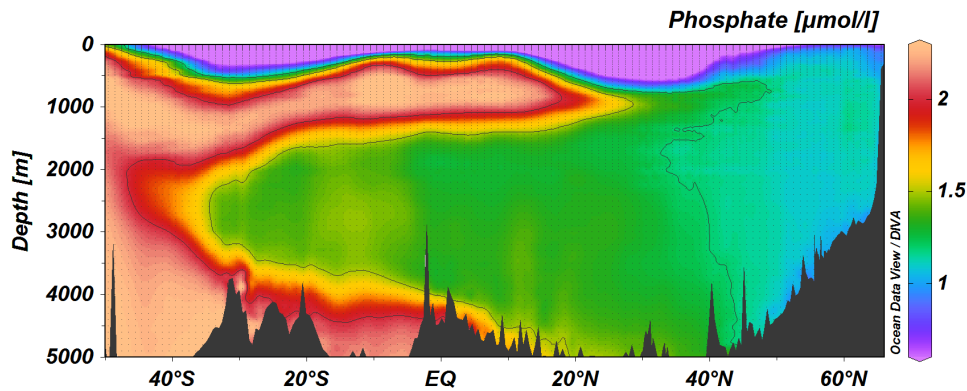


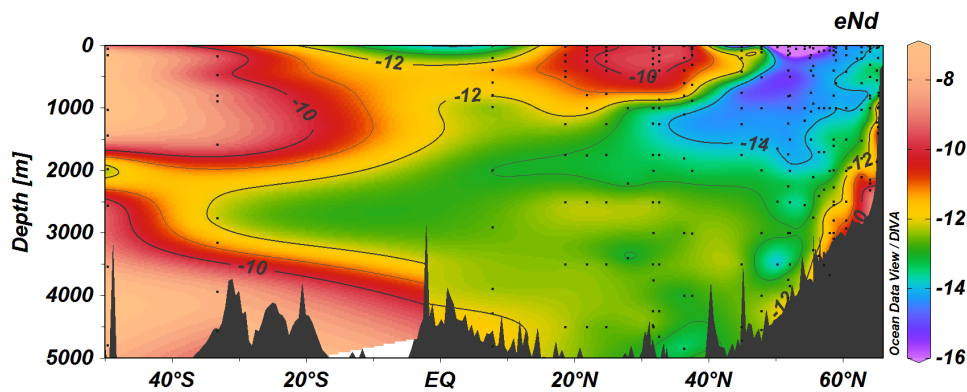
Figure 2.1: Schematic view of the global Thermohaline Circulation with the main deep water formation zones. General upwelling zones are also shown, however these are not as well spatially confined as the deep water formation areas. This figure is extracted from Rahmstorf [2006].

2.1.1 Ocean circulation during the last glacial-interglacial cycle

The last glacial started around 116 thousand years (ka) before present (Capron et al. [2012], see Fig. 2.3). Cooling and continental ice formation led to a maximum global ice volume between 26.5 and 19.0 ka (Clark et al. [2009]), the so called Last Glacial Maximum (LGM). What followed was the period of the last deglaciation or Termination 1, which lasted until the start of the warm Holocene at about 11.7 ka, which continues until today (Walker et al. [2009]). Proxy data and ocean circulation models suggest that NADW production during the LGM was significantly shallower



(a) Dissolved phosphate content on a meridional transect across the west Atlantic Ocean. The conservative phosphate concentration follows the advection of the main water masses. These are (from top to bottom): northward flowing Antarctic Intermediate Water (red), southward flowing North Atlantic Deep Water (blue-green), and northward penetrating Antarctic Bottom Water (red). Data are taken from Garcia et al. [2013b].



(b) Nd isotope composition on a meridional transect through the western Atlantic. North Atlantic Deep Water is depleted in ^{143}Nd (lower values) relative to most other water masses and can thus easily be distinguished from the upper Antarctic Intermediate Water and the dense Antarctic Bottom Water. Black dots indicate positions of actually measured data, taken from the compilation by van de Flierdt et al. [2016].

Figure 2.2: Atlantic meridional transects of dissolved phosphate and Nd isotopes. Both follow roughly the same pattern, in particular below 1000m water depth, supporting the quasi-conservative behaviour of dissolved Nd isotopes in the ocean (c.f. Tachikawa et al. [2017]).

and weaker than today (McManus et al. [2004]) and consequently AABW flooded the deep Atlantic Ocean to a greater extent (Curry and Oppo [2005], Marson et al. [2015]). This shallower glacial water mass is commonly referred to as Glacial North Atlantic Intermediate Water (GNAIW). However, this weakening is not necessarily the case for the entire duration of the last glacial period, when NADW circulation may have been shallower than today, but was still vigorous (Böhm et al. [2015]). Termination 1 was a period of extreme climatic fluctuations, caused in part by instabilities of the retreating continental ice sheets of the northern hemisphere. After an initial global warming during the Bølling-Allerød interstadial, the Younger Dryas event (YD, start at around 12.5 ka) led to a strong cooling and reversion to near glacial conditions for several hundreds of years (Dansgaard et al. [1989]). The Holocene itself, while providing relatively stable climate conditions, exhibits a thermal maximum (Holocene Thermal Optimum) between around 9000 to 6000 years before present, followed by a slight cooling (Renssen et al. [2012]). All these climatic changes have been shown to be accompanied by variations in the strength and geometry of the Atlantic Ocean circulation (e.g. Sarinthein et al. [1994]; McManus et al. [2004]; Kissel et al. [2013]).

During the last glacial, the northern ice shields on Canada, Greenland, Iceland, and Europe exhibited recurring instabilities, leading to the emanation of large armadas of icebergs into the North Atlantic in relatively short episodes of a few decades to centuries. These so called Heinrich Events are evidenced by the presence of thick layers of ice rafted debris (IRD) that was carried by the icebergs and deposited on the sea floor once they melted (Heinrich [1988]). The melting of these icebergs furthermore led to the input of large amounts of fresh water, diluting the surface waters of the North Atlantic and thus decreasing their density. This is thought to have led to abrupt decreases or even stagnation in the formation rate of NADW, and consequently cooling of the northern hemisphere (Hemming, Sidney [2004]; McManus et al. [2004]), leading to the so called Heinrich Stadials.

2.1.2 Proxies for past ocean circulation

If we want to investigate the past ocean circulation, we must refer to variables preserved in marine archives, so called proxy data. A large suite of such proxies have been developed in order to reconstruct different parameters like water temperature, salinity, local or regional flow strength or water mass age and origin. Here, several proxies relevant for the discussions in this thesis will be briefly introduced.

Stable isotopes in foraminifera calcite skeletons are probably the most extensively employed oceanic proxies. Foraminifera are protozoans which form calcite shells (tests) that are preserved in deep sea sediments. The isotopic signature of the calcite depends on the isotopic signature and chemistry of the water the foraminifer grew in, its nutrition, and local temperature and salinity. Furthermore, different foraminifera species live either near the sea surface (planktic), or at the sediment-water interface (benthic). Thus, the stable isotopes of oxygen and carbon in foraminiferal calcite are commonly used to reconstruct the temperature and salinity, or the water nutrient

content (often used synonymous with water mass age) of surface and deep waters (e.g. Pearson [2012]).

The average grain size of sediment can be influenced by intense bottom water currents. Strong currents tend to flush away small and light sediment grains and deposit them in calmer waters. Thus, the mean grain size of the remaining sediment is shifted to larger diameters. The so called sortable silt (\overline{SS}) is thus a measure of the local bottom current strength (McCave et al. [1995]).

The abundance ratio of the isotopes protactinium (^{231}Pa) and thorium (^{230}Th) is used as a proxy for the regional ocean circulation strength. Both isotopes are produced in the water column due to the radioactive decay of two different primordial uranium isotopes. Since U is homogeneously distributed in the oceans due to its high solubility and according long residence time, both isotopes are produced in a constant ratio. However, the two daughter isotopes are particle reactive to a different degree, leading to short and individual residence times of around 40 a for Th and 250 a for Pa. Thus, in a stagnant water column, both isotopes are sedimented in the ratio they are produced in, but in an environment with active advection, more Th than Pa is sedimented locally, because Pa is exported over longer distances. As the seawater $^{231}\text{Pa}/^{230}\text{Th}$ ratio increases along the advection pathway, so does it in the sediments. The ratio of ^{231}Pa and ^{230}Th therefore correlates inversely with the regional advection strength, supposing changes of the chemical composition of sedimenting particles do not influence the local residence time of either element (e.g. Henderson [2003]).

The abundance of radiogenic neodymium, ^{143}Nd , was initially developed as a tool for the determination of the age of rocks. However, it has also been employed as a tracer of water mass origin. Nd isotope signatures are imprinted into water masses from the surrounding continents in regions in which deep waters are formed. Since Nd from bottom water is archived abiologically in sediments, it can be retrieved and used as a proxy for past deep water mass provenance (e.g. Ling et al. [1997]).

It is important to note that all these proxies are (by definition) indirect tracers of ocean state variables or combination of parameters. Much effort is needed to quantify and calibrate proxy properties and values to make sure the interpreted signal was actually controlled by the factors discussed. As Gideon Henderson puts it (Henderson [2002]):

All proxies respond to more than one variable, some of which can be overlooked.

A combination of mechanistically different proxies and a holistic view of changes in the archive (here deep sea sediments) are therefore beneficial for the reliable interpretation of palaeoclimatologic proxies. \overline{SS} and $^{231}\text{Pa}/^{230}\text{Th}$ are examples of 'kinematic' proxies, which are linked to the dynamics of the environment, whereas carbon, oxygen, and neodymium isotopes are examples of 'static' proxies, linked to the state of their surroundings. Consequently, the latter do not necessarily react as sensitively to short term changes in circulation vigour. However, their reconstruction over spatially and temporally significant ranges allows for the indirect assessment

of the dynamics inside the ocean under transient change. Yet, such reconstructions require the analysis of larger numbers of samples. Efficient analytical techniques yielding larger data sets are therefore important not only for the quantity of different reconstructions, but also for their quality.

2.2 Nd in the environment

Neodymium is the lanthanide with atomic number 60. Seven natural Nd isotopes with masses ranging from 142 to 150 u exist (see Table 2.1). Nd is also part of the rare earth elements (REEs), a group of 17 elements exhibiting very similar chemical properties. With an abundance of 32 μg per g in average shale, Nd (and the other REEs) are not as rare as the name might suggest (Nance and Taylor [1976]). Nd is not essential for biological processes and thus only passively cycled during metabolism. The natural isotopes of Nd are practically stable, and only ^{143}Nd is produced radiogenically by alpha decay of ^{147}Sm on Earth today. The half life of the mother isotope is estimated at 106 Ga and thus variations in the abundance of ^{143}Nd are small (Stosch [1999]). Nd is less compatible for minerals in Earth's mantle than Sm and is therefore enriched during the partial melting of mantle and the subsequent formation of rocks. Based on this enrichment and the radioactive production of ^{143}Nd by Sm, older rocks are depleted in ^{143}Nd compared to rocks of younger age, in which more Sm has decayed before it got depleted during partial melting. The ratio of ^{143}Nd to the other Nd isotopes can thus be used to date rocks. The variations of ^{143}Nd abundance, however, lies in the hundred parts per million (ppm) range, requiring precise measurements with modern mass spectrometers for its accurate determination. Commonly, ^{143}Nd is normalised to ^{144}Nd and the same ratio in the CHUR standard (Chondritic uniform reservoir, Jacobsen and Wasserburg [1980]), and the *radiogenic neodymium isotope composition* (Nd IC) is then given in epsilon notation (sometimes 'Nd' is also written as subscript):

$$\epsilon\text{Nd}_{\text{Sample}} = \left[\frac{(^{143}\text{Nd}/^{144}\text{Nd})_{\text{Sample}}}{(^{143}\text{Nd}/^{144}\text{Nd})_{\text{CHUR}}} - 1 \right] \cdot 10,000 \quad (2.1)$$

As all non-volatile elements, Nd is transferred from rocks to the rest of the environment by weathering. The Nd composition of a material can thus yield information about the age of the rocks the Nd was derived from. If the age of different lithogenic facies is known, the Nd IC can furthermore be used as a geographic tracer.

Table 2.1: Table of the natural abundances of all isotopes from nuclear numbers (N) 140 to 150. Values are given in % of the elemental abundance and come from de Laeter et al. [2003].

N:	140	141	142	143	144	145	146	147	148	149	150
⁵⁸ Ce	88.4		11.1								
⁵⁹ Pr		100									
⁶⁰ Nd			27.2	12.2	23.8	8.3	17.2		5.7		5.6
⁶² Sm					3.1			15.0	11.2	13.8	7.4

2.3 Nd isotopes as a water mass tracer

Nd is transferred to the oceans by river runoff, dust input, and exchange with sediments and continental margins (Lacan and Jeandel [2005b]; Rempfer et al. [2011]). In the pelagic ocean, the Nd IC (not the absolute Nd concentration) has a mean residence time of 200 to 1000 years, which is in the order of inter basin water exchange (Tachikawa et al. [2003]; Rempfer et al. [2011]). Variations in the Nd IC of the major water masses are thus tied to their advection and mixing (Piepgras et al. [1979]; Piepgras and Wasserburg [1980]). Conveniently, deep water masses tend to receive their individual Nd IC imprinted in the region of their formation. Thus, their origin can be retraced by measuring the Nd IC (see Fig. 2.2b). Due to old crustal formations on the North American and European continents, NADW is the most ¹⁴³Nd depleted (i.e. *unradiogenic*) of the major water masses in the oceans. The Pacific, in contrast, is surrounded by very young formations and therefore exhibits ¹⁴³Nd enriched (i.e. *radiogenic*) Nd ICs. The southern component waters in the Atlantic, Antarctic Intermediate Water (AAIW) and Antarctic Bottom Water, are significantly influenced by Pacific waters and contain Nd with an intermediate isotopic composition.

Concentrations of Nd in seawater lie mostly in the range between 10 and 50 pmol/kg, with a tendency of higher concentrations in deeper water (Lacan et al. [2012]). The most important sink of dissolved Nd in the oceans is scavenging by particles and subsequent transport to the sediment (see also next paragraph). However, there are still several unanswered questions regarding the Nd budget of the oceans (Lacan and Jeandel [2005b]; Rempfer et al. [2011]). For example, a process named boundary exchange has been invoked to play a major role in some regions where seawater intensely interacts with the continental margin (Lacan and Jeandel [2005b]; Carter et al. [2012]; Wilson et al. [2012]; Rickli et al. [2014]; Jeandel [2016]). In these areas, Nd is removed from the seawater and exchanged with Nd from the marginal sediments, without significantly influencing the dissolved Nd concentration. The exact process is not well understood, in particular because Nd concentrations are far from saturation in seawater. One region where boundary exchange plays an important role is the Labrador Basin in the subpolar North-West Atlantic (Lacan

and Jeandel [2005a]). The deep geostrophic flow is forced through the basin by the local bathymetry and on its passage the water reduces its Nd isotopic composition by several epsilon units. Another process that has recently been found to be important in certain localities is the upward flux of dissolved Nd from the pore waters of sea sediments into the water column (Abbott et al. [2015b]; Du et al. [2016]). However, this process has only been shown to play a role in the modern North East Pacific. In chapter 5, it is investigated whether such a mechanism played a role during or after events of extreme detrital sedimentation in the Northeast Atlantic Ocean. These processes and their uncertainties limit our ability to use Nd isotopes as a quasi-conservative water mass tracer and must be considered when interpreting Nd isotopes as a proxy for past water mass provenance.

Even though there are some processes which can modify the quasi conservative behaviour of ϵNd , its reconstruction for past seawater has proved to be an invaluable water mass tracer in palaeoceanography. One prominent example is shown in Fig. 2.3. Roberts et al. [2010], Gutjahr and Lippold [2011], and Böhm et al. [2015] reconstructed the seawater Nd IC in the abyssal Northwest Atlantic. It was thus shown, for example, that this ocean basin was flushed mostly with Antarctic Bottom Water during the Last Glacial Maximum. While stable carbon isotopes in foraminiferal calcite indicated the same (e.g. Sarnthein et al. [1994]), an additional proxy that is independent of biological processes is a valuable scientific gain. Interestingly, this circulation state does not apply to most of the glacial cycle, but only to its most extreme phase. Furthermore, these studies showed that the local Nd IC was even less radiogenic than the modern unradiogenic end member, NADW, at several time intervals. This is most evident during the early Holocene, but also coincident with several distinct short climatic events during the last glacial. These extremely unradiogenic isotopic signatures are a direct evidence that the deep northern water masses changed their Nd ICs at some times. Thus, for a detailed interpretation of Nd IC records in terms of water mass mixing involving the deep North Atlantic water masses, variations of the Nd IC in this end member need to be better understood and quantified. Since the formation of NADW involves several distinct water masses with different Nd ICs, water mass provenance investigations in the subpolar North Atlantic using Nd isotopes are an important step towards this quantification.

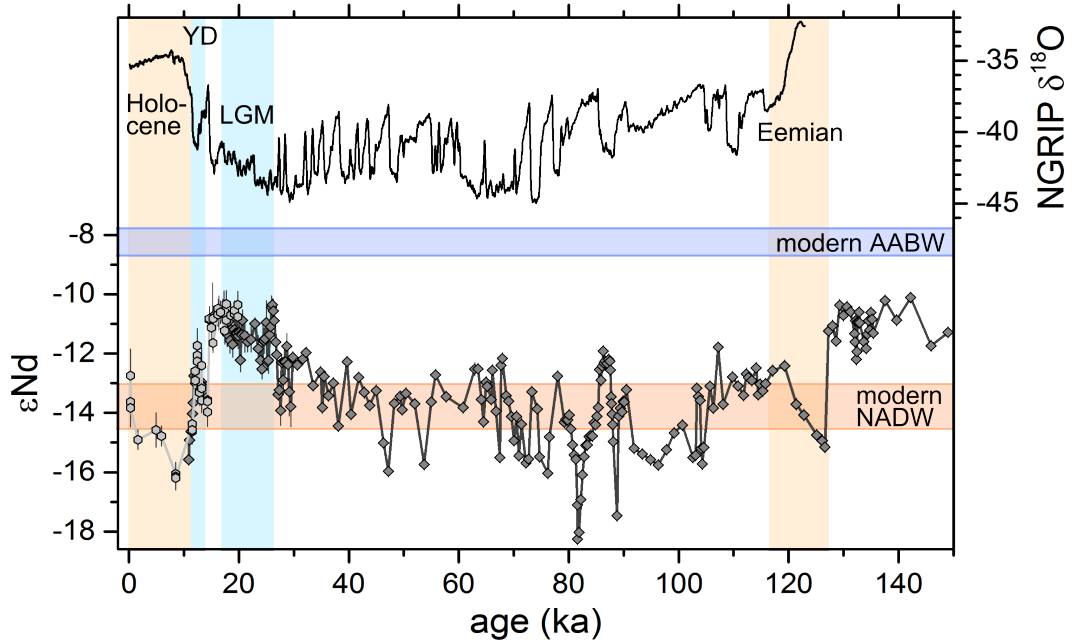


Figure 2.3: Greenland NGRIP ice core $\delta^{18}\text{O}$ (top) and reconstructed seawater Nd isotope compositions in the abyssal Northwest Atlantic (bottom) through the last glacial cycle. Lower $\delta^{18}\text{O}$ data reflect colder atmospheric temperatures. Yellow vertical bars mark warm stages, while blue vertical bars mark two important cold phases mentioned in the text. The horizontal bars indicate the range of the two modern end member water masses NADW and AABW. Clearly, the reconstructed seawater Nd IC data cannot be explained by a simple two end member mixing, unless the unradiogenic NADW end member changed its Nd isotope signature over time. Ice core data are taken from [NGRIP \[2004\]](#) and Nd IC data from [Roberts et al. \[2010\]](#) and [Böhm et al. \[2015\]](#).

2.4 Nd in deep sea sediments

Deep sea sediments in all their forms present valuable archives of oceanic and climatic parameters in the past. They can also be used to reconstruct the local bottom water Nd isotope composition. In order to understand the discussions of this thesis, it is necessary to understand the distribution of seawater-derived and detrital Nd in deep sea sediments.

2.4.1 Archives of seawater-derived Nd

Seawater derived Nd is transferred into ocean sediments mainly near the interface between bottom water and sediment ([Tachikawa et al. \[2003\]](#); [van de Flierdt and Frank \[2010\]](#)). An important mechanism is thought to be based on coprecipitation of the REEs together with Fe and Mn oxyhydroxides, which commonly form under oxic conditions during early diagenesis ([Koschinsky and Halbach \[1995\]](#)). Such

amorphous ferromanganese precipitates can cover all sediment particles and are rich in trace metals. For the reconstruction of past seawater Nd ICs, a wealth of different archives of authigenic Nd have been exploited through the recent years. Such archives include Fe-Mn crusts (e.g. [Abouchami et al. \[1999\]](#); [Frank et al. \[1999\]](#)), fossilised fish remains (e.g. [Staudigel et al. \[1985\]](#); [Martin and Scher \[2004\]](#)), cold water corals (e.g. [van de Flierdt et al. \[2006\]](#); [Colin et al. \[2010\]](#); [Wilson et al. \[2014\]](#)), chemically cleaned or uncleaned foraminifera (e.g. [Vance and Burton \[1999\]](#); [Klevenz et al. \[2008\]](#); [Roberts et al. \[2010\]](#)), and abovementioned dispersed Fe-Mn oxyhydroxides on particles of the bulk sediment (e.g. [Rutberg et al. \[2000\]](#); [Piotrowski et al. \[2004, 2008\]](#); [Crocket et al. \[2011\]](#)).

Reconstructions of past seawater Nd ICs have been achieved with all of these archives, and each of them has its own inherent advantages and disadvantages. In the past years, foraminifera and fish debris have become the most reliable archives for the reconstructions of continuous millennial scale changes of deep water mass provenance (e.g. [Roberts et al. \[2012\]](#)). Both of these sample types can be picked from the bulk sediment under a binocular microscope and can be cleaned physically of contaminating detrital particles. Therefore, methodological artefacts can be reduced or excluded. However, their picking is tedious work and neither archive is abundant in all sediments. Fish debris is generally rare and high resolution records are barely accomplishable based on fish remains alone. Foraminifera tests generally contain very little authigenic Nd and their abundance is subject to strong variations in space and time. A sediment core that is used for the reconstruction based on foraminifera would need to contain enough specimen throughout the time interval of interest, practically excluding many interesting regions from the reconstruction of local deep water sourcing.

Therefore, several studies have turned their focus on the acid-reductive extraction of trace metal enriched ferromanganese phases of the bulk sediment. This method holds the possibility of being applicable in almost every sediment and in the highest achievable resolution, since it does not require any special particle type. Furthermore, the leaching of a sediment sample is much more labour efficient than sieving sediment and picking of individual particles. Thus, higher temporal and spatial resolutions can be achieved, increasing the reliability of the tracer and our understanding of the Nd isotope proxy. However, acid-reductive leaching of bulk sediment is associated with the risk of extracting Nd from detrital (terrigenic or volcanic) particles. Several studies have encountered and highlighted such problems ([Bayon et al. \[2004\]](#); [Roberts et al. \[2010\]](#); [Elmore et al. \[2011\]](#); [Wilson et al. \[2013\]](#); [Molina-Kescher et al. \[2014\]](#)).

The methods most commonly employed for the extraction of seawater derived Nd bound to dispersed ferromanganese oxyhydroxides are rooted in the selective leaching scheme established by [Chester and Hughes \[1967\]](#). In recent years, this method has been adjusted and tested for the specific extraction of authigenic Nd bound in the ferromanganese phase (e.g. [Rutberg et al. \[2000\]](#); [Bayon et al. \[2002\]](#); [Piotrowski et al. \[2004\]](#); [Gutjahr et al. \[2007\]](#)). While these methods differ in details, most are based on the removal of carbonates with weak acids and the subsequent

acid-reductive extraction of ferromanganese oxyhydroxides. However, doubt has remained as to how well contamination from detrital phases can be reduced and constrained. Since detrital particles unavoidably get in contact with the leaching solution, it must be designed to not attack them significantly.

Recently, [Elmore et al. \[2011\]](#) and [Wilson et al. \[2013\]](#) identified radiogenic volcanic particles to present the most common source of contamination in sediment leaches. [Elmore et al. \[2011\]](#) compared foraminifera and leachate Nd ICs in North Atlantic core top sediments. They found that foraminifera signatures were in overall agreement with direct seawater measurements, whereas sediment leaches showed a systematic offset towards radiogenic sources in the vicinity of Iceland. Apparently, the leaching technique released Nd from young volcanic particles. [Wilson et al. \[2013\]](#) systematically investigated the leaching of sediments from the Indian Ocean with different leaching parameters. They also found significant radiogenic contamination in some extracts. Notably, the contamination was less when they did not remove the carbonate from the sediment beforehand. Similar results were also found by [Molina-Kescher et al. \[2014\]](#) in South Pacific sediments.

Picking and dissolving foraminifera is thought to be a method of reliably extracting the archived bottom water Nd isotope composition. [Roberts et al. \[2012\]](#) and [Tachikawa et al. \[2013\]](#) investigated the distribution of Nd in foraminifera calcite shells by laser ablation and microprobe analyses, respectively. The conclusion of both studies was that the Nd extracted from foraminifera is concentrated in microscopic ferromanganese deposits in the shell and between individual calcite layers. These authigenic phases must have been formed after the test was sedimented on the seafloor and therefore reflect bottom water compositions. The Nd in the calcite lattice itself, which is derived from surface waters in the case of planktonic foraminifera, is overprinted by these post-depositional processes. Even reductive cleaning of foraminifera tests is usually not effective enough to remove the early diagenetic authigenic phases ([Kraft et al. \[2013\]](#); [Piotrowski et al. \[2012\]](#); [Roberts et al. \[2012\]](#)). In chapter 4 it is shown that one can exploit this circumstance by leaching the authigenic Nd from bulk sediments including the carbonate fraction, thereby essentially extracting the same Nd as from picked foraminifera samples with less effort and also in absence of sufficient foraminifera tests.

2.4.2 Nd bearing components in common deep sea sediments

Common deep sea sediments are composed of a complex mixture of lithogenic, biological and authigenic (also referred to as hydrogenetic) substances, mainly in particulate form (see Fig. 2.4). Detrital lithogenic matter, for example, is eroded from the continents and deposited in the sediment via particulate transfer. Its Nd IC is therefore independent of the local seawater and a possible contaminant when extracting authigenic Nd for the reconstruction of deep water sourcing. These particles may not only contain Nd in their mineral lattices, but possibly also in authigenic coatings that were pre-formed in other environments like, for example, rivers ([Bayon et al. \[2004\]](#), [Crocket et al. \[2012\]](#)). Organic substances, calcium carbonates, detrital alu-

minosilicates and authigenically precipitated amorphous metal oxyhydroxides cover a wide range of different chemical properties. Their Nd ICs strongly depend on their origin and usually also vary significantly, especially in the North Atlantic. Different sub units of the individual phase may also exhibit variable chemical reactivities, which must be taken into account if the phase is not extracted quantitatively. Sr/Ca ratios in foraminifera, for example, can change with varying degrees of dissolution of the foraminifera sample (Nürnberg *et al.* [1996]; Hathorne *et al.* [2003]). From the phases illustrated in Fig. 2.4, the hydrogenetic oxyhydroxides dispersed on the sediment particles are the target fraction if we want to extract the bottom water Nd IC. As elaborated above, the Nd content of calcite lattice tests, and probably similarly of silica tests, do not contain significant amounts of Nd to pass as phases of possible contamination. On the other hand, organic matter does carry Nd from the surface waters (Freslon *et al.* [2014]), but is not abundant in most pelagic sediments due to its effective recycling by animals and bacteria. Pre-formed authigenic oxyhydroxides are probably of similar chemical composition to the hydrogenetic phases, but do not archive the local seawater Nd. They are therefore a potentially serious source of contaminant Nd, but are most commonly found in marginal sediments with a high particle flux directly from the continents such as estuaries (Bayon *et al.* [2004]; Kurzweil *et al.* [2010]; Crocket *et al.* [2012]; Kraft *et al.* [2013]). Lithogenic material from the small size fraction like wind blown continental clay is an important component of deep sea sediments. While small particles have the potential to harbour a significant amount of authigenic phases on their large surface area, the particles themselves are also significantly exposed to the leaching solution. Luckily, continental clays are not very reactive and weak leaching solutions should not significantly dissolve them. More reactive phases like young volcanic particles and detrital carbonates (DC), however, can present a significant and leachable source of contamination. Additionally, both phases play an important role in the North Atlantic and their Nd isotope signatures represent the radiogenic and unradiogenic end members in subpolar North Atlantic sediments. Therefore, their investigation receives stringent attention in this thesis. In chapter 4, their leaching in sediments is assessed in detail.

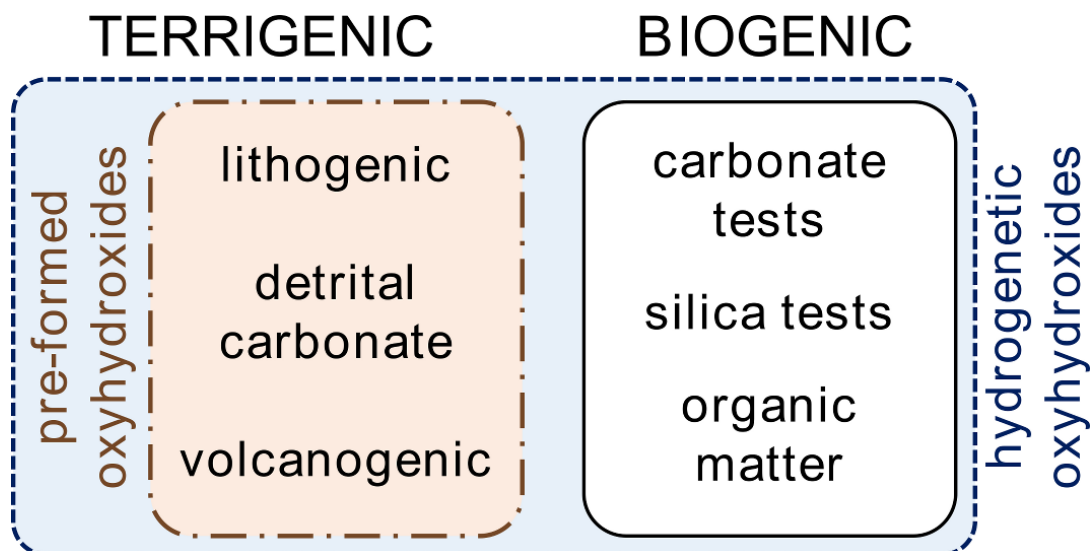


Figure 2.4: Conceptual view of Nd bearing deep sea sediment phases based on their origin. The significance of volcanogenic particles and detrital carbonate is highlighted in chapters 4 and 5. This figure is extracted from [Blaser et al. \[2016\]](#).

2.5 The role of the subpolar North Atlantic

The subpolar North Atlantic plays a special role in today's ocean circulation. As mentioned in section 2.1, the Labrador and Greenland Seas are the only sites with significant deep water production on the northern hemisphere. North Atlantic Deep Water is formed in the subpolar North Atlantic between Iceland, Greenland and Canada, and represents one of the major deep water masses flooding the world oceans. The deep water formation and its southward advection allow for a steady northward flow of warm surface water as well as supply of oxygen into depth. Thus, the latitudinal temperature difference and northern hemisphere ice volume are reduced. Less ice cover in turn reduces surface albedo, increasing the absorption of incoming radiation. Changes in the deep water formation therefore directly interact with the whole climate system. Variations in deep water formation furthermore lead to changes in the carbon storage in the deep ocean and thus affect atmospheric carbon dioxide concentrations. The subpolar North Atlantic is the region where the properties of NADW are set before it is exported into the Atlantic Ocean.

2.5.1 Hydrography of the subpolar North Atlantic

Today, the subpolar North Atlantic exhibits a complex hydrography. Several different water masses can be characterised and distinguished with hydrographic parameters like temperature and salinity. The deepest water masses are strongly confined to the bathymetry by the coriolis force and therefore form deep boundary currents. For a better understanding, evidence for these water masses is shown in depth transects for several sections in the appendix (section A.2). In addition to the basic

properties of different water masses of the subpolar North Atlantic, their Nd isotope characteristics will be briefly summarised (see also Table A.2 in the appendix). The latter are described in detail by [Lacan and Jeandel \[2005a\]](#) and [Lambelet et al. \[2016\]](#). Note, however, that the Nd isotope properties are based on spot samples taken in the last 3 decades and their temporal variability is therefore unknown. The basin names and schematised deep water flow of the subpolar North Atlantic can be found in Fig. 2.5.

SPMW

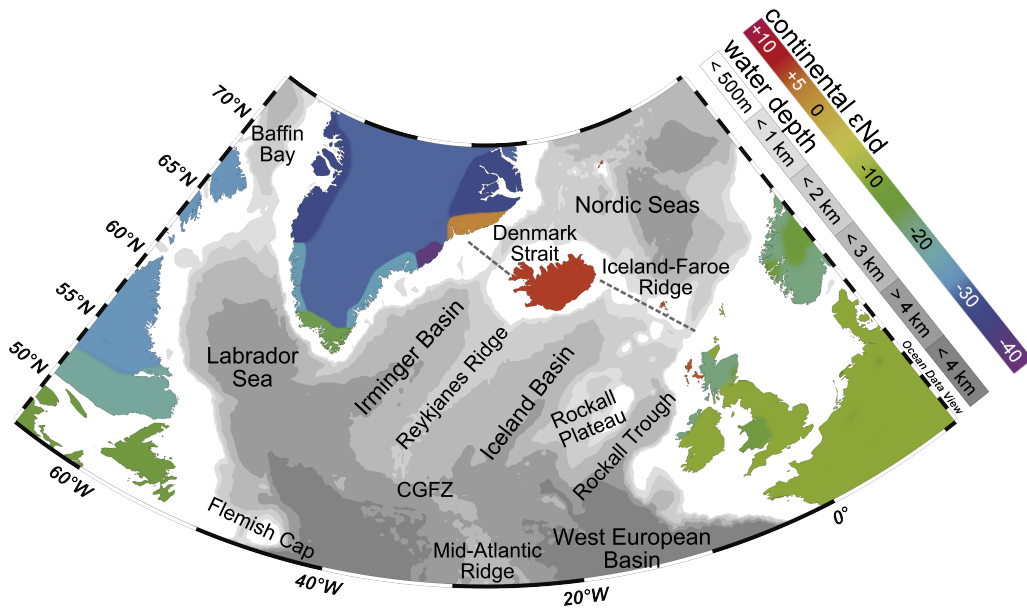
Subpolar Mode Water (SPMW) is a near surface water mass of almost homogeneous density ([Hanawa and D.Talley \[2001\]](#)). It occupies depths roughly between 1000 m and the surface waters. Its south-eastern part feeds the Greenland Sea with warm high salinity water, whereas its north-western part is the source water for the formation of denser Labrador Sea Water. Its Nd isotope signature was determined to -13.9 ± 0.3 epsilon units by [Lacan and Jeandel \[2005a\]](#).

LSW

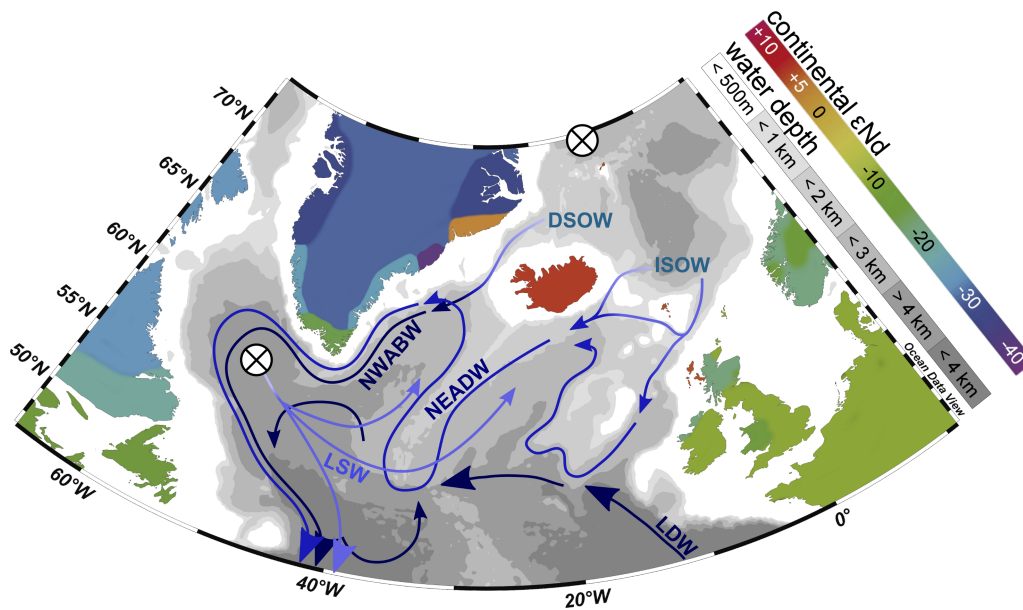
Labrador Sea Water (LSW) is formed by winter deep convection in the open Labrador Sea. It is characterised by high oxygen and relatively low salt content (compared to the other local water masses) underneath the SPMW down to roughly 2000 m. LSW spreads east and south into the Atlantic Ocean as upper NADW, and both the Iceland Sea and Irminger Sea, where it mixes with the underlying water masses. [Lacan and Jeandel \[2005a\]](#) determined its $\epsilon_{\text{Nd}} = -13.5 \pm 0.4$, which is practically identical to the overlying SPMW.

LDW

Lower Deep Water (LDW) is a southern component water mass which originated as Antarctic Bottom Water that is significantly modified by the admixture of northern component water masses, notably NADW and LSW. AABW enters the eastern Atlantic Basin through fracture zones in the equatorial Atlantic. LDW is advected northward into the subpolar North Atlantic along the European margin and recognised by its low oxygen and high silicate content (Fig. A.2). In the eastern subpolar North Atlantic and especially in the Iceland Basin it mixes with Iceland-Scotland Overflow Water and LSW to form North East Atlantic Deep Water (see below). It also passes into the western subpolar North Atlantic via the Charlie-Gibbs Fracture Zone (CGFZ). Along with LDW comes a moderately unradiogenic Nd IC of -12.5 ± 0.4 ([Lacan and Jeandel \[2005a\]](#)). This signature evidences the strong modification of the original AABW, which carries a Nd IC of ≥ -9 ([Rickli et al. \[2014\]](#)).



(a) Bathymetry of the subpolar North Atlantic. Names of prominent features, ridges and basins are given for reference in the text.



(b) Schematised deep water flows in the subpolar North Atlantic. Darker blue arrows indicate deeper waters. Crossed circles mark regions of active deep water formation by deep convection.

Figure 2.5: Map of the subpolar North Atlantic including (a) basin names and bathymetric features and (b) schematised deep water mass flows. Continental colours indicate their approximate Nd isotope compositions as estimated by Jeandel et al. [2007]. The bathymetric maps were created with Ocean Data View (GEBCO (General Bathymetric Chart of the Oceans) [1994]; Schlitzer [2016]).

ISOW

Iceland-Scotland Overflow Water (ISOW) is a dense water mass overflowing the Iceland-Faroe Rise and the Faroe-Shetland Seachannel, fed by intermediate and deep water in the Norwegian Sea. Its mean flux in the Iceland Basin was determined to be around 3 to 4 Sv (Kanzow and Zenk [2014]). During and after the overflow, ISOW mixes intensively with SPMW, LSW, and LDW, thus forming NEADW, which is advected along the Reykjanes Ridge into the western subpolar basins (see below). Lacan and Jeandel [2004b] determined the Nd IC of 'pure' ISOW to be -8.2 ± 0.6 . A minor part of ISOW also overflows the Wyville-Thompson Ridge directly into the Rockall Trough.

NEADW

Northeast Atlantic Deep Water is formed by mixing of LDW, ISOW and LSW in the Iceland Basin. It is then advected along the Reykjanes Ridge as a deep boundary current. Consequently, it passes the Irminger Basin and the Labrador Sea, before contributing to the central North Atlantic Deep Water. In the Irminger Basin, NEADW mixes with the underlying North West Atlantic Bottom Water. In the Labrador Sea, an intense modification of the Nd IC of NEADW takes place. Lacan and Jeandel [2005a] showed that there must be a boundary exchange process that significantly reduces the Nd IC of the water mass without a major shift in the Nd concentration. The Nd isotope signature thus decreases from a value around -11.2 epsilon units to -12.8 ± 0.2 (Lacan and Jeandel [2005b]). In the Labrador Basin, NEADW is marked by relatively high salinity and low chlorofluorocarbon (CFC) and oxygen contents, owed to the significant incorporation of LDW (see Fig. A.4 in the appendix).

DSOW

Denmark Strait Overflow Water (DSOW) is another dense water mass fed by intermediate waters from the Nordic Seas. It overflows the Denmark Strait between Iceland and Greenland, which has a sill depth of around 600 m today. The flux of DSOW is estimated between 2.1 and 3.3 Sv (Jónsson and Valdimarsson [2004] and references therein). DSOW is very dense, cold, and oxygen and CFC rich. It is the major contributor to NWABW. Its Nd IC at the Denmark Strait was determined to be -8.4 ± 1.4 (Lacan and Jeandel [2004a]). The relatively large uncertainty reflects significant variations in the overflow waters, probably due to strong interaction with the underlying sediments and basaltic rock formations in the Denmark Strait.

NWABW

Northwest Atlantic Bottom Water (NWABW) represents the densest water mass flooding the western subpolar North Atlantic. Originating from DSOW, it is formed by significant entrainment of SPMW and LSW during the overflow and strongly

incorporates NEADW along the Greenland margin. It contributes to the deepest part of NADW after looping through the Labrador Basin. Inside the Labrador Basin, it is strongly modified by Nd exchange, similar to NEADW. This leads to a Nd IC shift of 3.4 epsilon units from around -11.5 to -14.9 ± 0.4 , which is the most unradiogenic signature exported to the Atlantic Ocean (Lacan and Jeandel [2005a]).

NADW

North Atlantic Deep Water is the denomination for the northern sourced water that is finally exported into the world oceans. Its main advection path is as a deep western boundary current in the western Atlantic basin. According to the different source water masses, three distinct depth layers of NADW can be distinguished in the North Atlantic (Lacan and Jeandel [2005a]; Lambelet et al. [2016]). Lower, middle and upper NADW are essentially composed of NWABW, NEADW, and LSW, respectively. The Nd IC of upper NADW (i.e. LSW, $\epsilon\text{Nd} = -13.2 \pm 1.0$) is slightly less radiogenic than the lower components ($\epsilon\text{Nd} = -12.4 \pm 0.4$, Lambelet et al. [2016]), which incorporate about 1 Sv of western LDW at about 50°N (Lacan and Jeandel [2005b]).

2.5.2 Sedimentology of the subpolar North Atlantic

Diverse continental compositions, extensive ice rafting, and strong contour currents make the sedimentology of the subpolar North Atlantic rather complex. Furthermore, the abundance of foraminifera varies markedly, and is generally low. All these aspects can lead to complications when authigenic Nd isotopes shall be reconstructed from sedimentary archives, especially by bulk sediment leaches. For this method of extracting authigenic Nd, specific kinds of detritus can be particularly problematic. Firstly, as was shown by Elmore et al. [2011] and Wilson et al. [2013], volcanic particles present a serious source of radiogenic Nd, easily leading to contamination in conventional sediment leaches. Furthermore, as will be shown in chapters 4 and 5, detrital carbonate that is commonly delivered by iceberg rafting from the North American continent can lead to strong unradiogenic contamination in bulk sediment leaches. Furthermore, it is generally conceivable that physical glacial erosion leads to detrital fractions that are more susceptible to chemical weathering and laboratory leaching than detrital particles that already went through chemical erosion in temperate climates. Although such an effect has not been reported specifically, it may present another mechanism of contamination close to large continental ice shields like Greenland, as well as Iceland and North America during glacial times. Additionally, while drift sites provide elevated sedimentation rates and thus the potential for high temporal resolutions, the deposited particles may have travelled extended distances and the extracted authigenic Nd may thus represent a mixture of the bottom water properties along the drift path. The map in Fig. 2.6 illustrates the estimated or reported extents of these factors which may impact the reconstructed seawater Nd IC. From the distribution of these areas, it becomes clear that the extraction

of authigenic Nd for the reconstruction of past deep water provenance in the sub-polar North Atlantic can only be successful if an appropriate method is developed and understood (see chapter 4), and if the preservation of authigenic REEs in the sediment is properly constrained (see chapter 5).

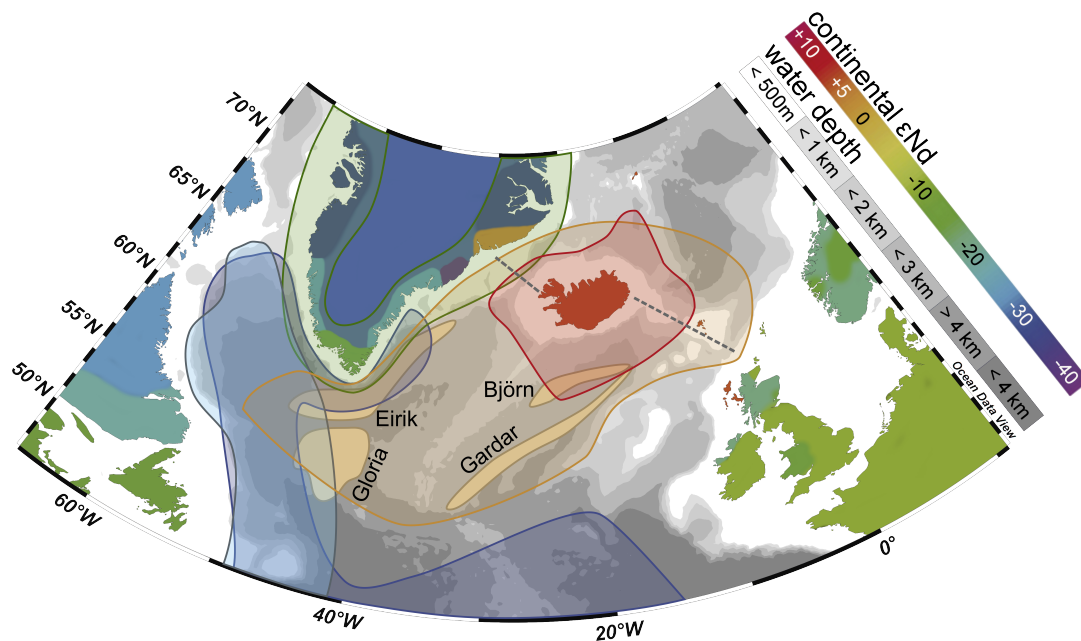


Figure 2.6: Map of the subpolar North Atlantic. The small beige areas mark the extent of some prominent sediment drift zones, which are formed by the local deep boundary currents (Eirik, Gloria, Björn and Gardar Drift). The large coloured zones indicate areas which reflect different detrital inputs, presenting a challenge for the reconstruction of seawater Nd ICs: red: > 10 % Icelandic volcanic glass in core top sediments (Bond et al. [2001]); orange: area, in which conventional core top bulk sediment leaches are contaminated by a volcanic source (Elmore et al. [2011]); light blue: > 5 % detrital carbonate in core top sediments (Bond et al. [2001]); dark blue: core area of detrital carbonate deposition during Heinrich Events 1 and 2 (Hemming, Sidney [2004]); green: area in which glacial erosion on Greenland may lead to significant easily leachable detrital fractions in the sediments.

3 Methods

The extraction of authigenic Nd from bulk sediment with an acid-reductive leaching technique are the fundament of this thesis throughout chapters 4 to 6. The method was developed by [Blaser et al. \[2016\]](#), summarised in chapter 4. This leaching method, the according measurements, and the assessment of their uncertainties are described below. Further methodological aspects specific to chapter 5 are outlined in the corresponding section 5.2.

3.1 Sample treatment

Neodymium was extracted from sediments in three different ways. Most importantly, the dried and pestled bulk sediment was leached for the extraction of authigenic Nd (see Fig. A.18 for a summary of the method). For comparison with another authigenic Nd reservoir, foraminifera samples were manually picked from selected sediment samples and afterwards analysed. Additionally, the leached sediment of selected samples was completely dissolved in order to access the detrital, chemically more resistant component. All three methods are described in the following.

3.1.1 Bulk sediment leaches

Sediment samples of one to two centimetres thickness were freeze dried and manually pestled for homogenisation. Sample splits of 250 to 300 mg were weighed into 15 ml centrifuge tubes for the subsequent leaching procedure. An initial rinse with a duration of 30 min with 10 - 12 ml high purity water (18.2 M Ω Milli-Q water) under constant agitation on a vertical rotating wheel was carried out to diminish contamination by dried fluids and loosely adsorbed fractions. The water was pipetted and discarded after thorough centrifugation at 4,000 rpm. Centrifugation took between 10 and 20 min, depending on the samples. Next, 10 ml of the acid-reductive leaching solution (described below) was added to the samples. The centrifuge tubes were then manually shaken and put on a vortex mixer until the sediment was completely dispersed. If necessary, CO₂ resulting from calcium carbonate dissolution was allowed to degas under sporadic agitation. After sufficient degassing, the sample tubes were put on a vertical tube rotator for constant agitation. Afterwards, the samples were centrifuged again, 8 ml of the leachate were carefully pipetted into Teflon vials, and the remaining leachate was discarded. The complete leaching time from dispersion to centrifugation was about one hour. The sediment residue was again rinsed with water for potential further treatment.

The leachates were dried down on hot plates at 110 to 130 °C in a clean lab environment. The addition of 1 ml concentrated nitric acid, subsequent evaporation, and repetition with 1 ml nitric acid combined with a few drops of 20 % hydrogen peroxide solution assured that organic compounds, mainly from the leachate itself, were sufficiently evaporated or broken down. Afterwards, the Teflon vials were filled with 3 ml 7 M HNO₃ and allowed to rest for a complete dissolution of the sample. From this solution, an aliquot of 500 µl was taken and diluted (usually 250 fold) for measurements of absolute element concentrations and concentration ratios. In some cases an additional aliquot of 1 ml was taken at this step and dried down for archive purposes. The remaining solution was evaporated again. This was followed by a dissolution in 9 M HCl, dried once, and a final dissolution in 1 M HCl for the following ion exchange column chromatography.

For the measurements of Nd isotopes, a purification of the Nd fraction is necessary in order to ensure equal solution matrix compositions between samples and standards and to avoid isobaric interferences. This purification consists of a two step column chromatography. The first column is conducted with 50WX8 resin (200-400 mesh size) for separation of the REEs from matrix elements following standard procedures (Cohen et al. [1988]). The matrix is thereby discarded and the REE aliquot dried down once again. After subsequent dissolution in 0.05 M HNO₃, a second chromatographic column for the isolation of Nd is used. This is carried out with reusable columns containing LN-Spec resin (100-150 µm particle size) from Eichrom (Pin et al. [1994]). The column chromatography protocol applied is efficient, but quantitative separation of Nd from the chemically similar REEs cerium (Ce) and praseodymium (Pr) is not achieved. Especially the presence of the former in higher abundance complicates measurements, because ¹⁴²Ce hydride can cause a non-negligible signal on the detector of mass 143 (see subsection 3.2.2). For the isotope ratio measurements, Nd samples were dried down, dissolved in 1.4 ml of 0.5 M HNO₃, and transferred into 1.5 ml centrifuge tubes. After an initial measurement of the REE concentrations, samples were diluted for the isotope ratio measurements.

The leaching solution

The applied leaching solution is based on the study by Gutjahr et al. [2007] and was refined in Blaser et al. [2016] (see chapter 4). The solution is a moderately acidic solution combined with hydroxylamine hydrochloride (HH) as a reducing chemical in order to decrease the reduction potential for a chemical reduction of the target phase, in this case ferromanganese oxyhydroxides. Furthermore, ethylenediaminetetraacetic acid (EDTA) is added as a chelating agent in order to keep particle reactive ions in solution and thus preventing them from re-adsorbing to sediment particles.

The final leaching solution contains 1.5 % (0.26 M) acetic acid, 0.005 M HH, and 0.003 M Na-EDTA, buffered to a pH of 4. For the buffering, concentrated sodium hydroxide was added during the study described in chapter 4, but changed to a 25 % ammonium solution in the treatment of the following samples described in chapters 5 and 6. The ammonium solution has the advantage of introducing less sodium

to the sample, which is a matrix element potentially decreasing the sensitivity of plasma source mass spectrometers as described in subsection 3.2.1 and shown in Fig. 3.2.

3.1.2 Total digestions

For the analysis of the detrital fraction the leached sediment residue was rinsed with water and afterwards transferred into teflon vials. The digestion was conducted with a mixture of concentrated hydrochloric, nitric, and hydrofluoric acids in a closed microwave system. After complete dissolution of the sediment, the acid was then fumed off in the same microwave system. The dried sample was redissolved in HCl and HNO₃ and slowly converted to nitrate form in order to proceed as was described above with the leaches. The digestion of several standard reference materials (SRMs) showed that in some cases particulate calcium fluoride was formed during the process which did not redissolve completely. Furthermore, silicon is fumed off together with the fluoride from the solution during the drying procedure. Therefore, Ca and Si concentrations in total digestions could not be determined quantitatively and can thus not be used for interpretations. Other elements may have been affected to a minor degree through coprecipitation. Apart from Ca and Si, the element concentrations from the SRMs were in general agreement with published results (see [Blaser et al. \[2016\]](#)).

3.1.3 Foraminifera analyses

The preparation of foraminifera samples followed the protocol proposed by [Tachikawa et al. \[2014\]](#). Mixed species of foraminifera were manually picked from the coarse fraction of the rinsed sediment. Around 10 to 60 µg were collected for the analysis. They were then crushed between two glass plates under a binocular microscope to open all the calcite test chambers. Afterwards, repeated ultrasonication in Milli-Q water and decantation was used to remove small particles like clay. The samples were not cleaned chemically, since diagenetic formations on the calcite are the actual target phases carrying the authigenic bottom water Nd ([Roberts et al. \[2012\]](#)). After clay removal, the samples were inspected again for residual detrital particles under the binocular microscope, which were then removed with a fine paintbrush. Finally, the samples were dissolved by slowly adding 500 µl water and then 1 M acetic acid in 100 µl steps until no further calcite dissolution was observed. Further treatment followed the method of the leachate samples outlined in the second paragraph of subsection 3.1.1.

3.2 Mass spectrometric measurements

The measurements of elemental abundance in the leachates were carried out with a Thermo Fisher iCap Qs inductively coupled plasma quadrupole mass spectrometer

(ICP-QMS). It allows for the fast measurement of many isotopes with intensities ranging over several orders of magnitude. Nd isotope abundance was measured with three different multi collector inductively coupled plasma mass spectrometers (MC ICP-MS). At the GEOMAR Hemholtz Centre in Kiel, Germany, one Nu Instruments MC ICP-MS and one Neptune Plus MC ICP-MS from Thermo Fisher were used. The third MC ICP-MS was a Neptune Plus at the Institute of Environmental Physics in Heidelberg.

3.2.1 Element abundance measurements

Element concentrations were measured with an ICP-QMS at the Institute of Environmental Physics in Heidelberg. The quadrupole mass spectrometer is particularly well suited to measure many different masses in succession, since mass selection with a quadrupole does not lead to hysteresis, as opposed to mass selection based on magnets. Therefore, low to medium precision element abundance measurements with a high throughput are well manageable. Its electron multiplier detector is capable of determining count rates of either up to about 10^6 counts per second (cps) in counting mode, or at higher intensities the detector can switch to an analogue mode. In this mode, the resulting voltage on a resistor is directly measured, which can then be calibrated to the counting mode to expand the detection range by three orders of magnitude. Additionally, helium gas can be introduced into a collision cell in the ion beam path. The gas interacts with the ion beam, preferably deflecting light and/or large ions. With a static quadrupole in the collision cell, the ion beam can be re-stabilised. The quadrupole voltages and the He gas flux can thus be tuned to reduce the transmission efficiency for lighter elements. Since many lighter elements are more abundant than the heavier ones in natural samples, this mechanism can be used to adjust the transmission efficiency for the different elements (see Fig. 3.1 for a typical transmission efficiency spectrum) and thereby adjust the calibration range to the sample composition.

The transmission efficiency and the background signals both vary significantly across the whole mass spectrum with ICP-MS. This leads to elevated lower calibration limits in the ppb range for several lighter elements like Al, Si, P, Mg, and Ca. For the measurements of Ni, Cu, and Zn, the background signal is elevated by 'contamination' from the mass spectrometer itself, most importantly from the sample and skimmer cones in the ion beam inlet system. Changing to Pt based cones may significantly reduce the background for these elements. The general sensitivity was increased by connecting an ESI APEX desolvator before the inlet system of the ICP-QMS. The desolvator heats and subsequently cools the sample solution, thereby precipitating the liquid from the sample aerosol. The reduction of water and acid abundance leads to increase in sensitivity of the measurements by an approximate factor of 5.

Measurements with an ICP-MS rely on equal ionisations and transmission efficiencies for standards and samples. Besides the type of acid and acid concentration used in the sample solutions, the elemental matrix can affect these parameters. This

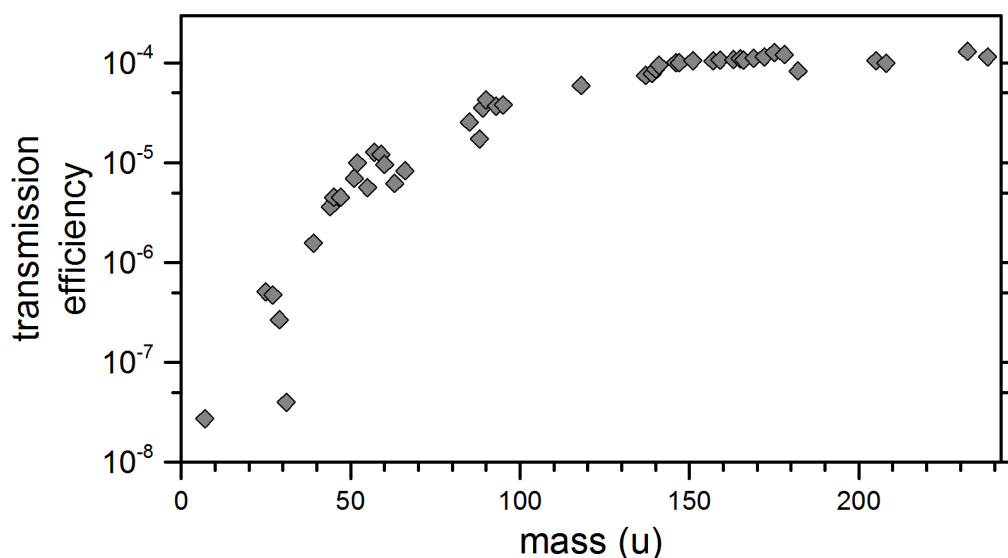


Figure 3.1: Transmission efficiency during a typical element abundance measurement. The transmission for lighter elements is artificially reduced by adding a He gas flow into the collision cell of the ICP-QMS. Thus, the more abundant lighter major elements can be measured from the same solution as the less abundant heavier trace elements. Note the logarithmic y-axis.

so called matrix effect can increase or decrease the transmission efficiency for different elements. For most samples in this thesis, Ca and Na were the most abundant matrix elements. Their effect on the transmission efficiency of other elements was measured with one sample spiked with different matrices, as shown in Fig. 3.2. It is clearly visible, that Ca exerts a more important matrix effect than Na. The effect of a matrix composed of 10 ppm or less of both Ca and Na, however, is negligible. Therefore, concentrations of these two elements was generally kept at a maximum of 10 ppm. The samples described in chapter 4 were kept at maximum 23 ppm Na, due to its high abundance from the NaOH buffer. In this case, the standards were adjusted to the same Na concentration.

Calibration of the instrument was carried out with multi element standards mixed from single element solutions. Instrument drift was corrected with a specific artificial drift standard measured every 6 to 12 samples. Several house mixed standard samples in addition to a certified 'SPSSW2' standard were measured as controls. Oxide formation was kept low through sample gas flux reduction (usually less than 1%) and interference from Ba and Ce oxides on Eu and Gd was assessed with a designated standard and corrected for. The establishment of a high throughput measurement routine was an important step for the realisation of the efficient leaching technique. The element abundances are therefore usually measured from one single 250 fold diluted solution of the respective sample aliquots. Figure 3.3 displays the typical calibration ranges for a set of elements measured with this high throughput routine.

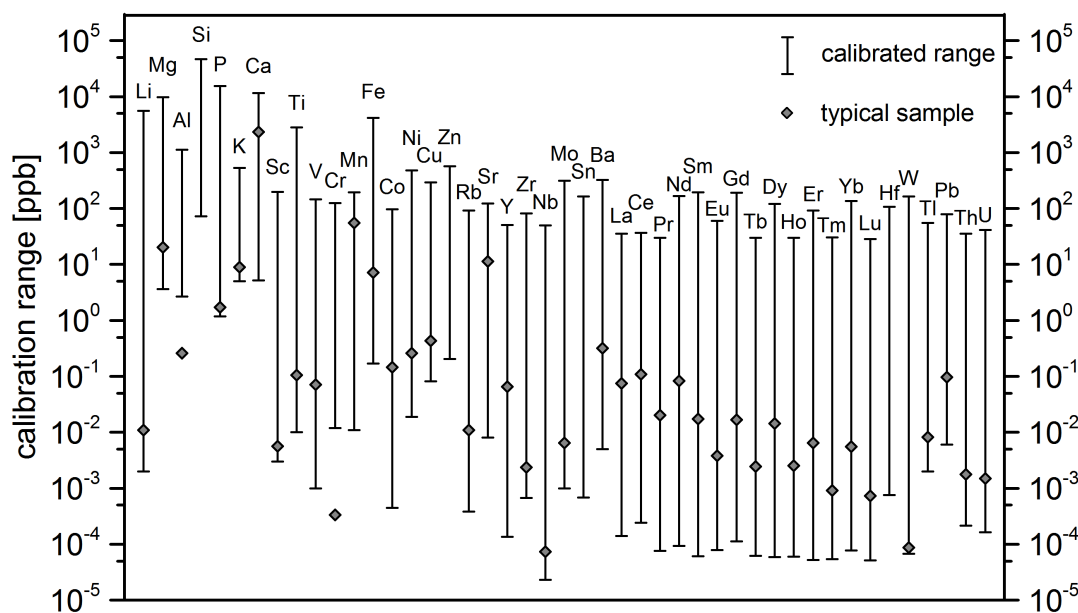


Figure 3.3: Calibration ranges of a typical measurement series (vertical whisker bars) for typically measured elements with the rapid scan technique described in the text. Also shown are the concentrations of a typical leachate sample solution in $250 \times$ dilution. Here, the calibration range was defined with the limit of quantification as the lower end and count rates of $2 \cdot 10^7$ cps as the upper end. This latter count rate lies in the range of the analogue detection mode and is calibrated to the cps scale. The upper detection limit presented is not a strict limit, since intensities of two magnitudes higher can be measured in analogue mode. However, such high intensities were avoided in order to protect the detector from wear and because the uncertainty of the calibration between both modes does then play an important role. Note the logarithmic y-axis.

most important elements needed for the interpretation of the leaches. The other two elements are Al and Ti, whose abundances do not lie as reliably in the calibration range. This is in part due to the fact that Al and Ti are low concentrated in leaches, and in part due to the relatively high background and low transmission efficiency of the ICP-QMS in this mass range. Therefore, for chapter 4 the major element concentrations in most samples were additionally measured with an ICP- optical emission spectrometer (OES) at the Institute of Earth Sciences, Heidelberg, which does not exhibit the same constraints in the low mass range (see [Blaser et al. \[2016\]](#)). Absolute element concentrations are reported in microgram per gram dry bulk sediment, i.e. in mass ppm, except for Ca, which is expressed as equivalent per cent CaCO_3 of the dry bulk sediment mass. Element ratios are reported dimensionless, except for the Sr/Ca mass ratio, which is usually small and thus reported in ‰ (i.e. the values are equivalent to μg Sr per mg Ca).

The relative amount of different rare earth elements in a given sample can yield information about its origin and chemical processes it went through. In order to

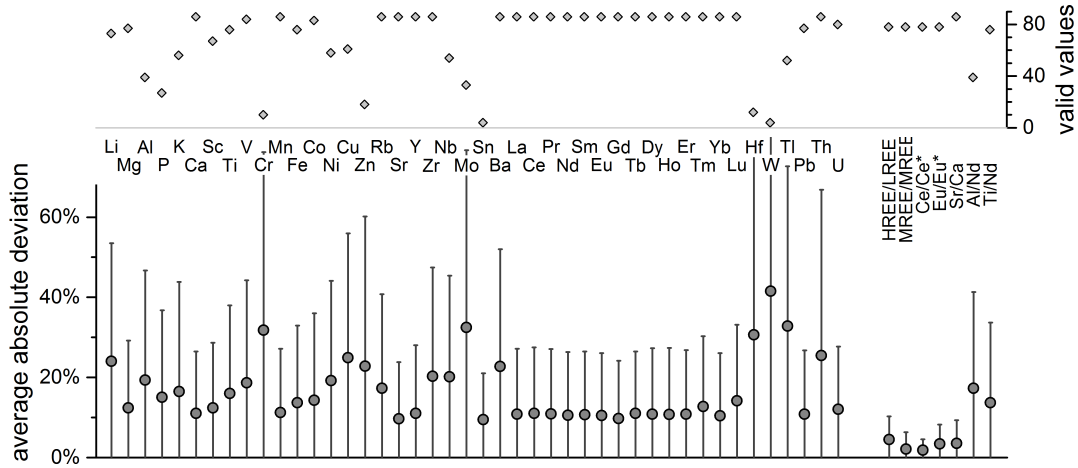


Figure 3.4: Precision of concentration determinations assessed with 41 total procedural replicates. Diamonds in the upper panel indicate the number of calibrated replicate data for the respective element, with a maximum of 86. The circle symbols in the lower panel denote the average of the absolute deviations of replicate measurements from the sample’s mean value (most replicates are duplicates). The error bars represent the 1 sigma standard deviation of the distribution of deviations from the mean values. Both these numbers are normalised to the mean concentration in the respective sample. Note that element concentration ratios (right hand side) are in average much better reproducible than absolute concentration data.

characterise the relative distribution of the REEs, several parameters have been developed. In this thesis the REE ratios as defined by [Martin et al. \[2010\]](#) are used. These parameters are based on the abundance of the different REEs relative to their respective abundance in a standard reference sample, in this case Post Archaean Australian Shale (PAAS) as described by [Nance and Taylor \[1976\]](#). The different parameters calculated to describe the REE patterns are:

$$\text{Cerium anomaly:} \quad Ce/Ce^* = [Ce]_n / \overline{[La]_n, [Pr]_n} \quad (3.1)$$

$$\text{Europium anomaly:} \quad Eu/Eu^* = [Eu]_n / \overline{[Sm]_n, [Gd]_n} \quad (3.2)$$

$$\text{Light REEs:} \quad LREE = \overline{[La]_n, [Pr]_n, [Nd]_n} \quad (3.3)$$

$$\text{Middle REEs:} \quad MREE = \overline{[Gd]_n, [Tb]_n, [Dy]_n} \quad (3.4)$$

$$\text{Heavy REEs:} \quad HREE = \overline{[Tm]_n, [Yb]_n, [Lu]_n} \quad (3.5)$$

$$\text{REE slope:} \quad HREE/LREE \quad (3.6)$$

$$\text{MREE bulge:} \quad MREE/MREE^* = MREE / \overline{LREE, HREE} \quad (3.7)$$

The square brackets denote element concentrations, horizontal bars of comma separated values stand for the arithmetic mean and ‘n’ indicates the normalisation to the PAAS reference concentration. Since the absolute concentrations of the different REEs exhibit a strong covariation, Nd is used as a representative for the general

REE concentrations throughout the manuscript. Examples of full rare earth element patterns are plotted in Fig. 4.6 in the next chapter.

3.2.2 Nd isotope measurements

Nd isotope abundance ratios were measured with three different MC-ICP-MS at the GEOMAR in Kiel and the Institute of Environmental Physics in Heidelberg. Nd, Ce, Pr, Sm, Ca, and Ba concentrations in the isotope samples were measured with the ICP-QMS beforehand in order to monitor matrix elements and adjust the samples to the desired Nd concentrations of 25 - 100 ppb. The sample solutions were introduced to the plasma through either an Elemental Scientific Apex or a Cetac Aridus II desolvator. Both these introduction systems dry the sample aerosol and thus reduce the matrix and increase the ionisation rate of the elements of interest, effectively increasing the transmission efficiency of the mass spectrometer. Beam intensities were measured with Faraday cups in a configuration shown in Table 3.1. The samples were bracketed with the JNdi-1 standard with a $^{143}\text{Nd}/^{144}\text{Nd}$ ratio of 0.512115 ± 0.000007 (Tanaka et al. [2000]). The measured $^{143}\text{Nd}/^{144}\text{Nd}$ ratios were corrected to $^{146}\text{Nd}/^{144}\text{Nd}$ of 0.7219 using an exponential mass bias law and then normalised to the corrected bracketing standards. The final Nd ICs are reported in epsilon notation (see Equation 2.1). The sensitivity of measured $^{143}\text{Nd}/^{144}\text{Nd}$ ratios to Ce abundance due to Ce hydride formation was assessed with a series of standards spiked with different amounts of Ce. In some samples, a correction for this effect was necessary, but the consequent shift in ϵNd was usually less than 1 epsilon unit, and the uncertainty in the applied correction is significantly smaller than the measurement uncertainty. Statistical uncertainties of individual samples are assessed and reported as the reproducibility of secondary standards in the same measurement sequence. For all samples analysed by the work group in the last two years, this external reproducibility lies between 0.10 and 0.56, with an average of 0.21 epsilon units (2 standard deviations, SD). During this time, 52 different samples were completely reproduced at least once as TPRs (see Fig. 3.5). The double SD of their deviations from the mean Nd ICs lies at 0.22 epsilon. This can be considered to be the average total reproducibility of the applied leaching method, including all treatment steps and sample inhomogeneity.

Table 3.1: Faraday cup configuration during Nd isotope measurements at the Neptune Plus MC-ICP-MS in Heidelberg.

Cup	H4	H3	H2	H1	C	L1	L2	L3
Resistor (Ω)	10^{10}	10^{11}	10^{11}	10^{11}	10^{11}	10^{11}	10^{11}	10^{11}
Mass (amu)	140	142	143	144	145	146	147	148

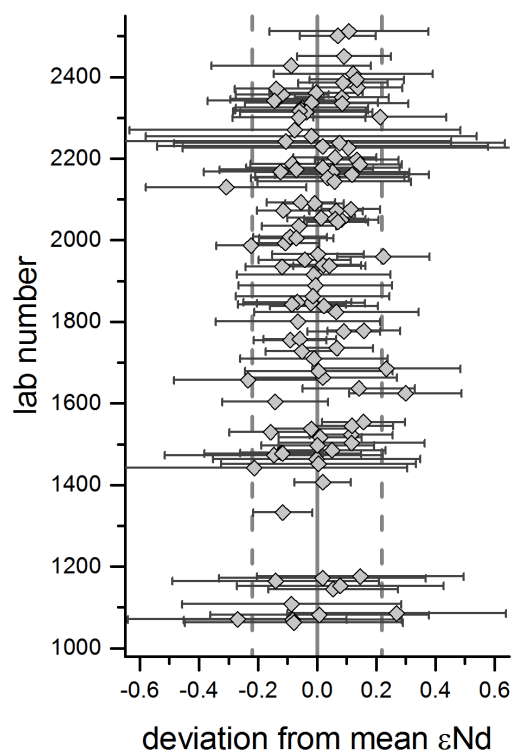


Figure 3.5: Deviations of radiogenic Nd isotope compositions from the respective mean sample values of total procedural replicates from 52 different samples. Error bars are the 2σ measurement uncertainty. From the ϵNd result of each measurement, the average value for the respective sample is subtracted. The 2σ standard deviation lies at 0.22 epsilon units (grey dashed lines).

4 The extraction of authigenic Nd from marine sediments

In this chapter the distribution of Nd together with other elements in the sediment and their extraction by leaching in the laboratory is investigated in detail. This was essential to improve the applicability of the leaching method from [Gütjahr et al. \[2007\]](#) and to better understand the processes that can lead to contaminations in the extracted authigenic Nd isotope composition. In particular in the subpolar North Atlantic conventional sediment leaches produced immense artefacts in Nd ICs, probably due to the leaching of Icelandic volcanogenic material ([Elmore et al. \[2011\]](#)). Foraminifera samples, however, yielded Nd ICs that were in general accordance with local deep water in the same study. A detailed investigation of the leaching process was thus necessary to pin down the source of this leaching artefact. This chapter is published as *'Extracting foraminiferal seawater Nd isotope signatures from bulk deep sea sediment by chemical leaching'* ([Blaser et al. \[2016\]](#)). Therefore the publication and its major findings will only be briefly summarised. The content of this chapter is extracted from the publication and the figures shown are the original ones.

4.1 Methods

In the original article ([Blaser et al. \[2016\]](#)) we investigated the distribution of Nd and other elements in the sediment and the effect of progressive leaching on the extracted components. The strategy was to take a set of samples with diverse compositions and ages, and repeatedly subject them to dilute versions of existing leaching solutions. Thus, the complete conventional leaching process could be investigated as it progressed. Additionally, foraminifera samples and the total digestions (labelled 'TD') were investigated for comparison with the leaches. This methodology proved to be very successful. The combination of Nd isotope and elemental concentration investigations provided considerable information on the processes taking place during the laboratory leaching process. Furthermore, analysis of the pH evolution during the leaching process allowed us to highlight the effect of calcium carbonate acting as an acid buffer that effectively determines the acidity during leaching.

The set of samples consisted of 11 core top samples ('CT') from sediments across the Atlantic Ocean with a focus on the North Atlantic (see Fig. 4.1 and Table 4.1). These young samples were complemented by 5 older ones from the penultimate glacial termination around 130 ka ('TII'). Additionally, one sample dominated by Icelandic ash ('ASH') and one dominated by detrital and/or authigenic carbonates ('IRD') were included to cover extreme cases of problematic sediment composi-

tions. For easier reference, we numbered the eleven sites from North to South. The foraminifera samples from site 7 were taken from another proximate sediment core not exhibiting the ash turbidite layer sample 7 ASH originates from. This allowed us to investigate whether the leaches in this sample agree with the actual contemporary seawater without taking any possible effects from the ash particles into account. Each sample was repeatedly leached with the acid-reductive leaching solution as de-

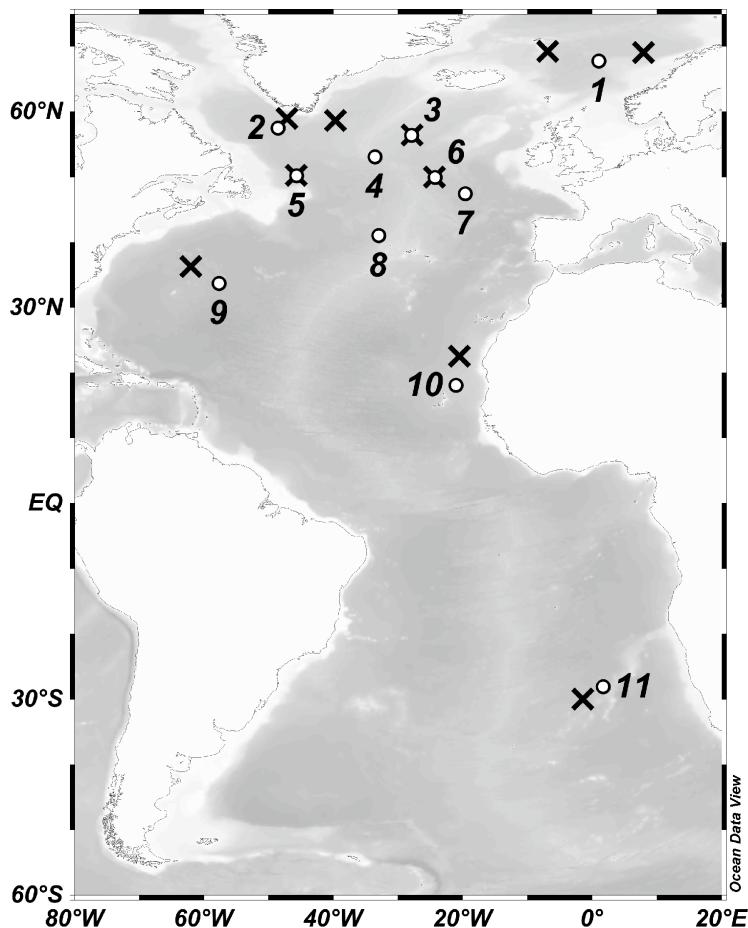


Figure 4.1: Sites of the sediment cores used for progressive leaching tests (circles). Black crosses are stations of seawater Nd isotope measurements used for comparison (Lacan et al. [2012]; Dubois-Dauphin et al. [2017]; Lambelet et al. [2016]).

scribed in chapter 3. After each leach the remaining sample was washed once with high purity water. This procedure was repeated 10 times. Following the literature, we called these the HH-leaches. The residual sediment was then completely digested. Additionally, the same method was carried out on a second aliquot of the same sediment samples, but applying a purely acidic leach. This second leaching solution consisted of 0.1 M solution of both acetic acid and Na-acetate, forming a buffer solution of pH 4.6, and was called 'Ac-leach'. After ten Ac-leaches the samples were washed and finally leached once more with the HH-leach solution ('AcHH-leach', see Fig. 4.2). This HH-leach after thorough decarbonation can be compared with 'conventional' leaches from the literature, in which an HH-leach (stronger than here) is commonly applied to fully decarbonated sediment (e.g. Bayon et al. [2004]; Gutjahr et al. [2007]; Piotrowski et al. [2004]; Elmore et al. [2011]).

In addition to measurements of elemental abundances with the ICP-QMS at the Institute of Environmental Physics as described in subsection 3.2.1, we measured major element concentrations with an Agilent ICP-OES 720 (optical emission spectrometer) at the Institute of Earth Sciences at Heidelberg University. Thus, results could be directly compared and thereby verified and concentrations of several light elements, notably Al, Ca, and Ti, could be determined at lower abundances.

Supplementing the article, an experiment concerning the pH in the leaching solution during the leaching process of about 1 hour was performed. For this experiment, three different fresh samples containing about 83 %, 29 %, and 0 % calcium carbonate were leached with the HH-solution. During the leaching process, the pH of the leaching solution in the sample tube was repeatedly measured using a calibrated digital pH meter (precision approximately 0.03 pH units, 2 SD). Additionally, the unused leaching solution was titrated with 30 % NaOH in order to characterise its intrinsic buffer behaviour. From the pH changes over time in the leached samples, the amount of protons taken up by neutralisation reactions from the solution could be calculated. Under the assumption that the dissolution reaction of calcium carbonate dominated the neutralisation reaction, the amount of CaCO_3 dissolved over time was calculated.

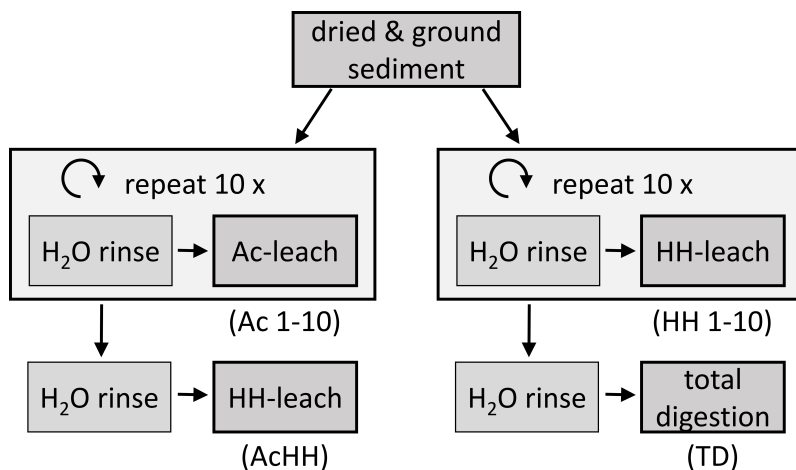


Figure 4.2: Schematic view of the progressive leaching tests. The two different leaches were repeated 10 times with a separate aliquot of the same sediment.

Table 4.1: Sediment samples processed following the progressive leaching protocols.

Site #	Core	Lat. (°N)	Long. (°E)	Water depth (m)	Sample depth (mcd)	CaCO ₃ ^a (%)	Sample label	Age model
1	ODP 643	67.72	1.03	2769	0 3.98	51 5	CT TII	Henrich and Baumann [1994]
2	IODP 1305	57.48	-48.53	3459	0 32.25	32 4	CT TII	Hillaire-Marcel et al. [2011]
3	IODP 1314	56.36	-27.89	2799	0 12.5	48 10	CT TII	Alvarez Zarikian et al. [2009]
4	IODP 1304	53.06	-33.53	3065	0.03	49	CT	
5	IODP 1302	50.17	-45.64	3556	0	38	CT	Hillaire-Marcel et al. [2011]
6	IODP 1308	49.88	-24.24	3873	0.02	70	CT	Hodell et al. [2008]
7	ME-68-91 VL	47.43	-19.58	4470	0 0.33	75 25	CT ^b ASH	Jantschik [1991]
7	ME-68-91 HL	47.43	-19.58	4470	0.51	34	IRD	
8	IODP 1313	41.00	-32.96	3413	0	78	CT	Stein et al. [2009]
9	ODP 1063	33.69	-57.62	4584	0.105	29	CT	Böhm et al. [2015]
10	ODP 659	18.08	-21.03	3071	0 4.20	58 21	CT TII	Kuechler et al. [2013]
11	ODP 1267	-28.10	1.71	4356	0 1.12	83 32	CT TII	Bowles [2006]

Notes: ^a CaCO₃ content estimated by assigning total amount of Ca extracted by 10 Ac-leaches to CaCO₃

^b Sample 7 CT was completely replicated once

4.2 Results

The abundances of several different elements varied over several orders of magnitude in the course of the repeated leaching process (see Fig. 4.4 and Fig. 4.5). The concentrations of Ca, Sr, and Mn are generally highest in the first leaches and decrease rapidly and monotonically by several orders of magnitude, especially in the HH-leaches. Depending on the calcium carbonate abundance in the samples, Ca and associated Sr concentrations can be saturated in the first leaches. The HH-leaches can dissolve up to about 35% calcium carbonate (relative to the sample weight), whereas the Ac-leaches dissolve approximately half as much CaCO_3 . The calcium carbonate thus reacts rapidly with the acidic component of the leaches and consequently exerts a control over the effective pH of the leaching solution for the remaining duration of the leach. This effect is clearly supported by the pH measurements during the HH-leaching procedure for three samples with different calcium carbonate contents (Fig. 4.3).

In contrast to Ca, Sr, and Mn, the concentrations of Al, Fe, show more complex trends. Both Al and Fe concentrations tend to increase or remain relatively constant throughout the repeated leaching procedures. The HH-leaches extract about an order of magnitude or more Al and Fe from the sediment than the Ac-leaches. Both leaches tend to remove less Al in the initial leaches, when there is still CaCO_3 present in the sediment. The exact evolutions of these two concentrations across the progressive leaching process is more diverse than for Ca, Sr, and Mn. The Nd concentration in the HH-leaches also decreases essentially monotonically, but more slowly and not as uniformly as for Ca, Sr, and Mn. In the Ac-leaches the extracted Nd peaks right after the extracted Ca concentration starts to drop in each sample and slowly decreases afterwards. In the initial Ac-leaches, barely any REEs are extracted.

The shale normalised REE patterns (as in equations 3.1 to 3.7) are relatively stable throughout the Ac-leaching process (figures 4.4, 4.5, and 4.6). Most notably, the Ce anomaly starts off negative and evolves towards 1 during progressive leaching. The REE slope (HREE/LREE) and bulge (MREE/MREE*) vary essentially around values of 1 and 2, respectively. The Eu anomaly is positive (> 1) in some samples at the beginning of the Ac-leach series. In the HH-leaches, the Ce anomaly also starts with an (in average smaller) depletion, but becomes positive for many samples in the mid of the leaching series, before trending towards 1 again. The Eu anomaly starts slightly elevated in average and exhibits a significant depletion in HH-leaching steps 5 to 9. The REE slope starts off around a value of 1 and reduces afterwards in most samples. And finally, the REE bulge in the HH-leaching series remains relatively constant around a value of 1.6 in average, but exhibits significant variations from sample to sample.

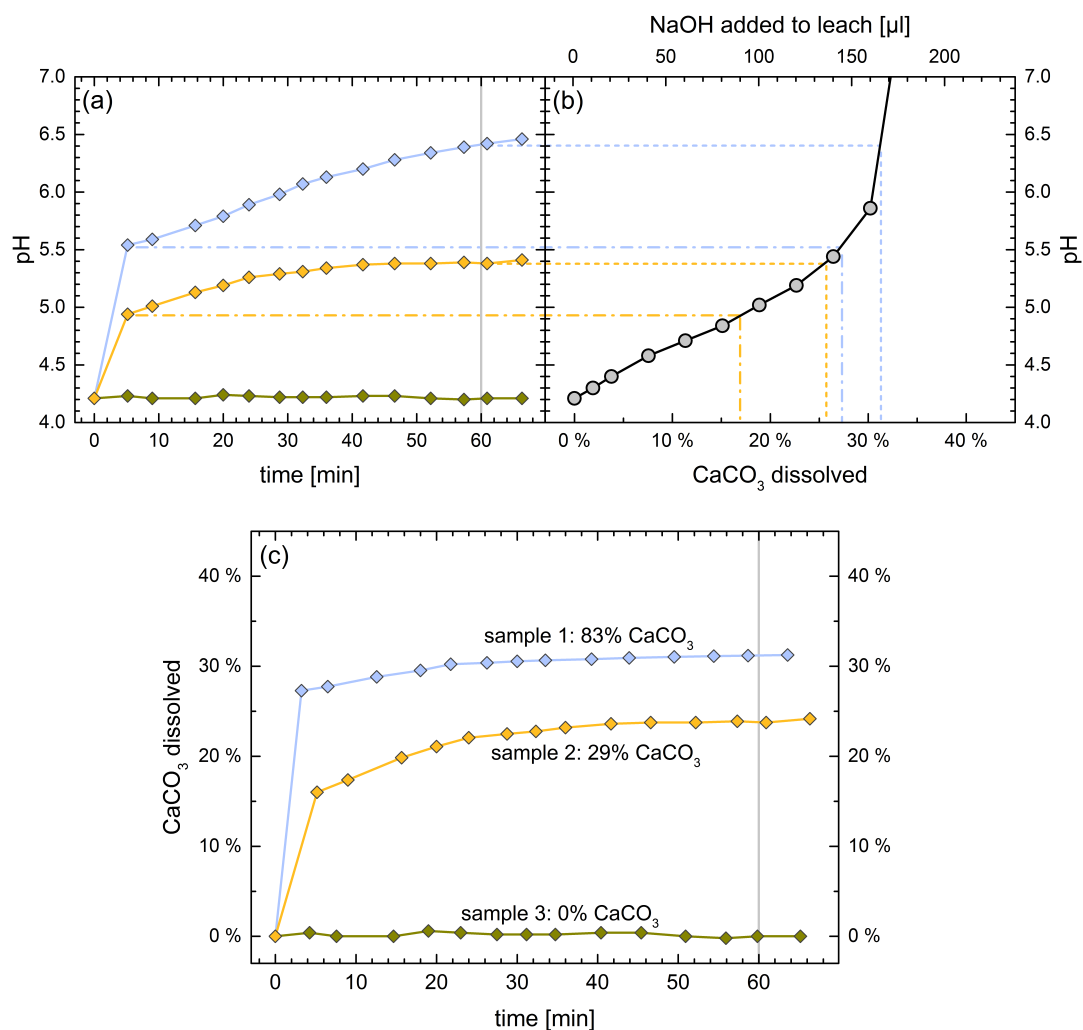


Figure 4.3: Results of the pH measurements during the HH-leaching process for three samples with different calcium carbonate contents (a). Titration of the leach with NaOH (b) allows for the calibration of the pH on the respective amount of CaCO₃ dissolved. Consequently, the dynamics of the dissolution process can be calculated (c). Almost all of the carbonate is dissolved in the first five minutes of the leaching duration. Accordingly, the pH increases by one pH unit or more during that time.

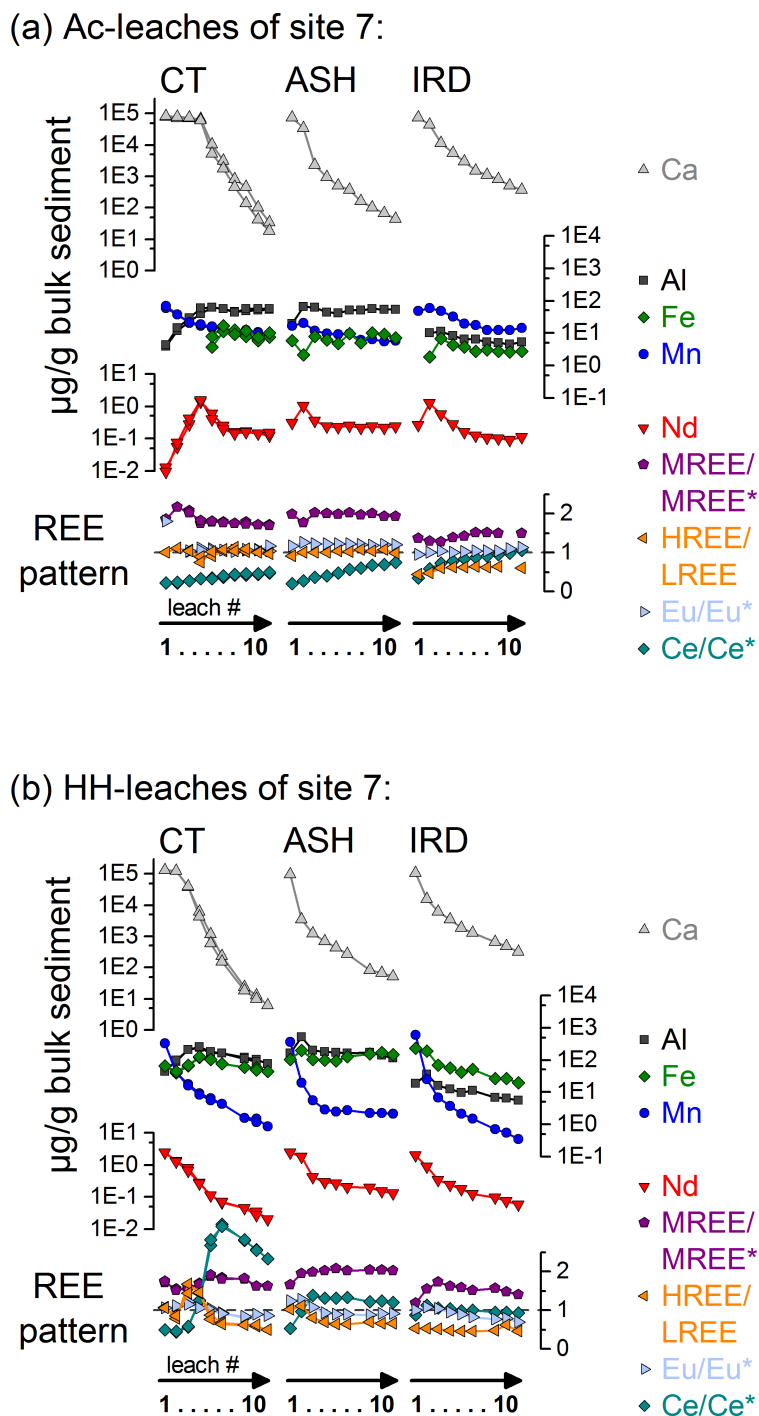


Figure 4.4: Results of element concentrations and concentration ratios for the three samples from site 7; (a) for repeated Ac-leaches, and (b) for repeated HH-leaches. Note that absolute concentration data are displayed on logarithmic y-axes. Sample 7 CT was completely replicated once.

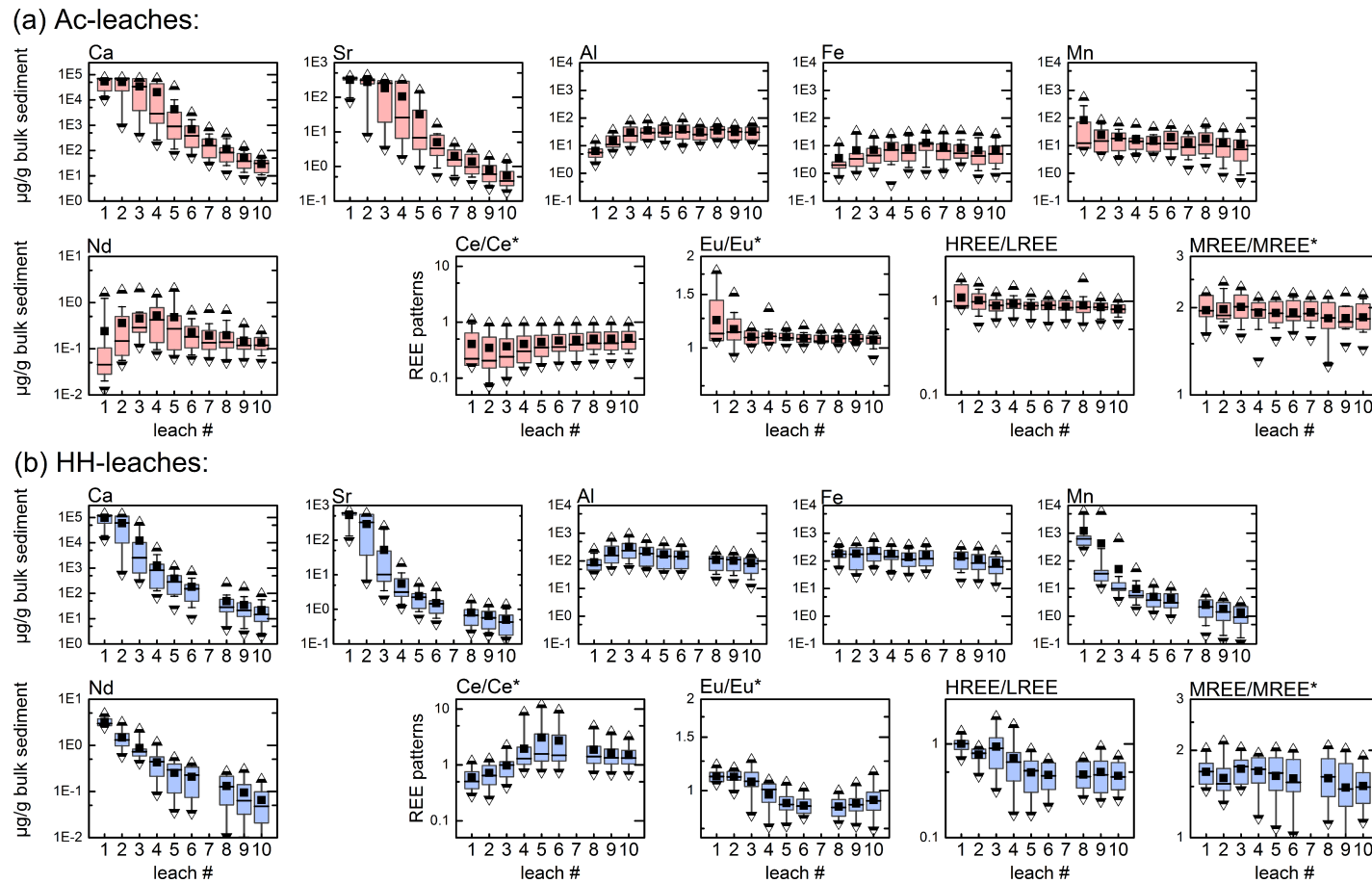


Figure 4.5: Statistical distribution of the elemental concentrations and REE ratios for (a) the repeated Ac-leaches and (b) the repeated HH-leaches. The distributions comprise the results from all samples except the ash and IRD samples from site 7. The black horizontal bars and squares mark the median and mean values, respectively. Half the results lie inside the boxes and 80% in between the whiskers. The triangles span the complete range of data. The solutions of HH-leaches from leaching step 7 were lost during preparation. Note the equal logarithmic y-axes in (a) and (b) for each element.

The Nd ICs of several samples evolve towards extremely radiogenic values during progressive HH-leaches (Fig. 4.7). This is especially the case for samples from the vicinity of Iceland, and counts both for young and old sediments. In sample 2 CT, and tentatively in samples 3 and 4 CT, this trend is stopped and even slightly reversed at leach number 5. However, the first HH-leaches and the first analysed Ac-leaches of all but the extreme samples ASH and IRD agree well with the Nd ICs extracted from picked and physically or chemically cleaned foraminifera. In most but not all cases these signatures also agree with the actual local deep water Nd IC. The samples for which this agreement is not given are mostly from the subpolar North Atlantic. As explained in subsection 2.5.1, this region exhibits a highly dynamic hydrography, which might explain part of these deviations. [Elmore et al. \[2011\]](#) already reported that their conventional leaches are far offset towards more radiogenic Nd ICs for samples near Iceland, agreeing well with our AcHH-leaches. However, the Nd ICs of AcHH-leaches lie close to foraminifera samples in the other sediments. Importantly, the residual detrital Nd ICs lie both above and below the foraminifera samples and do not exhibit any obvious correlation with the results of the leaches.

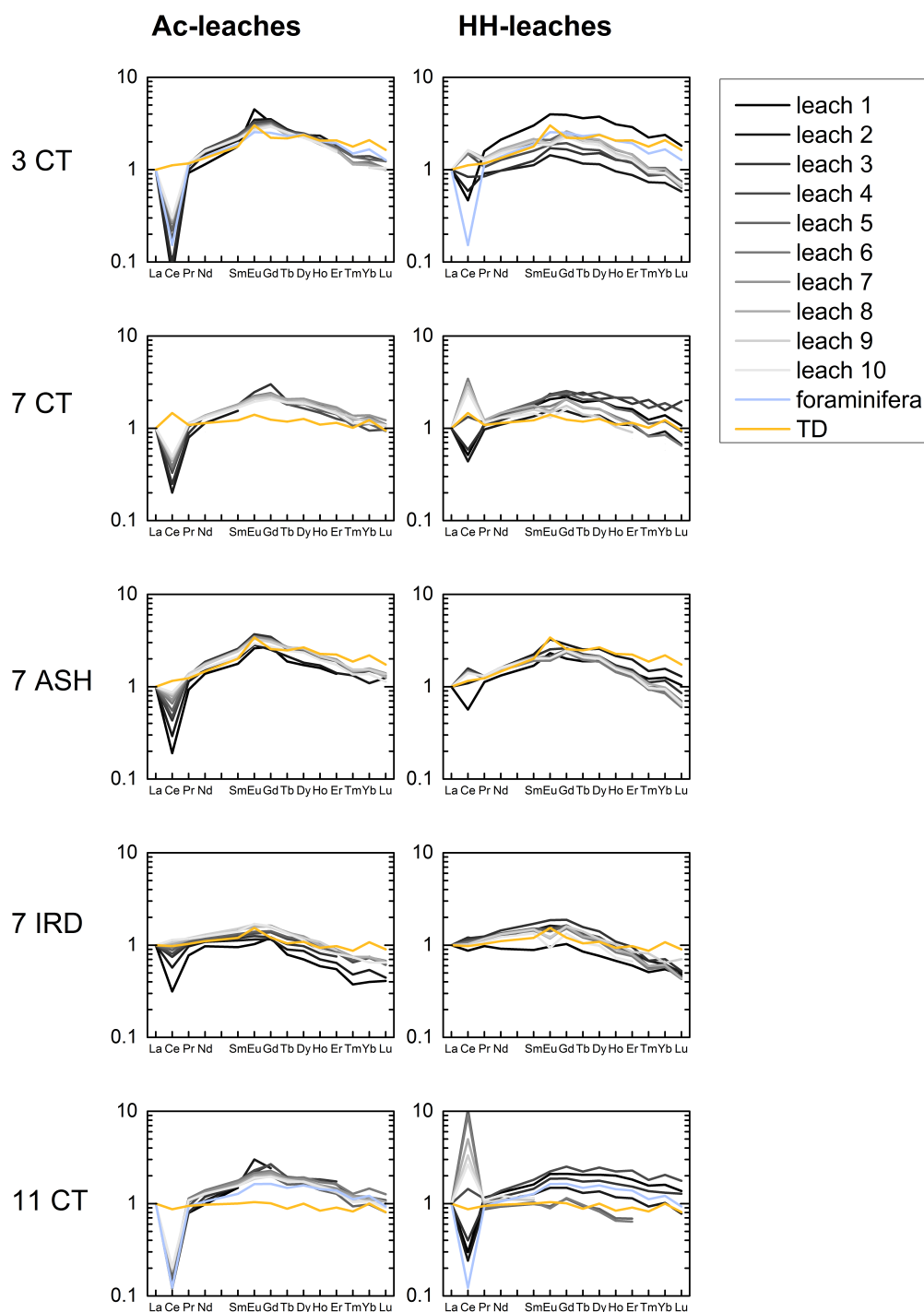


Figure 4.6: Full rare earth element patterns of selected samples during progressive leaching, in comparison with the respective foraminifera and total digestion data. The logarithmic y-axes indicate the REE abundances normalised to PAAS as well as to the respective La concentration. The positive mid REE bulges and heavy REE enrichment are obvious in most samples. The total digested residuals often exhibit patterns that are close to shale, i.e. straight lines at unity.

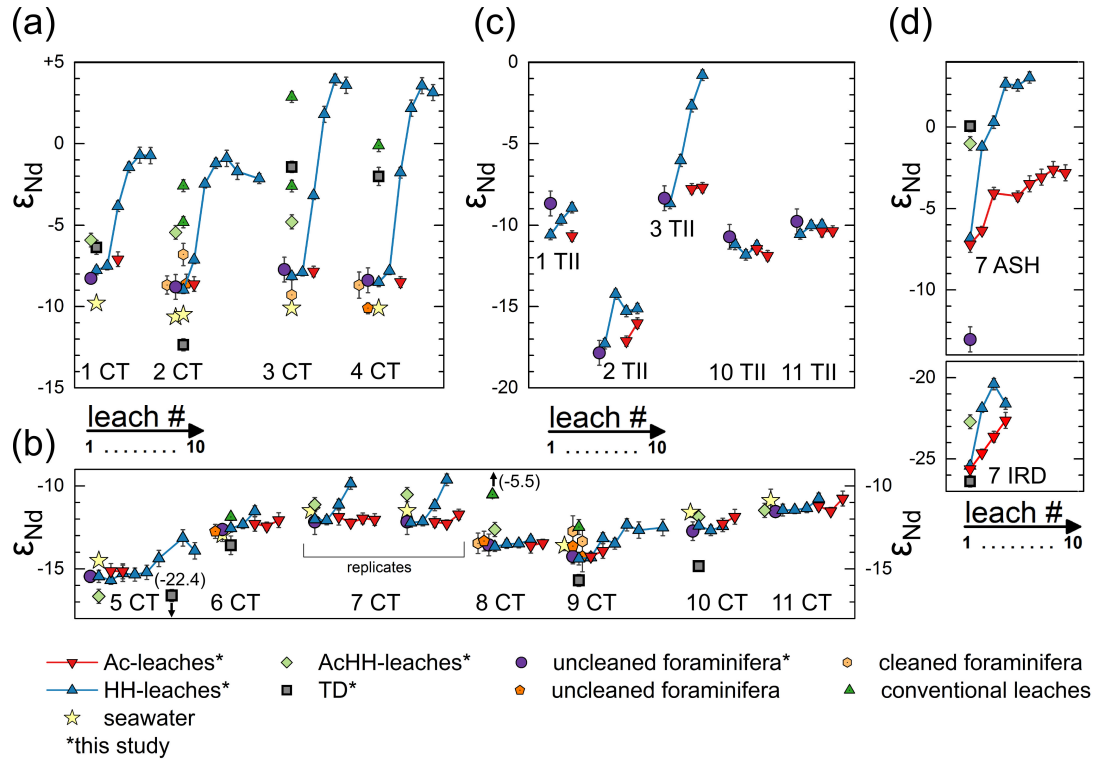


Figure 4.7: Evolution of the Nd isotope compositions during progressive leaching including literature data for each sample for comparison. Blue linked upward triangles are the HH-leaches from leach number 1 at the left for each sample, and progressive leaches following to the right. Similarly, red downwards triangles denote the progressive AC-leaches, of which most initial ones did not contain enough Nd to analyse its isotope composition. AcHH-leaches, total digestions, picked foraminifera samples from this study, foraminifera and conventional leaches from proximate sites (Elmore et al. [2011]), and proximate deep water data (as indicated in Fig. 4.1) are also shown with the respective samples. In (a) the core top samples from sites in proximity to Iceland are shown. (b) depicts the remaining core top samples, while the termination II samples are shown in (c) and the ash and IRD samples from site 7 are added in (d). The vertical intervals of one epsilon unit are equal in all panels.

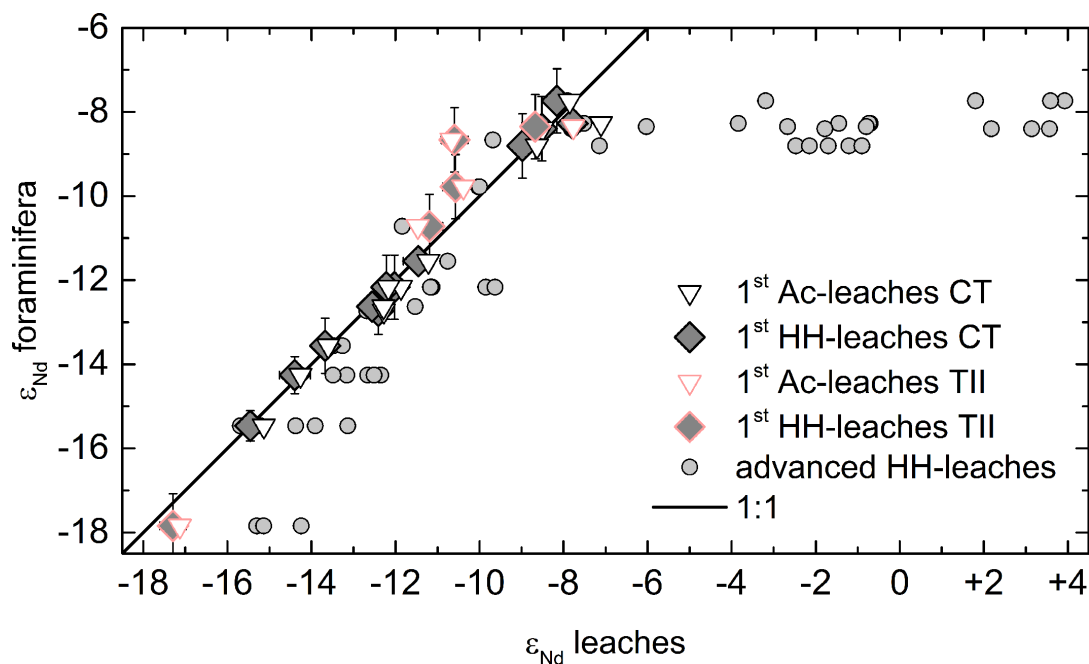


Figure 4.8: Comparison of Nd isotope compositions in the progressive Ac- and HH-leaches (x-axis) to those in foraminifera samples (y-axis). Note that the data cover the whole range of 10 epsilon units in isotope variability observed in the pelagic Atlantic Ocean today.

4.3 Discussion

4.3.1 Carbonate dissolution

The consistently high calcium concentrations in the first leaches across all samples containing sufficient calcium carbonate clearly reflect the quick reaction of carbonate with acids and the resultant acid buffering effect. As shown in the pH experiment (Fig. 4.3), this leads to an almost complete saturation of the HH-leaching solution with respect to calcium carbonate after less than 5 minutes. The pH increases by up to 1.5 pH units in the same time, depending on the absolute carbonate content of the sediment. Thus, the effective pH for at least 90 % of the leaching duration is essentially determined by the carbonate content of the sample instead of the actual pH of the leaching solution at the beginning of the leaching process. Hence, the mobilisation of other phases and elements may covary with the carbonate content of the sample. This observation has important implications for the remaining interpretation.

The Sr concentration is tightly coupled to the calcium carbonate dissolution, owed to the high Sr content of marine biogenic calcite lattices. The Sr/Ca ratio varies between 3.9 ‰ and 14.3 ‰ in the first leaches. The only exception is sample 7 IRD exhibiting a Sr/Ca value of only 1.3 ‰ and 1 ‰ in the first Ac and HH-leach, respectively. This Sr depletion reflects the dissolution of detrital or authigenic

carbonates as already described by Jantschik [1991] and Channell et al. [2012a].

4.3.2 Hydrogenetic Fe-Mn oxyhydroxides

Interestingly, Mn, Fe, and Nd are not extracted from the sediment concurrently in the HH-leaches. Mn is released most rapidly, followed by Nd, while Fe is extracted much later and mostly after CaCO_3 has been removed from the sediment. It is generally thought that an amorphous mixture of Fe and Mn oxyhydroxides precipitates on the sediment particles and incorporates REEs. The separate extraction of these elements thus highlights that the different components of ferromanganese oxyhydroxides are not as tightly coupled as may be expected, and instead react more or less independently from each other with the leachate. Consequently, the Fe/Mn ratio varies widely in the course of the progressive leaching process, increasing over several orders of magnitude in most samples. The fact that Fe is mostly released by HH-leaches after CaCO_3 has been removed (Fig. 4.4 and Fig. 4.5), points out that the dissolution of Fe is sensitive to both the pH and the Eh (reduction potential) of the leaching solution. If the pH played no important role, Fe would already be released in the first HH-leaches, and if the reduction potential were not important, the Ac-leaches would also release similar amounts of Fe after complete decarbonation. The relatively strong mobilisation of Mn in the Ac-leaches on the other hand, shows that the role of reduction for the dissolution of Mn is smaller than for Fe, although still relevant. In general, the same is true for Nd and the other REEs. The Fe/Mn ratios in our first leaches are generally smaller than in other publications applying conventional leaches, like Gutjahr et al. [2007, 2010]. This discrepancy can, however, easily be explained by differential dissolution of the Fe and Mn oxyhydroxides, since the leaching parameters in these studies differed from ours. Specifically, their leaching solution was higher concentrated and the sediment had been completely decarbonated beforehand, allowing for a higher effective pH and thus for a more effective Fe extraction. Our explanation of the sensitivity of Fe, Mn, and REE dissolution to pH and Eh is also supported by a comparison of their respective calculated (idealised) Pourbaix diagrams (Takeno [2005]).

There is one effect that may play a role but could not be disentangled by our study. Reprecipitation of different minerals or ions onto the remaining sediment particles after initial dissolution could diminish the effectiveness of the extraction of different elements during leaching. Theoretically, the EDTA contained in the leaching solution should act as a chelating agent and keep dissolved ions in solution. Yet, the relatively little EDTA may quickly be saturated, especially by the dominant Ca ions when calcium carbonates are dissolved. Thus, other elements initially mobilised would be adsorbed back into the sediment, in particular when the pH increases due to carbonate buffering. We cannot quantify the role of such a readsorption process. However, the results are well in accordance with theory and it will therefore be assumed that this process is not dominant.

4.3.3 Quantification of Nd contributions from different sediment fractions

The differences in ϵNd between foraminifera and 1st HH-leaches are generally small and average to $\Delta\epsilon\text{Nd} = -0.22 \pm 0.60$, 1 SD, $n = 16$ (see Fig. 4.8). Importantly, this is also true for sediments from the subpolar North Atlantic and from the vicinity of Iceland. Radiogenic contamination by volcanogenic material is only evident in these samples during progressive leaching and in the conventional and AcHH-leaches (apart from sample 7 ASH, see below). However, both foraminifera and first HH-leach samples often do not exactly match the local deep water Nd isotope signatures. This can have several reasons: First, the water sample stations used for comparison are not always at the same location as the respective sediment sites (see Fig. 4.1). Hence, they possibly do not exactly represent the bottom water Nd IC recorded by the core top sediments, especially in a highly dynamic region as the subpolar North Atlantic. Furthermore, while we cannot completely rule out a residual detrital contamination in these samples, it seems unlikely that uncleaned and cleaned foraminifera, and HH-leaches are all equally affected by such contamination. Another reason could be a temporal variation of the local deep water signatures in the past decades to centuries, as the sediment samples average over such a time range. Although many available palaeoceanographic Nd isotope records point towards invariable Nd distributions in the oceans during the late Holocene, there may still have been smaller or localised changes in some areas. Finally, since offsets between seawater and authigenic Nd isotopes are largest in the area around Iceland and are towards more radiogenic signatures, it might be that young volcanogenic sediment components supply radiogenic Nd to the pore water which then alters the authigenic ferromanganese fraction. Such a process was proposed by [Abbott et al. \[2015b\]](#), [Rousseau et al. \[2015\]](#) and [Du et al. \[2016\]](#), for example. An interaction between detrital and authigenic fraction via the pore water might thus be a serious challenge for the reconstruction of past deep water Nd isotope signatures, and may be very hard to identify from the sediment.

The only exception for which leachate data and foraminifera do not lie close to each other is sample 7 ASH. An offset towards radiogenic signatures by about 5-6 epsilon units already in the first HH-leach was measured in this sample. It is important to note, however, that the foraminifera were taken from a neighbouring core not containing the ash turbidite. While these foraminifera probably reflect local deep water signatures, foraminifera samples from the ash turbidite might be equally offset as the leachate data. Sample 7 ASH represents an extreme case of volcanogenic sediment components, as it mainly consists of ash derived from Iceland with only minor admixture from local sediment. The large offset from local bottom water Nd IC possibly comes from direct leaching of the ash particles, or from abovementioned in situ interaction between detrital and authigenic fractions via the pore waters. This problem will be further assessed in the following, but it is also an important topic in chapter 5.

The leached Nd ICs during progressive HH-leaching of samples 2, 3, and 4 reach

very radiogenic values and then slightly trend towards more unradiogenic signatures. This trend might indicate the successive leaching of at least three differently reactive sediment components with differing Nd isotope signatures. With a few assumptions, we can model a three end member mixing in these and some other samples and thus illustrate the characteristics of volcanogenic Nd release during leaching.

We define three inherently different end members. The first is the authigenic ferromanganese fraction, carrying the Nd isotope signature from seawater. In the HH-leaches, it is extracted at the beginning of the leaching series. We use the foraminifera Nd ICs as the true signature of this fraction. Secondly, the easily leachable volcanogenic component is mobilised early during the progressive leach sequence and carries a radiogenic Nd IC. We used a Nd IC value of +4.3 for this fraction, as was reported for glacial ash particles from North Atlantic sediments (Roberts and Piotrowski [2015]). The third end member is the 'bulk' leachable detritus. This component is mobilised later during the leaching sequence. We assume its Nd IC to be equal to that of the total digestions from the same samples after complete HH-leaching. Since the detritus can be a diverse mixture of minerals of different origins, this assumption might, however, not be exact. The two equations we work with are the conservation of Nd and of Nd isotopes:

$$c_{tot} = c_{hydr} + c_{volc} + c_{det} \quad (4.1)$$

$$c_{tot}\varepsilon_{tot} = c_{hydr}\varepsilon_{hydr} + c_{volc}\varepsilon_{volc} + c_{det}\varepsilon_{det} \quad (4.2)$$

Here, c denotes the Nd concentration and ε its Nd IC, 'tot' denotes the total mixture, 'hydr' the hydrogenetic fraction, 'volc' the leachable volcanogenic fraction and 'det' the leachable detrital fraction. Since two equations are insufficient for three variable concentrations we applied two more assumptions: Firstly, the detritus is not leached at the beginning of the leaching process. Hence, the initial leaching can be described by a two end member mixing ($c_{det} = 0$). Secondly, the contribution of the hydrogenetic fraction decreases exponentially after the first leaches so that only c_{volc} and c_{det} remain as variables at this stage. The transition from variable to parameterised hydrogenetic contribution is set to the leaching step in which the resulting total leached Nd is consistent with the measured value, i.e. where the necessary Nd from the three end members does not exceed the actually extracted Nd. This point of transition is reached after the second to fourth leach, depending on the sediment. These end member calculations allow us to investigate the leaching behaviour of the volcanogenic material more clearly (see Fig. 4.9).

These calculations show that up to one fourth of the extracted Nd during the complete HH-leaching series originates in leachable volcanogenic particles in the normal sediment samples. The bulk detrital contribution is calculated to 18 % in sample 5 CT, but significantly smaller in the other sediments. Sample 7 ASH starts off with a volcanogenic contribution of 36 %, and more volcanogenic than hydrogenetic Nd was extracted in the course of the leaching series. Overall, an estimated 15 % of the ash turbidite sample's mass consists of leachable volcanogenic matter. Interestingly, the non-hydrogenetic Nd isotope signature of the sediment was altered by about 1

to 2.5 epsilon units due to leaching of the detritus. This is an important finding for sediment provenance studies, in which the ferromanganese fraction is commonly removed with acids in order to investigate the detrital sediment origin based on Nd isotopes.

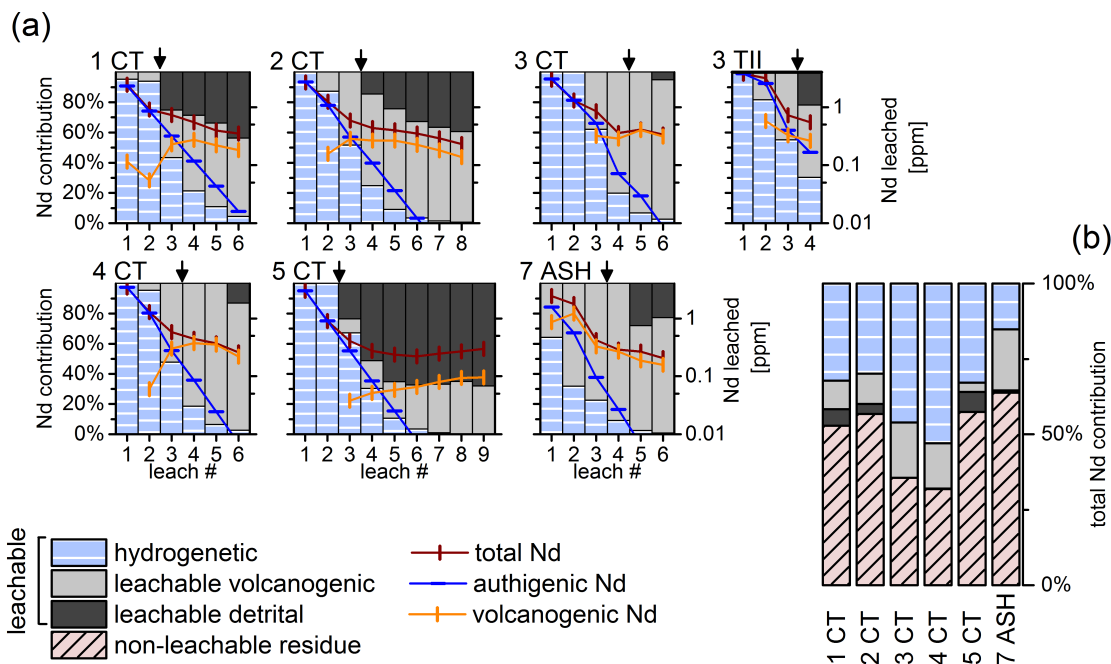


Figure 4.9: Calculated three end member contributions to the Nd isotope signatures during progressive HH-leaching. (a) Relative contributions of the end members to the leached Nd are shown as stacked columns (left y-axes), while the absolute concentrations are plotted above as lines (right y-axes). The successive leaching steps for each sample are ordered from left to right. The black arrows on top of each plot indicate the leaching step before which we switch from variable Nd_{hydr} to an exponential decay. (b) The complete distribution of Nd in the same samples, including the detrital fraction is shown.

The contribution of volcanogenic Nd in the leaches is inversely correlated to the (remaining) amount of carbonate in the sediment (Fig. 4.10). This correlation is even stronger for the ratio of calcium carbonate to volcanogenic material in the sediment. Since carbonates buffer the acid in the leach, this suggests that the volcanogenic component is mainly leached by the acidic component of the leaching solution. This observation is in line with those from Gislason and Oelkers [2003], who found that basaltic glass dissolves more than an order of magnitude faster at pH 4 (as the HH-leach at the beginning) than at pH 6 (as the HH-leach saturated with calcium carbonate). Furthermore, the concentration ratio of Al/Nd correlates well with the amount of non-hydrogenetic Nd extracted. Aluminium is most abundant in aluminosilicates, for example in clay minerals. The ratio can thus be used as an indicator of detrital contamination in the leachate, as suggested by Gutjahr

et al. [2007], for example. Furthermore, the negative europium anomaly associated with the leaching of detrital material further points towards a basaltic origin of the contaminant rare earth elements (e.g. S.P. Sinha [1982]).

The results for sample 7 ASH are somewhat off from the ordinary sediment samples in all of these instances. Specifically, the elemental parameters indicate less volcanogenic contribution than is manifested in the Nd IC. This may be another indication that in this extreme layer, the authigenic fraction did exchange Nd with the detrital fraction. This would lead to more radiogenic signatures in the modified authigenic fraction, and a resulting systematic overestimation of the contribution from the leachable volcanogenic fraction in the leachate.

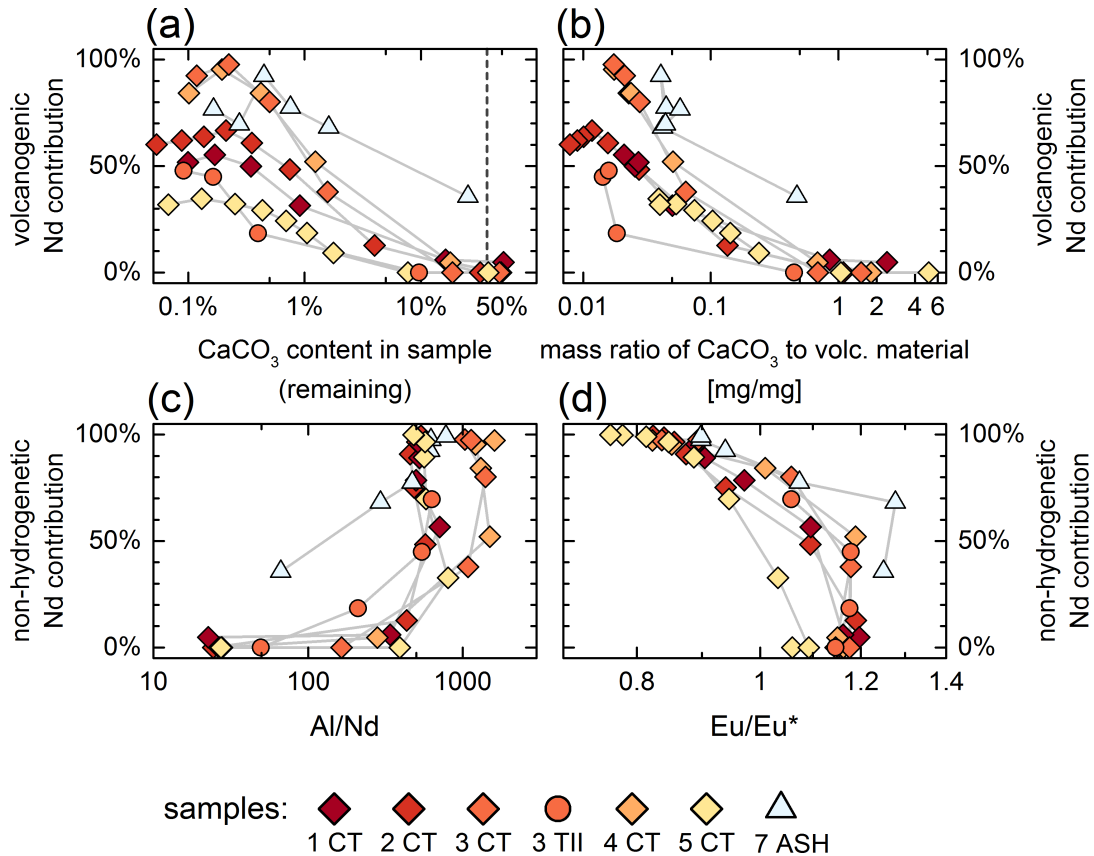


Figure 4.10: End member contributions to the leached Nd signal in relation to different leach parameters. (a) and (b) illustrate the volcanic Nd contribution in relation to the remaining CaCO₃ content of the sediment and in relation to the ratio of CaCO₃ mass to mass of leachable volcanic material in the sample, respectively. The dashed vertical line indicates the approximate maximum amount of carbonate dissolved during one leach. (c) and (d) depict the correlation of non-hydrogenetic contributions to Nd in relation to the leachate Al/Nd ratio and Eu anomaly, respectively. The colours code the different sites as illustrated underneath the plots. Note the logarithmic x-axes.

4.3.4 The influence of non-biogenic carbonates

As determined above, carbonates are the first fraction that gets dissolved and extracted during the leaching process. This is not a problem in the case of biogenic carbonate, which contains only very little Nd in the calcite lattice and plenty of post depositional authigenic bottom water Nd. Detrital or authigenically formed carbonates, however, present a serious source of contaminant Nd for leaching procedures without prior decarbonation. Moreover, detrital carbonate (DC) in the northern North Atlantic is often derived from northeastern Canada where continental Nd ICs are deeply radiogenic and can be as low as -40 epsilon units. Both authigenic carbonate and DC in the North Atlantic have been reported to be depleted in Sr (Channell et al. [2012b]; Jantschik [1991]).

The sediment composition of sample 7 IRD is reportedly dominated by authigenically recrystallised dolomite crystals (Jantschik [1991]). It thus represents an example of sediment contaminated with DC. Both the low Nd ICs in the Ac- and HH-leaches (-25.5 to -20) as well as the total digestion of the detrital fraction (-26) and the low Sr/Ca ratios in the leaches testify that authigenic and/or detrital carbonate was dissolved in this sample. Importantly, these Nd isotope signatures are much lower than any deep water mass in the contemporary Atlantic Ocean (\sim -15). The sample originates from a layer of ice rafted detritus, deposited during Heinrich Event 1. These layers are well known to contain DC from Canada (Heinrich [1988]; Broecker et al. [1992]).

Authigenic carbonates are not commonly formed in deep sea sediments. DC is deposited in the Northwest Atlantic Ocean near the Canadian shelf and in the North Atlantic Ocean during Heinrich Events, but is rather uncommon outside of these boundaries. Roberts and Piotrowski [2015] measured a Nd content in North Atlantic DC grains of 0.8 ppm and the initial HH-leaches of our sediments contained at least 2 μ g Nd per g bulk sediment. If the local seawater Nd IC of a hypothetical site were -10, then approximately 15 % of the sample mass in the form of DC would need to be dissolved in order to induce a contaminant Nd isotope shift of 0.5 epsilon units. Such high detrital (or authigenic) carbonate concentrations are, however, very unlikely outside of Heinrich layers and the Northwest Atlantic Canadian margin. While this contamination may not be prevented, it might be detected securely in the form of low Sr/Ca ratios in the leachate. Nd isotope signatures across DC Heinrich layers will be investigated in more detail in chapter 5.

4.3.5 Elemental ratios as proxies for non-hydrogenetic contamination

Several studies have proposed elemental ratios in the leachate as parameters for the verification of the authigenic origin of the extracted Nd. For example, Al/Nd has been suggested as an indicator of lithogenic contamination (Gutjahr et al. [2007]), and the distribution of rare earth elements for their general origin (Bayon et al. [2002]; Martin et al. [2010]). With the progressive leaching study we can simulate

the application of one HH-leach of varying strength by integrating the leachate content from the first to the n^{th} leach. Thus, $n = 1$ simply denominates the first leach, whereas $n = 10$ equals a very strong leach. We then compare the difference between the integrated Nd IC to that of foraminifera samples from the same site with different integrated elemental ratios in order to see whether they correlate (see Fig. 4.11).

The Al/Nd ratios in the integrated leaches of individual samples vary widely between 14 and 480 and exhibit high correlations to the offset in Nd ICs (average $r = 0.94 \pm 0.1$; 1 SD; $n = 17$). Exceptions are samples 10 CT and 10 TII, in which the Nd IC does not vary significantly during progressive leaching. However, the correlation between Al/Nd and $\Delta\epsilon\text{Nd}$ is smaller for the whole assemblage of leaches across all samples ($r = 0.73$, $n = 79$). While this correlation is still significant, it also shows that the exact correlation also depends on other parameters like the Nd ICs of the leached detritus and the authigenic fraction, the abundance of hydrogenetic Nd, the carbonate content, and probably also the mineralogy of the detritus. Thus, while Al/Nd can be used for the detection of detrital contamination, it should be assessed individually for each sediment core, or even better for each lithologic unit of a sediment core.

Compared to the Al/Nd ratio the four REE parameters in Fig. 4.11 (c) - (f) appear to be more complex and less well suited for the tracing of detrital contamination. While there is some correlation between the Nd IC offset and REE parameters in some cases, none of them appear on a similar scale for most samples simultaneously. Low HREE/LREE values, for example, correlate well with contamination in samples 1 and 2 TII, but the absolute values are very different in the two samples. Thus, while the REE ratios may indeed yield useful information about the origin of leached Nd, no absolute values can be given for any specific sources of contamination. Ideally, a covariation between REE patterns and extracted Nd IC in sediment cores can be observed and assigned to a detrital source. Most importantly, both high and low europium anomalies may indicate volcanogenic contamination, as this parameter is near 1 in most non-volcanogenic materials. An additional experiment furthermore showed that the extracted HREE/LREE ratio and Ce anomaly are sensitive to the carbonate content of a sample, which limits their application for the indication of REE origin (this experiment was conducted after the publication of [Blaser et al. \[2016\]](#), see Fig. A.16).

4.3.6 Implications for an improved acid-reductive leaching method

The results from successive leaching show that the first HH-leach applied to non-decarbonated bulk sediment fulfils all necessary requirements for an efficient, widely applicable, reliable, and verifiable method to extract seawater-derived Nd from deep sea sediment. We could show that the extracted Nd IC is basically equal to that from foraminifera in a wide range of sediment compositions. Importantly, this also

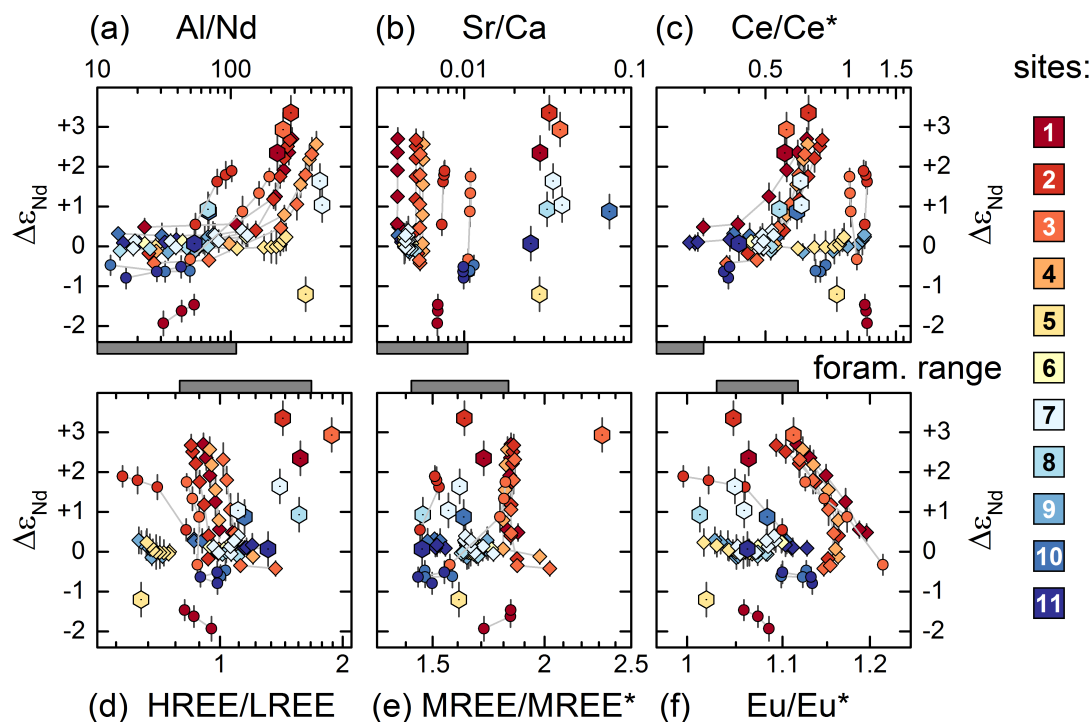


Figure 4.11: Cross plots of the integrated Nd isotope signature offsets between the leaches and foraminifera samples in relation to the integrated leachate element ratios. The data are integrated from the first to the n^{th} leach in order to simulate leaching of increasing strength. The different element ratios are (a) Al/Nd for the detection of the leaching of lithogenic detritus, (b) Sr/Ca for the detection of the leaching of non-biogenic carbonates, and (c) to (f) the REE ratios as general indicators of changing contributions from different sediment components. The colours code the different sites, while symbols code the different sample types: diamonds and circles for core top and termination II HH-leaches, respectively and hexagons for core top AcHH-leaches. The grey bars at the central x-axes mark the element ratio ranges in our foraminifera samples. Note that the x-axes are logarithmic.

counts for the area around Iceland, where conventional leaching did not reach this target. Elemental ratios can help to verify the leachates, with elevated Al/Nd ratios pointing towards lithogenic contribution, low Sr/Ca ratios indicating DC dissolution, and REE patterns possibly tracing contributions from different detrital components, most importantly volcanogenic material. The latter two detrital species, DC and fresh volcanogenic material, probably present the most important sources of contamination for bulk sediment leaches. Their in situ interaction with the ferromanganese fraction is further investigated in chapter 5.

4.4 Summary

The successive leaching method proved very successful for the investigation of the leaching process in the laboratory. Additionally, several conclusions about natural leaching (or chemical weathering) processes can be drawn. For example, the fundamentally different chemical reactivities of different detrital components leads to the fact that the Nd IC of the bulk detritus gives only very limited information about potential sources of contamination. Radiogenic volcanogenic material represents the most susceptible detrital fraction even in sediments in which it is only present in trace amounts and possibly not detected. Nonetheless, the refined weak leaching method is capable of extracting authigenic Nd isotope signatures even from many problematic sediments. Importantly, the agreement of bulk sediment leaches and foraminifera (which are picked from the coarse fraction) in sediments from drift sites indicates that the relocation of fine sediment by bottom currents does not significantly impact the viability of leach-extracted Nd. This method is thus promising for an application in the subpolar North Atlantic.

5 Reactivity and mobility of Nd in Northeast Atlantic sediments

Fresh labile volcanic material from Iceland represents a highly reactive detrital fraction in the subpolar North Atlantic, which can lead to contamination of the leached authigenic Nd IC (Elmore *et al.* [2011]; Wilson *et al.* [2013]; Blaser *et al.* [2016]). However, the in situ weathering of such material could also mobilise detrital Nd, which may exchange with the authigenic fraction or be released into the local bottom waters as a flux of benthic Nd (Abbott *et al.* [2015a]; Du *et al.* [2016]). Similarly, detrital carbonate (DC) from the North American continent may transport unradiogenic Nd into the Labrador Basin, and into the North Atlantic during Heinrich Events. Furthermore, Nd is generally a particle reactive element, and therefore increased particle flux in the water column as it occurred during Heinrich Events, for example, could have led to increased vertical transport, possibly disturbing the quasi conservative behaviour of the dissolved Nd IC. In order to better understand how the bottom water Nd IC and the archived authigenic fraction respond to varying fluxes of detrital material, sediment cores from the Northeast Atlantic containing distinct detrital layers are investigated in this chapter.

5.1 Introduction

Recent investigations at east Pacific continental margin sites dominated by slow deep water mass exchange questioned the robustness of archived seawater Nd ICs in sedimentary authigenic phases. For example, Abbott *et al.* [2015a, 2016] investigated sediments, pore water and seawater from the Oregon margin. Their results suggest that a diagenetic flux of Nd derived from both detrital and authigenic sediment components controlled the local bottom water Nd IC instead of vice versa. More recently, Du *et al.* [2016] showed that the detrital material in sediments of the Gulf of Alaska slowly exchanges Nd with the archived authigenic fraction, thus altering the archived bottom water Nd IC towards a detrital Nd IC over time. However, it was additionally proposed that such an effect may not be relevant in settings with a stronger deep water circulation such as the Atlantic Ocean, because the lateral supply of Nd would dominate the benthic flux.

In this chapter, it is investigated whether such processes have a significant impact on the robustness of the Nd isotope signatures recorded by sediments from the deep Northeast Atlantic. Instead of an analysis of bottom and pore waters and their comparison with surface sediments, the assessment is based on detailed analyses of sedimentary data. Thus, only indirect conclusions on the processes in pore

and bottom waters can be drawn. The advantage of this methodology, however, is the investigation of such exchange processes in the past using data from extreme sedimentologic events in a pelagic environment.

The eastern North Atlantic between 47°N and 53°N (Fig. 1) exhibits a moderate deep circulation strength today, which was probably more sluggish during the last glacial (e.g. Baas et al. [1998]). During Heinrich Events (HEs) 1 and 2 (Heinrich [1988]; Broecker et al. [1992]) the study region experienced an intense supply of ice rafted debris (IRD), forming so called Heinrich Layers (HLs). HE2 and HE1 occurred before and after the Last Glacial Maximum, respectively, and both were associated with IRD supply mainly derived from the Laurentide Ice Sheet. Additionally, an Icelandic turbidite deposited large quantities of basaltic material into the study area during the last deglaciation (Jantschik [1991]). These sedimentation events provide the ideal framework for an investigation of the exchange of Nd and other elements between detrital and authigenic fractions in the sediments, as well as a possible vertical diffusive flux within pore waters of the sediment column or even into the local bottom water.

Here, a high resolution record of authigenic Nd isotopes and element distribution from the deep Northeast Atlantic spanning the last 25 ka is presented, including the three abovementioned distinct detrital sedimentation events. Focus is placed on the analysis of past in situ exchange between the detrital and authigenic fractions in these distinct sediment layers and the mobility of Nd inside the pore waters of the sediment. Furthermore, with a regional comparison supplemented by analysis of three other sediment cores, it is assessed whether the mobilisation of sedimentary Nd may have led to a significant imprint in the Nd IC of the local and regional bottom waters.

5.2 Methods

5.2.1 Sites and sediment samples

Analyses were carried out on sediment samples from four sites in the deep eastern North Atlantic covering the last 25 ka (see Fig. 5.1 for a regional map and subsection 5.2.1 for a list of all cores discussed). The results from core Me68-91 VL (VL stands for trigger core; 47°26.60'N, 19°35.50'W; 4470 m water depth), located at the northern foot of the so-called 'Großer Dreizack' deep sea mountain at 47°30'N, 19°30'W, provide the main record of these investigations (see Table 5.1 for details on the general stratigraphy). The core site was affected by several prominent sedimentological events, as described below. Together with the two shallower sites Me68-89 (47°26.10'N, 19°33.40'W; 4260 m depth) and PO08-23 (47°24.67'N, 19°32.90'W; 3900 m depth; Fig. 5.1, Jantschik [1991]) on the Dreizack mountain the records form a depth transect from 4470 to 3900 m water depth. Additionally, IODP Leg 303 Site U1308 Hole C (a reoccupation of Site DSDP 609), located further northwest (49°53'N, 24°15'W; 3871 m depth) was investigated for comparison. The Dreizack

mountain is situated at the southern end of the Maury Channel system (Fig. 5.1), while Site IODP U1308 is located on an elevation northwest above the southern part of the Maury Channel.

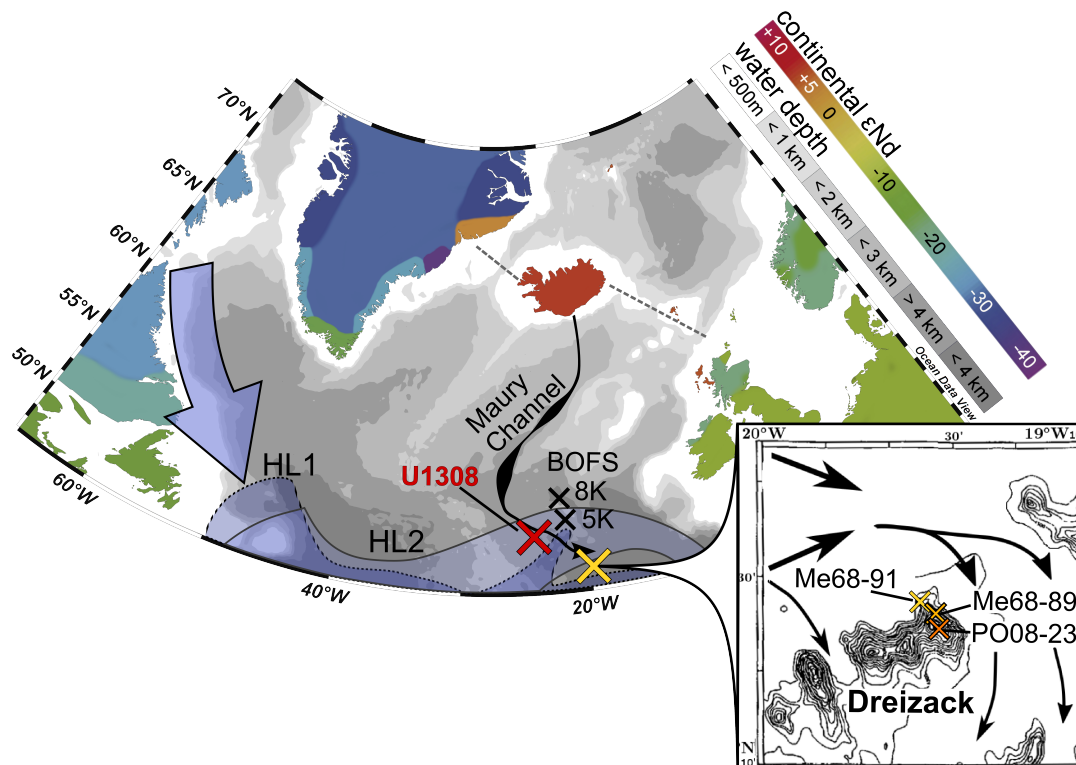


Figure 5.1: Discussed sites in the North Atlantic. Symbols mark the locations of the Dreizack seamount (yellow, see inlay), Site U1308 (red), and BOFS 5K and 8K (black, Roberts and Piotrowski [2015]). The inlay illustrates the area of the Dreizack seamount (Heinrich [1988]; Jantschik [1991]). Black arrows indicate the pathway of the Icelandic ash turbidite. The blue arrow indicates the main drift path of icebergs during HEs 1 and 2, blue areas mark the (northern) extent of the central IRD belts from Heinrich Events 1 and 2 (after Hemming, Sidney [2004]). The bathymetric map was created with Ocean Data View (Schlitzer [2016]).

The study area presented is well known from previous studies of the North Atlantic IRD layers deposited during HEs. Consequently, all cores presented contain HLs of about 10 to 15 cm thickness deposited during HEs 1 and 2. The general sediment composition is dominated by foraminiferal oozes with up to 80 % carbonate in the Holocene sections and higher detrital contributions in the last glacial sediments leading to carbonate contents below 30 %. Organic carbon contents are low and vary between 0.1 and 0.5 % at site Me68-91. Apart from the IRD events, an ash turbidite from the Vedde Ash event (Mangerud et al. [1984]) was transported via the Maury Channel system from southern Iceland to the study location. It can easily be identified as a black layer within core Me68-91 VL. Similar turbidites have been transported repeatedly through the Maury Channel and are reported to mainly

Table 5.1: Stratigraphy of sediment core Me68-91 VL as described by Jantschik [1991].

Sediment layer	Depth (cm)	Composition	Approximate age
1	0 – 50	Foraminiferal ooze	Holocene
2	17.5 – 38.5	Ash turbidite	Vedde Ash
3	50 – 64	Cemented marl	Heinrich 1
4	64 – 91	Diamicton	LGM
5	91 – 105.5	Cemented marl	Heinrich 2
6	From 105.5	Diamicton	last glacial

consist of coarse fresh volcanic material (Ruddiman [1972]; Lonsdale et al. [1981]). Site U1308 is thought to have received finer grained material from at least some of these turbidity currents (Ruddiman et al. [1987]), including the Vedde Ash (Bond et al. [1993]). For the two sites uphill the Dreizack sea mount no significance of an ash-layer has been reported from the expected stratigraphic depth of the aforementioned ash turbidite (Jantschik and Huon [1992]; Huon et al. [1993]).

Average sedimentation rates for sites U1308 and Me68-91 are about 7 and 3 cm/ka during the Holocene, and 4 and 5 cm/ka during the LGM, respectively, and decreasing for the higher located sites at the Dreizack. When core Me68-91 VL was sampled for sediment leaches, it was dried out and the ash turbidite had partly fallen apart and was lost, leading to a gap of 4.5 cm in the sampling resolution (see original core description of Jantschik [1991]). Depths are reported in original depth of the trigger core and data are corrected for the gap accordingly. Apart from this, the core was sampled at a high resolution of 1 to 3 cm intervals for sediment leaches. Site U1308 was sampled at a lower resolution of 2 to 12 cm, and from the other two Dreizack sites only a few samples were leached for comparison. Additionally, Nd isotope data were also recovered from twelve samples of chemically uncleaned foraminifera, mainly next to or within the original ash layer of site Me68-91. Thirteen total digestions of the residual sediment after initial leaching provide additional information about the bulk composition of the detritus. In addition to the presence of the Vedde Ash and the Heinrich Layers, chronostratigraphy was constrained with seven new ^{14}C ages for site Me68-91 and two new ^{14}C ages supplementing the 15 existing age tie points of Site U1308 (Bond et al. [1992]; Obrochta et al. [2012, 2014]).

5.2.2 Sediment handling and measurements

Radiocarbon measurements were carried out on ultrasonically cleaned, dry-sieved size fractions of the planktic foraminiferal species *Globigerina bulloides* or *Globorotalia inflata* with a MICADAS AMS at the LARA laboratory of the University of Bern, Switzerland (Table S.3). Lightness and magnetic susceptibility of cores Me68-

91 VL and Me68-89 were measured at the Department of Geosciences of the University of Tübingen, Germany. A hand-held spectrophotometer (Pausch Messtechnik Haan, Germany) with a measuring diameter of 1 cm was used to analyse the moistened sediment samples packed in plastic bags at 1 cm resolution. Colour values are presented in the L*a*b colour space system and are presented here by the channel of sediment Lightness L*. Bulk magnetic susceptibility was measured with an MFK1-FA bridge (Geofizka Brno, Czech Republic), at 200 A/m and 976 Hz, assuming a constant sample volume of 10 cm³ and sample weight of 10 g (mass magnetic susceptibility, Stoner and Andrews [1999]). Since the volume of each sample was similar, but not exactly equal, the susceptibility data are only used as semi-quantitative estimate of the sedimentary concentrations of magnetic (primarily iron) minerals. For the freeze-dried samples of a few g, magnetic susceptibility is given in units per gram. The data show that IRD and ash are reliably traced, given that the observed susceptibility changes are several orders of magnitude higher than the effects of potential variations in volume.

Sample preparations and the analyses of Nd ICs and elemental abundances were carried out as described in chapter 3. The presented sediment leaches from site Me68-91 were carried out by MSc. Frerk Pöppelmeier in the course of his Master's thesis (Pöppelmeier [2016]) as part of this dissertation project. See Fig. 5.2 for the Nd isotope results of site Me68-91, Fig. A.5 for the same data from Site U1308, and Fig. 5.4 for a summary of the Nd ICs from all sites discussed in this chapter. For the element concentrations and concentration ratios from core Me68-91 VL see Fig. 5.3, and figures A.6, A.7, and A.8 in the appendix for results from the other investigated sites.

5.3 Results

5.3.1 Sediment stratigraphy

Clear sediment age constraints are provided by the known ages of the Heinrich Layers and the Vedde Ash layer, which are confined by peaks of magnetic susceptibility and lightness in core Me68-91 VL. The Vedde Ash was deposited at a ¹⁴C age of 10.3 ka BP (Birks et al. [1996]) and HL1 and HL2 were dated to radiocarbon ages of 14.3 – 17.1 ka (Hodell et al. [2017]) and 21.1 – 21.9 ka (Bond et al. [1992, 1993]) at Site U1308. Their calibration to calendar ages, however, is complicated by the fact that surface reservoir ages underwent significant variations during these times, possibly becoming larger than 1000 years (Thornalley et al. [2011b]; Stern and Lisiecki [2014]; Sarnthein et al. [2015]). At Site U1308, together with the new ¹⁴C datings, the stratigraphy was established based on 17 tie points for the last 30 ka, whereas ¹⁴C measurements from six depths are now available for site Me68-91. New ¹⁴C datings are reported as ages BP, calibrated to the Marine13 curve (Reimer et al. [2013]) with a constant reservoir age of 400 years using the Calib 7.10 online tool (Stuiver et al. [2017]). The shallower sites from the Dreizack are cor-

related to site Me68-91 with the help of the IRD layers and assuming undisturbed core tops (linearly interpolated).

The magnetic susceptibility data of core Me68-91 VL further provide information on the exact distribution of different detrital species (Fig. 5.2). The deposition of the ash turbidite coincides with the largest peak in susceptibility, paralleled by a dip in sediment lightness, approximately between 18 and 39 cm depth (Fig. 5.2 D). Both parameters show a considerable sharp lower edge of the deposited ash material, whereas the upper boundary is blurred by bioturbation, indicating a rapid deposition of the ash turbidite. The main IRD layers are recognised by significant drops in porosity data of Meischner [1987] centred at around 56 and 103 cm depth (CM, Fig. 5.2). The low porosity originates from IRD deposition and sediment diagenesis in these layers, during which authigenic dolomite crystals formed, occupying the sediment pore space (Heinrich [1989]; Jantschik [1991]; Bond et al. [1992]). The susceptibility and lightness data, however, cannot be interpreted as simply around the IRD events (Fig. 5.2). The low porosity HL1 is embraced by small peaks in susceptibility. The deeper HL2 is more homogeneous in its magnetic susceptibility composition, although the lightness suggests that this event could also be separated into an older darker and a younger brighter part. About 10 cm below HL1, another peak in magnetic susceptibility indicates a localised input of detrital material that has not been reported before. This peak is also present in the new susceptibility record from site Me68-89.

Magnetic susceptibility data of Hole U1308C are available at a resolution of 2.5 cm per data point (Channell et al. [2010]) and clearly indicate the two IRD layers centred at depths of 95 and 133 cm. While these layers were originally recorded as smooth peaks in the magnetic susceptibility, a recent study found that HL1 is made up of two distinct layers at Site U1308 (Hodell et al. [2017]). In Hole C, the authors found HL1 in a depth from 88 to 95 cm, with the separation of the two individual detrital layers at around 90 – 91 cm core depth. ^{14}C dates, counts of lithogenic particles and the presence of the Vedde Ash layer are reported from Core DSDP 609 from the same site (Bond et al. [1993]; Bond and Lotti [1995]; Obrochta et al. [2012]). A refined correlation between DSDP 609 and U1308 was published by Hodell et al. [2008].

5.3.2 Radiogenic Nd isotopes

The isotopic composition of the reductively extracted Nd from core Me68-91 VL (Fig. 5.2 A) follows the general trend observed in Atlantic deep-sea sediments (e.g. Piotrowski et al. [2005]; Gutjahr et al. [2008]; Roberts et al. [2010]; Lippold et al. [2016], see Fig. 2.3 for an example from the deep Northwest Atlantic). Radiogenic ϵNd values around -9 in the glacial section between 91 and 80 cm depth and more unradiogenic values of about -12 in the Holocene foraminiferal ooze section are observed. However, in marked contrast to the abovementioned ϵNd profiles from the West Atlantic, this overall trend is interrupted by several distinct events with extreme values far beyond any water mass in the open Atlantic Ocean today. These

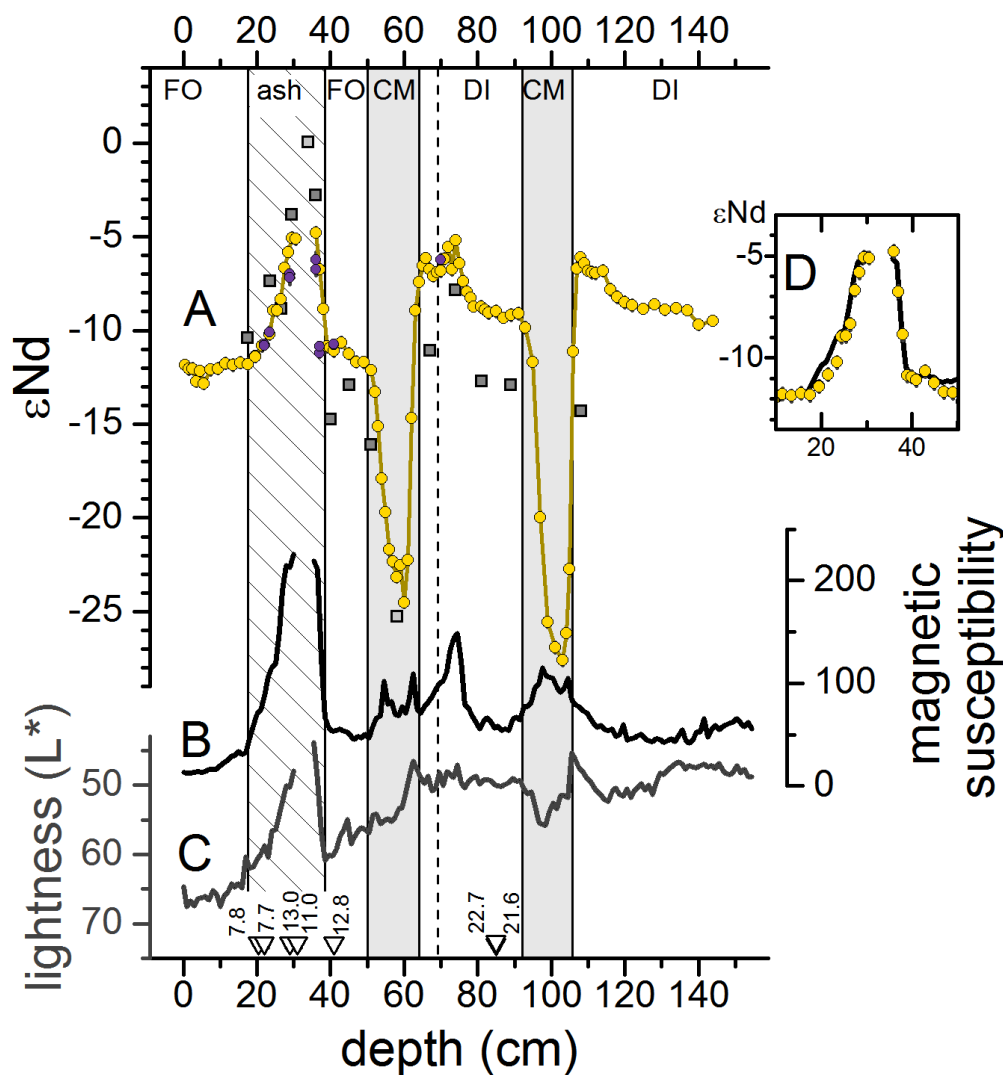


Figure 5.2: Stratigraphy and Nd IC profile of site Me68-91. Shown are the Nd ICs (A) of the leachates (yellow connected circles), foraminifera samples (pink circles), and total digestions (grey squares). Additionally, calculated Nd ICs of total digestions after the first HH-leach from chapter 4 are included as light grey squares. The weight-corrected magnetic susceptibility (B) and lightness (C, inverted) are also shown. The zoom on 10 – 50 cm (D) illustrates the exact match of the leached Nd ICs (yellow symbols in front) and the magnetic susceptibility (black line). Error bars in (A) are smaller than the symbols. Grey vertical bars indicate the detrital carbonate Heinrich Layers. The diagonally lined vertical bar marks the depth of the ash turbidite and the vertical dashed line indicates the position of the small peak in magnetic susceptibility. Small triangles along the bottom x-axis mark the depth of ¹⁴C datings in calibrated ka BP. Abbreviations at the top axis correlate to the original stratigraphic descriptions as in Table 5.1: foraminiferal ooze (FO), ash turbidite (ash), cemented marl (CM), and diamicton (DI). The gap at 37 cm depth in the leachate, magnetic and lightness records is the result of the dried out ash layer.

excursions reach Nd ICs of up to -4.8 in the ash layer, as well as -24.5 and -27.6 during the HLs 1 and 2, respectively. Additionally, immediately below both unradiogenic excursion intervals, smooth radiogenic peaks in the leachates reach values of up to -5.2 and -6.1 , respectively.

Similar to the comparison of magnetic susceptibility, the extracted Nd isotope data from Site U1308 follows the general trend of the Dreizack location, but with less variability (see Fig. 5.4 and Fig. A.5 in the appendix). The record evolves around ϵNd values of -7.5 below 104 cm and around -12.5 in the upper 50 cm. Both Heinrich Layers are marked by well defined unradiogenic excursions to $\epsilon\text{Nd} \approx -22$. These distinct signals correlate with peaks in DC counts at this site (Bond and Lotti [1995]). The smooth radiogenic excursions below the unradiogenic dips seen at site Me68-91, however, are missing at Site U1308. Above the HL1, at about 66 cm depth corresponding to the depth of the recorded Vedde Ash (Bond et al. [1993]; Hodell et al. [2008]), a broad excursion to slightly more radiogenic compositions is recorded, which leads to Nd isotope values of up to -9.8 .

5.3.3 Leachate composition

Detrital carbonates present in North Atlantic Heinrich Layers delivered from the Canadian Shield are commonly associated with a depletion of Sr relative to biogenic carbonates such as foraminifera shells (Jantschik [1991]; Channell et al. [2012a]). In the leachates of the HLs of core Me68-91 VL, a sharp drop in Sr/Ca can be observed (Fig. 5.3 A). In the same leachates, the Nd isotope ratios are deeply unradiogenic, which is also characteristic for DC derived from old Canadian rocks. Comparable results in Sr/Ca as well as ϵNd can be observed in the leachates of the Heinrich Layers of all three other investigated cores (see Fig. 5.3 and figures A.6 – A.8 in the appendix).

The measured concentrations of Fe and Mn in the leachates of core Me68-91 VL behave similarly throughout the analysed 144 cm, albeit with different absolute concentrations (Fig. 5.3 B). Below HL2, Mn concentrations amount to $\approx 100 \mu\text{g/g}$, whereas in the Holocene sediments above HL1 they reach up to $600 \mu\text{g/g}$. In between, three peaks can be identified. Two of these Mn peaks occur at the lower flanks of the low Sr/Ca layers, in which Mn concentrations of up to $3000 \mu\text{g/g}$ are reached. One broader and less pronounced peak is identified in the diamicton between 75 and 90 cm core depth. Similar peaks occur in the Fe content of the leachates. Here, concentrations below the low Sr/Ca layers rise to up to $670 \mu\text{g/g}$, from a background level of less than $300 \mu\text{g/g}$.

Titanium is an element which is most abundantly found in lithogenic particles, although authigenic Ti also exists, similar to Al. The variations in the amount of leached Ti closely follow those of Fe, but show an additional increase from 25 to up to $215 \mu\text{g/g}$ Ti within the central ash layer between 26 and 33 cm core depth. Throughout the low Sr/Ca layers, Ti concentrations are remarkably low with less than $10 \mu\text{g/g}$.

Concentrations of Al are between 200 and $450 \mu\text{g/g}$ in last glacial sediments and

low in the Holocene samples. In addition, they show a peak within the ash layer similar to that in Ti and also low concentrations in the low Sr/Ca layers.

The amount of leached Nd shows an almost linear trend for most of the record, decreasing from 6 $\mu\text{g/g}$ at 115 cm to around 4 $\mu\text{g/g}$ in the upper part. The only exceptions occur in the low Sr/Ca layers, in which only about half the amount of Nd was extracted from the sediment.

Finally, the concentration of U in the leachates is consistently low around 0.05 $\mu\text{g/g}$, but increases by a factor of 30 - 40 inside the low Sr/Ca layers. Remarkably, these peaks are characterised by sharp increases at the bases and smaller gradients towards the upper boundaries of these layers.

Both the REE slope (HREE/LREE) and bulge (MREE/MREE*) are relatively constant throughout the record, but show sharp interruptions to lower values in the low Sr/Ca layers. The REE slope is furthermore slightly higher in the foraminiferal ooze than in the diamicton between the HLs (HREE/LREE values of 1.1 and 0.9, respectively). While the presence of the ash layer does not lead to distinct REE patterns, a slight increase in HREE/LREE is coincident with the more radiogenic Nd isotope values below HL1. The Eu and Ce anomalies both increase from the core top (values of 0.9 and 0.4) towards the lower end of the record (values of 1.15 and 1). Again, this overall trend is interrupted by the HLs, in which the leachates are depleted in Eu and enriched in Ce, relative to the surrounding sediments ($\text{Eu}/\text{Eu}^* \approx 0.85$, $\text{Ce}/\text{Ce}^* \approx 0.80$ to 0.85). A slight increase in the Eu anomaly of about 0.1 is found in the centre of the ash turbidite layer and coincides with the increases in extracted Al and Ti.

Elemental concentrations of leachates obtained from the two shallower sites on the Dreizack seamount (Fig. A.7 and Fig. A.8) are generally similar to those of site Me68-91 at the same stratigraphic depth, with two exceptions. Firstly, the Mn concentrations below HL1 do not seem to peak in core PO08-23. More important, none of the elements and parameters displays any excursions in the stratigraphic depth in which the ash layer in core Me68-91 VL is present. The elemental record of Site U1308 (Fig. A.6) roughly follows the same pattern, but again with less variability. Only the HLs lead to significant excursions in the element concentrations of Site U1308, which are generally smaller than in core Me68-91 VL, in particular for the Ce and Eu anomalies.

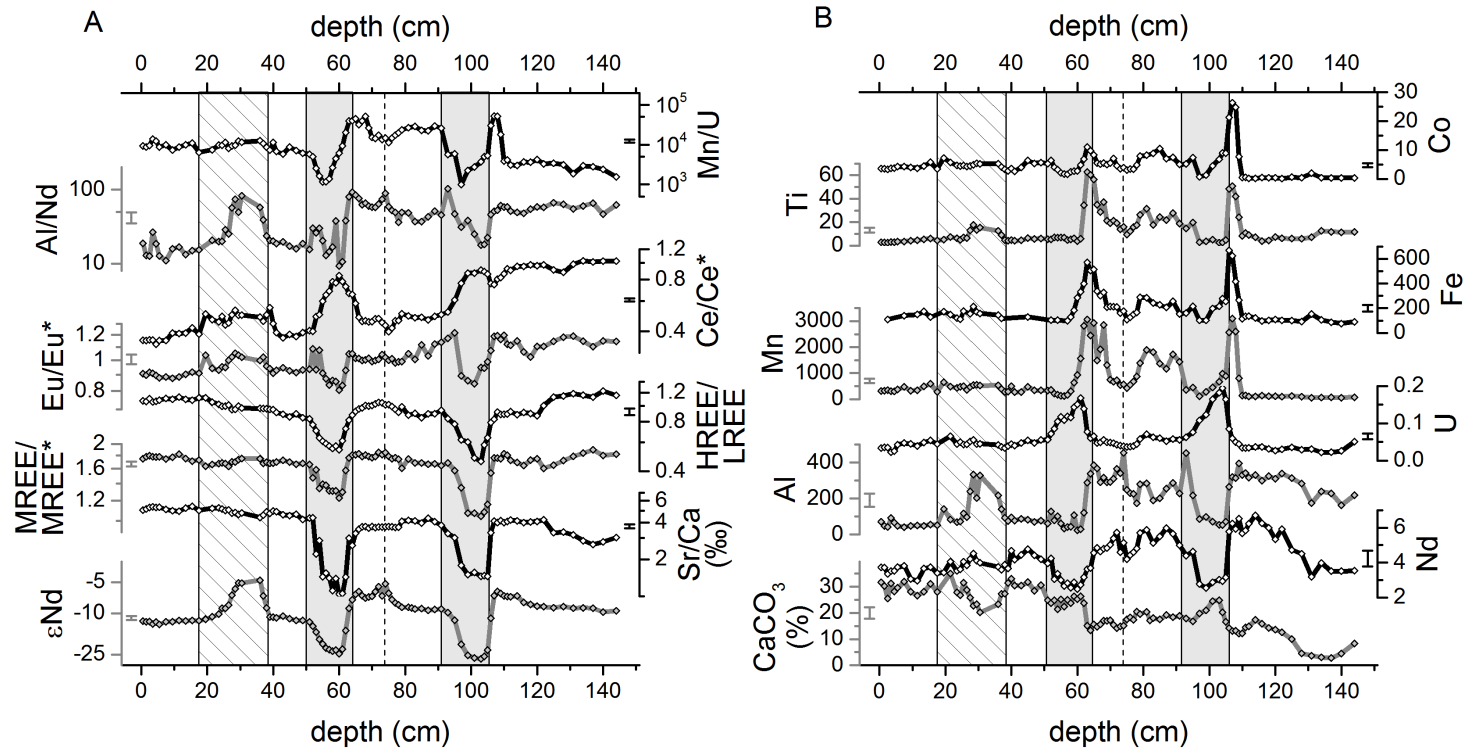


Figure 5.3: Elemental concentrations and ratios of core Me68-91 VL against depth in core. In the left panel (A), elemental and Nd isotope ratios are plotted on logarithmic vertical axes. In B, concentrations of different elements and calcium carbonate in the leachate are plotted in $\mu g/g$ bulk sediment ($CaCO_3$ in % of bulk sediment) on linear vertical axes. Left axes belong to the grey data plots, and right axes to the black and white data plots. Next to the respective vertical axes the average 1 sigma standard deviation from total procedural replicate sample measurements of the respective element or element ratio is shown (2 sigma SD for Nd isotopes) at the average concentration level. The vertical bars mark the Vedde Ash turbidite and Heinrich Layers as in Fig. 5.2. Vertical dashed line indicates the position of the small peak in magnetic susceptibility.

Table 5.2: Location of all sites discussed in this chapter and their respective mean authigenic Nd IC during the late Holocene and the LGM. Late Holocene data are averaged over the uppermost 12 cm of sediment, whereas LGM data are averaged over all undisturbed data between HL1 and HL2 (see Fig. 5.4). The hash designates the number of averaged values.

Site	Lat. (°N)	Long. (°E)	Depth (m)	ϵ Nd mean late Holocene	ϵ Nd median late Holocene	SD late Holocene	#	ϵ Nd mean LGM	ϵ Nd median LGM	SD LGM	#
BOFS 8K	52.5	-22.1	4045	-12.41	-12.43	0.44	3	-7.14	-7.03	0.48	6
BOFS 5K	50.7	-21.9	3547	-12.78	-12.78	0.06	2	-6.59	-6.71	0.34	3
U1308	49.9	-24.2	3871	-12.37	-12.37	0.02	2	-7.73	-7.64	0.18	5
Me68-91	47.4	-19.6	4470	-12.18	-12.07	0.36	9	-9.02	-9.07	0.22	7
Me68-89	47.4	-19.6	4260	-12.62	-12.62	0.23	2				
PO08-23	47.4	-19.5	3900	-12.78	-12.77	0.02	3				

5.4 Discussion

The following discussion will mainly be based on the results obtained from site ME68-91 and Site U1308. The other two investigated cores, as well as cores BOFS 5K and 8K (Roberts and Piotrowski [2015]) will serve for comparison in section 5.4.4 and section 5.4.4. The discussion focuses on the reconstruction of diffusional processes in the sediment column, as well as exchange processes between the different detrital layers and the authigenic fraction. Additionally, with the inclusion of proximate sediment cores, it is assessed whether exchanges with the detrital layers changed the local bottom water Nd IC, which would have important consequences for the applicability of ϵNd as a water mass tracer in the North Atlantic. Finally, the reconstructed evolution of the deep water Nd IC in the Northeast Atlantic is briefly discussed.

5.4.1 No evidence for vertical diffusion of REEs in the sediment

The concentrations and concentration ratios of the investigated elements of core Me68-91 VL show spatially confined excursions coinciding with the stratigraphic patterns as stated above. However, the concentrations of Mn, Fe, Ti, and Co show another peculiar feature (Fig. 5.3 B). These four elements exhibit distinct concentration peaks at the bases of both HLs. These peaks exhibit enrichment factors of 25 in Mn, 4 in Fe, 6 in Ti, and 60 in Co compared to the sediment below, for example in the peak below HL2. This feature appears to be an effect of vertical diffusion of these elements in the sediment column under increasing sedimentation rates and depleted oxygen concentrations. Previous studies have already identified sub- or anoxic conditions in Heinrich layers of the Northeast Atlantic (Baas et al. [1998]; Hoogakker et al. [2014a]), in particular in the dolomite bearing DC layers of the Dreizack region (Heinrich [1989]). An oxygen deficit is also supported by the increase of the U concentrations in the leaches of the DC layers, since U commonly precipitates under suboxic conditions (e.g. Mangini et al. [2001]). Recently, Hodell et al. [2017] also found distinct peaks in Mn at Site U1308, which correlate well with the leachate data from this site. They explained these enrichments in a similar way as it is done in the following.

The oxygen deficit in the deep waters at the time of deposition of the Heinrich Layers probably already led to redox boundaries close to the sediment surface, inducing upward migration of redox sensitive elements and their enrichment in a thin layer near the sediment surface, where oxygen supply was sufficient for their re-oxidation (e.g. Froelich et al. [1979]). Once the IRD started to be deposited and the sedimentation rate grew, the oxygen deficit became even larger, leading to highly reducing conditions. While the mobilised elements started to migrate into the developing IRD layer (especially in HL1), the deposition of fine material led to a significant reduction in porosity of the IRD layer, thus inhibiting further pore water diffusion through the IRD layer from below and effectively conserving the redox

boundary underneath (Hodell et al. [2017]). The conditions inside the IRD layer must have become highly reducing themselves, leading to the formation of cementing authigenic dolomite and the intrusion and precipitation of U originating from the bottom waters above. While authigenic dolomites were observed at Site U1308 and site SU90-09 in the West Atlantic as well (Tamburini et al. [2002]; Hodell et al. [2017]), it seems that their formation was strongest at the Dreizack location. Possibly, the preconditioning with oxygen depleted bottom water was most pronounced in the region of the Dreizack.

It is noteworthy that while Mn and Co are commonly seen as authigenic elements that are highly sensitive to changing redox chemistry, the mobilisation of Fe usually requires more extreme redox conditions (e.g. Bonatti et al. [1971]; Takeno [2005]). Ti is commonly not seen as an element susceptible to remobilisation. The diffusion of the latter two elements thus supports highly reducing conditions in the pore waters.

Sholkovitz et al. [1992] observed the release of REEs together with Fe from sediments during the seasonal anoxia in pore and bottom waters of Chesapeake Bay. This release was amplified for the lighter REEs and Ce, leading to a fractionation among the REEs. However, neither the Nd concentration in the leachates, the REE ratios, nor the radiogenic Nd isotope signatures show any indication of a similar reduction or diffusion process in the sediments below the IRD layers (Fig. 5.3). The slight dip in Ce/Ce* at 108 cm depth can probably be attributed to the general trend, which is intercepted by the decrease in Ce anomaly within HL2. Thus, the REEs seem to be less susceptible to dissolution and/or transport in the pore water than Mn, Fe, Ti and Co at the study site. This is especially interesting since it is usually assumed that authigenic REEs coprecipitate on sediment particles together with ferromanganese (oxy-)hydroxides supplied by the bottom water (Koschinsky and Halbach [1995]). The decoupling of REEs and Fe and Mn thus either indicates that the REEs bearing compounds in the authigenic ferromanganese hydroxides are relatively resistant to dissolution under suboxic conditions in pelagic sediments or the REEs exhibit higher particle reactivities within the sediment column under suboxic environments, leading to rapid reprecipitation and in effect to insignificant pore water diffusion. This observation is important for the interpretation of seawater Nd isotope signatures reconstructed from deep sea sediments, as it supports the viability of this approach even across (palaeo-) redox boundaries in the sediment. Our observations are also in accordance with interpretations of Martin et al. [2010], who showed that acid-reductive leaches extracted Nd isotope signatures and REE concentration changes similar to those archived in fish teeth around Ocean Anoxic Event 2, even though the sediments had lost most of their Fe and Mn oxides due to prevailing anoxic conditions.

5.4.2 Interaction between detrital and authigenic phases

The Nd isotope record of core Me68-91 VL reveals ϵNd signatures near -12 at the core top and in the Holocene foraminiferal ooze layer. In the glacial diamicton between 80 and 91 cm depth the signatures reflect more radiogenic deep water sig-

natures around -9 and slightly above (see Table 5.2). The Holocene and core top values are in good agreement with present seawater measurements (Dubois-Dauphin *et al.* [2017]) and the difference between Holocene and last glacial signatures is comparable to other sites in the deep Atlantic (cf. Lippold *et al.* [2016]). As no other measured parameter indicates a detrital contamination, both sections can be assumed to reflect archived deep water signatures. However, the Nd ICs in leaches of the ash and Heinrich Layers, as well as directly below both HLs show extreme deviations from the surrounding Holocene and glacial sediments, which have not been recorded in any other published North Atlantic locations. Therefore, the extracted Nd in these layers supposedly reflects a mixture of archived authigenic and detrital Nd, as explained below.

Two systematically different processes may have led to a detrital contribution to the leachates. Either Nd could have been released from the detrital material during reductive leaching in the laboratory, which would make the observed Nd ICs an analytical artefact. Alternatively, the detrital material may have released Nd to the pore water some time after sediment deposition. This re-dissolved Nd would subsequently reprecipitate and either be added to the authigenic fraction or exchange with the same (e.g. Du *et al.* [2016]). In that case, the authigenic Nd fraction was altered during early diagenesis and the archived seawater Nd isotopic composition is essentially lost for reconstruction.

Ash turbidite

The Nd IC from several samples of physically cleaned foraminifera within the ash layer of site Me68-91 was extracted in addition to the leaches (Fig. 5.2). The measured foraminiferal ϵNd values follow the trend of a broad radiogenic peak observed in the leachates. Three replicated foraminiferal Nd ICs indicate sufficiently cleaned samples, so that their isotope signatures were not significantly contaminated from residual detrital material in the laboratory. An analytical artefact that equally influences bulk sediment leachates and (duplicated) foraminiferal samples is highly unlikely, even if there were residual detrital particles incorporated in the foraminifera tests. Therefore it can be concluded that the observed radiogenic peak generally reflects the Nd isotope signature of the authigenic fraction and not an analytical artefact. Noteworthy to mention is a slight elevation in some element concentrations coinciding with the central part of the Nd IC peak of the ash layer. The Eu anomaly and the extracted Al and Ti contents exhibit small increases between 25 and 38 cm core depth. These may indicate a small additional contribution from leached volcanogenic material confined to the centre of the ash layer (Blaser *et al.* [2016]). The central ash layer also contains less carbonate (Fig. 5.3 and Jantschik [1991]), hence the increased concentrations of Al and Ti could also be explained as an effect of reduced carbonate buffering. The concentration of leached Nd does not change throughout the ash layer.

These observations suggest that the initially archived seawater Nd IC ($\epsilon\text{Nd} \approx -12$) must have been altered during early diagenesis and partially exchanged Nd

with the volcanic material during this process (ϵNd between 0 and +4, see [Blaser et al. \[2016\]](#), or up to +7 if it is similar to the Icelandic Eyjafjallajökull tephra). The constant Nd concentrations in the leachates across the ash layer suggest that detrital Nd was not simply added to the authigenic Nd pool, but must have exchanged with it. A similar exchange of sedimentary Nd has been reported previously in the Indian and Pacific Oceans ([Wilson et al. \[2013\]](#); [Du et al. \[2016\]](#)), as well as in Oligo-Miocene sections of the Ceara Fan off the Amazon delta ([Stewart et al. \[2016\]](#)). [Schacht et al. \[2010\]](#) recognised a similar process in mildly reducing sediments from the Pacific Central American margin.

Such an exchange between authigenic and detrital phases likely took place through the initial dissolution of Nd from detrital and possibly authigenic phases and release into pore water. In principle, such an effect can lead to increased pore water Nd concentrations and consequently to vertical diffusion of radiogenic Nd out of the ash layer. However, the radiogenic peak in leachate Nd IC does not exceed the peak in magnetic susceptibility which traces the distribution of ash particles (Fig. 5.2 D). Both peaks are blurred upwards by bioturbation, but if an additional significant pore water diffusion had taken place at any stage then the radiogenic Nd IC peak would need to be broader than the peak in magnetic susceptibility. Thus, any potential pore water diffusion of detrital Nd must have been significantly weaker than bioturbation, which exhibits a total length of about 13 cm in this layer.

Interestingly, the increase in Al/Nd in the central ash layer is smaller in amplitude than assessed in subsection 4.3.5. Peak Al/Nd ratios reach values of 83, but a significant imprint of radiogenic Nd is already observed accompanying a smaller local increase. Thus, while peaks in Al/Nd are a useful tool to indicate detrital influence on the leached Nd IC, the ratio may not always be sensitive enough to trace small detrital inputs.

IRD layers

Only few foraminifera are present in the IRD layers of the Dreizack sediment cores, hence only the Nd ICs from leaches were reconstructed. Since a considerable amount of DC and authigenic dolomite was deposited in these layers, which can easily be dissolved with acids, the leaches may be directly contaminated by these labile detrital and early diagenetic phases. However, [Blaser et al. \[2016\]](#) demonstrated that even in completely decarbonated samples from HL1 the extracted Nd IC is still clearly influenced by detrital Nd ($\epsilon\text{Nd} = -22.7$). The non-biogenic carbonates thus cannot be the only source of detrital Nd. The redeposition of dolomite must have involved the dissolution and subsequent precipitation of other phases of the sediment. This may be a mechanism through which Nd exchanges between detrital and archived seawater reservoirs. Again, this process must occur via the pore waters as transfer medium. However, no unradiogenic Nd isotope anomalies are present outside the actual IRD layers, indicating that vertical transport in the pore water column did not play a major role.

The low Sr/Ca ratios in core Me68-91 VL (Fig. 5.3) give evidence for the dis-

solution of Sr depleted non-biogenic carbonates in the IRD layers (Channell et al. [2012b]; Blaser et al. [2016]). The linear correlation coefficient (r) between ϵNd and Sr/Ca in HL1 and HL2 is 0.8. However, the extracted REE patterns also change in the IRD layers. In fact, the REE bulge and slope correlate even better with the Nd IC changes ($r = 0.94$ and $r = 0.95$, respectively). The Ce anomaly also exhibits a clear negative correlation coefficient of -0.76 with the Nd ICs. Thus, these REE ratios could be used to trace the influence of DC on the leachates. Importantly, the correlations in the IRD layers of Site U1308 are similar. The correlation of altered Nd ICs, Sr/Ca ratio and the mid REE bulge will be used in chapter 6 to trace the influence of DC on leachates in the subpolar North Atlantic (Fig. 6.4).

Pre-IRD layers

Immediately below both DC layers in core Me68-91 VL, the extracted Nd ICs are more radiogenic than the average local bottom water composition further below (Fig. 5.2 A). Below HL2 this radiogenic Nd IC maximum is preceded by a continuous change from $\epsilon\text{Nd} \approx -8.7$ to -6.6 over 13 cm, accompanied by an increase in magnetic susceptibility and a reduction in optical sediment lightness (Fig. 5.2 B, C). In contrast, directly below HL1, low magnetic susceptibility coincides with more radiogenic Nd isotope signatures. Another earlier peak indicates a change in detrital input about 11 cm below HL1. This latter excursion is also accompanied by a shift of the Nd IC in the detritus towards more radiogenic values ($\epsilon\text{Nd} = -7.8$). The result gives the assumption of a superposition of a slow increase in the Nd IC of the leachates (just as observed below HL2) and a short radiogenic peak in its centre. In both pre-IRD layers, the leaches extracted slightly increased amounts of Al, and the Al/Nd ratio closely traces the double peak below HL1 (Fig. 5.3 A, B). Outside the layer of increased magnetic susceptibility, the detrital Nd ICs remain low and in the range of glacial sediments. Two samples below HL1 of site PO08-23 show similarly radiogenic Nd ICs. However, none of these observations occurs at Site U1308. Furthermore, the trend towards radiogenic Nd ICs does not match with the distinct peaks in Mn, Fe, Ti and Co described in subsection 5.4.1.

Possibly, the increasingly radiogenic Nd ICs below HL1 and HL2 reflect the palaeoceanographic signal of northward penetrating, oxygen depleted southern sourced water (SSW) at the study site. These waters would have been more radiogenic than those present during the LGM, and would not have reached Site U1308, where such an increase in leached Nd IC is not observed. An early arrival of SSW in the Northwest Atlantic before the peak of Heinrich Event 2 ice rafting has been reported by Gutjahr and Lippold [2011]. A more radiogenic Nd IC of the bottom water may also be the result of e.g. a reduced admixture of Labrador Sea sourced Nd to the prevailing SSW. The SSW may still have been present during the peak of the IRD events but cannot be traced due to the overprinting of the signatures by the IRD layers. This water mass was likely depleted in oxygen and contributed to the low oxygen conditions found for the Northeast Atlantic at shallower sites off the Iberian margin (Baas et al. [1998]; Hoogakker et al. [2014a]), which would be consistent with the

observed Mn and Fe remobilisation. Such a water mass change was, however, not observed in a recently published study on Mauritanian margin sediments at around 20°N (Howe et al. [2016a]).

Another possible cause for these distinct radiogenic Nd isotope features at site Me68-91 could be the interaction between early Heinrich Event ice rafted debris and authigenic phases or the leaching solution, as described above for the ash layer. IRD derived from the British Ice Sheet or Iceland has been reported for several sites in the North Atlantic (Grousset et al. [2000]) and could deliver detritus carrying radiogenic Nd. The elevated Al/Nd ratios below HL1 indicate an increased contribution from a detrital source (Blaser et al. [2016]), although Al/Nd does not accompany the radiogenic Nd ICs below HL2. Even though the bulk detrital Nd ICs directly underneath the DC layers are relatively unradiogenic (Fig. 5.2), deposition of a minor labile fraction may have led to radiogenic signatures in the authigenic fraction or the leachates if it is preferentially dissolved (Wilson et al. [2013]; Blaser et al. [2016]; Du et al. [2016]). The cause for the radiogenic signatures and their gradual increase directly before the DC layers cannot be determined unambiguously. Both an early arrival of radiogenic bottom waters and the influence of a minor fraction of labile radiogenic detrital particles are possible and further investigations at sites located farther south would be necessary to solve this ambiguity.

5.4.3 Characteristics in the record from Site IODP U1308

Similar to the Dreizack location, Site U1308 reportedly contains extended IRD layers including DC corresponding to Heinrich Layers (Broecker et al. [1992]; Obrochta et al. [2012]; Hodell et al. [2017]). Consequently, the Nd isotopic signatures and trends of the leachates are comparable between these two localities (see Fig. 5.4 and Fig. A.5 in the appendix). Site U1308 also features a radiogenic excursion of the leached Nd IC between 52 and 82 cm core depth. This layer corresponds to the Vedde Ash layer, similar to core Me68-91 (Bond et al. [1993]). Therefore the radiogenic excursion probably also results from exchange of Nd between authigenic and detrital phases as in core Me68-91 VL. The magnitude of the radiogenic excursion at Site U1308, however, is smaller, probably due to a smaller input of volcanic material.

There is one distinctive feature in the analysis of Core U1308C. Three total replicate analyses of two sediment samples from HL1 (91 and 93 cm core depth) resulted in significantly different leachate compositions. Specifically, while two of the samples exhibit Nd ICs and elemental compositions typical for the DC layers, the three replicates yielded signatures in the normal range of seawater and carbonate ooze samples. This indicates that the sediment was insufficiently homogenised in this case and that the aliquots of 0.25 – 0.3 g taken for analyses contained differing amounts of DC. This observation further highlights the inhomogeneity of HL1 at Site U1308 (Hodell et al. [2017]) and that this IRD layer did not experience early diagenesis as extensive as those from the Dreizack seamount and, as a consequence, does not contain as much authigenic carbonate cementing the sediment. Thus, intense exchange of Nd between authigenic and detrital phases in the IRD layers

did likely not occur at Site U1308. This is consistent with the observation that extracted Nd ICs are not as unradiogenic as in the Dreizack sediments. The leachates of replicates without DC yield Nd ICs of about -11 , which is intermediate between Holocene and LGM values (Table 5.2 and Fig. 5.4).

5.4.4 Impact of detrital sediments on local bottom water Nd IC

The observation that detrital and authigenic fractions exchanged Nd during events of detrital deposition in the Northeast Atlantic raises the question whether part of the detrital Nd escaped the sediment pore waters after mobilisation and influenced the regional bottom water Nd isotope signature. Even though it was shown that there is no indication of vertical diffusion of Nd in these sediments, Nd may still have been released from the detrital sediment layers while they were located at the interface of bottom water and sediment. Therefore, the newly reconstructed Nd isotope records are compared with those of nearby sites with no similar detrital inputs.

Comparison with nearby sites

While the two shallower sites at the Dreizack do contain IRD layers like site Me68-91, they are located too high above the deep sea plains and channels to be directly reached by the ash turbidite. Several samples above HL1 in cores Me68-89 and PO08-23 were leached and analysed (Fig. 5.4). The expected depths of the ash turbidite event at these sites based on lower sedimentation rates compared to site Me68-91 are indicated by the diagonally lined bars and are well covered by the sample resolution. However, none of the samples show any evidence of a radiogenic anomaly that could indicate the supply of Nd from the massive ash turbidite to the local bottom water.

Additionally, the new data can be compared with those from sites BOFS 5K and 8K (Roberts and Piotrowski [2015]), located at similar depths but further north outside the central IRD belt (Fig. 5.1). The Nd IC record from core BOFS 5K contains one data point that indicates a slight radiogenic excursion of about 1 epsilon magnitude next to the maximum of Vedde Ash particles (Barker et al. [2004]; Roberts and Piotrowski [2015]). This could indicate that a similar exchange as in core Me68-91 VL also occurred in the sediments of core BOFS 5K, or that altered bottom water was advected northward. However, data of the neighbouring core BOFS 8K do not show any hint of a radiogenic influence on the archived Nd IC, even though they are sampled in a relatively high resolution (approximately every 3.8 cm or 0.8 ka). This indicates that the early diagenetic alteration of the archived authigenic Nd at site Me68-91 did not result in a significant imprint of radiogenic Nd onto the regional deep water masses and instead appears to be a local pore water process.

As discussed above in subsection 5.4.3, the replicates produced from HL1 at Site U1308 suggest that there was no significant exchange of Nd between the authigenic

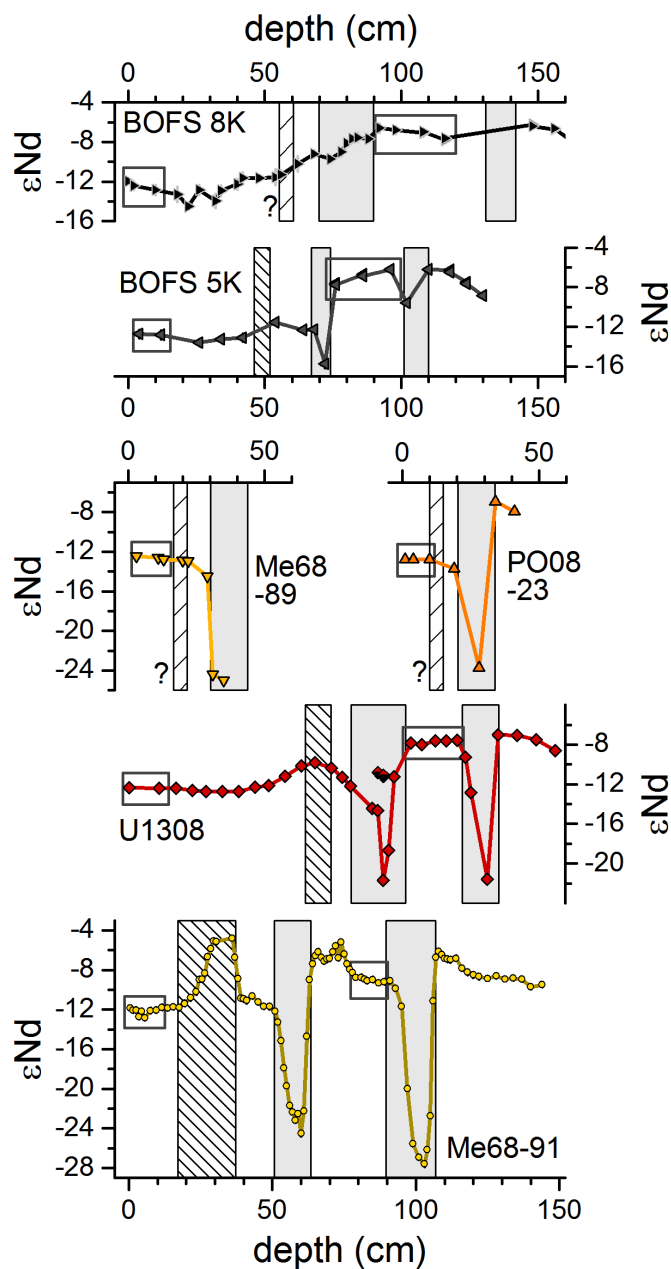


Figure 5.4: Nd isotope records from the Northeast Atlantic. Site details are given in Fig. 5.1 and Table 5.1. Small open boxes indicate the averaged Nd IC values of Table 5.2. Grey vertical bars indicate the depth range of Heinrich Layers. The ruled vertical bar indicates the depth of ash particles from the Vedde Ash at sites Me68-91, U1308, and BOFS 5K. In the profiles from sites Me68-89, PO08-23, and BOFS 8K it indicates the approximate stratigraphic depth of a potential direct or indirect imprint of the ash turbidite (based on the depth between HL1 and core top). The half black half red diamonds in HL1 of Site U1308 are replicate samples without imprint from detrital carbonate (see subsection 5.4.3). Data from BOFS cores are from Roberts and Piotrowski [2015].

phase and the IRD from HL1 at this site. Roberts and Piotrowski [2015] point out that the data from sites BOFS 5K and 8K contain a few points in layers with high DC counts which point to an unradiogenic influence in their Nd ICs. The authors note that an exchange of Nd within the pore water cannot be excluded, similar to the here presented data from core Me68-91 VL. However, none of the excursions is present in the records of both sites BOFS 5K and 8K. This further suggests that no advective transport of an altered bottom water mass during these IRD events in the Northeast Atlantic was present.

In summary, clear evidence is found that the detrital phases in sediment layers of the Vedde Ash turbidite and HL1 and HL2 exchanged Nd within pore waters at site Me68-91 and Site U1308. However, a detrital influence on the bottom waters of the area is not observed, which points to insignificant contributions of Nd to the regional bottom waters during these detrital events.

Quantitative constraints on a potential flux of Nd from the Vedde Ash turbidite

Significant fluxes of Nd from sediments to bottom waters were inferred in two regions in the Northeast Pacific. Abbott et al. [2015a] calculated that a benthic flux of up to 32 pmol/cm²yr of Nd from the sediment into the water column is required in order to explain the local seawater Nd IC profile at the Oregon margin. This released Nd was possibly derived from trace amounts of basaltic ash in the sediments. Similarly, Du et al. [2016] assessed that benthic fluxes of radiogenic Nd between 10 and 100 pmol/cm²yr of Nd can explain the spatial trend of the Nd IC of deep waters across the Pacific.

Volcanic material has been shown to be a highly reactive component of sediments that readily releases or exchanges large amounts of Nd with extremely radiogenic isotopic signatures (Pearce et al. [2013]; Wilson et al. [2013]; Blaser et al. [2016]; Du et al. [2016]). The deposition of the massive Vedde Ash turbidite in the Northeast Atlantic would thus be expected to have introduced large amounts of radiogenic Nd into the regional deep waters. If even traces of basaltic ash in sediments indeed lead to a significant benthic flux of Nd in North Pacific sites, released Nd from the Vedde Ash basaltic turbidite may have exerted a strong influence on the local deep water Nd IC in the Northeast Atlantic. The turbidite may furthermore have left an ash-bearing benthic nepheloid layer, which could lead to high exchange rates of Nd between detritus and deep water for years after the actual turbidite deposition (McCave [1986]).

Contrary to this scenario, described above in section 5.4.4, the data from two shallower Dreizack sites and site BOFS 8K do not show any indication of a modification of the deep water in the Northeast Atlantic. However, this observation is only a qualitative argument. A small modification of the deep water Nd IC might be concealed by a high degree of dilution with ambient water or strong bioturbation in the sediment. It is therefore not proven that there was no benthic flux of Nd. Based on a few assumptions, the maximum benthic flux that may have occurred without

an imprint in the authigenic Nd IC of samples from the abovementioned sites can be calculated.

For this calculation a steady benthic flux, steady deep circulation, and variable Nd isotope composition and concentration in the local deep water for a duration equivalent to 1 cm of sediment deposition will be assumed. This duration approximates to 500 years for the two shallower sites from the Dreizack sea mount and 250 years in the case of site BOFS 8K. Furthermore, a well-mixed bottom water layer of 1000 m height and an initial Nd concentration of 25 pmol/kg (Stichel et al. [2015]) will be assumed. The Nd IC of the benthic flux is taken as +7, as in the North Atlantic tephra from the 2010 Eyjafjallajökull eruption (Sigmarsson et al. [2011]). The largest gaps in between two samples from sites Me68-89 and BOFS 8K are 5 cm. If bioturbation at these sites is comparable to that in the ash turbidite from site Me68-91, the minimum shift in deep water Nd IC in order to be definitely recorded in these data sets can be assessed. The result is that a modified deep water Nd IC of -8 would lead to a shift of more than 0.5 epsilon units in at least one of the samples. Since several cores with samples taken at different stratigraphic depths are employed, it is unlikely that such a radiogenic excursion is exactly missed in all records. Thus it appears improbable that the deep water Nd IC was modified above a value of $\epsilon_{Nd} = -10$. For a volume of deep water covering the length L , width D and height H , advected with the speed v , the exchange time T can be given as

$$T = L/v \quad (5.1)$$

The total benthic flux of Nd into this water volume F_B is

$$F_B = f_B \cdot L \cdot D \quad (5.2)$$

where f_B is the flux per surface area of sediment in contact with the water volume in pmol per cm^2 and year. If the Nd concentration and isotopic compositions of the water are denoted with c and ϵ , respectively, and the subscripts DW and M for the initial and modified deep waters, then

$$H \cdot D \cdot v \cdot c_M = H \cdot D \cdot v \cdot c_{DW} + F_B \quad (5.3)$$

and

$$H \cdot D \cdot v \cdot c_M \cdot \epsilon_M = H \cdot D \cdot v \cdot c_{DW} \cdot \epsilon_{DW} + F_B \cdot \epsilon_B \quad (5.4)$$

represent the conservations of total Nd and of Nd isotopes, respectively. Combining equations 5.1 to 5.4 yields

$$\epsilon_M = \frac{f_B T \epsilon_B + H c_{DW} \epsilon_{DW}}{f_B T + H c_{DW}} \quad (5.5)$$

$$f_B = \frac{H c_{DW}}{T} \cdot \frac{\epsilon_M - \epsilon_{DW}}{\epsilon_B - \epsilon_M} \quad (5.6)$$

Equation 5.6 is the basis for Fig. 5.5. If ε_M is kept constant, the benthic flux thus scales linearly with the height of the mixed water layer and inversely with the time the water is exposed to this flux. If the mixing water volume was in contact with fresh unmodified water, then the required benthic flux would scale linearly with the increase in water volume taking up detrital Nd. However, the main uncertainty in these calculations is the effective time of exchange between deep water and benthic Nd. Today, the area of the Dreizack seamount is dominated by water flow speeds between 2 and 6 cm/s (Jantschik [1991]). On a direct flow path between the Dreizack seamount and site BOFS 8K, the exchange time between sediments and bottom water could therefore be as low as a year or less. Deviations caused by topography and recirculation may significantly increase the exchange time between these two sites. An estimated effective exchange time of a few years leads to maximum benthic fluxes of a few 10s of pmol/cm²yr. This maximum flux is in the same range as the results from Abbott et al. [2015a] and Du et al. [2016]. However, a lower limit of the benthic flux cannot be constrained and it may therefore be significantly smaller or even non-existent.

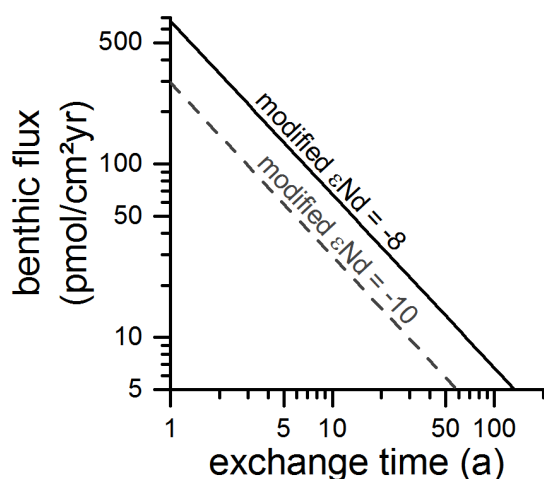


Figure 5.5: Estimation of the benthic flux of Nd from the Vedde Ash turbidite in relation to the mean exchange time and the possibility to detect the bottom water modification in neighbouring sediment cores. The two lines highlight the inverse relationship between exchange time and the maximum strength of the possible benthic flux of Nd into the bottom water for modified deep water Nd ICs of -8 and -10 . Note that both axes are logarithmic.

In the abovementioned studies from the North Pacific, trace contents of volcanic ash or other basaltic material in the sediment were likely responsible for the benthic fluxes of radiogenic Nd to the seawater. In the case of the Vedde Ash turbidite, large parts of the local ocean floor were covered in cm to metres thick layers of basaltic ash and the local nepheloid layer may have carried fine ash particles for years. By simple scaling one may expect that the volcanic detritus in this environment released much more radiogenic Nd to the bottom waters than in the steady state North Pacific situation. Yet, above calculations show that the flux was probably either comparable or smaller in the ash turbidite scenario. Similarly, Lambelet et al. [2016] highlight that they did not find any influence from the massive deposition of fresh tephra from the Icelandic Eyjafjallajökull eruption in surface waters in the North Atlantic (Sigmarsson et al. [2011]). Following this apparent contradiction, it seems that small amounts of volcanic material mixed into the ambient sediment are more efficient in releasing Nd to sedimentary pore waters than free floating particles or

thick surface layers of volcanic ash. An important factor controlling the release rate of Nd from volcanic particles may be the pH of the reacting solution. The surface water in the case of the Eyjafjallajökull tephra, and also of the bottom water to which the Vedde Ash turbidite was exposed during and shortly after sedimentation, should have had a pH of around 8. Pore water environments, however, can become more acidic due to the microbial degradation of organic matter and the involved production of carbonic acid in the sediment. Particularly in sediments with no or only little calcium carbonate to buffer the acidifying pore waters this effect plays a role (e.g. Jourabchi et al. [2008]). Pore water pH may thus be reduced by as much as 1 pH unit, and possibly even more in microenvironments. In addition, Gislason and Oelkers [2003] found that the dissolution rate of basaltic glass strongly depends on pH and is lowest in the neutral range, as assessed by the Si release rate. Leaching experiments support a dominant role of pH in the effectiveness of release of Nd from volcanic phases (Wilson et al. [2013]; Blaser et al. [2016]). The activity of microbes may also play a role to enhance the dissolution rate in micro environments (Staudigel et al. [1998]) and thus promote exchange of radiogenic Nd with pore water.

In the Northeast Pacific, only little CaCO_3 is buried in the sea floor and ash is dispersed in the sediments by bioturbation. The Oregon margin sediments analysed by Abbott et al. [2015a] and Abbott et al. [2016] contains both little CaCO_3 and relatively high amounts of organic carbon (1.4 – 2.2%). It is thus conceivable that small amounts of reactive basaltic material in an environment of residual organic carbon and little calcium carbonate can be significantly leached in situ and thus release radiogenic Nd into pore water throughout the upper sediment column, as described by Abbott et al. [2016] and Du et al. [2016]. In contrast, in the case of the Vedde Ash turbidite, the bottom water environment was not acidic and/or reducing enough to leach the volcanic particles with a comparable efficiency. Yet, once the thick ash layer was mixed with overlying sediment containing organic carbon, microbial activity potentially enhanced the release of Nd to the pore water. Thus, even though the Holocene sediments in the Dreizack area are rich in calcium carbonate, microbially dominated micro environments in the pore space may have mobilised enough Nd from ash particles to significantly exchange with the authigenic phase. Vertical diffusional transport in the pore water may have been prevented because the pore water offered an environment in which REEs rapidly re-precipitated, similar to the scenario for the lower glacial sediments of core Me68-91 VL in subsection 5.4.1. Such a process could explain the significant imprint of the ash signal in the Nd IC of the authigenic fraction, while the elemental composition of the authigenic fraction remained the same as in the surrounding pelagic sediment. The flux of sedimentary ash-derived radiogenic Nd to the deep water thus probably depends, in addition to the presence of ash, also on the organic matter and carbonate contents in the sediment, as well as the sedimentation rate and local deep water oxygen content.

5.4.5 Northeast Atlantic deep water Nd ICs during the LGM

Combined with the two deepest sites from Roberts and Piotrowski [2015], a data set of bottom water Nd ICs during the late Holocene and the LGM in the Northeast Atlantic can be constructed. It spans the area from 47.4° to 52.5° N and 3550 m to 4470 m water depth (see Table 5.2). Since the origin of the radiogenic Nd ICs immediately below the Heinrich Layers at site Me68-91 cannot be determined unambiguously, they will not be discussed further and instead the homogeneous Nd isotope signatures between 79 and 91 cm core depth will be assumed to represent the state during the LGM, which is dated by ^{14}C to about 22 ka BP at 81 cm depth.

All reconstructed Nd ICs from these sites during the late Holocene form a narrow range between -12.2 and -12.8 , indicating a homogeneous deep water distribution. During the LGM, however, Nd ICs systematically vary from relatively unradiogenic values of -9.0 at the deepest and southernmost site to values of -6.6 to -7.0 at the northern and shallower sites. This pronounced gradient in regional deep water Nd IC points to a mixing process between strongly modified AABW from the South and a radiogenic water mass in the North. Roberts and Piotrowski [2015] found that all of their sites, ranging from 1150 m to 4045 m water depth, recorded a similarly radiogenic water mass during the peak glacial. They concluded that there must have been a radiogenic relabelling of the local waters throughout the entire water column. If this is the case, then the area where this process takes place in the deep waters can be confined to north of 50°N. However, without a detailed assessment of the Nd IC distribution during the LGM in a larger region, such consideration would remain speculation. It will therefore be further discussed in section 6.4.2.

5.5 Summary

New high resolution records of authigenic Nd isotope compositions as well as element concentrations were presented. These records from the deep Northeast Atlantic span the last 25 ka and include the detrital sedimentation events of the Vedde Ash turbidite and Heinrich Events 1 and 2. Based on the new data it is possible to identify exchange processes between detrital and authigenic phases and pore waters in the sediments.

Two distinct spikes of extreme enrichments of Mn, Fe, Ti and Co provide evidence for vertical diffusion of these elements in the pore water under reducing conditions. However, neither the REE patterns nor Nd ICs follow a similar trend, suggesting that neither were affected by vertical diffusion. This highlights the immobility of authigenically precipitated REEs even under reducing conditions.

At the same time, significant overprinting of archived bottom water Nd ICs took place during phases of massive IRD supply and subsequent diagenesis of the sediment under reducing conditions at site Me68-91. Similarly, in the Vedde Ash turbidite volcanic material must have exchanged Nd with the surrounding authigenic phases without significantly increasing the concentration of leachable Nd. The detrital

Nd isotope signatures in the authigenic sediment fractions provide evidence that detrital Nd must have been released to pore water in all these layers. Yet, none of these sedimentation events shows any sign of significant vertical diffusion, promoting the idea that REEs quickly reprecipitated after being released from the detritus. Low Sr/Ca and MREE/MREE* ratios reliably indicate the influence of Laurentide detrital carbonate on the Nd isotope composition in the IRD layers of Site U1308 and the Dreizack seamount. Conversely, the radiogenic imprint from the ash particles was not as clearly reflected by elemental proxies. It was only indicated by moderate increases of the Eu anomaly as well as the Al/Nd and Ti/Nd ratios in the centre of the ash layer.

It is assessed that the Vedde Ash turbidite material did not release as much radiogenic Nd as an upscaling of the Northeast Pacific situation described by [Abbott et al. \[2015a\]](#) and [Du et al. \[2016\]](#) would suggest. Apparently the volcanic material remained thus relatively inert while exposed to bottom water. A comparison of Nd isotope trends in neighbouring Northeast Atlantic sediment sites suggests that Nd was neither released in sufficient quantities nor over a time period long enough to significantly alter the local deep water Nd isotope composition. In light of this observation, it is hypothesised that a reduced pore water pH and microbial activity in microenvironments may promote the release of REEs from fresh basaltic particles in the sediment, especially in the absence of calcium carbonate as an acid buffer. For estimations of the benthic Nd flux and possibly of boundary exchange, the sediment composition and pore water chemistry probably play an important role and have to be taken into account.

The release of Nd from volcanic phases in the sediment is therefore likely more effective in the Pacific than the Atlantic Ocean, which needs to be considered in future assessments of the release of radiogenic Nd from sediments. Additionally, the short exchange times in the Atlantic compared to the Pacific, owed to the vigorous overturning, helps to reduce the impact of such sedimentary Nd input on the Atlantic water Nd budget.

6 Nd isotopes in the subpolar North Atlantic during the deglaciation

The subpolar North Atlantic is the region where NADW is formed by mixing of different water masses as described in subsection 2.5.1. These source waters are dense overflows from the Nordic Seas, in situ formed Labrador Sea Water, and southern sourced LDW today. Owing to the complex process and the exposition to large climatic variations at high latitudes, this formation varied significantly during the last glacial cycle. Furthermore, glacial erosion together with differing circulation patterns had the potential to completely change the Nd IC of the local water masses and thus also that of NADW. Circulation and water mass provenance changes in the subpolar North Atlantic have been reconstructed with different biogeochemical and physical proxies. The additional investigation with Nd isotopes serves two purposes: Firstly, the inferred oceanic changes will be compared to those already postulated in order to find out whether interpretations based on Nd isotopes agree or yield additional information. Secondly, if Nd isotope data disagree with existing interpretations based on a simple interpretation of mixing with modern Nd IC end members, changes in the end member isotope compositions can be inferred. Such changes are important because they can be passed on into the Atlantic and the Southern Ocean, affecting interpretations based on Nd isotopes on a large scale.

6.1 Introduction

In this chapter the results of reconstructed authigenic Nd isotope profiles obtained from four sediment cores across the subpolar North Atlantic covering the last 35 ka are discussed. Apart from a study on core top sediments (Elmore et al. [2011]), authigenic Nd has not been reconstructed from sites spread across the subpolar North Atlantic before. Palaeoceanographic studies employing authigenic Nd isotopes have been restricted to the (northern) Nordic Seas (Werner et al. [2014]; Teschner et al. [2016]), the Rockall Trough (Crocket et al. [2011]; Crocker et al. [2016]) and Rockall Plateau (Roberts and Piotrowski [2015]), or further south in the Atlantic Ocean. This may be due to the shortage of sedimentary foraminifera in this region (required for studies based on foraminifera as archive) and due to the results of Elmore et al. [2011], who highlighted the possibility of severe contamination of leached Nd isotopes in this region. With the overhauled leaching method and an improved understanding on the distribution, reactivity, and mobility of Nd in marine sediments, the reliable reconstruction and interpretation of the past deep water provenance in this highly dynamic region now appears feasible.

6.2 The hydrography of the subpolar North Atlantic since last glacial

For easier discussion of the results, the major changes of the subpolar North Atlantic hydrography from the late glacial until today will be briefly summarised, as far as they have been reconstructed. The diversity of involved water masses and detrital input, strong western boundary currents, and in some cases a lack of foraminifera make such reconstructions harder than in many other regions. However, there have been several studies employing a number of proxies in order to constrain past water mass provenance, flow strength, and deep water formation in this area. Furthermore, palaeoceanographic investigations further South in the Atlantic Ocean yield indirect constraints on the water mass import into and export from the subpolar North Atlantic.

The hydrography during the Last Glacial Maximum

During the LGM, deep water production in the North Atlantic was probably restricted to shallower depths than today, and the resulting water mass is thus termed Glacial North Atlantic Intermediate Water (GNAIW, Duplessy et al. [1988]; Labeyrie et al. [1992]). Simulations and some sparse data suggest that open ocean Labrador Seawater production ceased during this time (Hillaire-Marcel et al. [2001]; Cottet-Puinel et al. [2004]). Deep water formation in the Greenland Sea was probably reduced or inhibited due to extended sea ice cover and reduced import of saline Atlantic surface waters. Accordingly, Iceland-Scotland Overflow Water flux seems to have been reduced and the Northeast Atlantic Deep Water apparently shallowed (Elmore et al. [2015]). Similarly, Denmark Strait Overflow may have been weakened and shallowed (Millo et al. [2006]), and did not form a strong bottom current as it does today (Fagel et al. [2002]). Sediment provenance studies from the southern Labrador Sea suggest that there existed a sluggish persistent deep gyre inside the Labrador Sea (Fagel et al. [1997, 1999]). Due to the less vigorous deep water formation in the North Atlantic, southern sourced water masses penetrated further into the subpolar North Atlantic. Benthic foraminiferal carbon isotopes suggest that Glacial Lower Deep Water flooded the southern Gardar Drift (Elmore et al. [2015]) and it supposedly occupied a larger part of the deep water column (Oppo and Lehman [1993]; Manighetti and McCave [1995]; Yu et al. [2008]). There is indirect evidence by ocean circulation models and stable isotope studies that there was an active intermediate or deep convection cell south of Iceland (e.g. Millo et al. [2006]; Duplessy et al. [1991]; Sarnthein et al. [1994]).

The hydrography during the deglaciation and early Holocene

During the interval between LGM and Holocene, the hydrography in the subpolar North Atlantic underwent significant reorganisations and short term changes. While

northern hemisphere ice sheets were melting, they delivered large fluxes of freshwater to the Arctic, Nordic, and Labrador Seas. The resulting reduction of sea surface salinity may have diminished deep water formation in these regions. [Praetorius et al. \[2008\]](#), for example, found evidence for weakened northern sourced water formation during Heinrich Stadials 1 and 2 and the Younger Dryas, and strengthening at the start of the Holocene at around 11 ka. Overall, however, the North Atlantic Deep Water production was slowly initiated and strengthened from 16 to 8 ka ([Marchitto et al. \[1998\]](#)). During the early Holocene, LSW production was probably absent ([Hillaire-Marcel et al. \[2001\]](#)), but sediment provenance studies imply that ISOW and NEADW flow strength increased ([Fagel et al. \[1997, 2004\]](#)) and so did the deep boundary currents in the Labrador basin ([Fagel et al. \[1999\]](#)). By about 8 ka before present, it is generally thought that modern circulation was established ([Ledbetter and Balsam \[1985\]](#); [Fagel et al. \[2002\]](#); [Thornalley et al. \[2010\]](#)). Nonetheless, [Hoogakker et al. \[2011\]](#) infer indications for a shoaling of LDW and increasing LSW presence in the eastern subpolar North Atlantic after 7 ka and [Thornalley et al. \[2013\]](#) point out a parallel weakening of ISOW. Interestingly, [Roberts et al. \[2010\]](#) reconstructed peak unradiogenic Nd isotope signatures in the bottom waters of the deep Northwest Atlantic at around 8 ka, and a trend towards more radiogenic modern signatures afterwards (Fig. 2.3).

6.3 Study sites

The reconstruction of deglacial deep water mass evolution in the subpolar North Atlantic will be mainly based on four sites. They were cored with modern advanced piston coring techniques during IODP expeditions 303 and 306. In the following their most relevant features will be summarised, including the sediment core sections used and palaeoceanographic reconstructions from nearby cores. The sites are listed in Table 6.1 and marked in the map in Fig. 6.1.

Site U1302

Site IODP U1302 is located in the southwestern Labrador Sea at the Orphan Knoll feature near the Canadian margin (50.17°N, 45.64°W). While it is situated at around 3556 m water depth, the proximity to the margin and the Northwest Atlantic Mid-Ocean Channel lead to a sedimentation pattern that is dominated by continental input ([Channell et al. \[2010\]](#)). Furthermore, the site is situated underneath a major iceberg drift path, which led to increased detrital sedimentation also in the larger particle size fraction during HEs and more localised detrital events ([Stoner et al. \[1996\]](#)). The sedimentation rate was high reaching 15.7 cm/ka in average for the last 30 ka. Analyses were carried out at core sections D 1-1 to D 1-3, followed by E 1-3 to E 1-4 down to 4.7 mcd (metres composite depth). The carbonate content is less than 10 % in last glacial sediments, when much of the carbonate was delivered from the Canadian continent ([Channell et al. \[2012b\]](#)), and increases to about 35 % and

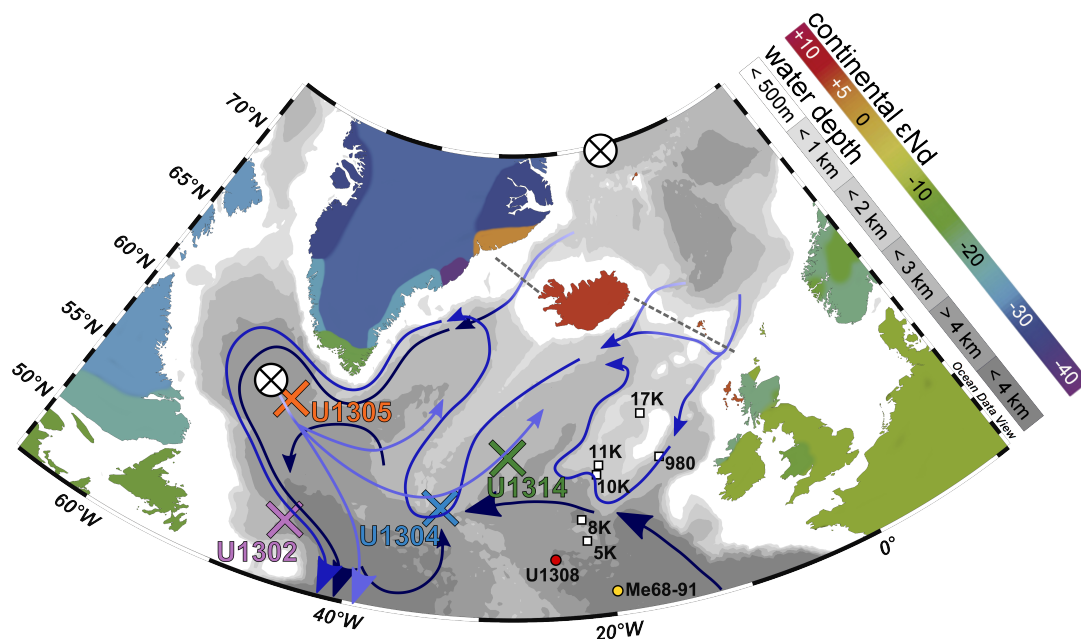


Figure 6.1: Map of study sites in the subpolar North Atlantic. The illustrated deep ocean currents are the same as in Fig. 2.5b. The four coloured crosses represent the sites in the centre of this investigation and the colours are the same as in the following figures. Additionally, the two sites investigated in chapter 5 are marked with circles. Additional sites at which Nd isotopes have been investigated in the literature are indicated with open squares (Roberts and Piotrowski [2015]; Crocket et al. [2011]; Crocker et al. [2016]). Modern deep water formation zones are indicated with big crossed circles and the Iceland sills with dashed grey bars. The bathymetric map was created with Ocean Data View (Schlitzer [2016]).

more in the Holocene sediments. The age model employed is based on IRD layers and their correlation to nearby sediment cores (Crocket et al. [2012]). This provides five tie-points between 12 and 38 ka age. Today, Site U1302 is bathed by NWABW, which is termed lower NADW directly south of the site.

Several palaeoceanographic studies have been carried out at this and nearby sites spanning a similar time range. However, most of them are based on the detrital or bulk sediment, since foraminifera, especially benthic species, are scarce (Hillaire-Marcel et al. [2011]). Fagel et al. [1999] investigated the Sm-Nd characteristics of the detrital clay fraction in nearby piston core HU91-045-094. Their results suggest an increasing presence of NEADW at the site from 14.3 ka on. A study of authigenic Pb isotopes at Site U1302 found variable continental weathering signals, which peaked during the HEs and Younger Dryas (Crocket et al. [2012]). Interestingly, they inferred that the detrital material delivered during these events contained high amounts of pre-formed authigenic Fe-Mn oxyhydroxides, which may also represent a source for contamination of authigenic Nd.

Site U1305

Site IODP U1305 is located in the central northern Labrador Sea (57.48°N, 48.53°W) at 3459 m depth. The sediment is situated at the southwestern tip of Eirik Drift, formed by the deep western boundary currents. Like Site U1302, this site is also influenced by the deposition of detritus, including detrital carbonate (DC), from the North American Continent via ice rafting and bottom currents. Its position on a drift led to very high sedimentation rates around 72 cm/ka during the Holocene and lower rates (14 - 20 cm/ka) during the late glacial (Hillaire-Marcel et al. [2011]). The first 14 metres composite depth were investigated here from core sections B 1-1 to B 1-6, followed by one sample from section C 2-2 and B 2-1 to B 2-4. The carbonate content is only between 2 - 5 % in late glacial samples and ranges from 20 to 50 % in Holocene sediments. Detrital carbonate was deposited abundantly during glacials, and Heinrich Events resulted in large detrital inputs (Stoner et al. [1996]). The sediments used are constrained in age by an extensive set of 14 ^{14}C datings between core top and 8 ka (Stoner et al. [2013]) and four stratigraphic $\delta^{18}\text{O}$ tie points between 10 and 57 ka (Hillaire-Marcel et al. [2011]). Additionally, detrital input during the final drainage of the glacial North American melt water lake Agassiz provides another tie point at 5.15 mcd. Today, Site U1305 is bathed by NWABW before this water mass enters the Labrador Basin where significant boundary exchange leads to a depletion of its ^{143}Nd content, as described in subsection 2.5.1.

Similar to Site U1302, the Canadian work group around Hillaire-Marcel, Fagel and de Vernal also investigated cores near Site U1305. These studies comprise Nd-Sm and Pb isotope systematics of the clay fraction to constrain the provenance of the detrital sediment fraction (Fagel et al. [1999, 2004]). Planktic foraminiferal stable isotopes were studied at a nearby piston core by de Vernal and Hillaire-Marcel [2006] and combined with dinocysts in Hillaire-Marcel et al. [2001]. The latter authors found that LSW deep convection above this site was absent during the early Holocene and only commenced around 7 ka ago.

Site U1314

Site U1314 is located on the central Gardar Drift east of the Reykjanes Ridge (56.36°N, 27.89°W) at 2799 m water depth. The drift is formed by the downslope flow of NEADW, which includes ISOW. Sedimentation rates were generally high in the Holocene (16 - 27 cm/ka) and reduced during the late glacial (4 - 5 cm/ka). Samples from core sections C 1-1 to C 1-3 and two samples from section A 1-1 were used for bulk sediment leaches. The carbonate content here is higher than in the Labrador Sea, roughly between 10 and 20 % in last glacial sediments and up to 50 % in Holocene samples (Grützner and Higgins [2010]). Organic carbon content is mostly below 0.25 %, and traces of volcanic ash were deposited by the deep western boundary current, especially during interglacials (Grützner and Higgins [2010]). The same authors also developed an age model by tuning sediment reflectance measurements to an orbitally tuned age model from Site ODP 983. This yielded five tie

points from 0 to 50.5 ka. Today, Site U1314 is bathed by ISOW or young NEADW, the distinction of which is not definite in this region.

Besides the abovementioned sediment provenance study by Grützner and Higgins [2010], recent work by Elmore et al. [2015] provides benthic carbon isotope signatures as nutrient tracers from neighbouring piston core KN166-14 11 JPC.

Site U1304

Site U1304 is situated at the southern limit of Gardar Drift in a semi-enclosed basin (53.06°N, 33.53°W) just North of the eastern Charlie-Gibbs Fracture Zone (CGFZ) at 3065 m water depth. The CGFZ provides an important pathway for deep water masses from the eastern to the western subpolar North Atlantic (and vice versa) across the Mid Atlantic Ridge (MAR). Core sections B 1-1 to B 1-4 were used in this study. The site exhibited sedimentation rates around 7 cm/ka during the late glacial and higher ones between 22 and 36 cm/ka during the deglacial and Holocene. The carbonate content in LGM samples lies at around 10 % and around 50 % in the Holocene section. The site is located at the northern edge of the Heinrich IRD belt and thus received some IRD during the glacial, especially during HEs. Initial analyses indicated that the sediment contains up to 1 % volcanic glass (Channell et al. [2010]). The age model employed was developed by Xuan et al. [2016] and relies on correlation to the well dated neighbouring piston core KN166-14-13JPC. The correlation is based on magnetic susceptibility and provides six tie points during the last 41 ka. Today, Site U1304 lies down stream of Site U1314 and is thus also bathed by ISOW or more evolved NEADW.

The abovementioned core 13JPC was studied by Hodell et al. [2010], who also reported benthic and planktic stable foraminiferal isotopes. Furthermore, Fagel and Mattielli [2011] and de Vernal and Hillaire-Marcel [2006] provided a further set of clay provenance studies from another proximate sediment core (HU 91-045-080P).

Table 6.1: Subpolar North Atlantic sites investigated for their authigenic Nd ICs with bulk sediment leaches. The respective symbols are used throughout the figures in this chapter.

Symbol	Site	Latitude (°N)	Longitude (°E)	Depth (m)
■	IODP U1302	50.1664	-45.6379	3555.7
●	IODP U1305	57.4751	-48.5302	3459.2
▲	IODP U1314	56.3647	-27.8885	2799.1
▼	IODP U1304	53.0567	-33.5297	3065.4

6.4 Results and Discussion

For the calibration of sediment core depths to ages linear interpolation between tie points and recent core tops were assumed for all sites (Fig. 6.2). Obviously, the two sites U1302 and U1305 from the Labrador Basin span a much wider range in ϵ_{Nd} (down to -24 and -21, respectively) than the two Gardar Drift sites U1314 and U1304 (Fig. 6.3). While the Labrador sites exhibit relatively stable and radiogenic Nd ICs at the upper (Holocene) part of the cores, the extracted Nd IC is much more variable and in part unradiogenic in the lower (glacial) parts of the records. Apart from these unradiogenic excursions, most variability is evident around the LGM section of Site U1314, during the transition from LGM to Holocene and during the mid- to late Holocene in all cores. Furthermore, sites U1305, U1314, and U1304 show strong similarity in their trend after about 6 ka.

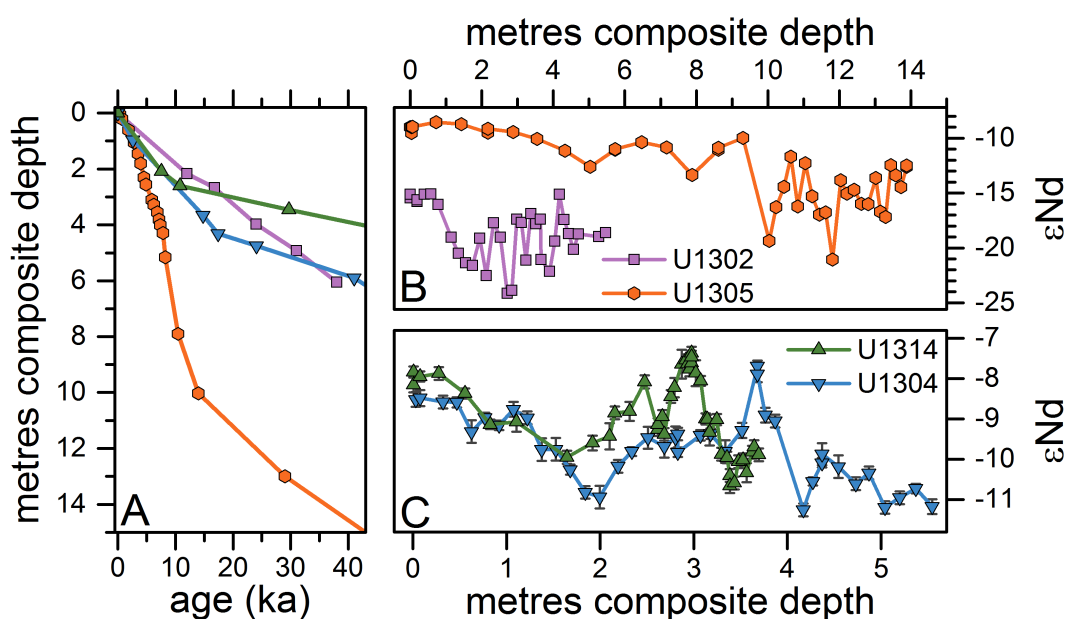


Figure 6.2: Depth-age models (A) and Nd IC results of bulk sediment leaches from the two Labrador Sea Sites U1302 and U1305 (B) and the two Gardar Drift Sites U1304 and U1314 (C). The age models are from [Crocket et al. \[2012\]](#) for Site U1302, [Stoner et al. \[2013\]](#) and [Hillaire-Marcel et al. \[2011\]](#) for Site U1305, [Xuan et al. \[2016\]](#) for Site U1304, and from [Grützner and Higgins \[2010\]](#) for Site U1314. Additionally, recent core tops were assumed for each composite core. Note the differently scaled axes in B and C.

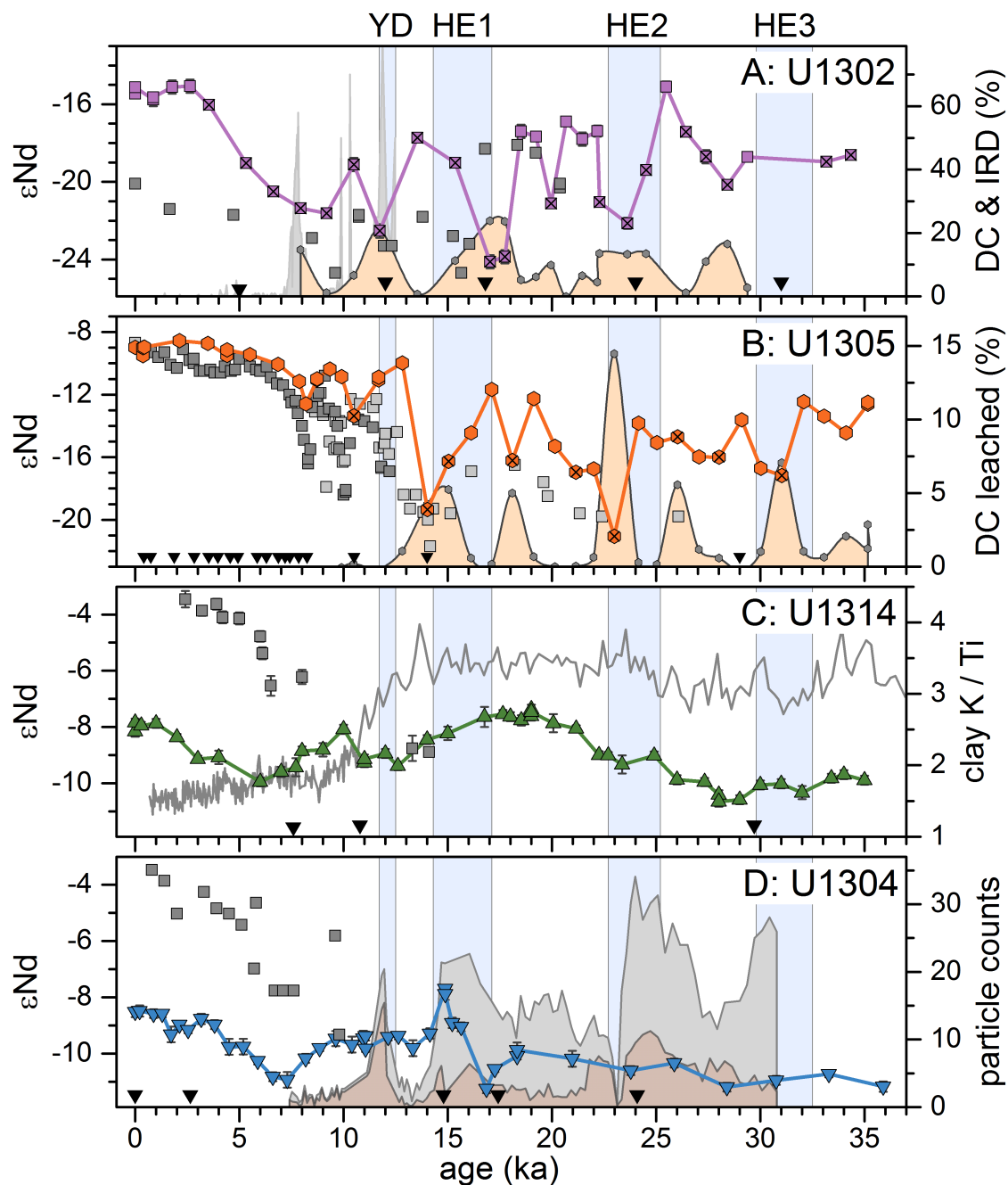


Figure 6.3: Nd ICs together with sedimentologic parameters plotted versus age in ka. Lines with symbols mark leached Nd ICs. Crossed symbols are not interpreted as seawater signatures (see section 6.4.1). Grey squares mark Nd ICs of the carbonate free clay fractions from nearby piston cores. Ochre surfaces in A and B indicate the amount of DC leached. **A:** Site U1302, with clay Nd IC (Fagel et al. [1999]) and IRD % in the sediment until the YD (grey shaded area Hoogakker et al. [2014b]) from two neighbouring cores. **B:** Site U1305, together with clay Nd IC from two nearby cores (light grey and dark grey squares, respectively; Fagel et al. [1999, 2004]). **C:** Site U1314, with clay Nd IC from Fagel and Mattielli [2011] and clay K/Ti ratio as an indicator of provenance (grey line, Grützner and Higgins [2010]). **D:** Site U1304, with clay Nd IC from Fagel and Mattielli [2011] and total lithic and volcanic glass counts (grey and brown surfaces, Hodell et al. [2010]) from two neighbouring cores. Black triangles indicate age tie points. Blue vertical bars mark cold climate events.

6.4.1 Integrity of leached Nd ICs as past bottom water signatures

Before the results of the sediment leaches are discussed in terms of deep water provenance, it must be assessed whether the extracted Nd ICs reflect true archived seawater signatures. While there is no unambiguous prove for this, a look at known indications of detrital or other contaminations in the elemental and Nd isotopic data of the leaches may give sufficient information. These indications have mostly been covered in the previous two chapters and are based on correlation of the composition of the sediment and the leachates with the extracted Nd IC, and comparison to actual seawater measurements.

Comparison with local deep water Nd IC

As was already discussed in [Blaser et al. \[2016\]](#), the core top Nd ICs at these sites are relatively close to available seawater data, but are not completely in agreement with them (see Fig. 6.6). The leachate signatures from U1302 are about 0.5 epsilon units too unradiogenic, whereas core top leachate signatures of the other three sites are up to two units too unradiogenic. The reasons for this could be plenty, since the region is very complex both in terms of hydrography and sedimentology. For example, the core top samples may not represent strictly recent sediment, but rather be several hundreds to thousand years old and reflect signatures integrated over 100s of years. Furthermore, the seawater samples, although taken from close to the ocean bottom and close to the respective sites (see Fig. 4.1), may not have sampled exactly the same seawater (with respect to Nd isotopes) as the one that is archived in the sediment. Alternatively, a slight but potentially continuous interaction between detrital and authigenic phases via pore water may have modified the extracted Nd, as was described in chapter 5. Importantly, a leaching artefact was already excluded in chapter 4, since foraminifera show the same offset from seawater data.

The agreement between foraminifera and bulk sediment leachate Nd ICs also testifies against a biasing influence of sediment transport, even at sites U1305, U1314, and U1304, which are located at the Eirik and Gardar drifts. Foraminifera are picked from the coarse sediment fraction and are rather resistant to redeposition by bottom currents due to their size, in contrast to the fine fraction, which dominates the bulk sediment. Thus, the agreement of foraminifera and bulk sediment leachate Nd ICs from three core top and two Termination II samples investigated in chapter 4 (see Fig. 4.7, samples 2, 3, and 4) indicates that the redistribution of sediment does generally not significantly affect the extracted Nd IC.

For the discussion in this chapter, it will be assumed that the extracted core top signatures represent the local bottom water Nd isotope signatures, except for some samples in which detrital contamination can be identified (see next paragraph).

Contamination by detrital carbonate

The most unradiogenic Nd isotope signatures at Sites U1302 and U1305 correlate with significant reductions of the mid REE bulge and Sr/Ca ratios in the leachates (Fig. 6.5). A similar correlation was observed in the DC Heinrich Layers from sites U1308 and Me68-91, shown in chapter 5. In a two end-member mixing scenario, the mixing data of MREE/MREE* and ϵ Nd plot on a straight mixing line, since both scale with the Nd concentration, whereas the data of Sr/Ca and ϵ Nd scale with different concentrations (Ca and Nd, respectively) and thus plot on asymptotes. From Fig. 6.4, it is obvious that the end members of the mid REE bulge in HL1 and HL2 are essentially the same, whereas the ones for Sr/Ca differ significantly. Consequently, the adjusted coefficients of determination (R_{adj}^2) for the individual mixing asymptotes between Sr/Ca and ϵ Nd are significantly larger (0.72 and 0.78) compared to only 0.58 for the assemblage of the data across both HLs. Importantly, the variations occur in both end members, that is the detrital and biogenic carbonates deposited during normal pelagic sedimentation. The variability of Sr/Ca ratios in DC are also evidenced by investigations from [Obrochta et al. \[2014\]](#), who measured the ratio directly from picked individual DC grains in Heinrich Layers of Site U1308. They found Sr/Ca ratios around 1.1 and 0.57‰ for HLs 1 and 2, respectively (median values of five analyses each). The variation in the biogenic end member is probably correlated to the local water temperature and the species composition from which the archived tests are derived. These data were used to calculate the amount of detrital carbonate that was extracted with the leach from Sites U1302 and U1305 (brown shaded curves in Fig. 6.3 A and B). As glacial biogenic end members Sr/Ca values from uncontaminated glacial samples of 3 and 4.5‰ were used respectively, which may not be accurate throughout the glacial record, but only influence the absolute numbers of leached DC, and not its trend. Clearly, the unradiogenic Nd ICs of the leaches correlate with peaks in extracted DC. The peaks in DC can furthermore be attributed to well dated DC layers and so-called Low DC (LDC) layers from the Labrador Basin ([Stoner et al. \[1996\]](#)), some of which correlate to Atlantic Heinrich Layers.

The mid REE bulge correlates linearly with an $R_{adj}^2 = 0.91$ with the Nd IC in the DC Heinrich layers (Fig. 6.4). It can therefore be used to detect contamination by detrital carbonate and associated phases in the leaches. However, it is not entirely clear what determines the REE bulge in the leachate. [Haley et al. \[2004\]](#) associated it with authigenic Fe phases, but a similar observation was not made in the investigations in chapter 4. While the REE bulge generally remained in a similar range during progressive leaching, some samples deviated significantly (see Fig. 4.5). Furthermore, the MREE/MREE* value in the initial HH-leaches was also rather variable from site to site, and especially the more southern sites 10 and 11 exhibited significantly lower values around 1.4 to 1.5 (see Fig. 4.11). This suggests that the authigenic MREE/MREE* end member may be site or water mass specific. In the uppermost Holocene age leaches of sites U1305, U1314, and U1304, MREE/MREE* values range mostly between 1.7 and 1.9 and the values go down

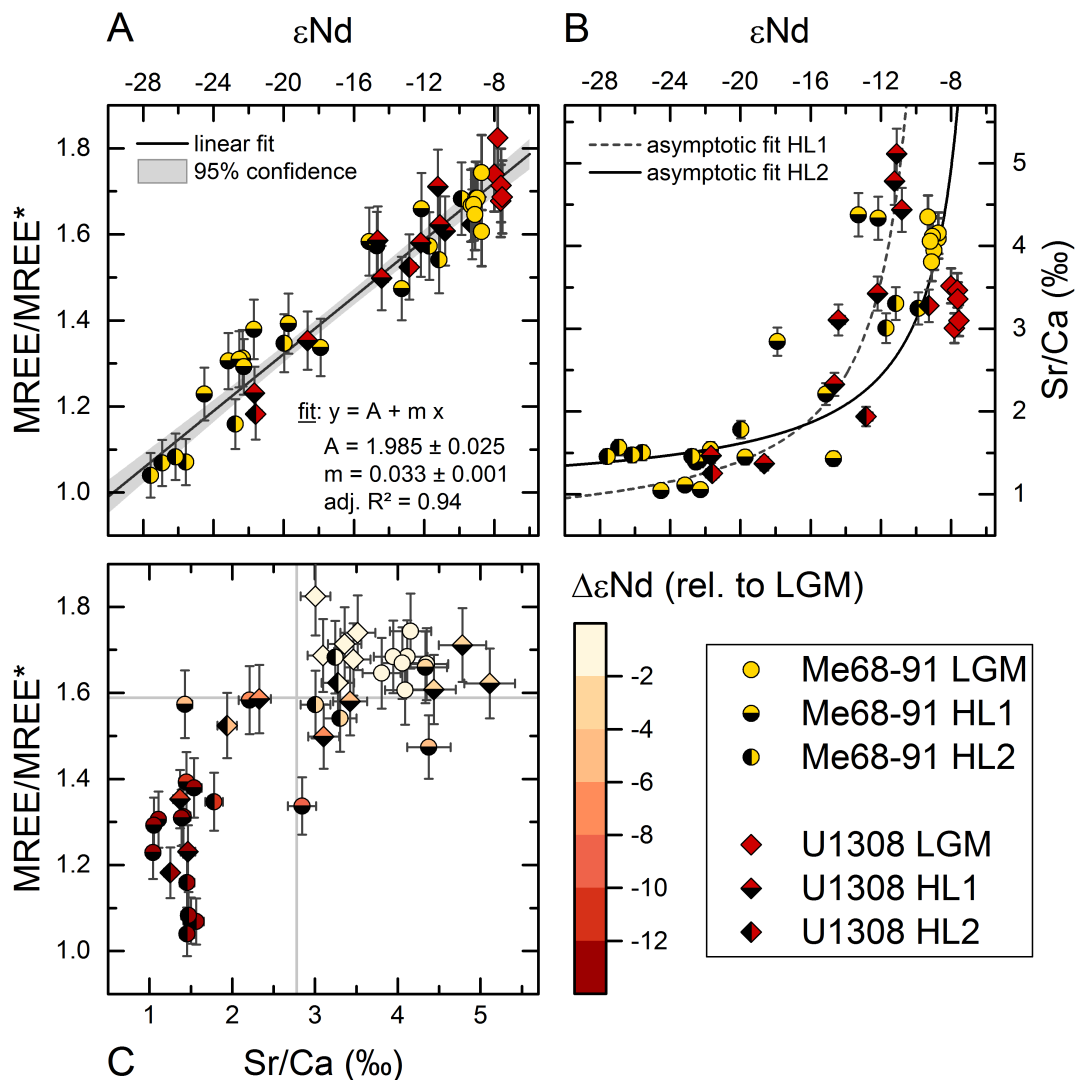


Figure 6.4: Correlation of the Nd IC to the mid REE bulge (MREE/MREE*, **A**) and the Sr/Ca elemental ratio (**B**) in leachates of Heinrich layers 1 and 2 and uncontaminated LGM data in cores Me68-91 VL and Site U1308C (from chapter 5). In **C**, the same data are plotted in element ratio space and the redness code the offset in Nd IC from the LGM signatures.

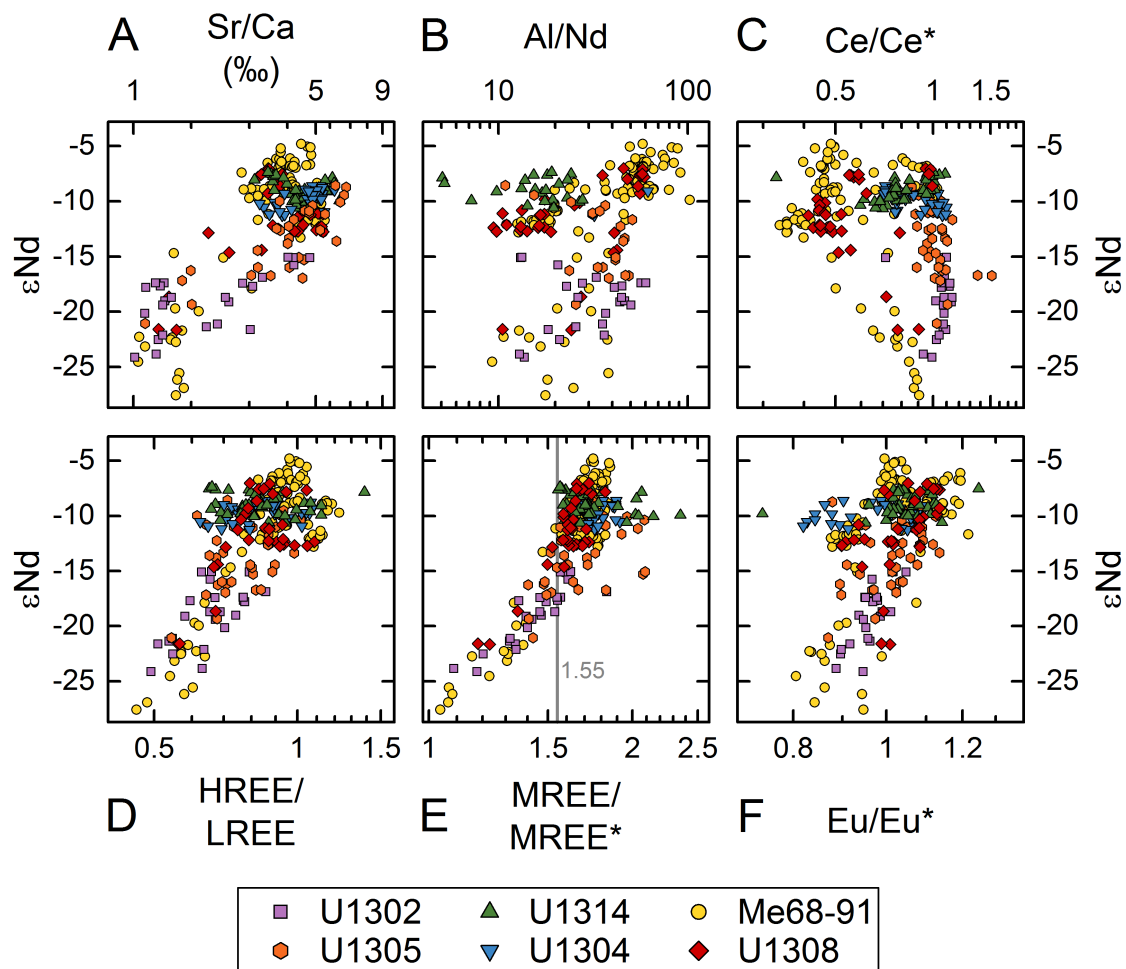


Figure 6.5: Relationship of elemental ratios and the extracted Nd isotope signatures of all leaches from sites U1302, U1305, U1314, U1304, as well as from sites U1308 and Me68-91VL from chapter 5. Nd isotope signatures are plotted on equal y-axes in each panel. The elemental ratios are plotted on logarithmic x-axes, individually scaled for each panel. **A:** Sr/Ca ratio; **B:** Al/Nd ratio; **C:** Ce anomaly; **D:** REE slope; **E:** REE bulge, grey vertical line indicates a mid REE enrichment factor of 1.55; **F:** Eu anomaly. Note that significantly fewer Al/Nd ratios are available, as mentioned in section 3.2.

to approximately 1.55 in leaches that do not exhibit any signs of DC contamination (i.e. no low Sr/Ca ratios or unradiogenic Nd ICs). It will thus be assumed that Nd ICs associated to MREE/MREE* values lower than 1.55 may be contaminated by DC or associated detrital fractions. These data will therefore be ignored for the interpretation of deep water provenance. For Site U1302, the late Holocene signatures lie lower, approximately at 1.6 and the threshold value is accordingly adjusted down to 1.47, below which the Nd IC data are discarded. For the three leachates between 4 and 7 ka of Site U1302, no elemental data are available and they will therefore also be excluded from further interpretations regarding deep water mass provenance (see Fig. 6.3). Data from sites U1314 or U1304 are not affected by this truncation. Obviously, most glacial data from Site U1302, and several from Site U1305 are discarded this way, including all of the most unradiogenic data points (c.f. Fig. 6.3 and Fig. 6.6). This truncation method based on the mid REE bulge is not very exact, and a potential correction in order to retrieve the original authigenic Nd ICs is therefore not attempted. Furthermore, the remaining glacial data points at sites U1302 and U1305 need to be assessed with caution, firstly because the determination precision of MREE/MREE* itself lies in the order of 0.1 units, equating 3 epsilon units of Nd IC shift according to the linear fit in Fig. 6.4. And secondly because the authigenic end member may have shifted due to changes in water mass provenance or weathering, even though it appears to be relatively stable through time for all investigated subpolar sites (Fig. A.12).

Contamination by other detrital fractions

Apart from the influence of DC, no other indications of detrital contaminations can be found in the leachate records. Al/Nd ratios are generally relatively low and do not appear to correlate with Nd ICs, except for low values in samples with DC contamination (see Fig. 6.5, and Fig. A.10 and Fig. A.12 in the appendix). At sites U1314 and especially U1304, Al contents are often below the limit of quantification (and thus not shown). Eu contents from Site U1304 are significantly depleted in some leaches, but these low values are spread across the record and do not covary with Nd ICs, suggesting no influence on the latter's interpretation. Furthermore, while there is some similarity in the trends of the Nd ICs in leachates and clay fractions of nearby sites, the absolute values are generally not close to each other except at Site U1305 (Fig. 6.3). The generally similar trends of the Nd ICs in the clay fractions and the leaches could indicate a leaching of the detrital fraction at first glance. Alternatively, both could well be rooted in deep water circulation changes, which is in line with the original interpretations of the clay records (Fagel *et al.* [1999, 2004]; Fagel and Mattielli [2011]). Furthermore, the absolute differences in Nd ICs between clay and leached fractions at the four sites are very different and variable, and the Nd ICs of clays and leaches at Site U1305 decouple during two sedimentation events at around 8 and 10.5 ka. Therefore, the similar trends in clay and leachate data do probably not imply an influence of the detrital fraction on the leach-extracted Nd. Finally, leached Nd ICs do not covary with the amount

of volcanic glass particles at Site U1304. A contamination through the leaching of volcanic material is therefore also unlikely.

6.4.2 Changes in past deep water provenance

The remaining data after eliminating leachates with a probable DC contamination are shown in Fig. 6.6 and will be assumed to reflect the evolution of deep water mass provenance at the four sites. For the following interpretations it is important to keep in mind that the age models behind these data are relatively coarse in most core sections. Significant variations of sedimentation rates, especially at the drift sites, could result in considerable unaccounted horizontal shifts in the data. Nonetheless, the major features of the four profiles are clear and sufficiently constrained by the available age models.

Recent Nd IC at the three eastern sites

In order to discuss the past Nd IC evolution, the modern situation and how it is reflected in the core top sediments needs to be understood first. Sites U1305, U1314, and U1304 all exhibit very similar Nd ICs between -8 and -9 in the uppermost sediment layers. The two Gardar Drift sites U1314 and U1304 are bathed by the same water mass, and the similar signatures thus indicate strong advection of ISOW from Site U1314 to U1304. The slight offset of approximately 0.5 epsilon units towards a less radiogenic signature at the deeper Site U1304 may indicate an addition of LDW to the prevailing NEADW ($\approx 12\%$ LDW admixture). Such an admixture of LDW fits into the picture of an evolving NEADW east of the Reykjanes ridge. Although the core top Nd IC at Site U1305 is very similar (average of the two samples in the uppermost 5 cm: $\epsilon\text{Nd} = -9.3$), it is important to keep in mind that this site is bathed by a different water mass today (NWABW). As discussed above in section 6.4.1, these three sites all exhibit core top Nd ICs more radiogenic than seawater measurements would suggest. These more radiogenic signatures could indicate that the archived Nd is more representative of the actual overflow waters ISOW and DSOW instead of NEADW and NWABW respectively, to which they contribute a major portion. Possibly, more pristine overflow signatures are preserved and transported right at the sediment interface than several 10s of meters above, where the water samples were taken.

Deep water mass evolution in the late glacial

During most of the late glacial, the LGM, and also in the early Holocene the two Gardar Drift sites U1314 and U1304 recorded Nd ICs that were more different from each other than they are today. A larger difference between these two sites can probably be related to increased advection of LDW to the lower site. This can be caused by a weakening of ISOW or its shallowing so that the deeper site received less of this water mass or none at all. Similar reasoning was given by Kissel *et al.*

[2013] for magnetic particles transported by ISOW and by Elmore et al. [2015] for benthic $\delta^{13}\text{C}$ archived in foraminifera for the difference in these characteristics between central and deep Gardar Drift sites.

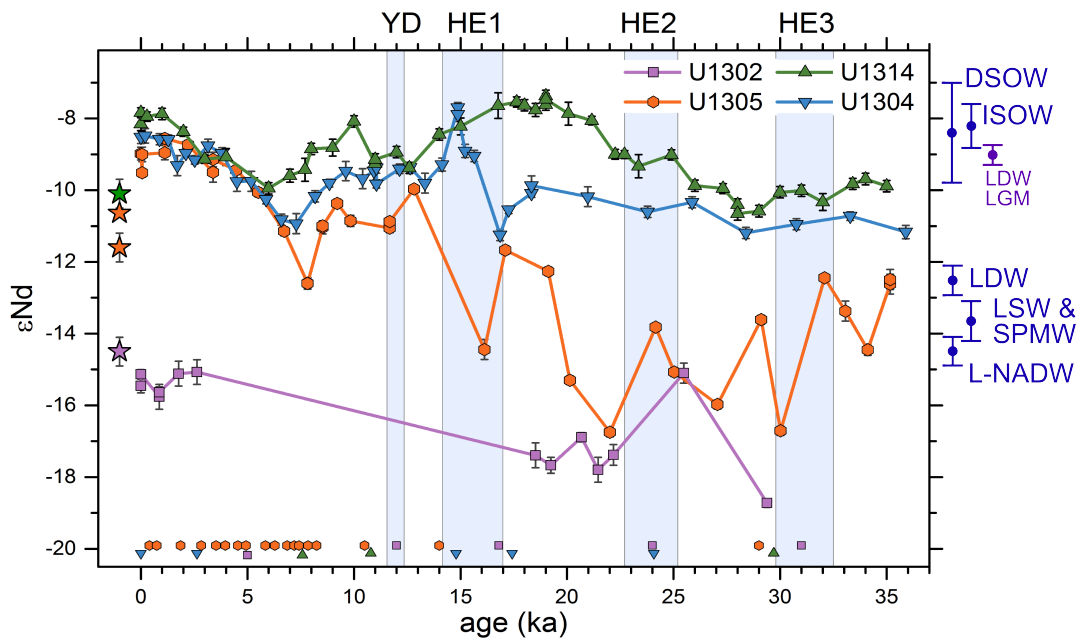


Figure 6.6: Authigenic Nd ICs profiles from the four subpolar sites. Data with low MREE/MREE* ratios from sites U1302 and U1305 were removed as they may be contaminated, as described in the text. Stars indicate Nd ICs of nearby deep water measurements. Symbols at the lower axis mark age tie points. Blue vertical bars indicate approximate ages of Heinrich and Younger Dryas Events. The ranges given in blue at the right y-axis indicate the Nd ICs of the relevant water masses today (Lacan and Jeandel [2005a]) and of LDW during the LGM.

The difference in authigenic Nd ICs, $\Delta\epsilon\text{Nd}$, between Sites U1304 and U1314 was small ($\Delta\epsilon\text{Nd} \approx -1$) but persistent during the late glacial between 35 and 25 ka (Fig. 6.7). Following the abovementioned reasoning, this difference indicates that ISOW was slightly weaker and/or shallower during the last glacial than today. This difference significantly increases to -3 during the LGM and then further increases and culminates at -4 right before HE1 at the end of the last glacial. Afterwards follows a rapid decrease towards zero difference in less than two thousand years during the start of the deglaciation. This pattern is accordingly interpreted as a further shallowing of ISOW during the LGM, combined with a northward penetration of LDW. Around 16.8 ka ISOW rapidly resumes to interglacial strength so that it dominates both Gardar sites. Importantly, the fast resumption is dominated by changing authigenic Nd ICs in the sediments from Site U1304, whose ages are constrained by two tie points in this depth range. The interpretation of a shallowing ISOW and increasing volume of southern sourced waters in the Iceland Basin is in agreement with studies based on stable isotopes and ocean climate models (Yu et al.

[2008]; Elmore et al. [2015]; Marson et al. [2015]). However, $\Delta\epsilon\text{Nd}$ may not reflect the shallowing of ISOW quantitatively, since once Site U1304 does not receive any more ISOW, the Nd ICs between sites U1314 and U1304 are decoupled and could evolve independently.

Specifically, Elmore et al. [2015] made similar investigations in a compilation of seven sites along the Gardar Drift based on stable carbon isotopes in benthic foraminifera, but they did not record such a rapid resumption of ISOW depth. This may in part be caused by much larger scatter in the reconstructed carbon isotopes, or it may be a true difference in the records. It could then be caused by secondary processes affecting one or both of these tracers. For carbon isotopes this could be a seawater temperature change or nutrient supply effect, for example, and for Nd a change in the isotopic signatures of the prevailing water mass at Site U1314 simultaneous to convection depth might be involved (see section 6.4.2).

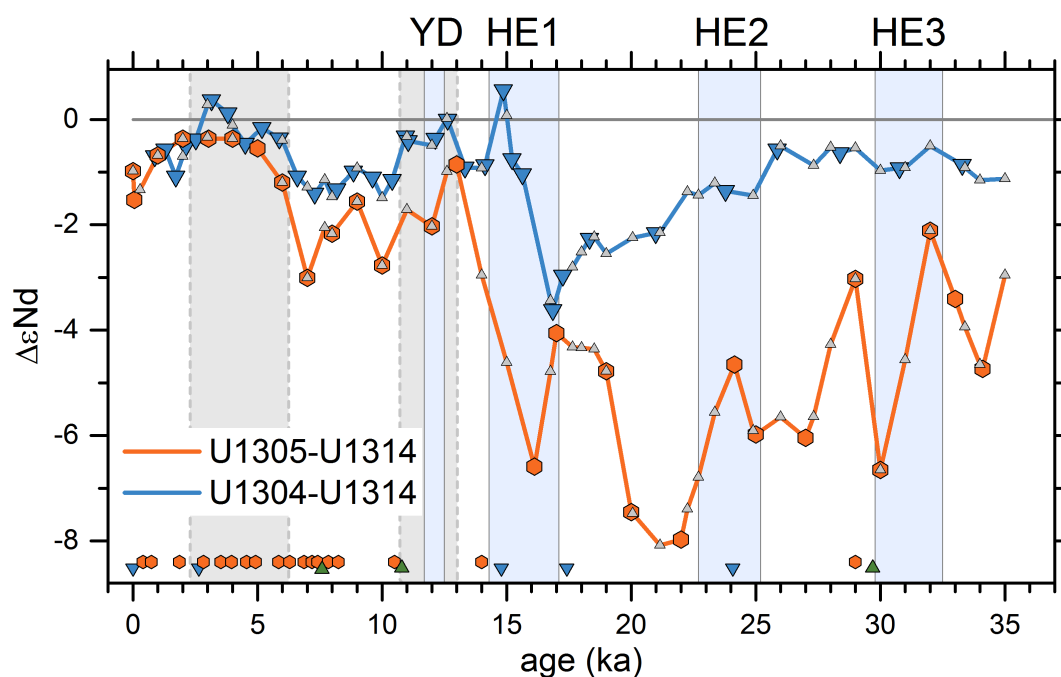


Figure 6.7: Difference in leachate ϵNd between sites U1305 and U1314, and sites U1304 and U1314. The data are linearly interpolated in order to subtract ϵNd values for unequal ages, the temporal resolution thus appears higher than it actually is. Orange and blue symbols indicate positions of measured data from U1305 and U1304, small grey triangles mark positions of measured data from Site U1314. Symbols at the lower x-axis mark age tie points. Blue vertical bars indicate approximate ages of HEs. Grey vertical bars mark time intervals in which sites U1304 and U1314 exhibit equal Nd ICs.

The authigenic Nd ICs of Site U1305 during the last glacial were significantly more unradiogenic than today (Fig. 6.6). They were also much closer to those from Site

U1302 and more different to those from the Gardar sites between 26 and 19 ka than they are today. This has two implications: Firstly, neither modern-like DSOW nor ISOW can have reached the deep Labrador basin similar to today during the end of the last glacial period, since they would have supplied radiogenic Nd. If there had been active DSOW supply, then it would have had to be much less radiogenic than today (ϵNd between -13 and -16). The active convection of less dense DSOW underlain by a local water mass is not excluded. This result is in accordance with conclusions from Fagel *et al.* [2002]. Additionally, Millo *et al.* [2006] inferred a shallower DSOW in the Irminger Basin during the LGM. Secondly, there was probably a regional exchange of water between the two Labrador sites, since their authigenic Nd isotope signatures are quite similar. If there had been no exchange of water between these two sites, the intrusion of relatively radiogenic southern sourced water would probably have led to a larger difference across the Labrador Basin. Fagel *et al.* [1999] drew a similar conclusion from their clay provenance study.

Recently, Keigwin and Swift [2017] found evidence for the presence of a Glacial North Atlantic Bottom Water (GNABW) mass during the late glacial, which must have been denser than local Glacial Antarctic Bottom Water. GNABW thus apparently flooded the deepest part of the Northwest Atlantic Basin. Similarly, Howe *et al.* [2016b] found indirect evidence for a glacial northern sourced deep water mass that must have supplied unradiogenic Nd to the deep Atlantic ocean during the LGM. Taking the above observations from the Labrador Sea into account, it can be estimated that any glacial bottom or deep water mass formed in or traversing the western subpolar North Atlantic probably exhibited a Nd IC between -15 and -18 . This estimation is thus in accordance with the conclusions of Howe *et al.* [2016b] and would allow for a reliable identification of this water mass employing authigenic Nd isotopes in the abyssal Northwest Atlantic.

Radiogenic imprint in the eastern subpolar North Atlantic during the LGM

Site U1314 exhibits a broad peak in Nd IC during the LGM and into the deglaciation of about two epsilon units above the signatures before and after the LGM. The exact time interval of this peak, however, is poorly constrained, with the closest age-depth tie points at 11 and 30 ka. The peak radiogenic Nd IC during this interval is -7.4 . This broad radiogenic excursion closely resembles the one at Site U1308 (from chapter 5) and at five sites across the depth transect from 1100 to 4000 m at Rockall Bank reconstructed by Roberts and Piotrowski [2015] (see map in Fig. 6.1 and data in Fig. 6.8).

Manighetti and McCave [1995] and Yu *et al.* [2008] reconstructed local flow speeds with particle size measurements and local water mass carbonate and nutrient contents with B/Ca and $\delta^{13}\text{C}$ in foraminifera, respectively, from the same BOFS cores around Rockall Bank. Both studies found that the southern sourced waters occupied a larger volume during the LGM, i.e. that the interface between southern and northern water masses shallowed. Yu *et al.* [2008] assessed that the boundary must have been at around 2.8 km water depth. Directly above this boundary, the

lower portion of Glacial North Atlantic Intermediate Water (GNAIW) was mainly formed by carbonate ion rich and ^{13}C depleted overflow waters. Since the records of Roberts and Piotrowski [2015] exhibit radiogenic Nd ICs throughout the water column during the LGM, these results were not in accordance with established theories of unradiogenic northern and radiogenic southern water masses. After critically excluding local artefacts from their samples and sites, Roberts and Piotrowski [2015] concluded that the cause for this radiogenic homogenisation throughout the depth transect must have been a 'radiogenic relabelling' of the local water masses due to increased flux of radiogenic IRD during the LGM and HEs. This would mean that Nd isotopes cannot be used to trace different water masses in this area between 30 and 15 ka.

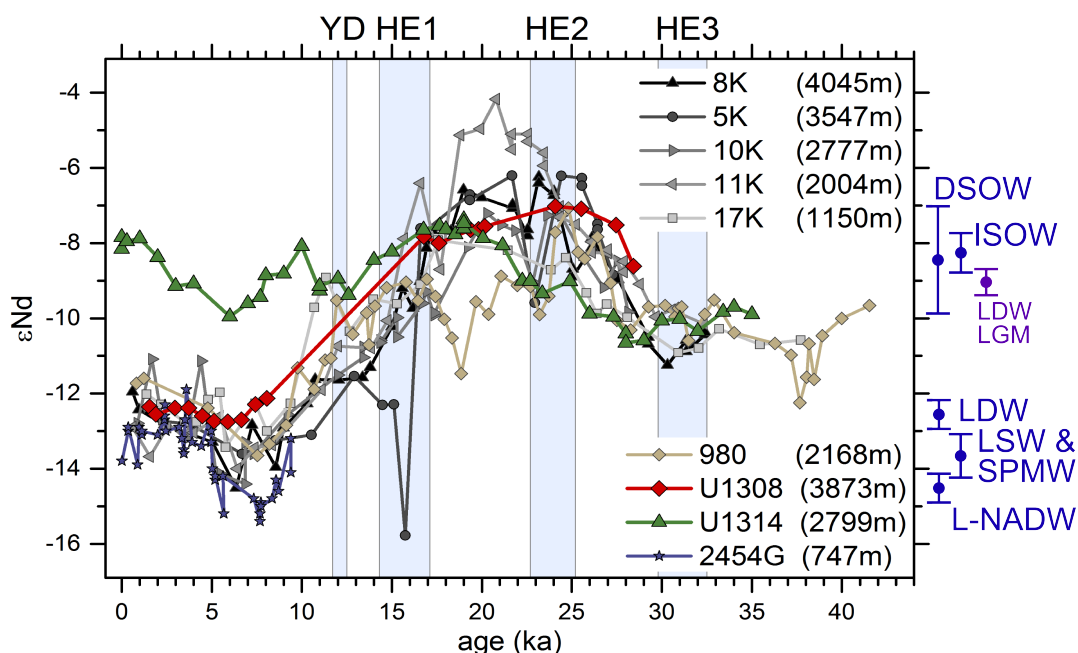


Figure 6.8: Compilation of authigenic Nd isotope records around Rockall Bank in the eastern North Atlantic. See map in Fig. 6.9 for the exact site locations. Records from BOFS 8K, 5K, 10K, and 17K are based on foraminifera from Roberts and Piotrowski [2015] and span a depth transect from 4045 to 1150 m. The record from site 980, situated in the Rockall Trough east of Rockall Bank, is also based on foraminifera (Crocker et al. [2016]). The deep sea coral record from Colin et al. [2010] is from core MD01-2454G, on the Rockall Bank slope above site 980. For the data from U1308 contaminated samples of HEs 1 and 2 and the ash turbidite were excluded. The unradiogenic excursions from BOFS cores 8K and 5K may be due to residual contamination in the foraminifera samples (Roberts and Piotrowski [2015]). Blue vertical bars mark Heinrich and Younger Dryas Events. The ranges given in blue at the right y-axis indicate the Nd ICs of the relevant water masses today (Lacan and Jeandel [2005a]) and of LDW during the LGM. See Table A.1 for a complete list of the sites.

This interpretation, however, is hard to reconcile with the conclusions from chapter 5. There it was clearly demonstrated that overprinting of the local seawater Nd IC is not simply achieved by the deposition of large amounts of volcanic particles in the water column. And large deposition events of volcanic material over a wide area are not reported for this time in the Iceland Basin and around Rockall Bank. The analysis in chapter 5 showed that a release of Nd from the detrital fraction is much more likely if it is dispersed in the sediment than while it is exposed to open seawater. In their investigation of core top Nd ICs in foraminifera, [Palmer and Elderfield \[1985\]](#) and [Elmore et al. \[2011\]](#) report Nd ICs extracted from foraminifera directly south of Iceland at almost 2 km depth that are far too radiogenic to represent pure local deep water ($\epsilon\text{Nd} = -5.6$ and $\epsilon\text{Nd} = -2.3$). This suggests that on the eastern Reykjanes Ridge near the southern Iceland margin, the authigenic Nd fraction intensely interacts with the detrital fraction already in the surface sediments, similar to the process in the ash turbidite at site Me68-91 (section 5.4.2). While this does not seem to have an impact on the seawater Nd IC under today's vigorous circulation regime, it could have been different during the Last Glacial Maximum. Furthermore, with the new Nd IC records from four sediment cores in the northern Northeast Atlantic, the region which is influenced by this effect can be constrained to the Iceland Basin, Rockall Bank, and the deep East Atlantic basin towards the Mid Atlantic Ridge (red numbers in the Fig. 6.9).

In principle, a change in the Nd IC of ISOW could have delivered more radiogenic Nd to the eastern subpolar North Atlantic. If these waters sank to depths between 2.8 and 2 km, this would explain the largest amplitude of the radiogenic LGM excursion at around 2000 m depth at Rockall Bank. The problem of this mechanism, however, is that it cannot explain how this radiogenic Nd was transported to 4000 m water depths if the radiogenic water mass was underlain by southern sourced waters. However, if the advance of southern sourced water was sluggish during the LGM, a modification of its Nd composition would have been more easily accomplished than today. Similarly, if the density difference of the southern and northern water masses was small, mixing would have been promoted.

Another possibility is that the water mass identified as overflow waters by [Yu et al. \[2008\]](#) was actually dominated by in situ deep convection near the South Iceland margin. Such local deep convection would have been rather susceptible to reactive volcanic phases and a possible benthic flux of radiogenic Nd from the marginal sediments south of Iceland. Furthermore, if the source waters were not surface waters in direct exchange with the atmosphere, but deep surface or shallow intermediate waters, the oxygen content of this water mass could have been relatively low and CO_3^{2-} content high (as reconstructed by [Yu et al. \[2008\]](#)), which would have further enhanced the release of Nd from sediment. However, [Thornalley et al. \[2011a\]](#) found that the deep water in this region exhibited ^{14}C ventilation ages of up to 3000 years, i.e. was very old. While this circumstance could explain the high carbonate ion content, it is hard to imagine an in situ formed deep water mass with such high ventilation ages. Therefore, aged overflow waters as proposed by [Thornalley et al. \[2015\]](#) or a mixture of overflow and local deep convection may be more realistic as a

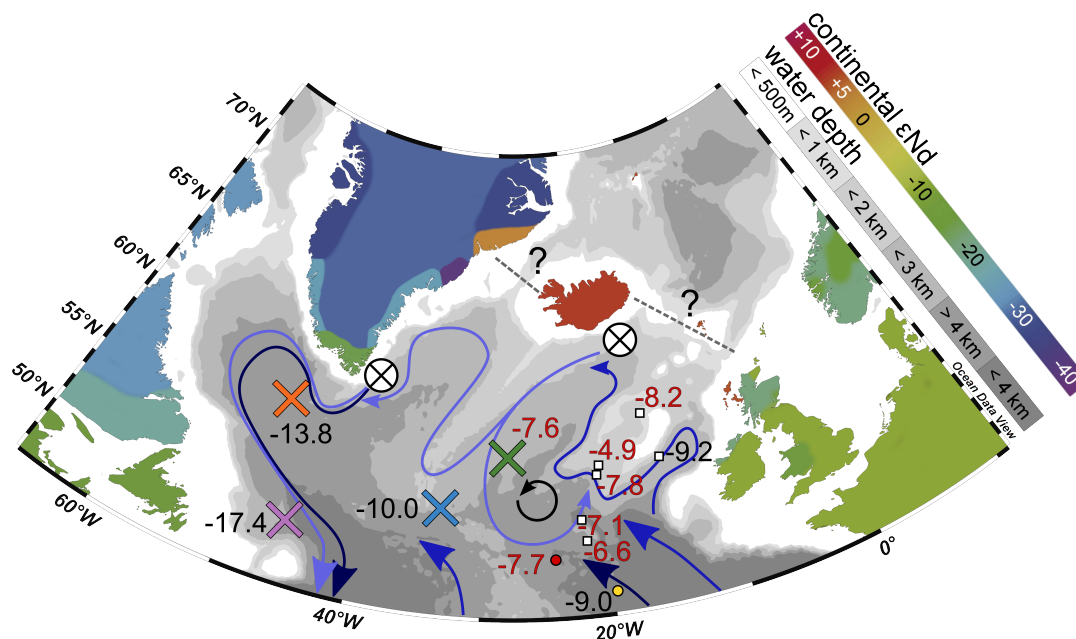


Figure 6.9: Map of the subpolar North Atlantic with Nd isotope compositions in sediments during the LGM and a possible LGM circulation pattern. White crossed circles mark areas of deep water convection. The sites and Nd IC values from the eastern North Atlantic are from Roberts and Piotrowski [2015] and Crocker et al. [2016], and site Me68-91 from chapter 5. The coloured crosses mark sites U1302, U1304, U1305, U1308, and U1314. See Fig. 6.1 for site names.

candidate for intermediate water supply in the Northeast Atlantic during the LGM. It can be hypothesised that this Intermediate Water incorporated radiogenic Nd from the South Iceland margin, sank to depths between 2.8 and 2 km and advanced southward to at least 50°N in the eastern North Atlantic basin. There, its imprint on the deeper water by successive modification could explain the radiogenic Nd ICs in the eastern subpolar North Atlantic between 1000 and 4000 m depth.

Subpolar deep water evolution during the deglaciation and early Holocene

Taking into account uncertainties of the age models and interpolation between individual data points, the authigenic Nd IC at Sites U1304 and U1314 remained basically equal between 15 and 11 ka (Fig. 6.7). The similar signatures imply that ISOW flow remained strong and deep throughout this interval. This is surprising since North Atlantic freshwater discharges associated with Heinrich Events and the Younger Dryas are often brought into relation with reduced deep water production and a resulting tailback in the northward transport of surface waters, as well as a northward penetration of southern sourced deep water (e.g. McManus et al. [2004]; Millo et al. [2006]; Thornalley et al. [2010]; Marson et al. [2015]). On the other hand, between approximately 11 and 6 ka, the difference in authigenic Nd ICs between the two Gardar sites was around -1.2 epsilon units, implying weaker ISOW

again. In this time range, works on other proxies suggest a strengthening of ISOW and NEADW (Fagel et al. [2004]; Thornalley et al. [2013]).

The apparent contradiction could be caused by a change in the composition of the southern sourced end member. Sites BOFS 8K and 5K recorded the Nd IC of the local LDW (and its modification during the LGM, see Fig. 6.8). These evidence that the shift from radiogenic LGM to modern signatures occurred in the time interval between approximately 17 and 8 ka. Between 15 and 11 ka, both ISOW and local LDW exhibited similar and concurrently changing Nd ICs (1 to 2 epsilon units offset, compared to more than 4 today). Between 11 and 6 ka, the difference between LDW and ISOW rapidly increased, making the Gardar site gradient more sensitive to ISOW advection strength and depth. Furthermore, as stated earlier, the age model of Site U1314 before 11 ka is rather badly constrained. Thus, an interpretation of the Nd IC gradient at the Gardar sites during the deglacial is problematic at present.

The authigenic Nd isotope signatures at Site U1305 became much more radiogenic during the deglacial interval. This evidences an increasing supply of radiogenic Nd by a dense water mass. Most likely, this supply was carried by a strengthening dense DSOW. However, it could also be caused by a deepening NEADW reaching the site in the absence of DSOW. These two possibilities cannot be distinguished with the present data set.

Subpolar deep water evolution during the mid to late Holocene

The seawater Nd isotope record from Site U1305 exhibits a distinct unradiogenic excursion at around 8 to 8.5 ka. At this time, the last large freshwater outflow from the melting of glacial ice sheets arrived in the North Atlantic in the form of the final drainage of Canadian glacial lakes Agassiz and Ojibway (Barber et al. [1999]; Hillaire-Marcel et al. [2007]). The event is also concurrent with moderately increased detrital input at the location of Site U1305 (Fagel et al. [2004]). However, element data do not suggest a significantly increased contamination in the leachate by this detrital event at Site U1305. Furthermore, Kissel et al. [2013] interpreted a distinct signal at sites near the western end of the Charlie-Gibbs Fracture Zone as a period of weakened bottom circulation caused by the increased freshwater flux during this event. The unradiogenic data could thus indeed indicate a change in bottom water Nd IC, caused by decreased presence of overflows.

By 7 ka sites U1305 and U1314 acquired equal Nd ICs, and by 6 ka this counts for all three eastern sites (Fig. 6.6). Even after this spatial homogenisation, however, all three sites still underwent a transient evolution of increasingly radiogenic Nd ICs. This trend towards radiogenic signatures led to a change in ϵNd of 4 units between 8 ka and today for Site U1305, and about 2.5 and 2 epsilon units for Sites U1304 and U1314, respectively, within shorter durations. Other proxies indicate that by 8 ka, the modern circulation regime was essentially established (e.g. Sarnthein et al. [1994]; Ledbetter and Balsam [1985]), including active deep water formation of LSW (Hillaire-Marcel et al. [2001]). Therefore, the three sites were probably already bathed by the same water masses as today. On the other hand, Thornalley et al.

[2013], for example found evidence for a weakening ISOW after 8 ka, and Kissel et al. [2013] for reducing NEADW and NWABW flow speeds between 6 and 2 ka.

The trend from relatively unradiogenic towards radiogenic Nd ICs at Site U1305 followed by the Gardar sites resembles the evolution in the abyssal Northwest Atlantic, where seawater Nd ICs increased by 2.4 epsilon units from ≈ 8.5 ka to today (Fig. 6.10). This suggests that whatever caused the isotopic shift in the overflows is also responsible for the similar shift in the lower part of the evolved NADW in the North Atlantic. Contrary to what Howe et al. [2016c] concluded, this unradiogenic signal therefore does not represent a local signal emerging from a post-glacial weathering pulse in the Labrador Sea, but was cycled throughout the subpolar North Atlantic. This modification was probably significantly weaker at intermediate depth in the North Atlantic due to mixing with the overlying LSW. There are two possibilities to explain these changes in NEADW and NWABW. Firstly, the relative contribution of the unradiogenic source water mass may have decreased over time. The unradiogenic end member sources are LSW and SPMW, which are entrained by the overflow waters from the Nordic Seas to form NEADW and NWABW. However, the entrainment of these waters cannot be independent from the overflow flux itself, which causes the entrainment. Today, entrained LSW/SPMW and pure overflow waters contribute to a comparable extent to the final overflows, and it is conceivable that this ratio was not completely different in the past. The least radiogenic signature at Site U1305 at around 8 ka (-12.6) would imply a LSW contribution of 86 % (assuming modern Nd end members). Unless LSW was deep enough to sink to a depth of 3500 m by itself, which is very unlikely given that other studies imply a circulation scheme similar to today, this contribution cannot be reached by pure entrainment. The other possibility is a change in the Nd IC of one or several of the end members. Since both NEADW and NWABW are affected by a similar shift in Nd IC, a change in a common end member is a likely cause. Thus, either LSW or a common source in the Nordic Seas can be considered. If only one of these two end members underwent the change in Nd IC, then it must have been approximately 4 epsilon units less radiogenic at around 8 ka than today, if the relative water fluxes and Nd concentrations remained constant.

Additionally shown in Fig. 6.10 is an exponential fit through the mid- to late Holocene data from sites U1305 and U1304. Naturally, this fit depends on the quality of the age models at these two sites. While the age model for Site U1305 is extraordinarily well constrained in this time period, only two age-depth tie points are available for Site U1304, and especially the onset of the transient Nd IC change is badly constrained. Based on the applied age models, the trend at Sites U1305 and U1304 is well reproduced by an exponential fit converging towards $\epsilon\text{Nd} = -8.5 \pm 0.3$ today. Such a converging exponential trend may be caused by a certain reservoir volume of water with unradiogenic Nd that is steadily flushed with a constant flux of modern-like, more radiogenic water.

On the other hand, Fig. 6.11 illustrates an antiparallel evolution of Iceland-Scotland Overflow strength reconstructed with a stacked sortable silt record (Thorvalley et al. [2013]) and the seawater Nd IC at the three eastern sites throughout

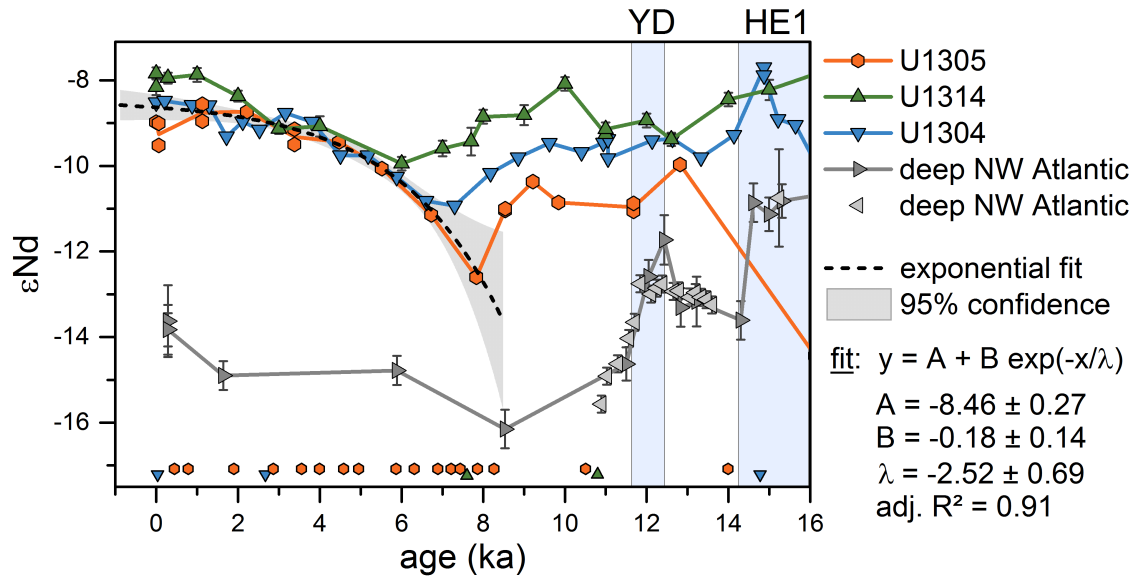


Figure 6.10: Nd IC records from the subpolar in comparison to the deep Northwest Atlantic during the Holocene and deglaciation. Results from the deep Northwest Atlantic (Bermuda Rise) are from Roberts et al. [2010] and Böhm et al. [2015]. An exponential curve was fitted to the data from Sites U1305 and U1304 between 7 and 0.8 ka. Symbols at the lower x-axis mark age-tie points. Blue vertical bars indicate the approximate ages of the Younger Dryas and Heinrich Event 1.

the Holocene. Overflow strength peaked around 7 ka and gradually decreased afterwards. The anti-correlation of overflow strength is strongest with the Nd IC record of the deep Gardar Drift Site U1304. However, a correlation of stronger overflow with more unradiogenic Nd isotope signatures is not self-evident. Thornalley et al. [2013] propose that the mid to late Holocene decrease in overflow strength was caused by changes in deep water convection in the Nordic Seas, which was weakened by surface freshwater export in the form of Arctic sea ice drift. Since overflow from the Nordic Seas provides the radiogenic end member of contemporary NEADW and NWABW, a reduction of this overflow export should not have yielded more radiogenic seawater signatures downstream. Hence, an easier explanation would be that both overflow strength and overflow Nd IC, and possibly Nd concentrations were controlled by the intensity of deep convection in the Nordic Seas. A stronger convection would thus have led to overflow with more unradiogenic Nd and/or lower overall Nd concentrations. The detailed effects causing the transient changes in Holocene Nd ICs of sites U1305, U1314, and U1304 are beyond this work, but their investigation in future studies may significantly enhance the knowledge of seawater Nd isotope systematics.

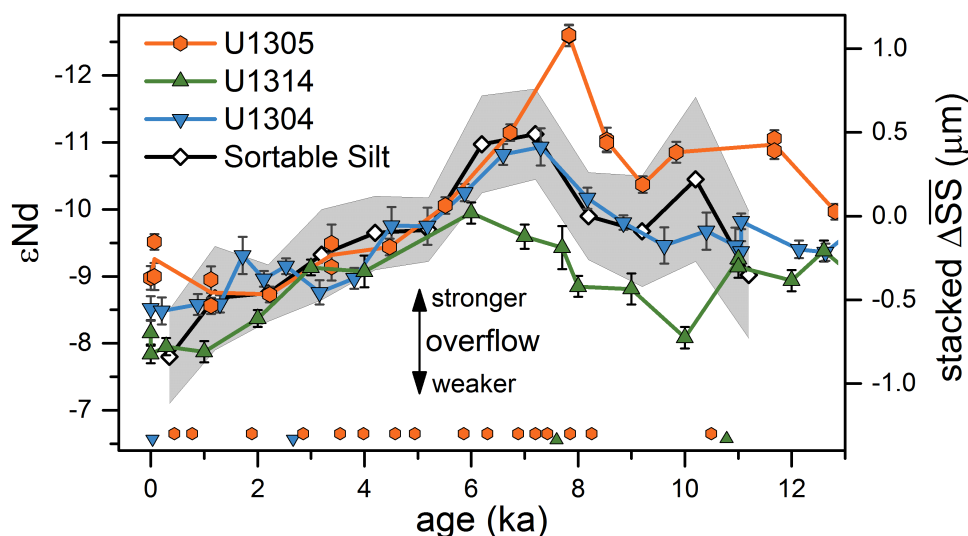


Figure 6.11: Comparison of subpolar authigenic Nd IC and Iceland-Scotland overflow strength during the Holocene. Leachate Nd ICs from sites U1305, U1314, and U1304 are plotted on an inverted y-axis. The black curve and grey surface are a weighted stacked record of sortable silt deviation and its 2SE uncertainty from Björn Drift north of Gardar Drift between 1200 and 2250 m depth from [Thornalley et al. \[2013\]](#). It indicates the relative current strength of ISOW, with higher values indicating stronger overflow. The peak in overflow strength clearly correlates with the most unradiogenic Nd ICs of the overflow, and its weakening is paralleled by the transient change towards more radiogenic Nd ICs.

6.5 Synthesis and summary

The four investigated records of deep water Nd IC exhibit a wide range of variations. Several conclusions can already be drawn from them, but further investigations at additional critical sites would greatly improve their interpretability by improving the boundary constraints. Furthermore, higher resolution age models could allow for more detailed interpretations, especially during the deglacial and early Holocene.

Unaffected by these shortcomings it was shown that these four records of authigenic Nd ICs spread across the subpolar north Atlantic already allow for several important conclusions which have not been published before. For example, the reduction of overflow waters during the peak glacial led to a stark separation between the eastern and western subpolar basins in terms of Nd isotopes. This has important implications for the formation of North Atlantic water masses and their Nd isotope budgets. For example, if there was a Glacial North Atlantic Bottom Water mass exported from the western subpolar North Atlantic as proposed by [Howe et al. \[2016b\]](#) and [Keigwin and Swift \[2017\]](#), then it would surely have had a very unradiogenic Nd IC, probably in the range of -18 to -15. Furthermore, it seems that the whole eastern subpolar North Atlantic was dominated by radiogenic Nd during the LGM. While the observations of chapter 5 and the now constrained spatial extent of this

radiogenic imprint suggest that the explanation given by [Roberts and Piotrowski \[2015\]](#) must be modified, it is still not clear how exactly this radiogenic Nd reached water depths of 4000 m. This calls for the implementation of Nd isotopes in regional ocean circulation and climate models in order to find a realistic explanation for this mechanism. Independent of the exact way of distribution, the presence of radiogenic water masses in the eastern basin implies that there must have been a counter weight of unradiogenic water masses prevailing in the western subpolar basin at intermediate depths in order to yield combined Nd ICs of glacial North Atlantic Intermediate Water that are not completely different from NADW today ([van de Flierdt et al. \[2006\]](#); [Howe et al. \[2016b\]](#)).

The Nd IC profiles in the section between Last Glacial Maximum and mid Holocene are rather hard to interpret at this point, probably due to small differences in Nd ICs of the prevailing water masses and possibly due to the lack of age model constraints of the two Gardar Drift sites. Therefore, an improvement of the age models in the relevant time range may significantly increase the value of these deglacial reconstructions. Furthermore, the Holocene data from sites U1305, U1314, and U1304 indicate that the origin of the mid-Holocene unradiogenic Nd isotope signatures in the deep Northwest Atlantic lies not in the Labrador Sea (as argued by [Howe et al. \[2016c\]](#)), but rather further upstream of the deep boundary currents. The most probable source is a change in the Nd IC of the overflow waters from the Nordic Seas.

7 Conclusion and Outlook

At the start of this thesis, conventional leaching techniques were clearly not suited to be applied to sediments of widely varying compositions, as was evidenced by the study on core top sediments of the North Atlantic by [Elmore et al. \[2011\]](#). Yet, in order to increase our understanding and the accuracy of interpretations of Nd isotopes as a proxy for palaeo water mass sourcing, their investigation in variable sedimentological environments is an important step. Since North Atlantic Deep Water and its glacial counterpart represent crucial actors both in the global climate system and in the systematics of seawater Nd isotopes, the detailed examination of archived authigenic Nd isotopes in their source region promises valuable insights. Thus, the subpolar North Atlantic with its complex hydrography and sedimentation patterns, and its sensitivity to climatic fluctuation was the focus of this work.

Summary

In the frame of this thesis, the extraction of authigenic Nd was improved, the understanding of sedimentary processes and their potential impact on the extraction and interpretation of Nd isotopes as a palaeo water mass tracer enhanced, and authigenic Nd isotopes of the past 35,000 years were investigated across the subpolar North Atlantic for the first time. In chapter 4, a detailed investigation of the distribution of Nd in deep sea sediments led to the improvement of an existing method for the extraction of authigenic Nd isotopes of [Gutjahr et al. \[2007\]](#). The analysis of progressive leaches in a suite of different sediments showed that radiogenic Nd from volcanic sources presents the dominating detrital source of Nd in sediments, even if volcanic material constitutes only a minor sediment fraction. This is of particular importance in the subpolar North Atlantic, where Icelandic volcanic material is disseminated into marine sediments.

Another problematic sedimentary phase is detrital carbonate, which can easily contaminate bulk sediment leachates. However, with the supporting analysis of different element concentrations in the leachates, the imprint of such detrital phases can be detected. Thus, the refined weak leaches applied to non-decarbonated bulk sediment are a promising technique to extract authigenic Nd from a large variety of sediments efficiently and verifiably. This was demonstrated throughout chapters 4 to 6. It was furthermore shown that the Al/Nd, Sr/Ca, and different rare earth element ratios trace the contribution of detrital sources to the leachates. In particular the mid REE bulge proved to be a valuable parameter for the detection of contaminating influences from detrital carbonate and associated phases. Due to the versatile composition of deep sea sediments, these elemental proxies are interpreted most accurately when assessed in a broader context. Thereby, their relative trend can

be compared with sedimentological and Nd isotopic variations, which strengthens the quantification of detrital contribution to the leachate. Therefore, the leaching method is best suited for the generation of downcore profiles in individual sediment cores, rather than 'time slice' studies, investigating one short age interval at many different sediment sites.

Another important step was the detailed investigation of the effect of high detrital particle fluxes on seawater and pore water, as well as the mobility of Nd in the sediment column. The observations in chapter 5 showed that there can be intense exchange between labile detrital fractions and the remaining sediment with regard to Nd isotopes. In the presented sediment cores from the Northeast Atlantic, archived authigenic Nd ICs were overprinted by exchange of Nd with the detritus inside different detrital layers. Importantly, while this exchange could be reliably traced in the case of Heinrich IRD layers, elemental proxies failed to accurately track the contribution of radiogenic Nd from volcanic sources in an ash turbidite. Nonetheless, it could be demonstrated that Nd derived from detrital particles did not have a significant impact on the seawater Nd IC during times of increased particulate flux through the water column, nor while detrital layers were exposed at the sediment surface. Therefore, such detrital deposition events represent rather confined local sources for detrital contamination, without regional imprint on seawater Nd ICs. The generally vigorous Atlantic Overturning Circulation is a key factor for the insensitivity to regionally confined fluxes of detrital Nd. This presents an important difference to the situation in the marginal Northeast Pacific, for example. Importantly, vertical diffusion of Nd in the pore water column could be excluded both from the layers with detrital Nd imprint and under strongly reducing conditions. This is a crucial observation because it limits the imprint of detrital Nd to specific sediment layers.

Finally, four profiles of reconstructed deep water Nd ICs spanning the last 35 ka were discussed in chapter 6. A significant fraction of the data extracted from Labrador Sea sediments had to be excluded from the interpretation of deep water provenance because of significant detrital contamination in the leachates. Nonetheless, the remaining data of all four sites yield a coherent picture in general accordance with the results from other studies and, importantly, from other proxies. Together with the investigations by [Roberts and Piotrowski \[2015\]](#), the new data indicate that the generally radiogenic signatures in the Northeast Atlantic during the LGM was caused by the development of a regional southward stretching intermediate depth circulation cell carrying highly radiogenic Nd. Furthermore, during the mid to late Holocene, Nd isotope signatures of NEADW and NWABW went through a parallel transition towards more radiogenic imprint. This concurrent change was probably caused by a shift in the Nd IC of the source waters in the Nordic Seas and provides the first direct evidence for the cause of simultaneous changes observed in the deep Northwest Atlantic ([Roberts et al. \[2010\]](#)). Interestingly, this result is in direct contrast to a recent study claiming that the cause for this imprint of unradiogenic Nd in the deep Northwest Atlantic lies in Labrador Sea sediments ([Howe et al. \[2016c\]](#)).

Remaining questions about the extraction of archived seawater-derived Nd

Today, the leaching method for the extraction of authigenic Nd from bulk sediment is more efficient, more widely applicable, and better verifiable than at the start of this thesis. It is now possible to extract an authigenic Nd signal from sediments of considerably varying compositions. This will allow a rapid advance in our understanding of Nd isotopes in the environment and in their quantitative interpretation for the reconstruction of past water mass provenance and concomitant changes in ocean circulation. As was mentioned in subsection 2.1.2, static proxies like radiogenic Nd isotopes profit particularly from their wider spatial and temporal reconstruction, because this allows for more detailed investigations and quantifications of their variabilities and fluxes. Furthermore, it makes their implementation in general ocean circulation models more valuable. The spatio-temporal advancement of reconstructions based on authigenic Nd isotopes is thus not only necessary to access new regions and time intervals, but also leads to an improvement of the proxy itself. Yet, the leaching method can probably still be improved. The investigation in chapter 4 indicated that leaching at a higher pH, for example, may further decrease the susceptibility to volcanic contamination. Reducing the ratio of leaching solution volume to sediment mass, as proposed by [Wilson et al. \[2013\]](#), may have a similar effect. However, it should be noted that the elemental concentrations and concentration ratios extracted with a further modified leaching method can be considerably different from those presented here (c.f. Fig. A.16). Finally, the precision of the elemental abundance determinations could be significantly increased if desired. This can be achieved through longer measurements or an additional measurement run at lower dilution as described in subsection 3.2.1. Alternatively, the uncertainty introduced by sample treatment could be reduced by spiking the leaching solution with one or several elements that are not naturally abundant in the leachates. Inaccuracies from pipetting or sample evaporation could thus be corrected for.

There remains one profound problem with the reconstruction of bottom water Nd isotope signatures from sediments in the subpolar North Atlantic and possibly from other regions. As discussed in subsection 4.3.3 and section 6.4.1, the reconstructed Nd ICs from both foraminifera, and Ac and HH-leaches does not exactly match those measured in the surrounding bottom water, even if the water sample was taken 'directly' above. This could indicate that the ferromanganese fraction archives a pore water Nd signal with influence of detrital Nd rather than a pure bottom water signal. However, apart from the extreme detrital layers in the Northeast Atlantic and Labrador Sea, authigenic Nd ICs extracted with weak leaches do not show a significant covariation with the presence volcanic particles or changes in sediment provenance (see Fig. 6.3). Hence, the systematics of this difference between authigenic sedimentary and true bottom water Nd ICs remain unclear and their investigations are of highest importance for the detailed interpretation of archived Nd isotopes. The best way to find the cause for this difference probably is the parallel analysis of authigenic sediment fraction, pore water, and directly overlying seawater applying a multicorer system in the subpolar North Atlantic, as has been

done in the Southwest and Northeast Pacific (Molina-Kescher et al. [2014]; Abbott et al. [2015a]).

Further reconstructions of past seawater Nd ICs

The discussion in chapter 6 was repeatedly limited by the knowledge of the past Nd IC of overflow waters from the Nordic Seas. In fact, the presented results strongly suggest that the overflow Nd ICs changed over time. Since these overflows are one of the major sources for deep water in the subpolar region and consequently for NADW, their characterisation in terms of Nd ICs is essential for more detailed interpretations. Lacan and Jeandel [2004a,b] showed that the Nd ICs of the different water masses in the Nordic seas are modified through exchange of Nd with the surrounding margins prior to overflowing into the subpolar North Atlantic. Combined with the diverse Nd ICs of the marginal continents around the Nordic Seas, ranging from $\epsilon\text{Nd} \approx -35$ in East Greenland to $\epsilon\text{Nd} \approx -15$ in Scandinavia to $\epsilon\text{Nd} \approx +7$ on Iceland and the basaltic formations around it (Jeandel et al. [2007]; Lacan and Jeandel [2004b]), the Nd IC of the water masses in the Nordic Seas could have varied considerably in the past. In particular during past glacial periods, when glacial physical erosion delivered chemically unweathered detrital material and water exchange with the North Atlantic was limited, the Nd IC of Nordic Sea water masses may have been completely different from today. If weaker Atlantic surface currents around Iceland delivered less Icelandic detrital material into the Nordic Seas, it can be hypothesised that such a change in dissolved Nd IC may have been towards more unradiogenic signatures, which would generally agree with the new Holocene profiles from the subpolar North Atlantic from section 6.4.2. Since the mid-Holocene unradiogenic Nd isotope signatures in the deep Northwest Atlantic seem to originate in the Nordic Seas, it is reasonable to suggest that the pervasive unradiogenic signatures during the last glacial are linked to the same processes (c.f. Fig. 2.3). Most of these unradiogenic excursions observed in the deep Northwest Atlantic during the last glacial have been identified to coincide with short recurring Greenland warm events recorded in ice cores, so-called Dansgaard-Oeschger events. Hence, the warm North Atlantic climate during these short episodes could have allowed for stronger deep convection in the Nordic Seas and flushed glacial unradiogenic Nd into the deep Northwest Atlantic, just as during the Holocene. Certainly, studies of the past Nd IC in the Nordic Seas could help answer these open questions. The corresponding work on several sites across the Nordic Seas has already been started.

In the subpolar North Atlantic, the investigation of more sites or a direct combination with other radiogenic isotope systems such as Hf or Pb could also close several knowledge gaps. For example, reconstruction of the Nd IC of intermediate water in the subpolar basins between 1000 and 2500 m water depth would allow to additionally constrain the Nd IC of the upper NADW, which is the only depth layer of NADW not investigated in this study. It could furthermore help to constrain the role of deep water formation in the Labrador and possibly Irminger Seas. As mentioned earlier, the pervasive radiogenic signatures in the eastern subpolar basin

during the LGM suggests that active deep water formation in the western basin occurred simultaneously and formed a counterbalance, so that the resulting Nd IC of GNAIW was not completely different from that of NADW (Foster et al. [2007]; van de Flierdt et al. [2006]). Such a process may be directly detected with the study of intermediate sites in the western subpolar basin. Furthermore, high sedimentation rates at several different drift sites across the subpolar North Atlantic allow for detailed high resolution reconstructions of the authigenic Nd ICs. Such studies may be especially rewarding at the Gardar Drift sites, since these sites seem to not suffer under the deposition of highly reactive detrital material, like detrital carbonate in the Labrador Basin. Finally, the very long sediment cores drilled with the IODP programme generally cover sediments from the past few million years, allowing the reconstruction of seawater Nd ICs across many glacial-interglacial cycles or beyond. The Eemian interglacial around 125 ka before present or the Marine Isotope Stage 11 interglacial at around 450 ka, for example, occurred under similar boundary conditions as today, but were both a few degrees warmer, and could therefore give insight into climate under sustained global warming. The reconstruction of deep water provenance in the subpolar North Atlantic during these warm stages could tell us how northern deep water formation can be affected by future climate change.

Additional information gained from sediment leaches

Apart from further reconstructions of Nd isotope provenance, the abundance and abundance ratios of several elements contained in the leachates also yield valuable information possibly justifying further investigation. The implemented measurements with the ICP-QMS are highly efficient and concentrations of many elements beyond those discussed in chapter 4 to chapter 6 are routinely quantified. Investigations of isotope fractionations of different transition metals such as Cu and Zn are being increasingly investigated in order to assess their applicability as proxies for nutrients in seawater or biological productivity (Little et al. [2014]). However, in order to be able to use such novel isotope systems comprehensively, the ocean's budget of these elements needs to be understood and constrained. The abundance of these elements in the authigenic fraction of ocean sediments and variations therein may help to solve this problem (see section A.5 in the appendix for first thoughts on this topic). As another example, the concentration of uranium in the authigenic fraction may contain information about the oxygen content of local deep water masses above the sediment. Similarly, the Ce anomaly supposedly reacts sensitively to the oxygen concentration (e.g. Roberts et al. [2012]) and may thus also help to constrain deep water oxygenation or, consequently, deep water mass age. Finally, the reconstruction of past seawater Nd concentrations, as opposed to isotope ratios, has not been achieved yet. The accurate quantification of the authigenic Nd flux into the sediment, possibly normalised to another authigenic element flux, could provide a way to assess changes in the Nd concentration of past seawater. Such quantifications are necessary for the establishment of true water mass mixing calculations and would thus allow for an actual quantification of past deep water provenance.

8 Publications of the author

The following published peer-reviewed articles have been authored or co-authored by Patrick Blaser as of 18th April, 2017. The contents of [Blaser et al. \[2016\]](#) were used in chapters 2 and 4, as is also stated there.

Böhm, E., J. Lippold, M. Gutjahr, M. Frank, **P. Blaser**, B. Antz, J. Fohlmeister, N. Frank, M.B. Andersen, and M. Deininger
2015. Strong and deep Atlantic meridional overturning circulation during the last glacial cycle. *Nature*, v. 517, no. 7534, p. 73–76, doi: 10.1038/nature14059.

Blaser, P., J. Lippold, M. Gutjahr, N. Frank, J.M. Link, and M. Frank
2016. Extracting foraminiferal seawater Nd isotope signatures from bulk deep sea sediment by chemical leaching. *Chemical Geology*, v. 439, p. 189–204, doi: 10.1016/j.chemgeo.2016.06.024.

Lippold, J., M. Gutjahr, **P. Blaser**, E. Christner, M.L. Ferreira, S. Mulitza, M. Christl, F. Wombacher, E. Böhm, B. Antz, O. Cartapanis, H. Vogel, and S.L. Jaccard
2016. Deep water provenance and dynamics of the (de)glacial Atlantic meridional overturning circulation. *Earth and Planetary Science Letters*, v. 445, p. 68–78, doi: 10.1016/j.epsl.2016.04.013.

9 Bibliography

- Abbott, A. N., B. A. Haley, and J. McManus
2015a. Bottoms up: Sedimentary control of the deep North Pacific Ocean's ϵ Nd signature. *Geology*, 43(11):G37114.1.
- Abbott, A. N., B. A. Haley, and J. McManus
2016. The impact of sedimentary coatings on the diagenetic Nd flux. *Earth Planet. Sci. Lett.*, 449:217–227.
- Abbott, A. N., B. A. Haley, J. McManus, and C. E. Reimers
2015b. The sedimentary flux of dissolved rare earth elements to the ocean. *Geochim. Cosmochim. Acta*, 154:186–200.
- Abouchami, W., S. J. G. Galer, and A. Koschinsky
1999. Pb and Nd isotopes in NE Atlantic Fe-Mn crusts: Proxies for trace metal paleosources and paleocean circulation. *Geochim. Cosmochim. Acta*, 63(10):1489–1505.
- Adkins, J. F.
2013. The role of deep ocean circulation in setting glacial climates. *Paleoceanography*, 28(3):539–561.
- Alvarez Zarikian, C. A., A. Y. Stepanova, and J. Grützner
2009. Glacial-interglacial variability in deep sea ostracod assemblage composition at IODP Site U1314 in the subpolar North Atlantic. *Mar. Geol.*, 258(1-4):69–87.
- Baas, J. H., J. Schönfeld, and R. Zahn
1998. Mid-depth oxygen drawdown during Heinrich events: Evidence from benthic foraminiferal community structure, trace-fossil tiering, and benthic $\delta^{13}\text{C}$ at the Portuguese Margin. *Mar. Geol.*, 152(1-3):25–55.
- Barber, D. C., A. Dyke, C. Hillaire-Marcel, A. E. Jennings, J. T. Andrews, M. W. Kerwin, B. Bilodeau, R. McNeely, J. Southon, M. D. Morehead, and J.-M. Gagnon
1999. Forcing of the cold event of 8,200 years ago by catastrophic drainage of Laurentide lakes. *Nature*, 400(July):344–348.
- Barker, S., T. Kiefer, and H. Elderfield
2004. Temporal changes in North Atlantic circulation constrained by planktonic foraminiferal shell weights. *Paleoceanography*, 19(3):1–16.

- Bates, S. L., K. R. Hendry, H. V. Pryer, C. W. Kinsley, K. M. Pyle, E. M. S. Woodward, and T. J. Horner
2017. Barium isotopes reveal role of ocean circulation on barium cycling in the Atlantic. *Geochim. Cosmochim. Acta*, 204:286–299.
- Bayon, G., C. R. German, R. M. Boella, J. A. Milton, R. N. Taylor, and R. W. Nesbitt
2002. An improved method for extracting marine sediment fractions and its application to Sr and Nd isotopic analysis. *Chem. Geol.*, 187(3-4):179–199.
- Bayon, G., C. R. German, K. W. Burton, R. W. Nesbitt, and N. Rogers
2004. Sedimentary Fe-Mn oxyhydroxides as paleoceanographic archives and the role of aeolian flux in regulating oceanic dissolved REE. *Earth Planet. Sci. Lett.*, 224(3-4):477–492.
- Birks, H. H., S. Gulliksen, H. Hafliðason, J. Mangerud, and G. Possnert
1996. New Radiocarbon Dates for the Vedde Ash and the Saksunarvatn Ash from Western Norway. *Quat. Res.*, 45(2):119–127.
- Blaser, P., J. Lippold, M. Gutjahr, N. Frank, J. M. Link, and M. Frank
2016. Extracting foraminiferal seawater Nd isotope signatures from bulk deep sea sediment by chemical leaching. *Chem. Geol.*, 439:189–204.
- Böhm, E., J. Lippold, M. Gutjahr, M. Frank, P. Blaser, B. Antz, J. Fohlmeister, N. Frank, M. B. Andersen, and M. Deininger
2015. Strong and deep Atlantic meridional overturning circulation during the last glacial cycle. *Nature*, 517(7534):73–76.
- Bonatti, E., D. E. Fisher, O. Joensuu, and H. S. Rydell
1971. Postdepositional mobility of some transition elements, phosphorous, uranium and thorium in deep sea sediments. *Geochim. Cosmochim. Acta*, 35:189–201.
- Bond, G., W. S. Broecker, S. Johnsen, J. McManus, L. Labeyrie, J. Jouzel, and G. Bonani
1993. Correlations between climate records from North Atlantic sediments and Greenland ice. *Nature*, 365(6442):143–147.
- Bond, G., H. Heinrich, W. S. Broecker, L. Labeyrie, J. McManus, J. T. Andrews, S. Huon, R. Jantschik, S. Clasen, C. Simet, K. Tedesco, M. Klas, G. Bonani, and S. Ivy
1992. Evidence for massive iceberg discharges in the North Atlantic Ocean during the last glacial period. *Nature*, 360:249–345.
- Bond, G., B. Kromer, J. Beer, R. Muscheler, M. N. Evans, W. Showers, S. Hoffmann, R. Lotti-Bond, I. Hajdas, and G. Bonani
2001. Persistent solar influence on North Atlantic climate during the Holocene. *Science*, 294(5549):2130–2136.

- Bond, G. and R. Lotti
1995. Iceberg discharges into the North Atlantic on millennial time scales during the last glaciation. *Science*, 267(5200):1005–1010.
- Bowles, J.
2006. Magnetostratigraphy and Magnetic Mineralogy of Sediments from Walvis Ridge, Leg 208. *Proc. Ocean Drill. Program, Sci. Results*, 208(October 2005).
- Broecker, W. S.
1991. The great ocean conveyor. *Oceanography*, 4(2):79–89.
- Broecker, W. S., G. Bond, M. Klas, E. Clark, and J. McManus
1992. Origin of the northern Atlantic's Heinrich events. *Clim. Dyn.*, 6:265–273.
- Broecker, W. S. and T. Peng
1982. *Tracers in the Sea*. Lamont-Doherty Geological Observatory, Columbia University, Palisades, New York 10964.
- Cao, Z., C. Siebert, E. C. Hathorne, M. Dai, and M. Frank
2015. Constraining the oceanic barium cycle with stable barium isotopes. *Earth Planet. Sci. Lett.*, 434:1–9.
- Capron, E., A. Landais, J. Chappellaz, D. Buiron, H. Fischer, S. J. Johnsen, J. Jouzel, M. Leuenberger, V. Masson-Delmotte, and T. F. Stocker
2012. A global picture of the first abrupt climatic event occurring during the last glacial inception. *Geophys. Res. Lett.*, 39(15):1–8.
- Carter, P., D. Vance, C. D. Hillenbrand, J. A. Smith, and D. R. Shoosmith
2012. The neodymium isotopic composition of waters masses in the eastern Pacific sector of the Southern Ocean. *Geochim. Cosmochim. Acta*, 79:41–59.
- Channell, J., T. Sato, T. Kanamatsu, R. Stein, and C. Alvarez Zarikian
2010. Expedition 303/306 synthesis: North Atlantic climate. In *Proc. IODP, 303/306*, volume 303/306, Pp. 1–25. Integrated Ocean Drilling Program.
- Channell, J. E. T., D. A. Hodell, and J. H. Curtis
2012a. ODP Site 1063 (Bermuda Rise) revisited: Oxygen isotopes, excursions and paleointensity in the Brunhes Chron. *Geochemistry, Geophys. Geosystems*, 13(2).
- Channell, J. E. T., D. A. Hodell, O. E. Romero, C. Hillaire-Marcel, A. de Vernal, J. S. Stoner, A. Mazaud, and U. Röhl
2012b. A 750-kyr detrital-layer stratigraphy for the North Atlantic (IODP Sites U1302-U1303, Orphan Knoll, Labrador Sea). *Earth Planet. Sci. Lett.*, 317-318:218–230.
- Channell, J. E. T., T. Sato, M. J. Malone, S. Robinson, G. L. Bartoli, S. Chiyonobu, J. J. E. Damuth, L. De Abreu, A. De Vernal, A. Ennyu, E. Vazquez Esmerode,

- S. Funakawa, S. S. Henderson, D. A. Hodell, M. Ito, K. Kawamura, N. Kawamura, L. A. Krissek, S. N. Leigh, C. Liu, A. Mazaud, S. Obrochta, O. E. Romero, R. Schiebel, C. Shimada, J. S. Stoner, R. H. Wilkens, J. D. Wright, and M. Yamasaki
2005. North Atlantic Climate Ice sheet - ocean atmosphere interactions on millennial timescales during the late Neogene-Quaternary using a paleointensity-assisted chronology for the North Atlantic. Technical report.
- Chester, R. and M. Hughes
1967. A chemical technique for the separation of ferro-manganese minerals, carbonate minerals and adsorbed trace elements from pelagic sediments. *Chem. Geol.*, 2:249–262.
- Clark, P. U., A. Dyke, J. D. Shakun, A. E. Carlson, J. Clark, B. Wohlfarth, J. Mitrovica, S. Hostetler, and A. McCabe
2009. The Last Glacial Maximum. *Science*, 325(5941):710–714.
- Cohen, A. S., R. K. O’Nions, R. Siegenthaler, and W. L. Griffin
1988. Chronology of the pressure-temperature history recorded by a granulite terrain. *Contrib. to Mineral. Petrol.*, 98(3):303–311.
- Colin, C., N. Frank, K. Copard, and E. Douville
2010. Neodymium isotopic composition of deep-sea corals from the NE Atlantic: implications for past hydrological changes during the Holocene. *Quat. Sci. Rev.*, 29(19-20):2509–2517.
- Cottet-Puinel, M., A. J. Weaver, C. Hillaire-Marcel, A. De Vernal, P. U. Clark, and M. Eby
2004. Variation of Labrador Sea Water formation over the Last Glacial cycle in a climate model of intermediate complexity. *Quat. Sci. Rev.*, 23(3-4):449–465.
- Crocker, A. J., T. B. Chalk, I. Bailey, M. R. Spencer, M. Gutjahr, G. L. Foster, and P. A. Wilson
2016. Geochemical response of the mid-depth Northeast Atlantic Ocean to fresh-water input during Heinrich events 1 to 4. *Quat. Sci. Rev.*, 151:236–254.
- Crocket, K. C., D. Vance, G. L. Foster, D. A. Richards, and M. Tranter
2012. Continental weathering fluxes during the last glacial/interglacial cycle: Insights from the marine sedimentary Pb isotope record at Orphan Knoll, NW Atlantic. *Quat. Sci. Rev.*, 38:89–99.
- Crocket, K. C., D. Vance, M. Gutjahr, G. L. Foster, and D. A. Richards
2011. Persistent Nordic deep-water overflow to the glacial North Atlantic. *Geology*, 39(6):515–518.

- Curry, W. B. and D. W. Oppo
2005. Glacial water mass geometry and the distribution of $\delta^{13}\text{C}$ of CO_2 in the western Atlantic Ocean. *Paleoceanography*, 20(1):PA1017.
- Dansgaard, W., J. W. C. White, and S. J. Johnsen
1989. The abrupt termination of the Younger Dryas climate event. *Nature*, 339(6225):532–534.
- de Laeter, J. R., J. K. Böhlke, P. De Bièvre, H. Hidaka, H. S. Peiser, K. J. R. Rosman, and P. D. P. Taylor
2003. Atomic weights of the elements. Review 2000 (IUPAC Technical Report). *Pure Appl. Chem.*, 75(6):785.
- de Vernal, A. and C. Hillaire-Marcel
2006. Provincialism in trends and high frequency changes in the northwest North Atlantic during the Holocene. *Glob. Planet. Change*, 54(3-4):263–290.
- Du, J., B. A. Haley, and A. C. Mix
2016. Neodymium isotopes in authigenic phases, bottom waters and detrital sediments in the Gulf of Alaska and their implications for paleo-circulation reconstruction. *Geochim. Cosmochim. Acta*, 193:14–35.
- Dubois-Dauphin, Q., C. Colin, L. Bonneau, P. Montagna, Q. Wu, D. Van Rooij, G. Reverdin, E. Douville, F. Thil, A. Waldner, and N. Frank
2017. Fingerprinting Northeast Atlantic water masses using Neodymium isotopes. *Geochim. Cosmochim. Acta*.
- Duplessy, J.-C., L. Labeyrie, A. Juillet-Leclerc, F. Maitre, J. Duprat, and M. Sarnthein
1991. Surface salinity reconstruction of the North Atlantic Ocean during the Last Glacial Maximum. *Ocean. Acta*, 14:311–324.
- Duplessy, J.-C., N. J. Shackleton, R. G. Fairbanks, L. Labeyrie, D. W. Oppo, and N. Kallel
1988. Deepwater source variations during the last climatic cycle and their impact on the global deepwater circulation. *Paleoceanography*, 3(3):343.
- Elmore, A. C., A. M. Piotrowski, J. D. Wright, and A. E. Scrivner
2011. Testing the extraction of past seawater Nd isotopic composition from North Atlantic deep sea sediments and foraminifera. *Geochemistry, Geophys. Geosystems*, 12(9).
- Elmore, A. C., J. D. Wright, and T. B. Chalk
2015. Precession-driven changes in Iceland-Scotland Overflow Water penetration and bottom water circulation on Gardar Drift since $\sim 200\text{ka}$. *Palaeogeogr. Palaeoclimatol. Palaeoecol.*, 440:551–563.

- Fagel, N., C. Hillaire-Marcel, M. Humblet, R. Brasseur, D. Weis, and R. Stevenson
2004. Nd and Pb isotope signatures of the clay-size fraction of Labrador Sea sediments during the Holocene: Implications for the inception of the modern deep circulation pattern. *Paleoceanography*, 19(3).
- Fagel, N., C. Hillaire-Marcel, and C. Robert
1997. Changes in the Western Boundary Undercurrents outflow since the Last Glacial Maximum, from Smectite/Illite ratios in deep Labrador Sea sediments. *Paleoceanography*, 12(1):79–96.
- Fagel, N., C. Innocent, C. Gariépy, and C. Hillaire-Marcel
2002. Sources of Labrador Sea sediments since the last glacial maximum inferred from Nd-Pb isotopes. *Geochim. Cosmochim. Acta*, 66(14):2569–2581.
- Fagel, N., C. Innocent, K. Stevenson, and C. Hillaire-Marcel
1999. Deep circulation changes in the Labrador Sea since the Last Glacial Maximum: New constraints from Sm-Nd data on sediments. *Paleoceanography*, 14(6):777–788.
- Fagel, N. and N. Mattielli
2011. Holocene evolution of deep circulation in the northern North Atlantic traced by Sm, Nd and Pb isotopes and bulk sediment mineralogy. *Paleoceanography*, 26(4):1–15.
- Foster, G. L., D. Vance, and J. Prytulak
2007. No change in the neodymium isotope composition of deep water exported from the North Atlantic on glacial-interglacial time scales. *Geology*, 35(1):37.
- Frank, M., R. K. O’Nions, J. R. Hein, and V. K. Banakar
1999. 60 Myr records of major elements and Pb-Nd isotopes from hydrogenous ferromanganese crusts: Reconstruction of seawater paleochemistry. *Geochim. Cosmochim. Acta*, 63(11-12):1689–1708.
- Freslon, N., G. Bayon, S. Toucanne, S. Bermell, C. Bollinger, S. Chéron, J. Etoubleau, Y. Germain, A. Khripounoff, E. Ponzevera, and M. L. Rouget
2014. Rare earth elements and neodymium isotopes in sedimentary organic matter. *Geochim. Cosmochim. Acta*, 140:177–198.
- Froelich, P. N., G. P. Klinkhammer, M. L. Bender, N. A. Luedtke, G. R. Heath, D. Cullen, P. Dauphin, D. Hammond, B. Hartman, and V. Maynard
1979. Early oxidation of organic matter in pelagic sediments of the eastern equatorial Atlantic: suboxic diagenesis. *Geochim. Cosmochim. Acta*, 43:1075–1090.
- Garcia, H. E., T. P. Boyer, R. A. Locarnini, J. I. Antonov, A. V. Mishonov, O. K. Baranova, M. M. Zweng, J. R. Reagan, and D. R. Johnson
2013a. World Ocean Atlas 2013. Volume 3: dissolved oxygen, apparent oxygen utilization, and oxygen saturation. Technical report.

- Garcia, H. E., R. A. Locarnini, T. P. Boyer, J. I. Antonov, O. K. Baranova, M. M. Zweng, J. R. Reagan, and D. R. Johnson
2013b. World Ocean Atlas 2013 Volume 4: Dissolved Inorganic Nutrients (phosphate, nitrate, silicate). Technical report.
- GEBCO (General Bathymetric Chart of the Oceans)
1994. GEBCO Digital Atlas, British Oceanographic Data Center.
- Gislason, S. R. and E. H. Oelkers
2003. Mechanism, rates, and consequences of basaltic glass dissolution: II. An experimental study of the dissolution rates of basaltic glass as a function of pH and temperature. *Geochim. Cosmochim. Acta*, 67(20):3817–3832.
- Grousset, F. E., C. Pujol, L. D. Labeyrie, G. Auffret, and A. Boelaert
2000. Were the North Atlantic Heinrich events triggered by the behaviour of the European ice-sheets? *Geology*, 28(2):123–126.
- Grützner, J. and S. M. Higgins
2010. Threshold behavior of millennial scale variability in deep water hydrography inferred from a 1.1 Ma long record of sediment provenance at the southern Gardar Drift. *Paleoceanography*, 25(4):PA4204.
- Gutjahr, M., M. Frank, C. H. Stirling, L. D. Keigwin, and A. N. Halliday
2008. Tracing the Nd isotope evolution of North Atlantic Deep and Intermediate Waters in the western North Atlantic since the LGM from Blake Ridge sediments. *Earth Planet. Sci. Lett.*, 266(1-2):61–77.
- Gutjahr, M., M. Frank, C. H. Stirling, V. Klemm, T. van de Flierdt, and A. N. Halliday
2007. Reliable extraction of a deepwater trace metal isotope signal from Fe-Mn oxyhydroxide coatings of marine sediments. *Chem. Geol.*, 242(3-4):351–370.
- Gutjahr, M., B. A. A. Hoogakker, M. Frank, and I. N. McCave
2010. Changes in North Atlantic Deep Water strength and bottom water masses during Marine Isotope Stage 3 (45–35 ka BP). *Quat. Sci. Rev.*, 29(19-20):2451–2461.
- Gutjahr, M. and J. Lippold
2011. Early arrival of Southern Source Water in the deep North Atlantic prior to Heinrich event 2. *Paleoceanography*, 26(January):1–9.
- Haley, B. A., G. P. Klinkhammer, and J. McManus
2004. Rare earth elements in pore waters of marine sediments. *Geochim. Cosmochim. Acta*, 68(6):1265–1279.
- Hanawa, K. and L. D. Talley
2001. Chapter 5.4 Mode waters. In *Int. Geophys.*, volume 77, Pp. 373–386.

- Hathorne, E. C., O. Alard, R. H. James, and N. W. Rogers
2003. Determination of intratest variability of trace elements in foraminifera by laser ablation inductively coupled plasma-mass spectrometry. *Geochemistry, Geophys. Geosystems*, 4(12).
- Heinrich, H.
1988. Origin and consequences of cyclic ice rafting in the Northeast Atlantic Ocean during the past 130,000 years. *Quat. Res.*, 29(2):142–152.
- Heinrich, H.
1989. Geologisch-Geomorphologische Untersuchungen in der Westeuropäischen Tiefsee. Technical report.
- Hemming, Sidney, R.
2004. Heinrich events: Massive late Pleistocene detritus layers of the North Atlantic and their global climate imprint. *Rev. Geophys.*, 42(2003).
- Henderson, G. M.
2002. New oceanic proxies for paleoclimate. *Earth Planet. Sci. Lett.*, 203(1):1–13.
- Henderson, G. M.
2003. The U-series Toolbox for Paleoceanography. *Rev. Mineral. Geochemistry*, 52(1):493–531.
- Henrich, R. and K.-H. Baumann
1994. Evolution of the Norwegian Current and the Scandinavian Ice Sheets during the past 2.6 m.y.: evidence from ODP Leg 104 biogenic carbonate and terrigenous records. *Palaeogeogr. Palaeoclimatol. Palaeoecol.*, 108(1-2):75–94.
- Hillaire-Marcel, C., A. de Vernal, G. Bilodeau, and A. J. Weaver
2001. Absence of deep-water formation in the Labrador Sea during the last interglacial period. *Nature*, 410(6832):1073–1077.
- Hillaire-Marcel, C., A. de Vernal, and J. McKay
2011. Foraminifer isotope study of the Pleistocene Labrador Sea, northwest North Atlantic (IODP Sites 1302/03 and 1305), with emphasis on paleoceanographical differences between its “inner” and “outer” basins. *Mar. Geol.*, 279(1-4):188–198.
- Hillaire-Marcel, C., A. de Vernal, and D. J. W. Piper
2007. Lake Agassiz Final drainage event in the northwest North Atlantic. *Geophys. Res. Lett.*, 34(15):1–5.
- Hodell, D. A., J. E. T. Channell, J. H. Curtis, O. E. Romero, and U. Röhl
2008. Onset of ‘Hudson Strait’ Heinrich events in the eastern North Atlantic at the end of the middle Pleistocene transition (~640 ka)? *Paleoceanography*, 23(4):1–16.

- Hodell, D. A., H. F. Evans, J. E. T. Channell, and J. H. Curtis
2010. Phase relationships of North Atlantic ice-rafted debris and surface-deep climate proxies during the last glacial period. *Quat. Sci. Rev.*, 29(27-28):3875–3886.
- Hodell, D. A., J. A. Nicholl, T. R. R. Bontognali, S. Danino, J. Dorador, J. A. Dowdeswell, J. Einsle, H. Kuhlmann, B. Martrat, M. J. Mleneck-Vautravers, F. J. Rodríguez-Tovar, and U. Röhl
2017. Anatomy of Heinrich Layer 1 and its Role in the Last Deglaciation. *Paleoceanography*, 1.
- Hoogakker, B. A. A., M. R. Chapman, I. N. McCave, C. Hillaire-Marcel, C. R. W. Ellison, I. R. Hall, and R. J. Telford
2011. Dynamics of North Atlantic Deep Water masses during the Holocene. *Paleoceanography*, 26(4):1–10.
- Hoogakker, B. A. A., H. Elderfield, G. Schmiedl, I. N. McCave, and R. E. M. Rickaby
2014a. Glacial–interglacial changes in bottom-water oxygen content on the Portuguese margin. *Nat. Geosci.*, 8(1):40–43.
- Hoogakker, B. A. A., I. N. McCave, H. Elderfield, C. Hillaire-Marcel, and J. Simstich
2014b. Holocene climate variability in the Labrador Sea. *J. Geol. Soc. London.*, 172(2):272–277.
- Howe, J. N. W., A. M. Piotrowski, R. Hu, and A. Bory
2016a. Reconstruction of east–west deep water exchange in the low latitude Atlantic Ocean over the past 25,000 years. *Earth Planet. Sci. Lett.*, 1:1–10.
- Howe, J. N. W., A. M. Piotrowski, T. L. Noble, S. Mulitza, C. M. Chiessi, and G. Bayon
2016b. North Atlantic Deep Water production during the Last Glacial Maximum. *Under Rev.*, 7:1–8.
- Howe, J. N. W., A. M. Piotrowski, and V. C. Rennie
2016c. Abyssal origin for the early Holocene pulse of unradiogenic neodymium isotopes in Atlantic seawater. *Geology*, 1(10):G38155.1.
- Huon, S., R. Jantschik, and S. Huon
1993. Detrital silicates in Northeast Atlantic deep-sea sediments during the Late Quaternary : mineralogical and K-Ar isotopic data. *Eclogae Geol. Helv.*, 82(1):195–212.
- Jacobsen, S. B. and G. J. Wasserburg
1980. Sm-Nd isotopic evolution of chondrites. *Earth Planet. Sci. Lett.*, 50:139–155.

Jantschik, R.

1991. *Mineralogische und geochemische Untersuchungen spätquartärer Tiefseesedimente aus dem Westeuropäischen Becken (bei 47° 30'N und 19° 30'W)*. Phd thesis, Université de Neuchâtel.

Jantschik, R. and S. Huon

1992. Detrital silicates in Northeast Atlantic deep-sea sediments during the Late Quaternary : mineralogical and K-Ar isotopic data. *Eclogae Geol. Helv.*, 82(1):195–212.

Jeandel, C.

2016. Overview of the mechanisms that could explain the 'Boundary Exchange' at the land–ocean contact. *Philos. Trans. R. Soc. A Math. Eng. Sci.*, 374(2081):20150287.

Jeandel, C., T. Arsouze, F. Lacan, P. Téchiné, and J.-C. Dutay

2007. Isotopic Nd compositions and concentrations of the lithogenic inputs into the ocean: A compilation, with an emphasis on the margins. *Chem. Geol.*, 239(1-2):156–164.

Jónsson, S. and H. Valdimarsson

2004. A new path for the Denmark Strait overflow water from the Iceland Sea to Denmark Strait. *Geophys. Res. Lett.*, 31(3):L03305.

Jourabchi, P., C. Meile, L. R. Pasion, and P. Van Cappellen

2008. Quantitative interpretation of pore water O₂ and pH distributions in deep-sea sediments. *Geochim. Cosmochim. Acta*, 72(5):1350–1364.

Kanzow, T. and W. Zenk

2014. Structure and transport of the Iceland Scotland Overflow plume along the Reykjanes Ridge in the Iceland Basin. *Deep. Res. Part I Oceanogr. Res. Pap.*, 86:82–93.

Keigwin, L. D. and S. A. Swift

2017. Carbon isotope evidence for a northern source of deep water in the glacial western North Atlantic. *Proc. Natl. Acad. Sci.*, (7):201614693.

Kissel, C., A. Van Toer, C. Laj, E. Cortijo, and E. Michel

2013. Variations in the strength of the North Atlantic bottom water during Holocene. *Earth Planet. Sci. Lett.*, 369-370:248–259.

Klevenz, V., D. Vance, D. N. Schmidt, and K. Mezger

2008. Neodymium isotopes in benthic foraminifera: Core-top systematics and a down-core record from the Neogene South Atlantic. *Earth Planet. Sci. Lett.*, 265(3-4):571–587.

- Koschinsky, A. and P. Halbach
1995. Sequential leaching of marine ferromanganese precipitates: Genetic implications. *Geochim. Cosmochim. Acta*, 59(24):5113–5132.
- Kraft, S., M. Frank, E. C. Hathorne, and S. Weldeab
2013. Assessment of seawater Nd isotope signatures extracted from foraminiferal shells and authigenic phases of Gulf of Guinea sediments. *Geochim. Cosmochim. Acta*, 121:414–435.
- Kuechler, R. R., E. Schefuß, B. Beckmann, L. Dupont, and G. Wefer
2013. NW African hydrology and vegetation during the Last Glacial cycle reflected in plant-wax-specific hydrogen and carbon isotopes. *Quat. Sci. Rev.*, 82:56–67.
- Kurzweil, F., M. Gutjahr, D. Vance, and L. D. Keigwin
2010. Authigenic Pb isotopes from the Laurentian Fan: Changes in chemical weathering and patterns of North American freshwater runoff during the last deglaciation. *Earth Planet. Sci. Lett.*, 299(3-4):458–465.
- Labeyrie, L. D., J.-C. Duplessy, J. Duprat, A. Juillet-Leclerc, J. Moyes, E. Michel, N. Kallel, and N. J. Shackleton
1992. Changes in the vertical structure of the North Atlantic Ocean between glacial and modern times. *Quat. Sci. Rev.*, 11:401–413.
- Lacan, F. and C. Jeandel
2004a. Denmark Strait water circulation traced by heterogeneity in neodymium isotopic compositions. *Deep. Res. Part I Oceanogr. Res. Pap.*, 51(1):71–82.
- Lacan, F. and C. Jeandel
2004b. Neodymium isotopic composition and rare earth element concentrations in the deep and intermediate Nordic Seas: Constraints on the Iceland Scotland Overflow Water signature. *Geochemistry, Geophys. Geosystems*, 5(11):Q11006.
- Lacan, F. and C. Jeandel
2005a. Acquisition of the neodymium isotopic composition of the North Atlantic Deep Water. *Geochemistry, Geophys. Geosystems*, 6(12):Q12008.
- Lacan, F. and C. Jeandel
2005b. Neodymium isotopes as a new tool for quantifying exchange fluxes at the continent-ocean interface. *Earth Planet. Sci. Lett.*, 232(3-4):245–257.
- Lacan, F., K. Tachikawa, and C. Jeandel
2012. Neodymium isotopic composition of the oceans: A compilation of seawater data. *Chem. Geol.*, 300-301:177–184.
- Lambelet, M., T. van de Flierdt, K. C. Crocket, M. Rehkämper, K. Kreissig, B. Coles, M. J. A. Rijkenberg, L. J. A. Gerringa, H. J. De Baar, and R. Steinfeldt
2016. Neodymium isotopic composition and concentration in the western North

- Atlantic Ocean: Results from the GEOTRACES GA02 section. *Geochim. Cosmochim. Acta*, 177:1–29.
- Ledbetter, M. T. and W. L. Balsam
1985. Paleooceanography of the Deep Western Boundary undercurrent on the North American continental margin for the past 25 000 yr. *Geology*, 13(3):181–184.
- Ling, H., K. W. Burton, R. O’Nions, B. Kamber, F. von Blanckenburg, A. Gibb, and J. Hein
1997. Evolution of Nd and Pb isotopes in Central Pacific seawater from ferromanganese crusts. *Earth Planet. Sci. Lett.*, 146(1-2):1–12.
- Lippold, J., M. Gutjahr, P. Blaser, E. Christner, M. L. d. C. Ferreira, S. Mulitza, M. Christl, F. Wombacher, E. Böhm, B. Antz, O. Cartapanis, H. Vogel, and S. L. Jaccard
2016. Deep water provenance and dynamics of the (de)glacial Atlantic meridional overturning circulation. *Earth Planet. Sci. Lett.*, 445:68–78.
- Little, S. H., D. Vance, C. Walker-Brown, and W. M. Landing
2014. The oceanic mass balance of copper and zinc isotopes, investigated by analysis of their inputs, and outputs to ferromanganese oxide sediments. *Geochim. Cosmochim. Acta*, 125:673–693.
- Lonsdale, P. F., C. D. Hollister, and L. A. Mayer
1981. Erosion and deposition in interplain channels of the Maury Channel system, Northeast Atlantic. *Oceanol. Acta*, 4(2):185–201.
- Mangerud, J., S. E. Lie, H. Furnes, I. L. Kristiansen, and L. Lømo
1984. A Younger Dryas Ash Bed in western Norway, and its possible correlations with tephra in cores from the Norwegian Sea and the North Atlantic. *Quat. Res.*, 21(1):85–104.
- Mangini, A., M. Jung, and S. Laukenmann
2001. What do we learn from peaks of uranium and of manganese in deep sea sediments? *Mar. Geol.*, 177(1-2):63.
- Manighetti, B. and I. N. McCave
1995. Late Glacial and Holocene palaeocurrents around Rockall Bank, NE Atlantic Ocean. *Paleoceanography*, 10(3):611–626.
- Marchitto, T. M., W. B. Curry, and D. W. Oppo
1998. Millennial-scale changes in North Atlantic circulation since the last glaciation. *Nature*, 413(October):531–534.
- Marson, J. M., L. A. Mysak, M. M. Mata, and I. Wainer
2015. Evolution of the deep Atlantic water masses since the last glacial maximum based on a transient run of NCAR-CCSM3. *Clim. Dyn.*, 47(3):865–877.

- Martin, E. E., S. W. Blair, G. D. Kamenov, H. D. Scher, E. Bourbon, C. Basak, and D. N. Newkirk
2010. Extraction of Nd isotopes from bulk deep sea sediments for paleoceanographic studies on Cenozoic time scales. *Chem. Geol.*, 269(3-4):414–431.
- Martin, E. E. and H. D. Scher
2004. Preservation of seawater Sr and Nd isotopes in fossil fish teeth: Bad news and good news. *Earth Planet. Sci. Lett.*, 220(1-2):25–39.
- McCave, I. N.
1986. Local and global aspects of the bottom nepheloid layers in the world ocean. *Netherlands J. Sea Res.*, 20(2/3):167–181.
- McCave, I. N., B. Manighetti, and S. G. Robinson
1995. Sortable silt and fine sediment size/composition slicing: Parameters for palaeocurrent speed and palaeoceanography. *Paleoceanography*, 10(3):593–610.
- McManus, J. F., R. Francois, J.-M. Gherardi, L. D. Keigwin, and S. Brown-Leger
2004. Collapse and rapid resumption of Atlantic meridional circulation linked to deglacial climate changes. *Nature*, 428(6985):834–837.
- Meischner, D.
1987. Nordostatlantisches Monitoring Programm (NOAMP) Kolbenlot-Kerne aus dem Westeuropaeischen Becken - Abschlussbericht.
- Millo, C., M. Sarnthein, A. Voelker, and H. Erlenkeuser
2006. Variability of the Denmark Strait Overflow during the Last Glacial Maximum. *Boreas*, 35(1):50–60.
- Molina-Kescher, M., M. Frank, and E. C. Hathorne
2014. Nd and Sr isotope compositions of different phases of surface sediments in the South Pacific: Extraction of seawater signatures, boundary exchange, and detrital/dust provenance. *Geochemistry, Geophys. Geosystems*, 15(9):3502–3520.
- Nance, W. and S. Taylor
1976. Rare earth element patterns and crustal evolution—I. Australian post-Archean sedimentary rocks. *Geochim. Cosmochim. Acta*, 40:1539–1551.
- NGRIP
2004. North Greenland Ice Core Project Oxygen Isotope Data. Technical report, NOAA/NGDC Paleoclimatology Program, Boulder CO, USA.
- Nürnberg, D., J. Bijma, and C. Hemleben
1996. Assessing the reliability of magnesium in foraminiferal calcite as a proxy for water mass temperatures. *Geochim. Cosmochim. Acta*, 60(5):803–814.

- Obrochta, S. P., T. J. Crowley, J. E. T. Channell, D. A. Hodell, P. A. Baker, A. Seki, and Y. Yokoyama
2014. Climate variability and ice-sheet dynamics during the last three glaciations. *Earth Planet. Sci. Lett.*, 406:198–212.
- Obrochta, S. P., H. Miyahara, Y. Yokoyama, and T. J. Crowley
2012. A re-examination of evidence for the North Atlantic '1500-year cycle' at Site 609. *Quat. Sci. Rev.*, 55:23–33.
- Oppo, D. W. and S. J. Lehman
1993. Mid-depth circulation of the subpolar north atlantic during the last glacial maximum. *Science*, 259(5098):1148–1152.
- Paillard, D.
1998. The timing of Pleistocene glaciations from a simple multiple-stateclimatemodel Didier. *Nature*, 391(January):916–918.
- Palmer, M. R. and H. Elderfield
1985. Variations in the Nd isotopic composition of foraminifera from Atlantic Ocean sediments. *Earth Planet. Sci. Lett.*, 73(2-4):299–305.
- Pearce, C. R., M. T. Jones, E. H. Oelkers, C. Pradoux, and C. Jeandel
2013. The effect of particulate dissolution on the neodymium (Nd) isotope and Rare Earth Element (REE) composition of seawater. *Earth Planet. Sci. Lett.*, 369-370:138–147.
- Pearson, P. N.
2012. Oxygen isotopes in foraminifera: overview and historical review.
- Piepgras, D. J. and G. J. Wasserburg
1980. Neodymium isotopic variations in seawater. *Earth Planet. Sci. Lett.*, 50(1):128–138.
- Piepgras, D. J., G. J. Wasserburg, and E. J. Dasch
1979. The isotopic composition of Nd in different ocean masses. *Earth Planet. Sci. Lett.*, 45:223–236.
- Pin, C., D. Briot, C. Bassin, and F. Poitrasson
1994. Concomitant separation of strontium and samarium-neodymium for isotopic analysis in silicate samples, based on specific extraction chromatography. *Anal. Chim. Acta*, 298(2):209–217.
- Piotrowski, A. M., A. Galy, J. A. L. Nicholl, N. Roberts, D. J. Wilson, J. A. Clegg, and J. Yu
2012. Reconstructing deglacial North and South Atlantic deep water sourcing using foraminiferal Nd isotopes. *Earth Planet. Sci. Lett.*, 357-358:289–297.

- Piotrowski, A. M., S. L. Goldstein, R. Hemming, Sidney, and R. G. Fairbanks
2004. Intensification and variability of ocean thermohaline circulation through the last deglaciation. *Earth Planet. Sci. Lett.*, 225(1-2):205–220.
- Piotrowski, A. M., S. L. Goldstein, R. Hemming, Sidney, and R. G. Fairbanks
2005. Temporal relationships of carbon cycling and ocean circulation at glacial boundaries. *Science*, 307(5717):1933–1938.
- Piotrowski, A. M., S. L. Goldstein, R. Hemming, Sidney, R. G. Fairbanks, and D. R. Zylberberg
2008. Oscillating glacial northern and southern deep water formation from combined neodymium and carbon isotopes. *Earth Planet. Sci. Lett.*, 272(1-2):394–405.
- Pöppelmeier, F.
2016. Investigations of Authigenic Neodymium Sediment-Pore Water Interaction and Reconstruction of Deep Water Mass Sourcing in the North-East Atlantic.
- Praetorius, S. K., J. F. McManus, D. W. Oppo, and W. B. Curry
2008. Episodic reductions in bottom-water currents since the last ice age. *Nat. Geosci.*, 1(7):449–452.
- Rahmstorf, S.
2006. Thermohaline Ocean Circulation. In *Encycl. Quat. Sci.*, Pp. 1–10.
- Reimer, P. J., E. Bard, A. Bayliss, J. W. Beck, P. G. Blackwell, R. C. Bronk, C. E. Buck, H. Cheng, R. L. Edwards, M. Friedrich, P. M. Grootes, T. P. Guilderson, H. Haflidason, I. Hajdas, C. Hatté, T. J. Heaton, D. L. Hoffmann, A. G. Hogg, K. A. Hughen, K. F. Kaiser, B. Kromer, S. W. Manning, M. Niu, R. W. Reimer, D. A. Richards, E. M. Scott, J. R. Southon, R. A. Staff, C. S. M. Turney, and J. van der Plicht
2013. IntCal13 and Marine13 Radiocarbon Age Calibration Curves 0–50,000 Years cal BP. *Radiocarbon*, 55(4):1869–1887.
- Rempfer, J., T. F. Stocker, F. Joos, J.-C. Dutay, and M. Siddall
2011. Modelling Nd-isotopes with a coarse resolution ocean circulation model: Sensitivities to model parameters and source/sink distributions. *Geochim. Cosmochim. Acta*, 75(20):5927–5950.
- Renssen, H., H. Seppä, X. Crosta, H. Goosse, and D. Roche
2012. Global characterization of the Holocene Thermal Maximum. *Quat. Sci. Rev.*, 48:7–19.
- Rickli, J., M. Gutjahr, D. Vance, M. Fischer-Gödde, C.-D. Hillenbrand, and G. Kuhn
2014. Neodymium and hafnium boundary contributions to seawater along the West Antarctic continental margin. *Earth Planet. Sci. Lett.*, 394:99–110.

- Roberts, N. L. and A. M. Piotrowski
2015. Radiogenic Nd isotope labeling of the northern NE Atlantic during MIS 2. *Earth Planet. Sci. Lett.*, 423:125–133.
- Roberts, N. L., A. M. Piotrowski, H. Elderfield, T. I. Eglinton, and M. W. Lomas
2012. Rare earth element association with foraminifera. *Geochim. Cosmochim. Acta*, 94:57–71.
- Roberts, N. L., A. M. Piotrowski, J. F. McManus, and L. D. Keigwin
2010. Synchronous deglacial overturning and water mass source changes. *Science*, 327(5961):75–78.
- Rousseau, T. C. C., J. E. Sonke, J. Chmeleff, P. van Beek, M. Souhaut, G. Boaventura, P. Seyler, and C. Jeandel
2015. Rapid neodymium release to marine waters from lithogenic sediments in the Amazon estuary. *Nat. Commun.*, 6(May):7592.
- Ruddiman, W. F.
1972. Sediment redistribution on the Reykjanes ridge: Seismic evidence. *Bull. Geol. Soc. Am.*, 83(7):2039–2062.
- Ruddiman, W. F., R. Kidd, and E. Thomas
1987. *Initial Reports of the Deep Sea Drilling Project, 94*, volume 94 of *Initial Reports of the Deep Sea Drilling Project*. U.S. Government Printing Office.
- Rutberg, R., R. Hemming, Sidney, and S. Goldstein
2000. Reduced North Atlantic Deep Water flux to the glacial Southern Ocean inferred from neodymium isotope ratios. *Nature*, 405(6789):935–938.
- Sarnthein, M., S. Balmer, P. M. Grootes, and M. Mudelsee
2015. Planktic and Benthic ^{14}C Reservoir Ages for Three Ocean Basins, Calibrated by a Suite of ^{14}C Plateaus in the Glacial-to-Deglacial Suigetsu Atmospheric ^{14}C Record. *Radiocarbon*, 57(01):129–151.
- Sarnthein, M., K. Winn, S. J. Jung, J.-C. Duplessy, L. Labeyrie, H. Erlenkeuser, and G. M. Ganssen
1994. Changes in east Atlantic deepwater circulation over the last 30,000 years: Eight time slice reconstructions. *Paleoceanography*, 9(2):209+.
- Schacht, U., K. Wallmann, and S. Kutterolf
2010. The influence of volcanic ash alteration on the REE composition of marine pore waters. *J. Geochemical Explor.*, 106(1-3):176–187.
- Schlitzer, R.
2016. Ocean Data View.

- Sholkovitz, E. R., T. J. Shaw, and D. L. Schneider
1992. The geochemistry of rare earth elements in the seasonally anoxic water column and porewaters of Chesapeake Bay. *Geochim. Cosmochim. Acta*, 56(9):3389–3402.
- Sigmarsson, O., I. Vlastelic, R. Andreasen, I. Bindeman, J. L. Devidal, S. Moune, J. K. Keiding, G. Larsen, A. Höskuldsson, and T. H. Thordarson
2011. Remobilization of silicic intrusion by mafic magmas during the 2010 Eyjafjallajökull eruption. *Solid Earth*, 2(2):271–281.
- Skinner, L. C., S. Fallon, C. Waelbroeck, E. Michel, and S. Barker
2010. Ventilation of the deep Southern Ocean and deglacial CO₂ rise. *Science*, 328(5982):1147–1151.
- S.P. Sinha
1982. Systematics and the properties of the lanthanides. *Polyhedron*, 1(1):141.
- Staudigel, H., P. Doyle, and A. Zindler
1985. Sr and Nd isotope systematics in fish teeth. *Earth Planet. Sci. Lett.*, 76(1-2):45–56.
- Staudigel, H., A. Yayanos, R. Chastain, G. Davies, E. Verdurmen, P. Schiffman, R. Bourcier, and H. J. De Baar
1998. Biologically mediated dissolution of volcanic glass in seawater. *Earth Planet. Sci. Lett.*, 164:233–244.
- Stein, R., J. Hefter, J. Grützner, A. Voelker, and B. D. A. Naafs
2009. Variability of surface water characteristics and Heinrich-like events in the Pleistocene midlatitude North Atlantic Ocean: Biomarker and XRD records from IODP Site U1313 (MIS 16–9). *Paleoceanography*, 24(2):PA2203.
- Stern, J. V. and L. E. Lisiecki
2014. Termination 1 timing in radiocarbon-dated regional benthic $\delta^{18}\text{O}$ stacks. *Paleoceanography*, 29(12):1127–1142.
- Stewart, J. A., M. Gutjahr, R. H. James, P. Anand, and P. A. Wilson
2016. Influence of the Amazon River on the Nd isotope composition of deep water in the western equatorial Atlantic during the Oligocene–Miocene transition. *Earth Planet. Sci. Lett.*, 454:132–141.
- Stichel, T., A. E. Hartman, B. D. Duggan, S. L. Goldstein, H. Scher, and K. Pahnke
2015. Separating biogeochemical cycling of neodymium from water mass mixing in the Eastern North Atlantic. *Earth Planet. Sci. Lett.*, 412:245–260.
- Stoner, J. S. and J. T. Andrews
1999. The North Atlantic as a Quaternary magnetic archive. In *Quat. Clim. Environ. Magn.*

- Stoner, J. S., J. E. T. Channell, and C. Hillaire-Marcel
1996. The magnetic signature of rapidly deposited detrital layers from the Deep Labrador Sea: Relationship to North Atlantic Heinrich layers. *Paleoceanography*, 11(3):309.
- Stoner, J. S., J. E. T. Channell, A. Mazaud, S. E. Strano, and C. Xuan
2013. The influence of high-latitude flux lobes on the Holocene paleomagnetic record of IODP Site U1305 and the northern North Atlantic. *Geochemistry, Geophys. Geosystems*, 14(10):4623–4646.
- Stosch, H.-G.
1999. Einführung in die Isotopengeochemie.
- Stouffer, R. J., J. Yin, J. M. Gregory, K. W. Dixon, M. J. Spelman, W. Hurlin, A. J. Weaver, M. Eby, G. M. Flato, H. Hasumi, A. Hu, J. H. Jungclauss, I. V. Kamenkovich, A. Levermann, M. Montoya, S. Murakami, S. Nawrath, A. Oka, W. R. Peltier, D. Y. Robitaille, A. Sokolov, G. Vettoretti, and S. L. Weber
2006. Investigating the Causes of the Response of the Thermohaline Circulation to Past and Future Climate Changes. *J. Clim.*, 19.
- Stuiver, M., P. J. Reimer, and R. Reimer
2017. CALIB 14C Calibration Program.
- Tachikawa, K., T. Arsouze, G. Bayon, A. Bory, C. Colin, J.-C. Dutay, N. Frank, X. Giraud, A. T. Gourelan, C. Jeandel, F. Lacan, L. Meynadier, P. Montagna, A. M. Piotrowski, Y. Plancherel, E. Pucéat, M. Roy-Barman, and C. Waelbroeck
2017. The large-scale evolution of neodymium isotopic composition in the global modern and Holocene ocean revealed from seawater and archive data. *Chem. Geol.*
- Tachikawa, K., V. Athias, and C. Jeandel
2003. Neodymium budget in the modern ocean and paleo-oceanographic implications. *J. Geophys. Res.*, 108(C8):3254.
- Tachikawa, K., A. M. Piotrowski, and G. Bayon
2014. Neodymium associated with foraminiferal carbonate as a recorder of seawater isotopic signatures. *Quat. Sci. Rev.*, 88:1–13.
- Tachikawa, K., T. Toyofuku, I. Basile-Doelsch, and T. Delhaye
2013. Microscale neodymium distribution in sedimentary planktonic foraminiferal tests and associated mineral phases. *Geochim. Cosmochim. Acta*, 100:11–23.
- Takeno, N.
2005. Atlas of Eh-pH diagrams. *Geol. Surv. Japan Open File Rep.*, (419).
- Talley, L. D., J. L. Reid, and P. E. Robbins
2003. Data-based meridional overturning streamfunctions for the global ocean. *J. Clim.*, 16(19):3213–3226.

- Tamburini, F., S. Huon, P. Steinmann, F. E. Grousset, T. Adatte, and K. B. Foellmi
2002. Dyaerobic conditions during Heinrich events 4 and 5: Evidence from phosphorus distribution in a North Atlantic deep-sea core. *Geochim. Cosmochim. Acta*, 66(23):4069–4083.
- Tanaka, T., S. Togashi, H. Kamioka, H. Amakawa, H. Kagami, T. Hamamoto, M. Yuhara, Y. Orihashi, S. Yoneda, H. Shimizu, T. Kunimaru, K. Takahashi, T. Yanagi, T. Nakano, H. Fujimaki, R. Shinjo, Y. Asahara, M. Tanimizu, and C. Dragusanu
2000. JNdi-1: A neodymium isotopic reference in consistency with LaJolla neodymium. *Chem. Geol.*, 168(3-4):279–281.
- Teschner, C., M. Frank, B. A. Haley, and J. Knies
2016. Plio-Pleistocene evolution of water mass exchange and erosional input at the Atlantic-Arctic gateway. *Paleoceanography*, Pp. 1–18.
- Thornalley, D. J. R., S. Barker, W. S. Broecker, H. Elderfield, and I. N. McCave
2011a. The Deglacial Evolution of North Atlantic Deep Convection. *Science*, 331(6014):202–205.
- Thornalley, D. J. R., H. A. Bauch, G. Gebbie, W. Guo, M. Ziegler, S. M. Bernasconi, S. Barker, L. C. Skinner, and J. Yu
2015. A warm and poorly ventilated deep Arctic Mediterranean during the last glacial period. *Science*, 349(6249):706–10.
- Thornalley, D. J. R., M. Blaschek, F. J. Davies, S. Praetorius, D. W. Oppo, J. F. McManus, I. R. Hall, H. Kleiven, H. Renssen, and I. N. McCave
2013. Long-term variations in Iceland–Scotland overflow strength during the Holocene. *Clim. Past*, 9(5):2073–2084.
- Thornalley, D. J. R., H. Elderfield, and I. N. McCave
2010. Intermediate and deep water paleoceanography of the northern North Atlantic over the past 21,000 years. *Paleoceanography*, 25(1):1–17.
- Thornalley, D. J. R., I. N. McCave, and H. Elderfield
2011b. Tephra in deglacial ocean sediments south of Iceland: Stratigraphy, geochemistry and oceanic reservoir ages. *J. Quat. Sci.*, 26(2):190–198.
- van de Flierdt, T. and M. Frank
2010. Neodymium isotopes in paleoceanography. *Quat. Sci. Rev.*, 29(19-20):2439–2441.
- van de Flierdt, T., A. M. Griffiths, M. Lambelet, S. H. Little, T. Stichel, and D. J. Wilson
2016. Subject Areas : Neodymium in the oceans : a global database , a regional comparison and implications for palaeoceanographic research.

- van de Flierdt, T., L. F. Robinson, J. F. Adkins, R. Hemming, Sidney, and S. L. Goldstein
2006. Temporal stability of the neodymium isotope signature of the Holocene to glacial North Atlantic. *Paleoceanography*, 21(4).
- Vance, D. and K. W. Burton
1999. Neodymium isotopes in planktonic foraminifera: a record of the response of continental weathering and ocean circulation rates to climate change. *Earth Planet. Sci. Lett.*, 173(4):365–379.
- Walker, M., S. Johnsen, S. O. Rasmussen, T. Popp, J.-P. Steffensen, P. Gibbard, W. Hoek, J. Lowe, J. T. Andrews, S. Björck, L. C. Cwynar, K. A. Hughen, P. Kershaw, B. Kromer, T. Litt, D. J. Lowe, T. Nakagawa, R. Newnham, and J. Schwander
2009. Formal definition and dating of the GSSP (Global Stratotype Section and Point) for the base of the Holocene using the Greenland NGRIP ice core, and selected auxiliary records. *J. Quat. Sci.*, 24(1):3–17.
- Werner, K., M. Frank, C. Teschner, J. Müller, and R. F. Spielhagen
2014. Neoglacial change in deep water exchange and increase of sea-ice transport through eastern Fram Strait: Evidence from radiogenic isotopes. *Quat. Sci. Rev.*, 92:190–207.
- Wilson, D. J., K. C. Crocket, T. van de Flierdt, L. F. Robinson, and J. F. Adkins
2014. Dynamic intermediate ocean circulation in the North Atlantic during Heinrich Stadial 1: A radiocarbon and neodymium isotope perspective. *Paleoceanography*, 29(11):1072–1093.
- Wilson, D. J., A. M. Piotrowski, A. Galy, and J. A. Clegg
2013. Reactivity of neodymium carriers in deep sea sediments: Implications for boundary exchange and paleoceanography. *Geochim. Cosmochim. Acta*, 109:197–221.
- Wilson, D. J., A. M. Piotrowski, A. Galy, and I. N. McCave
2012. A boundary exchange influence on deglacial neodymium isotope records from the deep western Indian Ocean. *Earth Planet. Sci. Lett.*, 341-344:35–47.
- Xuan, C., J. E. T. Channell, and D. A. Hodell
2016. Quaternary magnetic and oxygen isotope stratigraphy in diatom-rich sediments of the southern Gardar Drift (IODP Site U1304, North Atlantic). *Quat. Sci. Rev.*, 142:74–89.
- Yu, J., H. Elderfield, and A. M. Piotrowski
2008. Seawater carbonate ion- $\delta^{13}\text{C}$ systematics and application to glacial-interglacial North Atlantic ocean circulation. *Earth Planet. Sci. Lett.*, 271(1-4):209–220.

Zweng, M. M., J. R. Reagan, J. I. Antonov, R. A. Locarnini, A. V. Mishonov, T. P. Boyer, H. E. Garcia, O. K. Baranova, D. Johnson, D. Seidov, and M. Biddle
2013. WORLD OCEAN ATLAS 2013 Volume 2: Salinity. Technical report.

Appendices

A Supplementary Material

A.1 Site locations

Table A.1: Table of all core sites discussed in chapters 5 and 6. Nd IC data of core MD01-2454G is taken from [Colin et al. \[2010\]](#), data of Site ODP 980 from [Crocker et al. \[2016\]](#), and data of the BOFS cores from [Roberts and Piotrowski \[2015\]](#) and [Yu et al. \[2008\]](#).

Station	Latitude (°N)	Longitude (°E)	Depth (m)
IODP U1302	50.1664	-45.6379	3555.7
IODP U1304	53.0567	-33.5297	3065.4
IODP U1305	57.4751	-48.5302	3459.2
IODP U1308	49.8778	-24.2381	3872.7
IODP U1314	56.3647	-27.8885	2799.1
Me68-91	47.43	-19.58	4470
Me68-89	47.43	-19.58	4260
PO08-23	47.43	-19.58	3900
MD01-2454G	55.52	-15.65	747
ODP 980	55.485	-14.702	2168
BOFS 5K	50.41	-21.52	3547
BOFS 8K	52.3	-22.04	4045
BOFS 10K	54.6	-20.6	2777
BOFS 11K	55.2	-20.33	2004
BOFS 17K	58	-20.33	1150

A.2 Hydrographic sections and water mass Nd characteristics

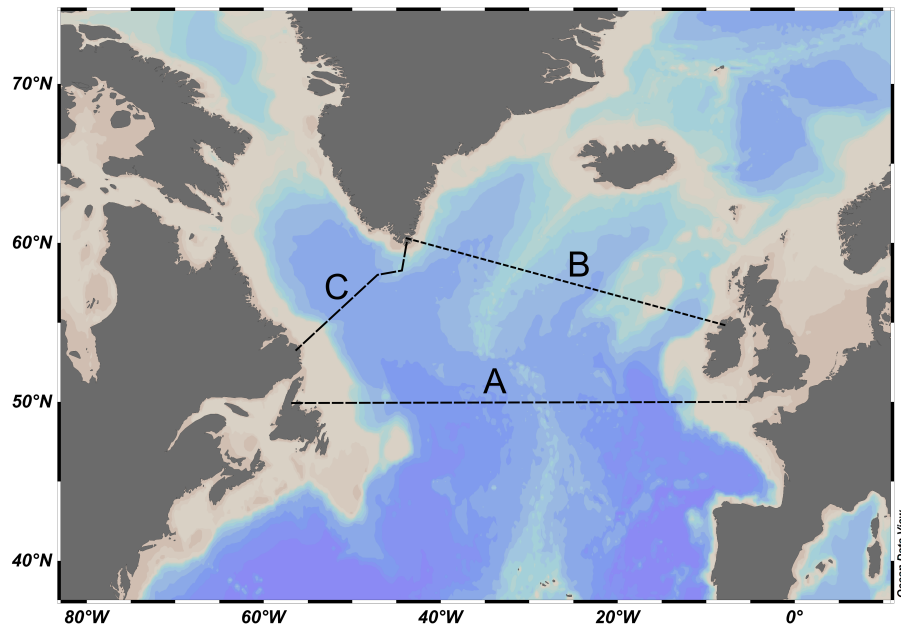
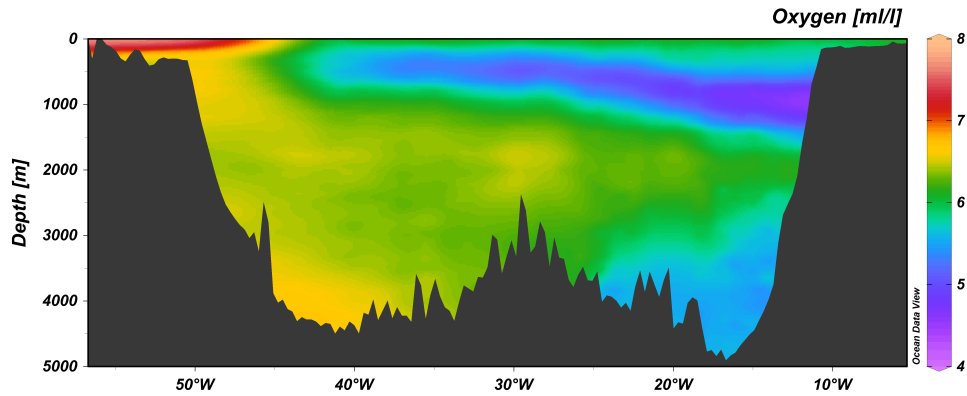


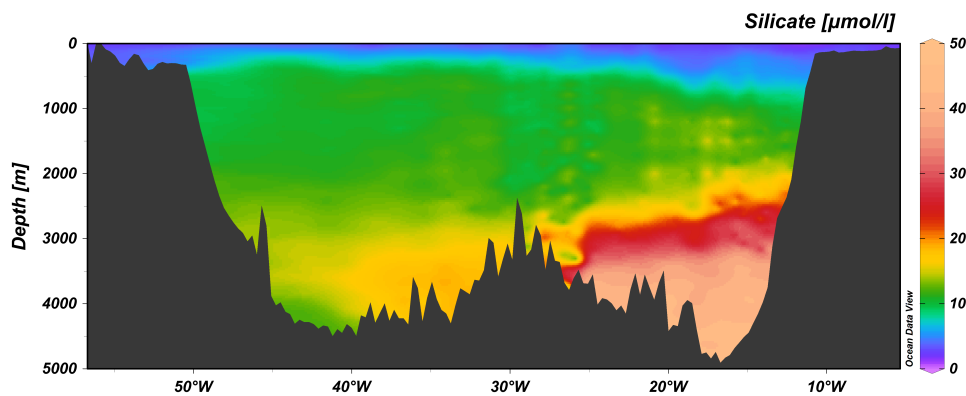
Figure A.1: Sections of the hydrographic property depth transects plotted in figures A.2 to A.4. A: Trans Atlantic at 50°N; B: Greenland to Scotland; C: Labrador Sea. The bathymetric map was created with Ocean Data View (Schlitzer [2016]).

Table A.2: Summary of the Nd concentrations and isotope compositions of the relevant water masses discussed in section 2.5.1. Data are from Lacan and Jeandel [2005b].

	SPMW	LSW	eastern LDW	pure ISOW	NEADW	DSOW	NWABW
[Nd]	2.7 ±0.1	2.5 ±0.2	3.4 ±0.4	3.1 ±0.3	2.6 ±0.2	3.2 ±0.5	2.8 ±0.2
ϵ Nd	-13.9 ±0.3	-13.5 ±0.4	-12.5 ±0.4	-8.2 ±0.6	-13.2 ±0.2	-8.4 ±1.4	-14.5 ±0.4

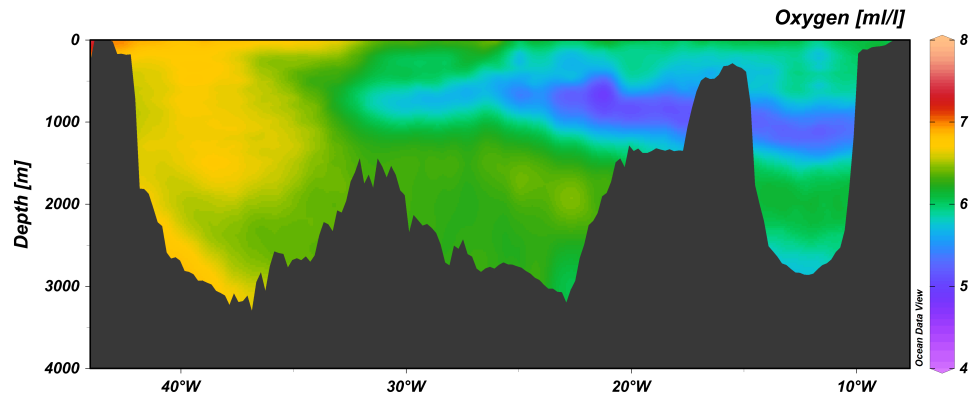


(a) Oxygen concentration at hydrographic transect A - 50°N

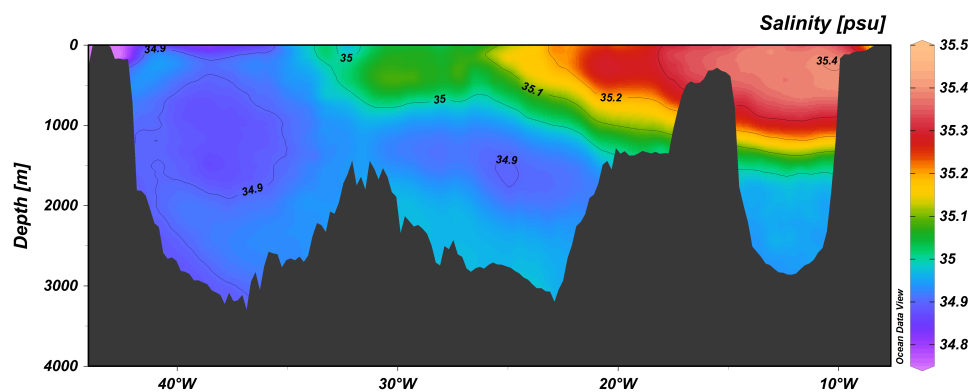


(b) Silicate concentration at hydrographic transect A - 50°N

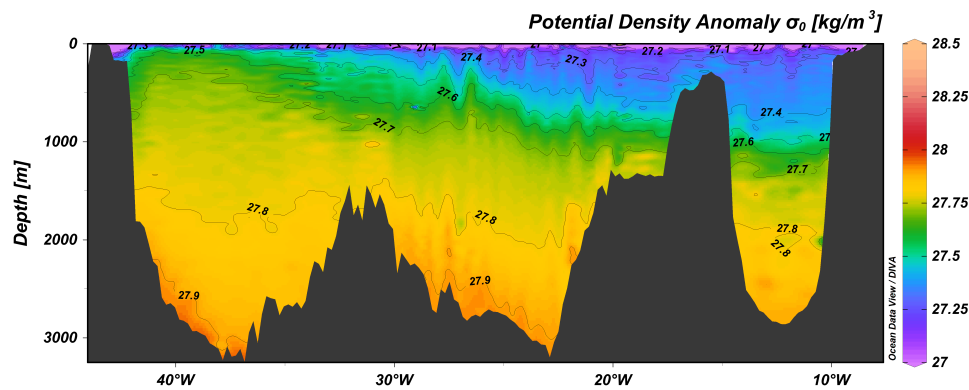
Figure A.2: Oxygen and silicate concentrations at hydrographic transect A - 50°N. LDW is evidenced by high silicate and low oxygen in the deep eastern basin. A smaller fraction of LDW also spreads at the western flank of the Mid Atlantic Ridge. SPMW is marked by lower oxygen concentration in the upper eastern waters. Lower NADW exhibits the highest oxygen concentrations in the deep western basin. Most of the water column is filled with NADW. The sections were created with Ocean Data View (Schlitzer [2016]) and data are from Garcia et al. [2013b,a].



(a) Oxygen concentration at hydrographic transect B - from Greenland to Scotland

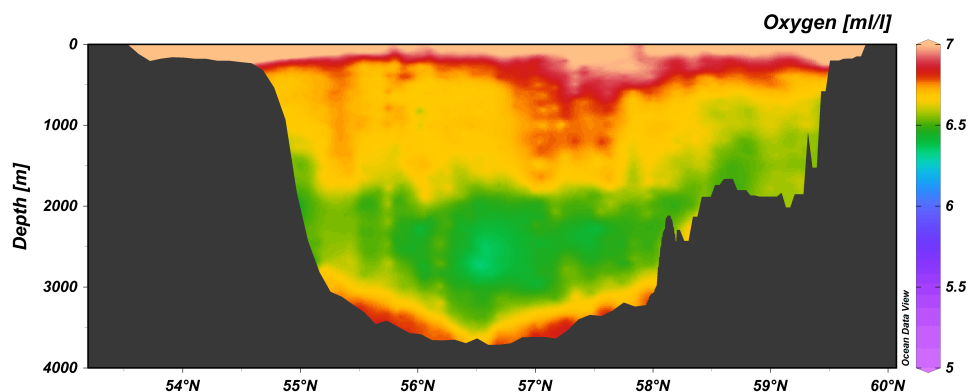


(b) Silicate concentration at hydrographic transect B - from Greenland to Scotland

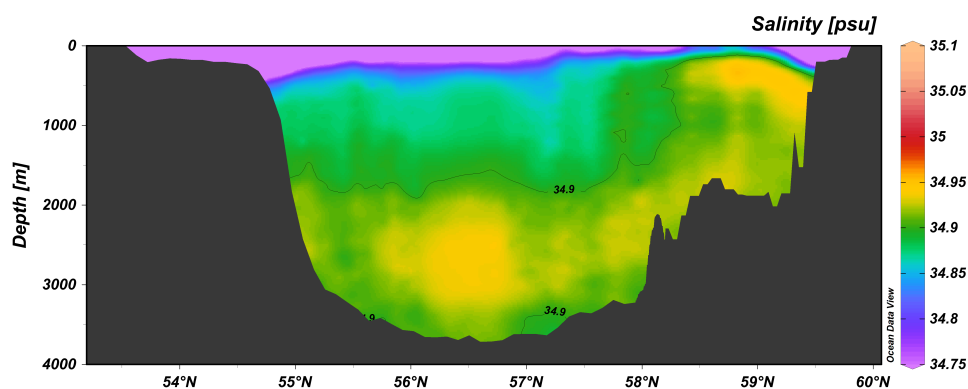


(c) Potential density at hydrographic transect B - from Greenland to Scotland

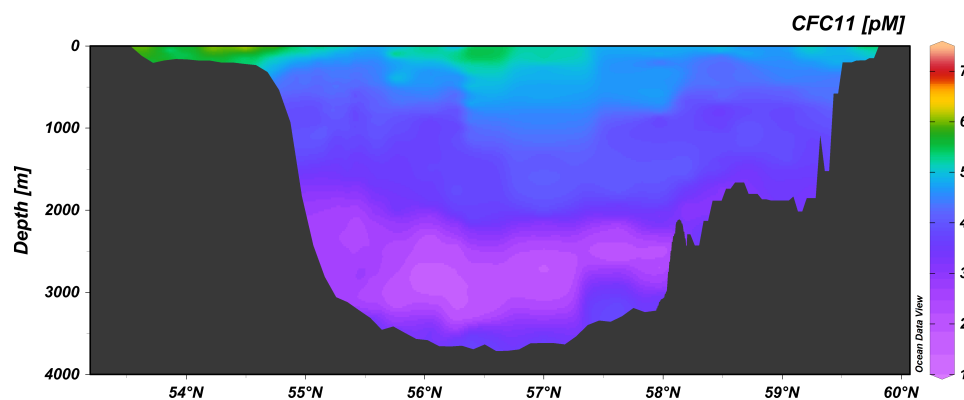
Figure A.3: Oxygen concentration, salinity and potential density at hydrographic transect B - from Greenland to Scotland. SPMW is marked with lower oxygen concentration in the upper eastern waters. LSW is characterised by a salinity minimum and high oxygen content in the intermediate depth Irvinger and Iceland Basins. LDW is present in the deep Rockall Trough (the confined easternmost basin). Thin layers of increased density at the eastern edges of the Reykjanes Ridge in the centre and at the Greenland margin in the West mark ISOW and DSOW, respectively. The high salinity surface waters in the East evidences NACW flowing towards the Denmark Sea. The sections were created with Ocean Data View (Schlitzer [2016]) and data are from Garcia et al. [2013b,a]; Zweng et al. [2013].



(a) Oxygen concentration at hydrographic transect C - Labrador Sea



(b) Salinity at hydrographic transect C - Labrador Sea



(c) (Anthropogenic) CFC11 concentration at hydrographic transect C - Labrador Sea

Figure A.4: Oxygen concentration, salinity and chlorofluorocarbon concentration (CFC11) at hydrographic transect C - Labrador Sea. Underneath surface waters with low salinity due to freshwater discharge, LSW is characterised by high CFC11 and oxygen concentrations. Between 2000 and 3200 m NEADW floods the Labrador Sea. The depletion of CFC11 and oxygen evidence its incorporation of southern sourced waters in the form of LDW. A thin layer of younger oxygen and CFC11 rich bottom water marks the inflow and outflow of dense NWABW as a deep boundary current. The sections were created with Ocean Data View (Schlitzer [2016]) and data are from Garcia et al. [2013b,a]; Zweng et al. [2013].

A.3 Supplement to chapter 5

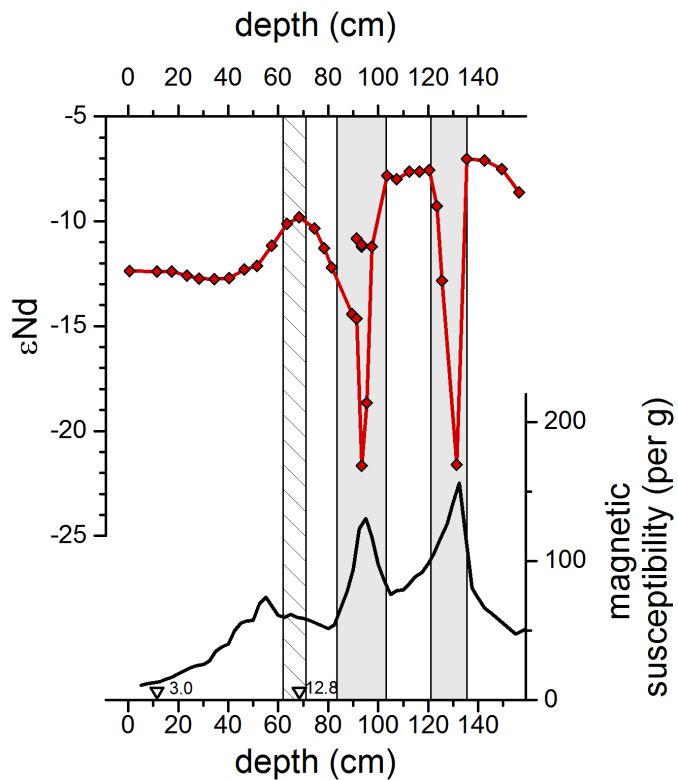


Figure A.5: Nd isotopic composition of leaches and magnetic susceptibility (Channell *et al.* [2005]) of bulk sediment in Core IODP U1308 C. Grey vertical bars mark the depth of the IRD layers and diagonally lined vertical bar marks the reported depth range of the Vedde Ash (from core DSDP 609, see Bond *et al.* [1993] and Hodell *et al.* [2008]). Triangles at the lower x-axes mark the depth of new planktic ^{14}C datings, numbers give the calibrated ages with a reservoir age of 400 years.

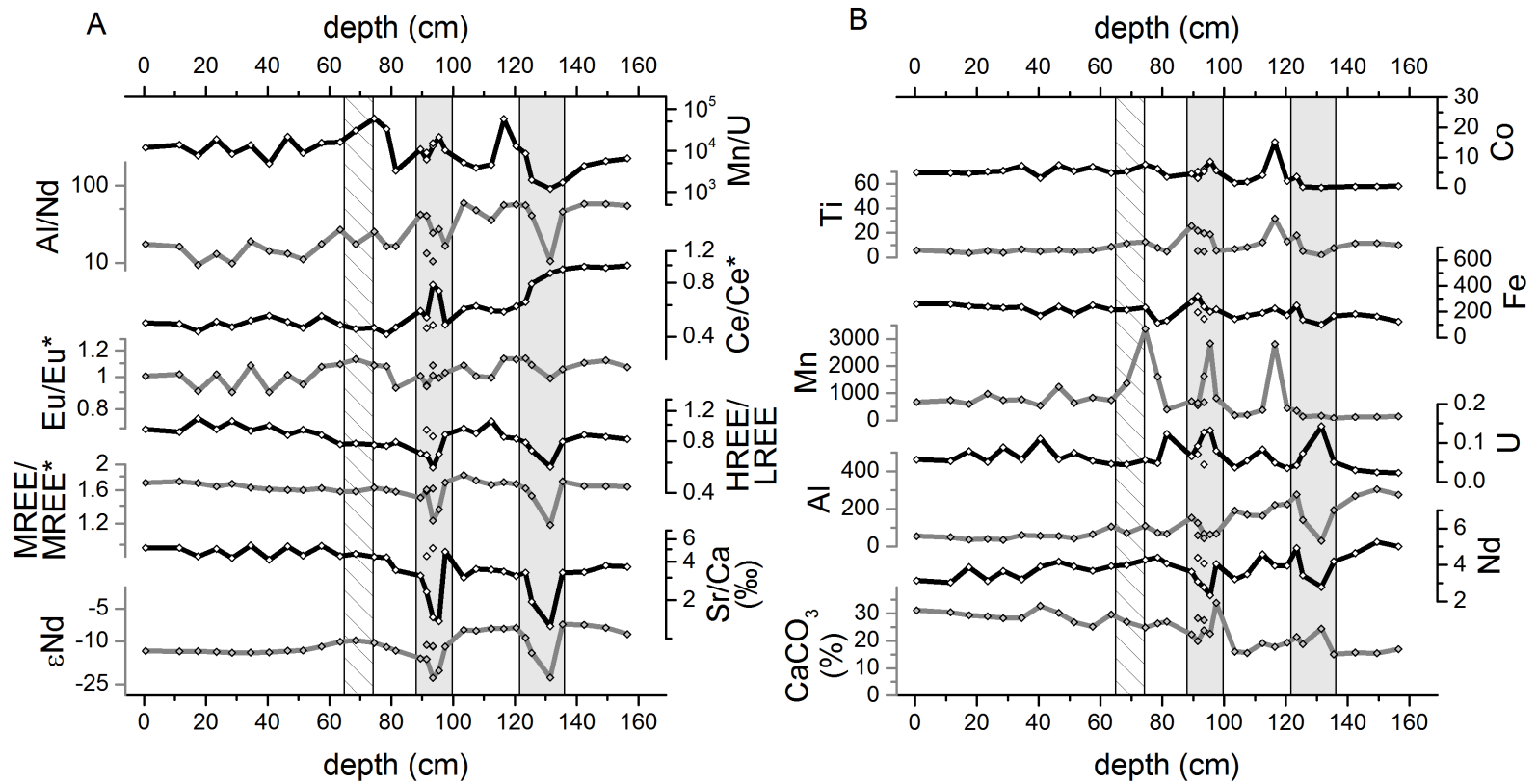


Figure A.6: Elemental analysis of core U1308C. In the left panel (A), elemental and isotope ratios are plotted on logarithmic vertical axes. In B, concentrations of different elements and calcium carbonate in the leachate are plotted on linear vertical axes. Left axes belong to the grey data plots, and right axes to the black and white data plots. Grey vertical bars indicate the detrital carbonate IRD layers. Diagonally lined vertical bar marks the area of the ash turbidite.

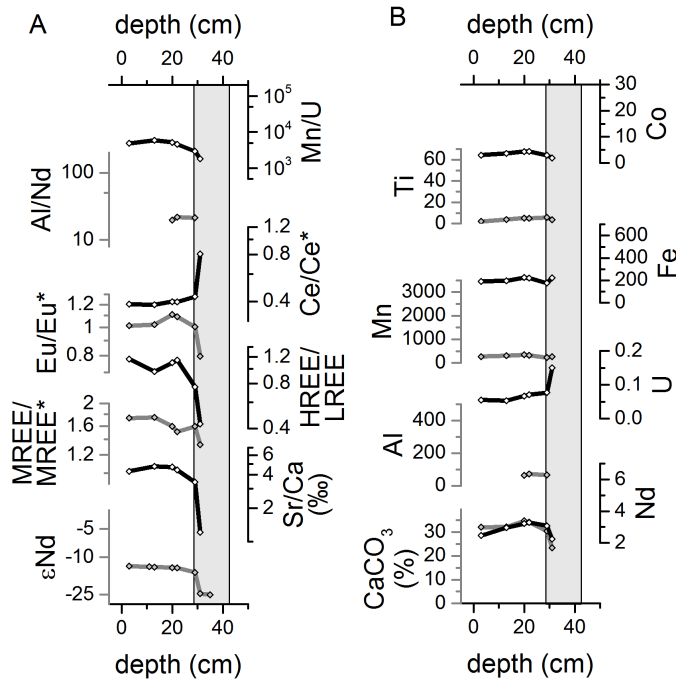


Figure A.7: Elemental and Nd isotopic results from core Me68-89 HL. In the left panel (A), elemental and isotope ratios are plotted on logarithmic vertical axes. In B, concentrations of different elements and calcium carbonate in the leachate are plotted on linear vertical axes. Left axes belong to the grey data plots, and right axes to the black and white data plots. Grey vertical bars indicate the detrital carbonate IRD layers. The depth size of these samples is 2 cm, which matches the symbol size.

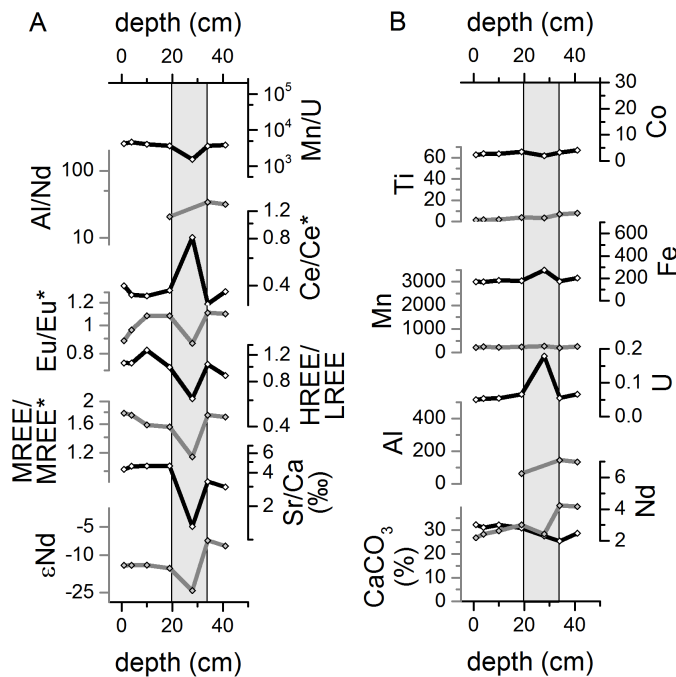


Figure A.8: Elemental and Nd isotopic results from core PO08-23 HL. In the left panel (A), elemental and isotope ratios are plotted on logarithmic vertical axes. In B, concentrations of different elements and calcium carbonate in the leachate are plotted on linear vertical axes. Left axes belong to the grey data plots, and right axes to the black and white data plots. Grey vertical bars indicate the detrital carbonate IRD layers. The depth size of these samples is 2 cm, which matches the symbol size.

A.4 Supplement to chapter 6

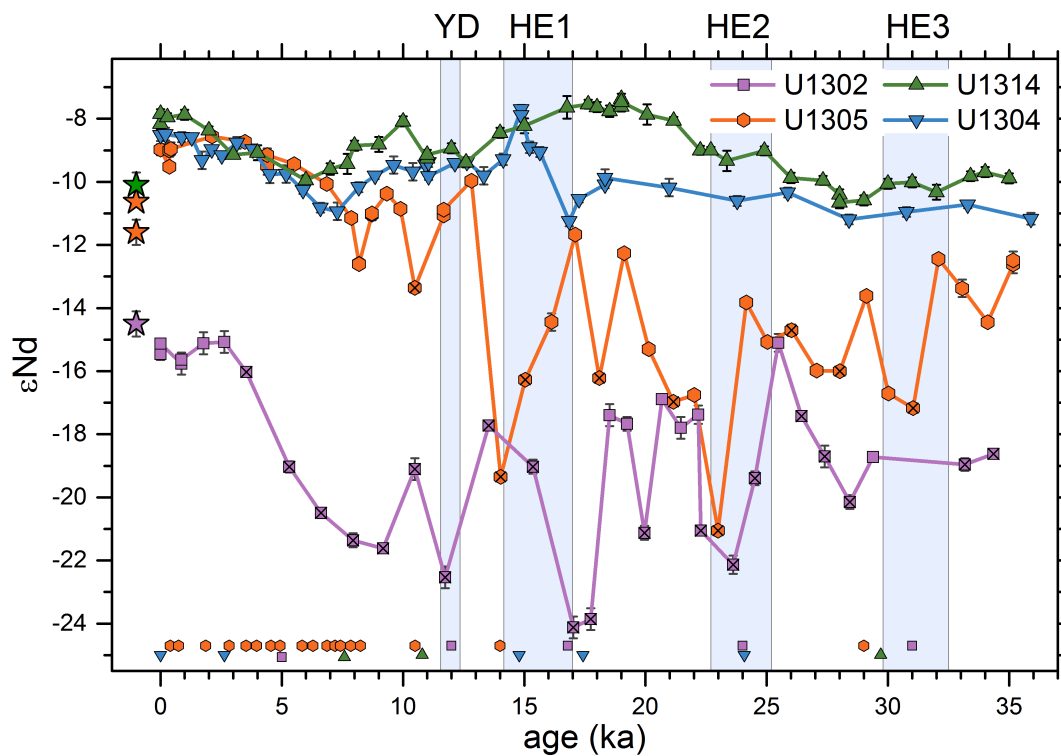


Figure A.9: Nd ICs of all leaches from the subpolar North Atlantic sites. Stars at the left hand side mark measurements from nearby deep waters. Crossed symbols are interpreted as contaminated data. Symbols at the lower x-axis mark age-tie points. Blue vertical bars indicate the approximate ages of the Younger Dryas and Heinrich Events.

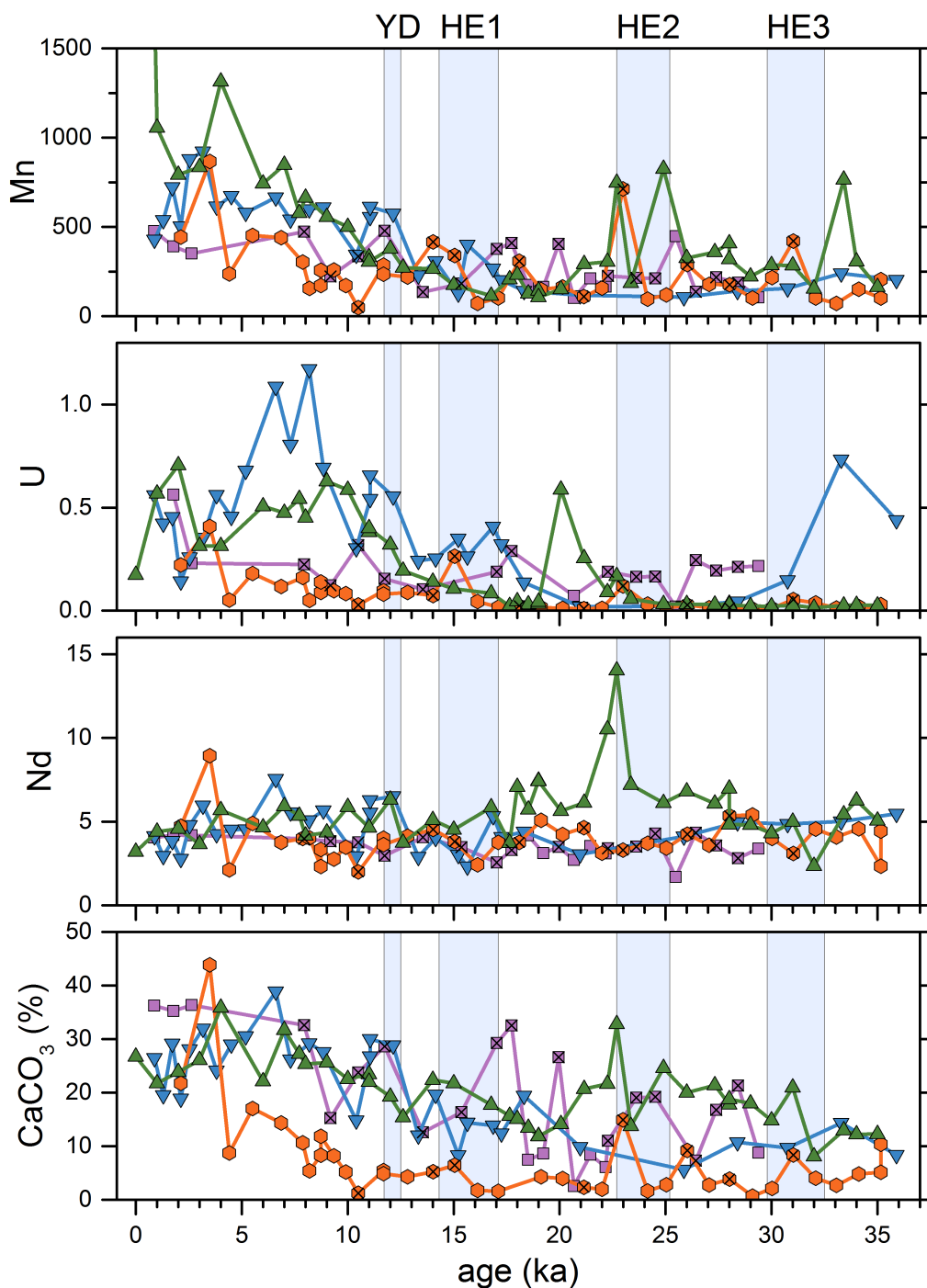


Figure A.10: Concentrations of Mn, U, Nd (all in $\mu\text{g/g}$), and CaCO_3 in leaches from the four subpolar North Atlantic sites U1302 (pink squares), U1305 (orange hexagons), U1314 (green upward triangles), and U1304 (blue downward triangles). Crossed symbols are interpreted as contaminated data. Symbols at the lower x-axis mark age-tie points. Blue vertical bars indicate the approximate ages of the Younger Dryas and Heinrich Events.

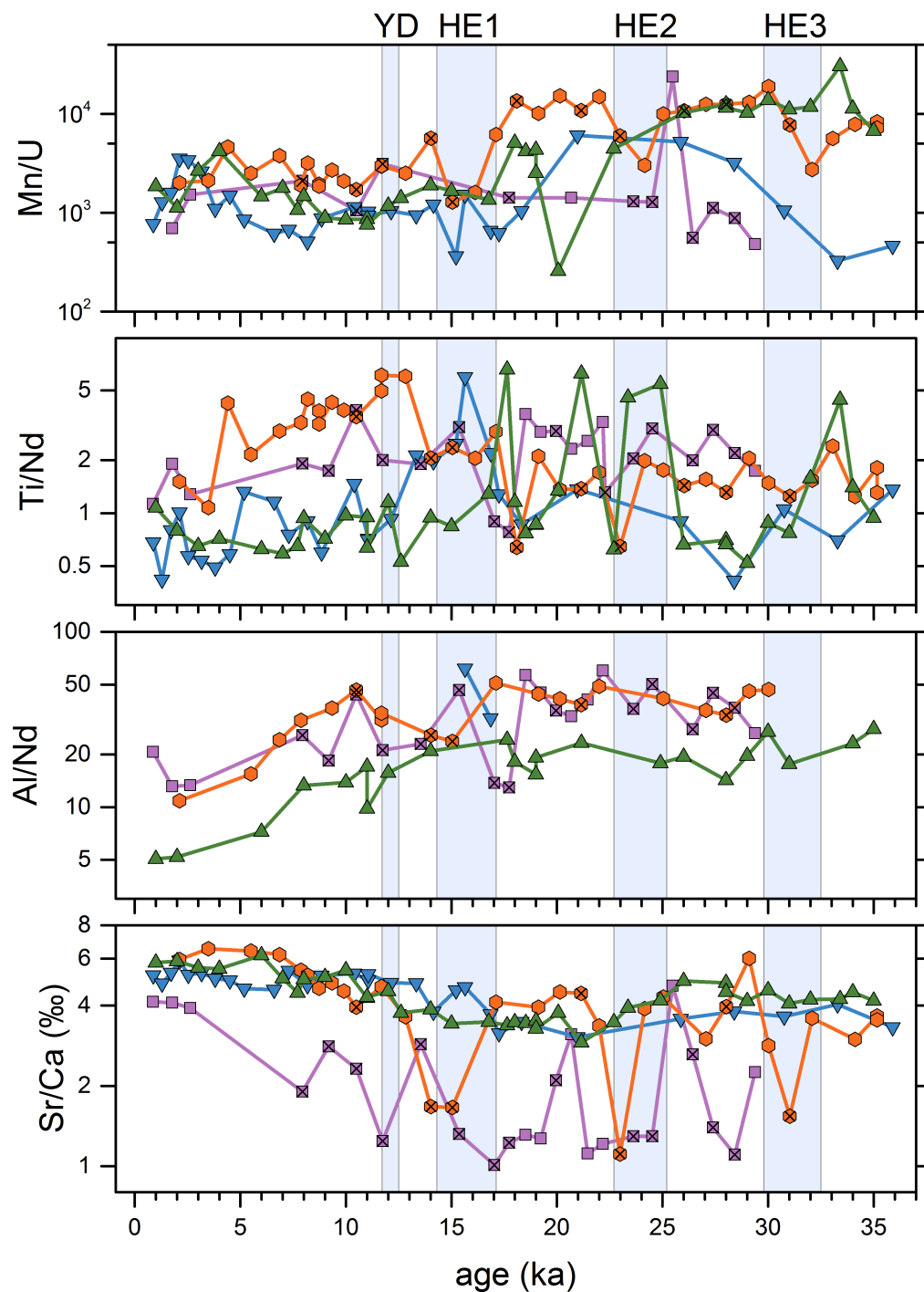


Figure A.11: Concentration ratios of Mn/U, Ti/Nd, Al/Nd, Sr/Ca in leaches from the four subpolar North Atlantic sites U1302 (pink squares), U1305 (orange hexagons), U1314 (green upward triangles), and U1304 (blue downward triangles). Crossed symbols are interpreted as contaminated data. Symbols at the lower x-axis mark age-tie points. Blue vertical bars indicate the approximate ages of the Younger Dryas and Heinrich Events. Y-axes are logarithmically scaled.

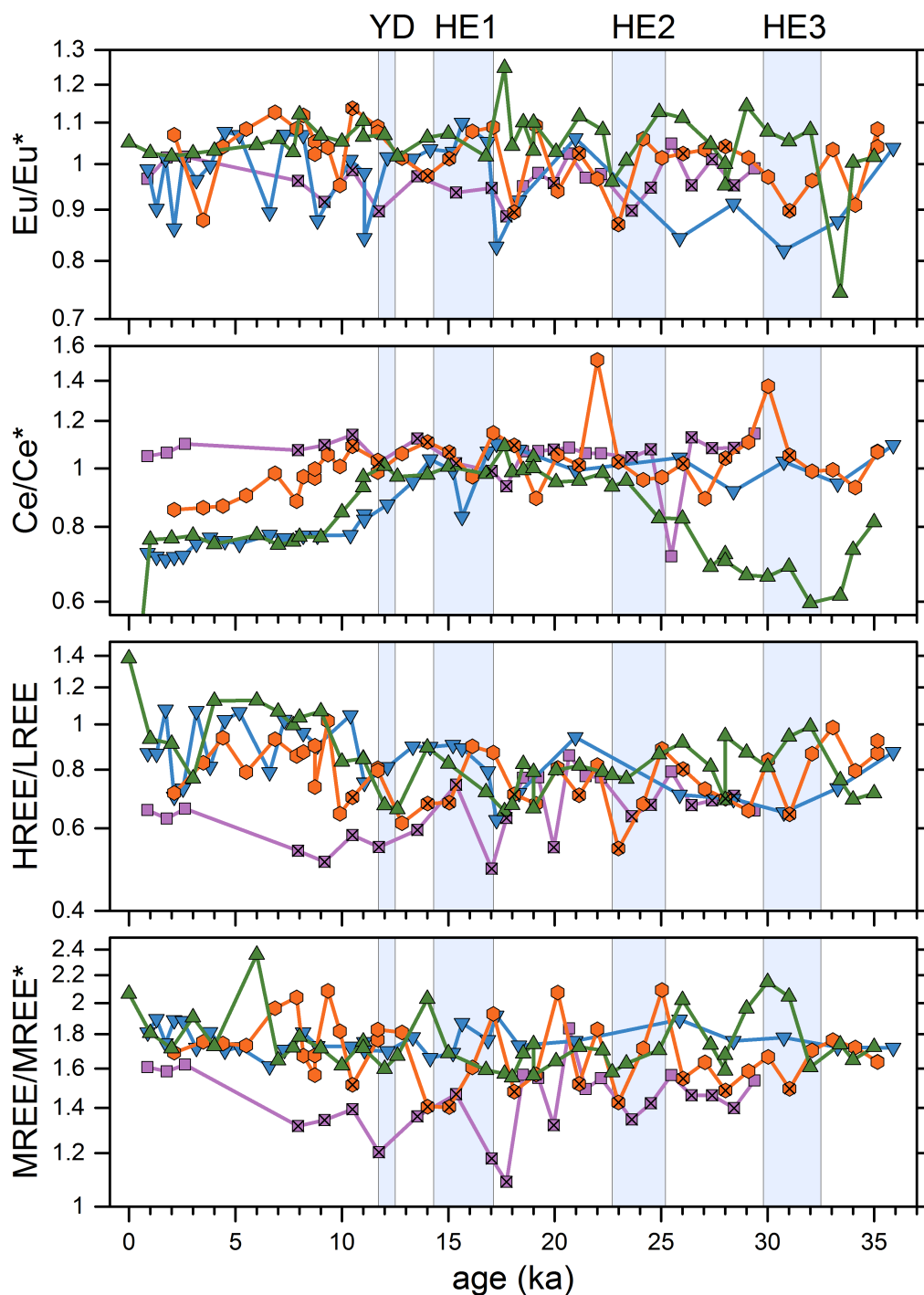


Figure A.12: REE ratios in leaches from the four subpolar North Atlantic sites U1302 (pink squares), U1305 (orange hexagons), U1314 (green upward triangles), and U1304 (blue downward triangles). Crossed symbols are interpreted as contaminated data. Symbols at the lower x-axis mark age-tie points. Blue vertical bars indicate the approximate ages of the Younger Dryas and Heinrich Events. Y-axes are logarithmically scaled.

A.5 Quantification of the authigenic fraction via sediment leaches

The element abundance measurements of the leachates yield a wealth of information about the leachate compositions. In chapter 4 it is shown that the contents of one initial HH-leach applied to the bulk sediment does not quantitatively extract the authigenic fraction, but it does not significantly leach the detrital component. It was also shown that it is not strait forward to assess which fraction of the leached elements under progressive leaching does originate in the authigenic component, and which from the detrital. If the fraction of the authigenic component extracted with the first HH-leach were constant, then the leachate data could be used to assess the authigenic budget of different elements in the sediments and its change over time. Together with sedimentation rates, the past authigenic flux of these elements into the sediment could be assessed. Such information could prove valuable for the construction of oceanic element budgets. Such budgets become more relevant because unconventional elements and their isotopes are being investigated as new proxies for oceanic parameters like oxygenation, redox conditions, or nutrient content of seawater. These include, for example, the transition elements Cu and Zn (Little et al. [2014]), or Ba (Cao et al. [2015]; Bates et al. [2017]).

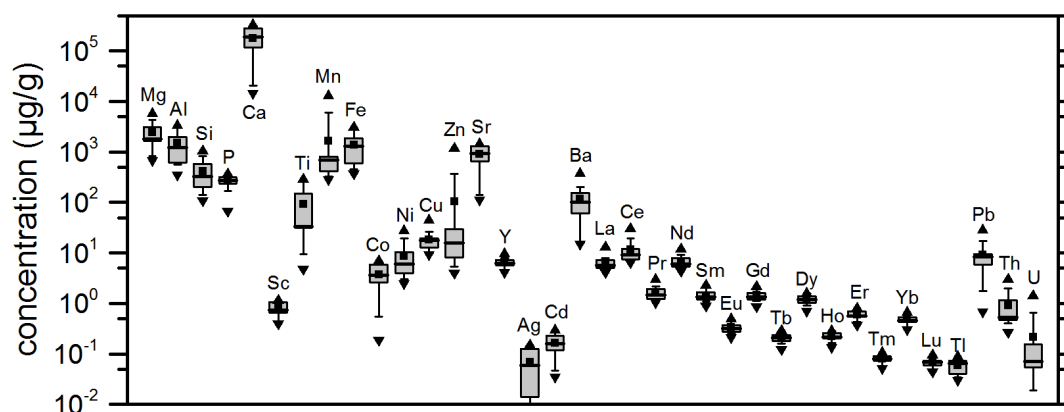


Figure A.13: Statistical distribution of the elemental abundance in the authigenic fraction, assessed by the content in the 10 HH-leaches from 17 different sediment samples from chapter 4 (excluding samples 7 ASH and IRD for simplicity). The average and median values are given by the black square and horizontal bar, respectively. Boxes mark the range of the central half of the data, and whiskers the central 80 %. Triangles mark the extreme values of the data set.

If we assume or define that the elements extracted with 10 HH-leaches from chapter 4 represent the complete authigenic fraction, then it can be tested whether the share contained in the first HH-leach is constant across these 17 samples. Figure A.13 shows the resulting abundance of the different quantified elements in the authigenic fraction and their statistical distribution. The amount of the same elements

contained already in the first HH-leach normalised to the sum in 10 HH-leaches and its statistical distribution across the 17 sediment samples is plotted in Fig. A.14. This figure clearly illustrates that the spread in the share of authigenic elements in the first HH-leach is very unequally distributed. Ideally, the share extracted with the initial leach would be high and its spread as low as possible. While the initial HH-leach extracted about 40 to 50 % of the REEs in all sediment samples, for example, the extracted amount of Co varies strongly from 20 to nearly 100 %. From these distributions, one may suppose that the amount of authigenic Sc, Mn, Cu, Zn, Y, REEs, and U could be fairly well quantified when applying a correction factor to the amount of these elements extracted with the first HH-leach.

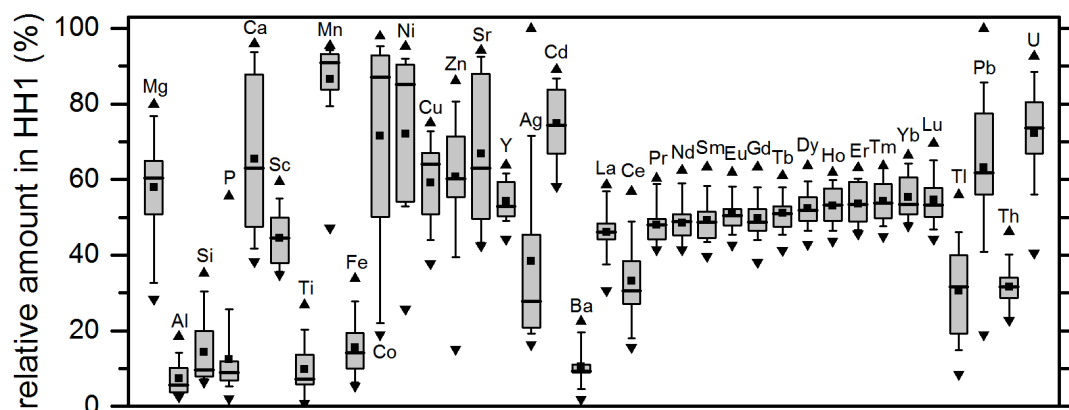


Figure A.14: Statistical distribution of the relative authigenic amount of the respective elements extracted with the first HH-leach. 100 % mean that leaches 2-10 did not contain any significant amount of the respective element, whereas 0 % designate that the first HH-leach did not contain any amount. The average and median values are given by the black square and horizontal bar, respectively. Boxes mark the range of the central half of the data, and whiskers the central 80 %. Triangles mark the extreme values of the data set.

However, for an assessment of the usefulness of these data, it is important to take the natural variability of the respective elements in the authigenic fraction into account. If the abundance of an element in the authigenic sediment fraction is highly variable across different sediments of different ages, then measured information on its abundance is more valuable than if its abundance is fairly constant. Therefore, the relative variability (1 SD) of the amount of the different elements in the authigenic fractions in these 17 sediment samples is compared to the uncertainty of their quantification via the first HH-leach in Fig. A.15. Data at a value of 1 exhibit the same natural variability as the uncertainty of the abundance quantification via the first HH-leach. At a value of 0.5, the uncertainty of the quantification is half as big as the natural variability and so on. This figure indicates that this method of quantification yields the most valuable information on the authigenic abundance of Mn, Zn, U, Cd, Th, the REEs, Ni, Cu, Mg, Y, and Pb. This preliminary assessment based on the 17 different samples may be premature, but it does indicate

that this authigenic budget estimation can be valuable for several elements. Since these data are readily available for samples analysed with the weak leaching and measuring routine outlined in this thesis, it may be worth while investigating this topic further.

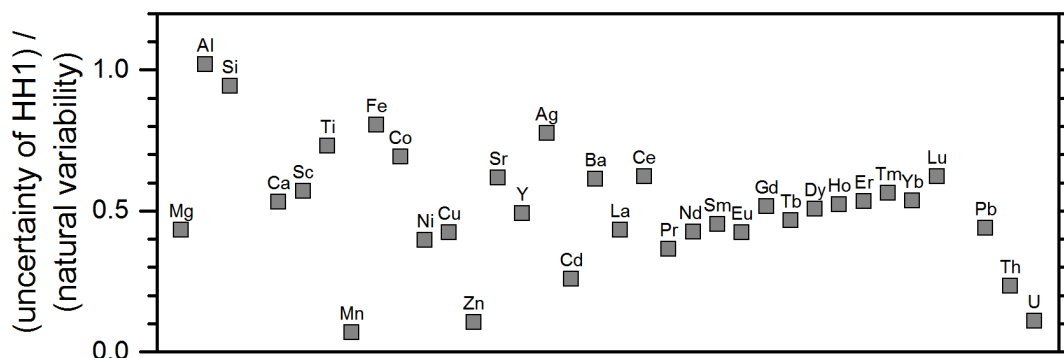


Figure A.15: Ratio of the uncertainty of the assessment of authigenic abundance based on data of the first HH-leach only and the natural variability in the authigenic fraction of the respective element in the 17 samples investigated in chapter 4.

A.6 Additional figures

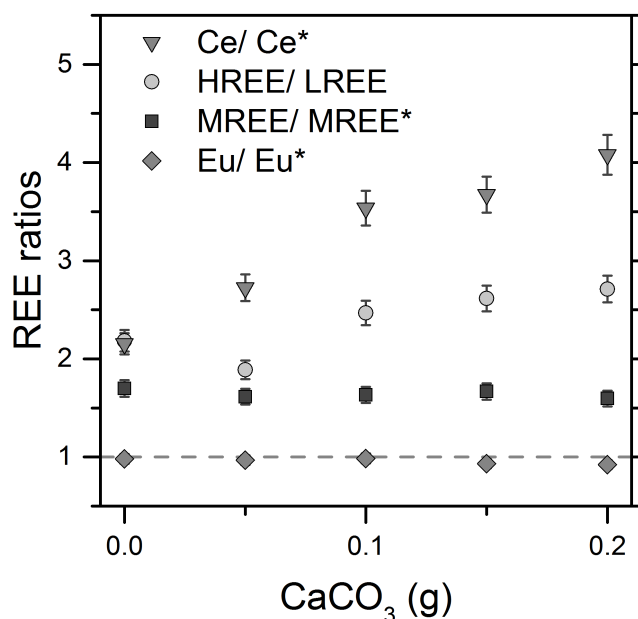


Figure A.16: Effect of carbonate content on extracted REE ratios. Each sample consisted of 30 mg of the Nod-A1 SRM, mixed with variable amounts of pure CaCO_3 (pA quality). While the carbonate does not contain REEs itself, it buffers the acid in the leachate and thus increases the effective pH of the solution (see section 4.3.1). This result evidences the sensitivity of the Ce anomaly (Ce/Ce^*) and the REE slope (HREE/LREE) in the leachate to the pH in the leaching solution. A higher pH correlates to higher values of these parameters. In contrast, the mid REE bulge ($\text{MREE}/\text{MREE}^*$) and the Eu anomaly are not influenced by the pH.

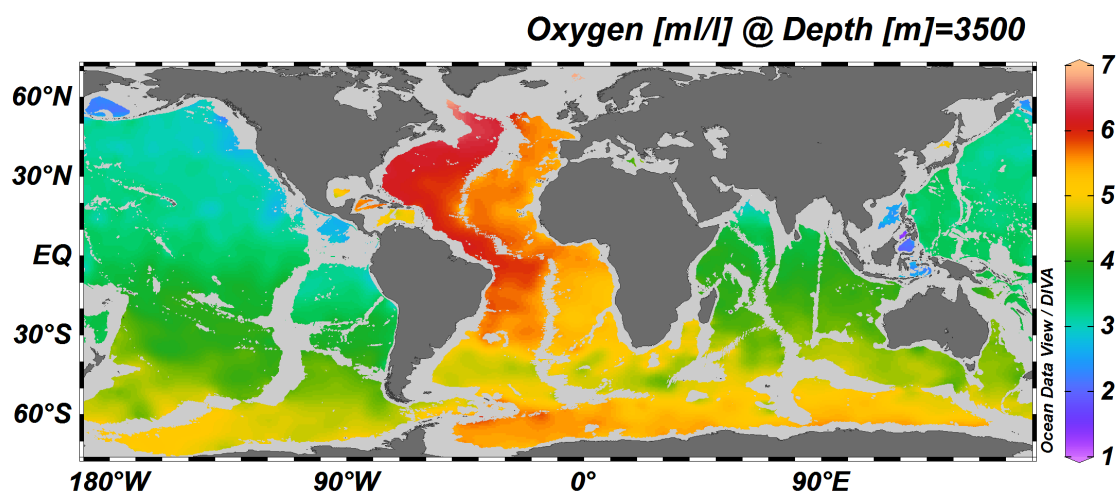


Figure A.17: O_2 concentration in global deep waters at 3.5 km depth in ml/l. The high oxygen concentrations in the deep Northwest Atlantic evidence the role of NEADW and NWABW in supplying oxygen to the deep oceans. It is furthermore an illustration of the important role of North Atlantic deep water formation in coupling the deep ocean to the atmosphere. The map was created with Ocean Data View (Schlitzer [2016]) and data are from Garcia et al. [2013a,b]; Zweng et al. [2013].

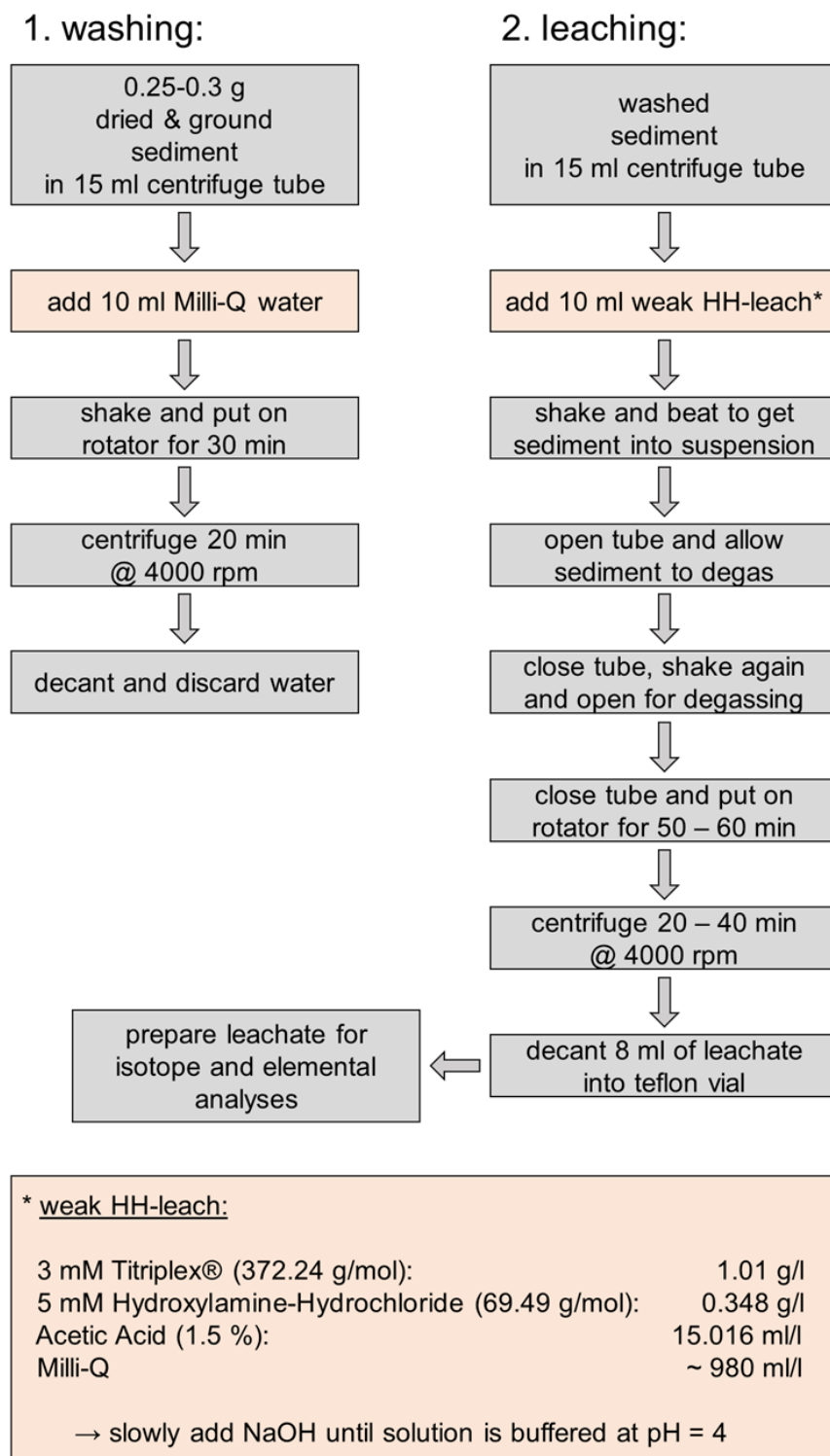


Figure A.18: Schematic illustration of the refined leaching method. The figure is extracted from the supplement of [Blaser et al. \[2016\]](#).

B Lists

B.1 List of Figures

2.1	Schematic view of the global Thermohaline Circulation	13
2.2	Atlantic meridional transects of PO_3 and ϵNd	14
2.3	Ice core $\delta^{18}O$ and reconstructed seawater Nd IC in the abyssal North West Atlantic	20
2.4	Nd bearing fractions of deep sea sediments	24
2.5	Maps of the subpolar North Atlantic including basin names and deep water flows.	26
2.6	Map of the subpolar North Atlantic with areas of complications for the extraction of authigenic Nd	29
3.1	Transmission efficiency during element abundance measurements . . .	34
3.2	Matrix effects from Ca and Na on element abundance measurements .	35
3.3	Calibration Ranges and sample concentration of a typical element abundance measurement	36
3.4	Reproducibility of TPR concentrations and concentration ratios . . .	37
3.5	Reproducibility of TPR Nd IC determinations	39
4.1	Sites of progressive leaching test sediments	41
4.2	Scheme of progressive leaching tests	42
4.3	pH evolution and carbonate dissolution during the HH-leaching process	45
4.4	Progressive leaching results for samples from site 7	46
4.5	Statistical distribution of the elemental concentrations and REE ra- tios during progressive leaching	47
4.6	REE patterns of selected samples during progressive leaching	49
4.7	Nd ICs from the progressive leaching tests and selected literature . .	50
4.8	Comparison of Nd ICs from progressive leaches and foraminifera. . . .	51
4.9	Calculated end member contributions to progressive leaching signals	55
4.10	End member contributions to the progressive leaches correlated in relation to different parameters	56
4.11	Cross plots of Nd IC offset to different element ratios	59
5.1	Map of the North Atlantic including sites and detrital input.	63
5.2	Stratigraphy and Nd IC profile of site Me68-91	67
5.3	Elemental concentrations and ratios of core Me68-91 VL	70
5.4	Nd isotope records from the Northeast Atlantic region	79
5.5	Estimation of the benthic flux of Nd from the Vedde Ash turbidite . .	82

6.1	Map of study sites in the subpolar North Atlantic	89
6.2	Age models and Nd IC results of subpolar North Atlantic sites	92
6.3	Nd IC and reported sedimentology of subpolar sites	93
6.4	Correlation of Nd IC with MREE and Sr/Ca in Heinrich Layers	96
6.5	Scatter plots of elemental ratios and Nd ICs of leachates	97
6.6	Authigenic Nd ICs of the four subpolar sites	100
6.7	Difference in Nd IC between the subpolar sites	101
6.8	Nd isotope records around Rockall Bank	103
6.9	Map of sedimentary Nd ICs and possible circulation during the LGM	105
6.10	Holocene Nd IC results from the subpolar and deep western North Atlantic	108
6.11	Holocene Nd ICs compared to variations in sortable silt	109
A.1	Depth transect sections in the subpolar North Atlantic	140
A.2	Chemical properties at hydrographic transect A - 50°N	141
A.3	Chemical and physical properties at hydrographic transect B - from Greenland to Scotland	142
A.4	Chemical and physical properties at hydrographic transect C - Labrador Sea	143
A.5	Stratigraphy and Nd IC profile of Site U1308	144
A.6	Elemental analysis of core U1308C	145
A.7	Elemental and Nd isotopic results from core Me68-89 HL	146
A.8	Elemental and Nd isotopic results from core PO08-23 HL	146
A.9	Nd ICs of all leaches from the subpolar North Atlantic	147
A.10	Concentrations of Mn, U, Nd, and CaCO ₃ in leaches from the subpolar North Atlantic	148
A.11	Concentration ratios of Mn/U, Ti/Nd, Al/Nd, Sr/Ca in leaches from the subpolar North Atlantic	149
A.12	REE ratios in leaches from the subpolar North Atlantic	150
A.13	Statistical distribution of the elemental abundance in the authigenic fraction	151
A.14	Statistical distribution of the relative authigenic amount extracted with the first HH-leach	152
A.15	Uncertainty of the calculated elemental abundance in the authigenic fraction compared to their natural variability	153
A.16	Effect of carbonate content on extracted REE ratios	154
A.17	O ₂ concentration in global deep waters	155
A.18	Scheme of the refined leaching procedure	156

B.2 List of Tables

2.1	Table of the natural abundances of all isotopes from nuclear numbers 140 to 150.	18
3.1	Faraday cup configuration during Nd isotope measurements in Heidelberg	38
4.1	Samples used during leaching tests	43
5.1	Stratigraphy of sediment core Me68-91 VL	64
5.2	Northeast Atlantic sites and Holocene and LGM Nd ICs	71
6.1	Investigated sites in the subpolar North Atlantic	91
A.1	Table of all core sites discussed in chapter 6	139
A.2	Nd characteristics of relevant water masses	140

B.3 List of abbreviations

AABW	Antarctic Bottom Water
AAIW	Antarctic Intermediate Water
AC	acetic acid
AMOC	Atlantic Meridional Overturning Circulation
CFC	chlorofluorocarbon
CGFZ	Charlie-Gibbs Fracture Zone
CHUR	Chondritic Uniform Reservoir
CT	core top sample
DC	detrital carbonate
DSOW	Denmark Strait Overflow Water
EDTA	ethylenediaminetetraacetic acid
GNABW	Glacial North Atlantic Bottom Water
GNAIW	Glacial North Atlantic Intermediate Water
HE	Heinrich Event
HH	hydroxylamine hydrochloride
HL	Heinrich Layer
HREE/LREE	rare earth element slope
ICP-OES	inductively coupled plasma optical emission spectrometer
ICP-QMS	inductively coupled plasma quadrupole mass spectrometer
IRD	ice rafted debris
ISOW	Iceland-Scotland Overflow Water
ka	thousand years
LDW	Lower Deep Water
LGM	Last Glacial Maximum
LSW	Labrador Sea Water
MC-ICP-MS	multicollector inductively coupled plasma mass spectrometer
MREE/MREE*	mid rare earth element bulge
NADW	North Atlantic Deep Water
NCW	northern component water
Nd IC	radiogenic neodymium isotope composition
NEADW	Northeast Atlantic Deep Water
NWABW	Northwest Atlantic Bottom Water
PAAS	Post Archaean Australian Shale
REE	rare earth element
SPMW	Subpolar Mode Water
SRM	standard reference material
\overline{SS}	sortable silt
SSW	southern sourced water
TPR	total procedural replicate
TII	Termination II sample
VL	trigger core ('Vorlot')
YD	Younger Dryas

Acknowledgements

Ein Projekt wie diese Doktorarbeit wird nicht im Alleingang bewältigt. Ich bedanke mich hiermit bei allen, die daran direkt und indirekt mitgearbeitet haben. Insbesondere gilt all den Leuten Dank, die im Labor Hand angelegt haben wie Jasmin Link, Frerk Pöppelmeier, Evan Border, Thomas Krenzel, Matthias Fladt, Benny Antz, Julia Hoffmann und René Eichstädter. Außerdem Marcus Gutjahr, der fast schon unzählige Nd Isotopenproben gemessen und dafür auch das ein oder andere Wochenende geopfert hat und Hartmut Schulz, der mit äußerster Sorgfalt und Motivation mit der Vermessung und Beprobung der Dreizack Kerne geholfen hat. Auch die Studenten, die ich direkt betreut habe, und die dadurch direkt oder indirekt mitgewirkt haben seien erwähnt. Durch die Arbeit mit Malu de Carvalho Ferreira, Philipp Eisinger, Richard Dietrich, Jasmin Link, und Frerk Pöppelmeier habe auch ich selbst vieles gelernt.

Ich bin Norbert Frank sehr dankbar, dass er mich für diese Arbeit aufgenommen und betreut hat. Besonders seine Ermutigung tiefer in so manche Systematik einzutauchen und so manche Bekanntmachung auf Konferenzen sowie in Heidelberg weiß ich zu schätzen. Jörg Lippold gilt besonders großer Dank, da er mich zur Paläoklimatologie gebracht und dort gehalten hat. Und natürlich dafür, dass er vor vier Jahren den erfolgreichen Antrag für dieses Projekt innerhalb von zwei Wochen nach nur einer Unterhaltung geschrieben und es damit überhaupt ermöglicht hat.

Dank gilt auch all jenen, die mir die nötigen Dinge beigebracht haben um diese Arbeit zu bewältigen. Das sind allen voran Norbert Frank und Jörg Lippold, Evelyn Böhm und René Eichstädter, und die Kollegen vom GEOMAR Marcus Gutjahr und Martin Frank. Aber auch die restliche Arbeitsgruppe hat immer wieder dazu beigetragen. Auch alle weiteren Kollegen überall auf der Welt mit denen ich interessante Unterhaltungen und Diskussionen hatte haben indirekt mitgeholfen, und dafür sei auch ihnen gedankt. Ich freue mich auf weitere interessante Jahre. Ganz konkreter Dank gilt außerdem allen, die diese Arbeit gewissenhaft korrektur gelesen und damit signifikant verbessert haben, den Mitbetreuern Kurt Roth und Martin Frank, und Werner Aeschbach als Zweitgutachter.

Abschließend gilt auch meinem privaten Umfeld Dank. Meiner Familie, die mich immer unterstützt hat, auch wenn ich Heimatbesuche schändlich vernachlässigt habe. All meinen Freunden dafür, dass es sie gibt, ganz besonders aber den Nerds für viele Tage und Abende voll Ablenkung und ebenso meinen Hobbiz für unzählige Sonntage und Wochenenden, bei denen man sich in angenehmer Atmosphäre mal so richtig auspowern konnte. Möge das alles weiterhin erhalten bleiben. Und meinen zauberhaften Kolleginnen und Kollegen Jörg, Evelyn, Benny, Freya, Jenny und alle anderen für eine generell angenehme Arbeitsatmosphäre und viele erholsame Pausen und Feierabende. Meiner Kollegin, Kommilitonin und Freundin Sanam, die mich schon seit zehn Jahren durch dick und dünn begleitet hat gilt ganz besonderer Dank für all die guten Zeiten und wichtigen Diskussionen und Motivationen dieser und der kommenden Jahre. Fast zum Schluss möchte ich mich herzlichst bei meiner Meret bedanken, dafür dass sie schon so lange ihr Leben mit mir teilt, mich immer wieder sehr aktiv, aber jeden Tag auch passiv unterstützt hat und das sicherlich auch weiterhin tun wird. Der letzte Dank gilt den kleinen Menschen Lenny, Kira und Jona, die durch ihre bloße Existenz das Leben schöner machen und mich daran erinnern, was sonst noch wichtig ist.